MODEM DESIGN
FOR
DIGITAL SATELLITE COMMUNICATIONS

BY

MOHAMMED TALAL, B.Sc., M.Sc.

A Doctoral Thesis

Submitted in partial fulfilment of the requirements for
the award of Doctor of Philosophy of the
Loughborough University

January 1997

Supervisor: Dr. W.G.Marshall

Department of Electronic and Electrical Engineering
Loughborough University
Loughborough
Leicestershire LE11 3TU
U.K

LIST OF CONTENTS

	Page number
ABSTRACT	i
ACKNOWLEDGEMENTS	iii
GLOSSARY	iv
Chapter 1: INTRODUCTION	1
1.1 Background	1
1.2 Modulation methods	2
1.3 Outline of investigation	4
Chapter 2: MODELLING OF THE DIGITAL COMMUNICATION CHANNEL	6
2.1 Baseband data-transmission system	6
2.2 Baseband signal waveform shaping	15
2.3 Data-transmission system for satellite links	21
2.4 Filter configurations for computer simulation	24
2.5 Nonlinearity	26
2.6 The baseband equivalent models of quadrature modulation systems	31
Chapter 3: COHERENT QUATERNARY PSK SYSTEMS OVER A LINEAR OR NONLINEAR SATELLITE CHANNEL	49
3.1 Description of coherent QPSK, DEQPSK and OQPSK systems	49
3.2 Error probability performances of coherent QPSK, DEQPSK and OQPSK signals	55
3.3 Baseband equivalent model of DEQPSK system, for computer simulation	57
3.4 Power spectra of QPSK, DEQPSK and OQPSK signals	61
3.5 Spectral estimation of QPSK, DEQPSK and OQPSK signals by computer simulation	62
3.6 Simulation results and discussion	64
Chapter 4: CONVOLUTIONAL ENCODING AND COHERENT 8PSK SYSTEMS OVER A NONLINEAR SATELLITE CHANNEL	91

4.1 Introduction 91
4.2 TDMA Frame structure 92
4.3 Convolutional code and coherent 8PSK (CE8PSK) system 93
4.4 Baseband equivalent model of CE8PSK system, with a nonlinear satellite channel, for computer simulation 100
4.5 Viterbi-algorithm decoder for CE8PSK signals 103
4.6 Frame synchronisation in TDMA 105
4.7 Carrier recovery scheme for CE8PSK signals 108
4.8 Performances of CE8PSK signal 111
4.9 Distance measure for minimum-distance decoding of CDE8PSK signals 112
4.10 Simulation results and discussion 114

Chapter 5: CONVOLUTIONAL ENCODING AND COHERENT DIFFERENTIALLY 8PSK SYSTEMS OVER A NONLINEAR SATELLITE CHANNEL 141
5.1 Introduction 141
5.2 Convolutional code and differentially encoded 8 phase-shift keying (CDE8PSK) technique 142
5.3 Baseband equivalent model of CDE8PSK system, with a nonlinear satellite channel, for computer simulation 144
5.4 Suboptimum decoder for CDE8PSK signals 145
5.5 Performance of CDE8PSK signal 148
5.6 Power spectra of CE8PSK and CDE8PSK signals 149
5.7 Simulation results and discussion 151

Chapter 6: BASEBAND LINEARIZER TECHNIQUE APPLIED TO PSK SIGNALS 163
6.1 Baseband linearizer technique 163
6.2 Modelling of the baseband linearizer 166
6.3 Model of the baseband linearizer in cascade with the HPA, used for computer simulation 169
6.4 Backoff factor of the baseband linearizer 170
6.5 Baseband equivalent model of the DEQPSK or CE8PSK system (or CDE8PSK system) with the use of the baseband linearizer 171
6.6 Simulation results and discussion 172

Chapter 7: IMPLEMENTATION OF A DEMODULATION AND FILTERING OF THE T-SAT MODEM USING DIGITAL SIGNAL PROCESSOR (DSP) 194

7.1 Introduction 194

7.2 The T-SAT modem 195

7.3 Development of the demodulation and digital filtering in the T-SAT using digital signal processor (DSP) 197

7.4 Discussion and results 201

Chapter 8: DIGITAL SIGNAL PROCESSOR IMPLEMENTATION OF A VITERBI-ALGORITHM DECODER FOR A CONVOLUTIONALLY ENCODED 8PSK SIGNAL 210

8.1 Introduction 210

8.2 Convolutionally encoded 8PSK signals 211

8.3 Viterbi-algorithm decoder 212

8.4 Digital signal processor implementation of the Viterbi-algorithm decoder 214

8.5 Discussion and results 223

Chapter 9: COMMENTS ON THE PROJECT 235

9.1 Recommendations for further study 235

9.2 Conclusions 237

9.3 Originality of the study 238

Appendices 241

Appendix A1: Matched-filter detection 242

Appendix A2: Impulse responses of the transfer functions giving a rectangular spectrum and sinusoidal roll-off spectrum 252

A2.1 Rectangular spectrum 252

A2.2 Sinusoidal roll-off spectrum 252

Appendix A3: The relationship of $2E_b/N_0$ between the uplink and downlink of a satellite channel 257

Appendix A4: Baseband equivalent models of symmetrical bandpass filters 258

A4.1 Baseband equivalent model of the BPF at the transmitter 258

A4.1 Baseband equivalent model of the BPF at the receiver 259

Appendix A5: Analysis of quadrature crosstalk in bandpass signals 262

Appendix A6: Proof of the complex signal representation of systems using quadrature modulated signal 265

A6.1 Representation of the modulated signal 265

A6.2 Representation of the demodulated signal 266

Appendix A7: Narrowband noise representation properties 268

Appendix A8: Bit-energy-to-noise density ratio ($2E_b/N_0$) calculation for computer simulation 273

A8.1 $1/2\,N_0$ Determination for computer simulation 273

A8.2 $2E_b/N_0$ Value calculation for computer simulation 275

Appendix A9: The scaling relationship between the continuous signal and the sampled signal 278

Appendix A10: Probability of error calculation for binary signals 279

REFERENCES 282

ABSTRACT

The thesis is concerned with the design of a phase-shift keying system for a digital modem, operating over a satellite link. Computer simulation tests and theoretical analyses are used to assess the proposed design.

The optimum design of both transmitter and receiver filters for the system to be used in the modem are discussed. Sinusoidal roll-off spectrum with different roll-off factor and optimum truncation lengths of the sample impulse response are designed for the proposed scheme to approximate to the theoretical ideal. It has used an IF bandpass filter to band limit the modulated signal, which forms part of the satellite channel modelling. The high power amplifier (HPA) at the earth station has been used in the satellite channel modelling due to its effect in introducing nonlinear AM-AM and AM-PM conversion effects and distortion on the transmitted signal from the earth station. The satellite transponder is assumed to be operating in a linear mode.

Different phase-shift keying signals such as differentially encoded quaternary phase-shift keying (DEQPSK), offset quaternary phase-shift keying (OQPSK) and convolutionally encoded 8PSK (CE8PSK) signals are analysed and discussed in the thesis, when the high power amplifier (HPA) at the earth station is operating in a nonlinear mode. Convolutional encoding is discussed when applied to the system used in the modem, and a Viterbi-algorithm decoder at the receiver has been used, for CE8PSK signals for a nonlinear satellite channel. A method of feed-forward synchronisation scheme is designed for carrier recovery in CE8PSK receiver.

The thesis describes a method of baseband linearizing the baseband signal in order to reduce the nonlinear effects caused by the HPA at the earth station. The scheme which compensates for the nonlinear effects of the HPA by predistorting the baseband signal prior to modulation as opposed to correcting the distortion after modulation, thus reducing the effects of nonlinear distortion introduced by the HPA. The results of the improvement are presented.

The advanced technology of digital signal processors (DSPs) has been used in the implementation of the demodulation and digital filtering parts of the modem replacing large parts of conventional circuits. The Viterbi-algorithm decoder for CE8PSK signals has been implemented using a digital signal processor chip, giving

excellent performance and is a cost effective and easy way for future developments and any modifications.

The results showed that, by using the various studied techniques, as well as the implementation of digital signal processor chip in parts of the modem, a potentially more cost effective modem can be obtained.

ACKNOWLEDGEMENTS

The author would like to express his gratitude to his supervisor, Dr. W.G.Marshall, for his considerable help and guidance.

The financial support of the Scientific Studies and Research Centre in Syria, is gratefully acknowledged.

The author would like to thank Dr. M.Abbasi, for his guidance and supervision part of the work in Syria.

A special thank to the author's mother, wife Iniam, children Majdi, Diya and Bahaa for their prays and encouragement.

GLOSSARY

Abbreviations

AWGN	additive white Gaussian noise
ADC	analog-to-digital converter
BER	bit error rate in the detected data
CE8PSK	convolutionally encoded 8 phase-shift keying
CDE8PSK	convolutionally and differentially encoded 8 phase-shift keying
CORPSK	correlative phase-shift keying
8PSK	eight phase-shift keying
D/C	down converter
DAC	digital-to-analog converter
DSP	digital signal processor
DEQPSK	differentially encoded quaternary phase-shift keying
E_b	energy per bit
E_s	energy per symbol
GMSK	Gaussian minimum phase-shift keying
FDMA	frequency-division-multiple-access
FEC	forward-error-correction
FFT	fast Fourier transform
F_{IF}	IF filter
h.f.c	high frequency components
HPA	high power amplifier
IBO	input backoff
IDFT	inverse discrete Fourier transform
IF	intermediate frequency
IJF-QPSK	intersymbol-interference free quaternary phase-shift keying
IJF-OQPSK	intersymbol-interference free quaternary offset phase-shift keying
ISI	intersymbol interference
MSK	minimum phase-shift keying
OBO	output backoff
OQPSK	offset quaternary phase-shift keying
PSK	phase-shift keying
QPSK	quaternary phase-shift keying
SNR	signal-to-noise power ratio
TDMA	time-division-multiple-access
TFM	tamed frequency modulation

TWTA travelling wave tube amplifier

U/C upconverter

List of principal mathematical symbols

$\hat{A}$ signal envelope, with the use of the HPA backoff factor M_c, at the input to the HPA.

C_i unitary distance between two vectors (used for decoding a CE8PSK signal).

c_i incremental distance for the sample received at time $t = iT$, when decoding a CE8PSK signal.

$C_i(j)$ unitary distance between two vectors (used for decoding a CDE8PSK signal).

$c_i(j)$ incremental distance for the sample received at time $t = iT$, when decoding a CDE8PSK signal.

$D_p(\delta_m), D_q(\delta_m)$ inphase and quadrature components of the conversion function $D(\delta_m)$ of the baseband linearizer.

E[.] average of (.).

$\hat{E}_i$ signal envelope, with the use of the baseband linearizer backoff factor L_c, at the input to the baseband linearizer.

E_b energy per bit.

E_s energy per symbol.

$e_i(j)$ for $j = 1,2,3$ binary coded symbols carried by e_i (for a CE8PSK or CDE8PSK signal).

Δf and $\Delta\omega$ frequency offset in Hz and rad/s.

$f(\delta_m)$ AM-PM conversion function of the baseband linearizer.

$f(t)$ impluse response of the baseband equivalent model of the transmitter or receiver filter.

f_m $m+1^{\text{th}}$ component of the vector $\{f_g\}$ which is obtained by sampling the impulse response $f(t)$ at a rate of $1/T_s$ samples per second.

f_{IF} and ω_{IF} intermediate frequency in Hz and rad/s.

f_c and ω_c carrier frequency in Hz and rad/s.

$F_T(f)$ transfer function of the modulation filter in cascade with the transmitter filter.

$g(\lambda_m)$ AM-PM conversion function of the assumed HPA.

$G_p(\lambda_m), G_q(\lambda_m)$ inphase and quadrature components of the conversion function $G(\lambda_m)$ of the assumed HPA.

$H_t(f)$ frequency response (transfer function) of the transmitter filter.

$H_r(f)$ frequency response (transfer function) of the receiver filter.

$H(f)$	frequency response (transfer function) of the baseband channel, i.e., $H_t(f)$ and $H_r(f)$ in cascade.
$H^*(f)$	complex-conjugate of $H(f)$.
$h(t)$	impulse response of the resultant transfer function of the baseband channel.
$h_t(t)$	impulse response of the transmitter filter.
$h_r(t)$	impulse response of the receiver filter.
k	constraint length of the convolutional code.
L	number of tested symbols.
L_c	baseband linearizer backoff factor.
M_c	HPA backoff factor.
$\frac{1}{2} N_0$	two-sided power spectral density of zero mean additive white Gaussian noise at the input to the receiver.
$N(t)$	bandpass noise function.
$n(t)$	baseband equivalent of the noise $N(t)$.
$n_c(t)$ and $n_s(t)$	real and imaginary components of the complex value noise waveform $n(t)$.
$n_{c,m}$ and $n_{s,m}$	real and imaginary components of $n(t)$ at time $t = mT_s$.
$p(t)$	impulse response of the modulation or demodulation filters.
p_m	m^{th} component of the vector $\{p_n\}$, which are obtained by sampling the impulse response $p(t)$ at the rate of $1/T_s$ samples per second.
P_e	probability of bit error in the detection of a received signal element.
q_i	i^{th} 4-level complex-valued symbol in DEQPSK or OQPSK signals or 8-level complex-valued symbol for CE8PSK or CDE8PSK signals.
r_i	i^{th} received sample of the complex-valued signal $r(t)$.
$S(t)$	bandpass signal.
$s(t)$	baseband equivalent signal of $S(t)$.
$\lvert s(t) \rvert$	magnitude of $s(t)$.
$\{S_L\}$	L-component data vector to be transmitted.
s_i	i^{th} 2-level data symbol in $\{S_L\}$.
T	unit of time which represents the length of time between adjacent transmitted symbols.
T_s	unit of time which represents the length of time between samples used in computer simulation.
u_m	m^{th} transmitted sample of the waveform $u(t)$ at the input to the modulator.
v_i	sample value of the filtered noise waveform $v(t)$ at the time $t = iT_s$.
X_L	L-component vector of the corresponding data symbol $\{S_L\}$.

y_i	i -component vector of the possible received symbols.
σ^2	variance of the additive white Gaussian noise at the input of the receiver.
α	sinusoidal roll-off factor.
$\delta(t)$	unit impulse function (Dirac function).
θ_i	arbitrary carrier phase $\theta(t)$ of the receiving signal at time $t = iT$.

CHAPTER 1

INTRODUCTION

1.1 Background

As the demand for all areas of communications services expands, it is inevitable that the demand for satellite services will increase.

Digital satellite systems offer the most cost-effective methods of signal transmission for many applications. Increasingly, new satellite systems are digital rather than analogue. There are a number of reasons for this, in addition to the fact that much of the new traffic is digital in nature [6]. Time Division Multiple-Access (TDMA) can be used as the multiple-access method in digital systems. This can achieve an increased capacity compared with analogue multiple-access systems [3]. TDMA transponders relay only one digitally modulated carrier at a time so that intermodulation is not as critical as in FDMA systems. This increased capacity, linked to the decreasing cost of Large Scale Integration (LSI) digital circuit components, enhances the economic viability of digital satellite systems, compared with the corresponding analogue systems. Digital systems are inherently more robust in an interference environment, and can be operated at lower transmitter power levels than the corresponding analogue, Frequency-Division Multiplex, Frequency Modulated, (FDM-FM), systems [6]. The bit streams which comprise the digital signal have similar properties, whether TV signals, voice signals, computer data, or ISDN services [8] which in analogue form all have very different properties. Thus signal multiplexing and processing is very much simpler in a digital system. Satellite signals are more easily interfaced to terrestrial systems, (optical fibre, cable, or microwave), when in digital form. The predominance of digital circuit components in a digital satellite system provides a very predictable and repeatable performance, which is not subject to drift with time.

The increased confidence in the reliability of digital systems has led, in the last few years, to consideration of the feasibility of performing more complex functions

on board the satellite, thereby simplifying the earth station hardware [97]. This is a very important step in reducing the cost of earth stations to the end-user who wishes to take advantage of the new satellite services.

The use for satellite services is where the broadcast nature of the service is of prime importance, in multi-point to point and point to multi-point communications such as mobile radio, electronic news gathering, remote printing, database transfer and updating, and as a back-up to terrestrial services.

The project will be used to perform experiments to demonstrate the advantages of on board processing with Molniya satellite orbits. A satellite in this orbit remains at a near-zenith elevation for 8 of the 12 hour orbit period [75]. The orbit alleviates many of the problems, since the satellite is essentially overhead during its operating period.

This thesis is concerned with one aspect of the new generation of digital satellite systems; the modulator/demodulator (MODEM), and the possibility of hardware implementation of the modem using the advanced technology of digital signal processing. This thesis is concerned with a station to ground channel, and the mobile to ground station link is not discussed. The remaining two sections in this chapter are concerned with the choice of the modulation methods for which appropriate detection processes are investigated, and with an outline of the contents of the thesis.

1.2 Modulation methods

The systems of interest here operate at a rate of 64, 128, 256 Kbit/sec over a satellite link. The modulation methods commonly considered for application to satellite systems can be classified in a number of different ways, but they all have one thing in common. In all cases the signals are either constant envelope or near-constant envelope; thus minimizing AM-AM and AM-PM conversion effects and band spreading of the transmitted signal, when the latter is fed through a nonlinear amplifier (when the signal level approaches the amplifier saturation region, it will cause: for a multicarrier signal, intermodulation occurs, and for a single bandlimited signal, envelope fluctuation will cause unwanted phase modulation and spectral spreading). The amplifier could be a high power amplifier (HPA) or satellite repeater that is operating at or close to saturation. At this point the typical HPA has a very nonlinear characteristic, so that an input signal with significant envelope variations, will be amplified such that the output signal has a significantly increased effective bandwidth, and is nonlinearly distorted. Therefore constant envelope, or near-constant envelope signals, are imperative. This means that only frequency or phase modulated signals are considered.

Many recently proposed signals, such as quaternary phase-shift keying (QPSK), offset quaternary phase-shift keying (OQPSK), minimum phase-shift keying (MSK) [98], [99], Gaussian minimum phase-shift keying (GMSK) [100], [101], tamed frequency modulation (TFM) [12], correlative phase-shift keying (CORPSK) [34], intersymbol-interference-free QPSK (IJF-QPSK) [6], [102], [103], IJF-OQPSK [11], convolutionally encoded 8PSK (CE8PSK) [31], [32] signals, and so on, have been developed for use over satellite links. Of these, CORPSK, TFM and MSK signals are the ones that achieve a truly constant envelope, the price paid for this being a rather wider bandwidth than that of the others. Bandlimiting of the signals results in the introduction of an envelope ripple and intersymbol interference (ISI). An OQPSK signal is a modified form of a QPSK signal but with a near constant envelope. In an OQPSK signal, the inphase data stream is delayed relatively to the quadrature data stream by half a symbol period. An IJF-QPSK signal [6], [102], [103] is also a near constant envelope scheme derived from an OQPSK signal by employing various transmitted pulse shapes to give a desired compromise between bandwidth and envelope ripple.

Of these proposed signals, the convolutionally encoded 8PSK signal [31], [32] although exhibiting considerable envelope variation, provides a coding gain of greater than 4 dB over an ideal uncoded QPSK signal for a code with a 4-bit memory, hence it can provide high-quality transmission over satellite links. However for the optimum detection of such signal, a complex valued demodulation process is required, involving both in-phase and quadrature coherent demodulators. The demodulated baseband signal obtained is complex-valued (having two separate components), and the detector has to compute, for each of a number of possible sequence of received data symbols, the unitary distance between the corresponding received sequence, in the absence of noise, and the sequence actually received. Such computations involve numerous operations of squaring or multiplication. Now, provided only that the transmitted-modulated carrier signal has a near constant envelope together with a large number of carrier cycles per signal element, then little or non useful information carried by the phase-modulated waveform is lost in the receiver by first slicing the received waveform in an amplifier limiter and then extracting the phase for subsequent use in the detection process.

Having described the general classes of modulation schemes which are being considered for future satellite services, an important feature is that the earth station should be simple, in order to make it cheap and reliable. The aim of the investigation is to determine the combination of the signal design and demodulation process leading to the potentially most cost-effective modem, in a system operating over a satellite link. In the investigation, it is assumed that time division multiple access

(TDMA) is used at the satellite and that the satellite transponder is operating at less than its full power, so that there will be no further nonlinear distortion caused by the satellite transponder. It is also assumed that the satellite is used in a highly elliptical orbit.

1.3 Outline of investigation

The investigation is mainly concerned with the tolerance to additive white Gaussian noise (AWGN) of various data-transmission systems studied, using DEQPSK, OQPSK, CE8PSK and convolutionally differentially encoded 8PSK (CDE8PSK) signals, with the use of different combinations of the signal design. The aim is to develop the most cost effective arrangement of the data-transmission system, leading to the potentially most cost effective modem for use over satellite links, in terms of hardware implementation using a digital signal processor (DSP) chip in the detection process. Computer simulation tests have been used to compare the system schemes with theoretical analysis. A Texas Instruments DSP device is used for implementing part of the hardware of the modem.

Chapter 2 describes modelling the satellite channel, which includes the design of shaping filters for the transmitter and receiver with a sinusoidal spectrum with different roll-off factors (25%, 40% and 100%), and designing the optimum truncation lengths of the sampled impulse response. The IF bandpass filters have been modelled in the satellite channel. The high power amplifier (HPA) at the earth station has been used in the satellite channel modelling for computer simulation because of its effect on distortion when operated at the saturation point introducing nonlinear AM-AM and AM-PM conversion effects.

Chapter 3 describes coherent, differentially coherent QPSK and offset QPSK (OQPSK) techniques which are analysed and simulated when transmitted over a nonlinear and bandlimited satellite channel. Different simulation models, used to evaluate the effects of nonlinear distortion on the error-rate performances are discussed.

Chapter 4 contains descriptions of the convolutional encoding when applied to QPSK signals. A convolutionally encoded coherent 8PSK (CE8PSK) system has been designed for the satellite modem in a TDMA scheme, when the modem transmitting data in a burst mode operation, and a Viterbi-algorithm decoder has been used for decoding the signal giving better performance when the system is operating over a nonlinear and bandlimited satellite channel. The baseband equivalent models of the CE8PSK systems, with a nonlinear channel, for computer simulation are derived. Feed forward synchronisation scheme has been designed for CE8PSK signals with the use of phase estimator scheme in carrier recovery circuit. The system

described above is original work proposed for use over satellite links. An assessment for frame synchronisation and unique word detection are analysed in this chapter.

In Chapter 5 a convolutionally differentially encoded 8PSK (CDE8PSK) system has also been designed and analysed for the satellite modem to solve the catastrophic failure of CE8PSK signals, caused by a wrong reference carrier phase recovered at the receiver. The results of computer simulation tests for CDE8PSK system on the error-rate performance in different situations are presented and compared with those of DEQPSK systems, which gives a more cost effective supports for the system originated in chapter 4 in comparison with uncoded QPSK signals.

Chapter 6 describes a new technique of baseband linearizing or predistortion used to compensate for the nonlinear effects of the HPA. By using this technique, inverse distortion is added to the HPA input to cancel HPA nonlinear distortion. The baseband equivalent model of the baseband linearizer for computer simulation is derived. This baseband linearizer technique has been applied to PSK signals, the results of error-rate performance tests of DEQPSK, CE8PSK and CDE8PSK signals, with the use of the baseband linearizer are discussed.

In Chapter 7, the technology of digital signal processing (DSP) is described when used in the implementation and development of the T-SAT modem. Large parts of demodulation and digital filtering using conventional digital circuits of the T-SAT modem can be replaced using a single chip digital signal processor. The technique discussed is valid for use in other applications for a digital modem using PSK signals, where cost, size and limited-power environments of the hardware are important.

Chapter 8 is concerned with the implementation of the Viterbi-algorithm decoder for convolutionally encoded 8 phase-shift-keyed (CE8PSK) signals which have been proposed for use over satellite links in Chapter 4. The DSP makes the hardware implementation of the Viterbi-algorithm decoder possible for the high data bit-rate used in satellite communications. The decoder implemented using a single DSP chip and is valid for use in other applications for a digital modem.

Chapter 9 contains comments on the project, and outline the proposed signal design of the systems discussed in the thesis, leading to most cost effective signals for use over a nonlinear and bandlimited satellite channel. Originality of the study is outlined in this chapter as well.

CHAPTER 2

MODELLING OF THE DIGITAL COMMUNICATION CHANNEL

2.1 Baseband data-transmission system

The derivation of the probability of error, P_e, performance of a matched-filter detector is shown in Appendix A1, where there is no discussion of intersymbol interference (ISI) (i.e., a single signal-element is assumed). The matched-filter detector is optimum for a single-shot transmission, that is, for systems in which only one signal-element is transmitted, and in wideband systems where each signal-element is confined to its duration (i.e., ISI is negligible). However for optimal spectral efficiency, (i.e., in the presence of ISI) the transmitter and receiver filters must be optimized in order to minimize the error probability [7].

2.1.1 Optimum design of transmitter and receiver filters [1]

It is required to determine the transfer functions $H_t(f)$ and $H_r(f)$ of the transmitter and receiver filters, that maximize the signal/noise power ratio at the input to the detector in Fig. 2.1.

A binary polar signal is assumed throughout the following discussion. The transmitted signal-element is statistically independent and equally likely to have either of the two possible values. In the regular sequence of impulses carrying the element values $\{s_i\}$, at the input to the baseband channel, $s_i = \pm k$. A single transmitted signal-element at the input to the transmission path has the waveform

$$s_i h_t(t - iT)$$

where $h_t(t)$ is the impulse response of the transmitter filter. The Fourier transform (frequency spectrum) of the signal element is

$$s_i \exp(-j2\pi fiT) H_t(f)$$

Thus the energy spectral density of an individual transmitted signal-element, at the input to the transmission path, is

$$\left|s_i \exp(-j2\pi fiT) H_t(f)\right|^2 = s_i^2 \left|H_t(f)\right|^2 \qquad 2.1.1$$

and its energy is

$$E_i = s_i^2 \int_{-\infty}^{\infty} \left|H_t(f)\right|^2 df \qquad 2.1.2$$

Since the signal-elements are statistically independent and have zero means, making them statistically orthogonal, the average transmitted energy per signal-element, at the input to the transmission path, is the average of expected value of E_i is

$$E = \overline{s_i^2} \int_{-\infty}^{\infty} \left|H_t(f)\right|^2 df \qquad 2.1.3$$

where $\overline{s_i^2}$ is the average value of s_i^2. Clearly, at a given element rate, E is a measure of the transmitted signal power level.

Assume that the signal fed to the transmission path is sufficiently bandlimited by the transmitter filter so that it experiences no further bandlimiting in transmission. Furthermore, the transmission path is taken to introduce no attenuation, no delay, no amplitude distortion, and no phase distortion over the signal frequency band, so that the signal experiences no attenuation, delay or distortion in transmission. Thus the transmission path and receiver filter, in Fig. 2.1 together form a baseband channel with transfer function

$$H(f) = H_t(f) H_r(f) \qquad 2.1.4$$

Let $$\int_{-\infty}^{\infty} \left|H(f)\right| df = k \qquad 2.1.5$$

where k is a constant.

The impulse response of the baseband channel is

$$h(t) = \int_{-\infty}^{\infty} H(f)\exp(j2\pi ft)df \qquad 2.1.6$$

so that a single received signal-element at the detector input has the waveform

$$s_i h(t - iT)$$

with the Fourier transform

$$s_i \exp(-j2\pi fiT)H(f)$$

Thus the energy spectral density of an individual received signal-element at the detector input, is

$$\left|s_i \exp(-j2\pi fiT)H(f)\right|^2 = s_i^2\left|H(f)\right|^2 \qquad 2.1.7$$

and its energy is

$$F_i = s_i^2 \int_{-\infty}^{\infty}\left|H(f)\right|^2 df \qquad 2.1.8$$

Clearly, the average energy per element of the signal at the detector input is the average or expected value of F_i and is

$$F = \overline{s_i^2}\int_{-\infty}^{\infty}\left|H(f)\right|^2 df \qquad 2.1.9$$

The signal waveform at the input to the detector (in the absence of noise) is

$$\sum_i s_i h(t - iT)$$

so that the resultant waveform at the detector input is

$$r(t) = \sum_i s_i h(t - iT) + v(t) \qquad 2.1.10$$

where $v(t)$ is the noise waveform.

Since the noise input to the receiver filter is white Gaussian noise with zero mean and a two-sided power spectral density of $\frac{1}{2}N_0$, $v(t)$ is a sample function of a Gaussian random process with zero mean and a power spectral density of

$$\frac{1}{2}N_0\left|H_r(f)\right|^2$$

where, $H_r(f)$ is the transfer function of the receiver filter [2]. Thus the average power of the noise waveform $v(t)$ is

$$N = \frac{1}{2}N_0\int_{-\infty}^{\infty}\left|H_r(f)\right|^2 df \qquad 2.1.11$$

The signal/noise power ratio at the detector input, expressed as the average per element of the signal divided by the average noise power, is

$$\frac{F}{N} = \frac{\overline{s_i^2}\int_{-\infty}^{\infty}\left|H(f)\right|^2 df}{\frac{1}{2}N_0\int_{-\infty}^{\infty}\left|H_r(f)\right|^2 df} \qquad 2.1.12$$

Consider now any given transfer function $H(f)$ of the baseband channel, where $H(f)$ satisfies Eqns. 2.1.4 and 2.1.5. Suppose that the value of $H_r(f)$ is multiplied by d, where d is any positive real constant that is independent of frequency. The average transmitted signal power at the input to the transmission path is constant, fixed by the transmission path, since the transmitted signal power is always assumed to be set at its maximum permissible value. Clearly, if the value of N in Eqn. 2.1.12 is multiplied by d^2, the value of $H_t(f)$ must be multiplied by d^{-1}, in order that Eqns. 2.1.4 and 2.1.5 are still satisfied. Thus, from Eqn. 2.1.3 the value of $\overline{s_i^2}$ is multiplied by d^2, so that the value of F in Eqn. 2.1.12 is also multiplied by d^2. It follows that if the value of $H_r(f)$ is multiplied by the constant d, where d may have any real positive value, the value of F/N in Eqn. 2.1.12 remains unchanged.

Assume therefore that the value of $H_r(f)$ is such that

$$\int_{-\infty}^{\infty}\left|H_r(f)\right|^2 df = b \qquad 2.1.13$$

where b is any positive real constant. It is clear from the previous discussion that F/N is independent of b, since $H_r(f)$ may be multiplied by the appropriate constant d so that Eqn. 2.1.13 is satisfied. Now

$$\frac{F}{N} = \frac{\overline{s_i^2}}{\frac{1}{2} N_0 b} \int_{-\infty}^{\infty} |H(f)|^2 \, df$$

$$= \frac{E \int_{-\infty}^{\infty} |H(f)|^2 \, df}{\frac{1}{2} N_0 b \int_{-\infty}^{\infty} |H_t(f)|^2 \, df} \qquad 2.1.14$$

from Eqn. 2.1.3, where E is the average transmitted energy per signal-element.

Since for any given application, the values of E, N_0 and $H(f)$ are given and are therefore not subject to modification, and since F/N is independent of b, it can be seen that to maximize F/N, the signal/noise power ratio at the detector input, it is necessary to minimize $\int_{-\infty}^{\infty} |H_t(f)|^2 df$.

By the Schwarz inequality [3],

$$\int_{-\infty}^{\infty} |H_t(f)|^2 df \int_{-\infty}^{\infty} |H_r(f)|^2 df \geq \left(\int_{-\infty}^{\infty} |H_t(f)| |H_r(f)| df \right)^2 \qquad 2.1.15$$

with equality when

$$|H_r(f)| = d |H_t(f)| \qquad 2.1.16$$

From Eqn. 2.1.4

$$|H(f)| = |H_t(f)| |H_r(f)| \qquad 2.1.17$$

So that, from Eqn. 2.1.5

$$\int_{-\infty}^{\infty} |H_t(f)| |H_r(f)| df = k \qquad 2.1.18$$

Thus, from Eqns. 2.1.13 and 2.1.15

$$\int_{-\infty}^{\infty} |H_t(f)|^2 df \geq k b^{-1} \qquad 2.1.19$$

with equality when

$$|H_r(f)| = b|H_t(f)| \qquad 2.1.20$$

Since now $d = b$, as can be seen from Eqns. 2.1.16, 2.1.13 and 2.1.19.

But when equality holds in Eqn. 2.1.19, $\int_{-\infty}^{\infty} |H_t(f)|^2 df$ has its minimum value, so that the signal/noise power ratio at the detector input now has its maximum value. Equation 2.1.20 therefore gives the condition that must be satisfied by the transmitter and receiver filters, in order to maximize the signal/noise power ratio at the detector input. The signal/noise power ratio is here defined as the ratio of the average energy per signal element to the average noise power. This is not the same as the definition of the signal/noise power ratio used for the matched filter in Appendix A1, which is the ratio of the instantaneous signal power, at the time instant $t = T$, to the average noise power.

From Eqn. 2.1.20, since $|H_t(f)|$ and $|H_r(f)|$ are the moduli of $H_t(f)$ and $H_r(f)$, respectively, their values are always positive. $H_t(f)$ and $H_r(f)$ are, however, often complex. The values of $|H_t(f)|$ and $|H_r(f)|$ are clearly independent of the respective phase characteristics. Each filter may therefore introduce any degree of phase distortion and therefore any degree of group delay distortion, so long as Eqns. 2.1.4 and 2.1.20 are satisfied, without affecting the signal/noise power ratio at the detector input.

The linear filter matched to any given signal-element, $s_0 h_t(t)$ where s_0 carries the symbol value and where $h_t(t)$ is nonzero only over the time interval 0 to T seconds, has an impulse response

$$g(t) = c h_t(T - t) \qquad 2.1.21$$

where c is any real constant. The transfer function of the linear filter is

$$G(f) = c[\exp(-j2\pi fT) H_t^*(f)] \qquad 2.1.22$$

where $H_t(f)$ is the Fourier transform of $h_t(t)$ and $H_t^*(f)$ is the complex conjugate of the $H_t(f)$. $h_t(t)$ is here taken to be the impulse response of the transmitter filter in Fig. 2.1, so that $s_0 h_t(t)$ is the received signal waveform at the input to the receiver filter, corresponding to an individual signal-element received in the absence of noise. When the signal element $s_0 h_t(t)$ is received in the presence of AWGN, the matched filter maximizes the output signal/noise power ratio at the time instant $t = T$, as

shown in Appendix A1. The received element value is detected by sampling the output signal from the matched filter at the time $t = T$ seconds, and comparing the sample value with the appropriate threshold levels.

The term $\exp(-j2\pi fT)$ in Eqn. 2.1.22 is the Fourier transform of a delay of T seconds. This delay can be neglected without affecting the significant points in the present discussion. Thus the transfer function of the matched filter can be taken to be

$$G(f) = cH_t^*(f) \qquad 2.1.23$$

and the received element value is detected here by sampling the output signal from the matched filter at the time instant $t = 0$. This is a non-physical system, (i.e., not physically realisable), but it can always be made physically realisable again by re-introducing the appropriate delay of T seconds.

From Eqn. 2.1.23

$$|G(f)| = b|H_t(f)| \qquad 2.1.24$$

Where $b = |c|$. If the matched filter is now used for the received filter in Fig. 2.1, $H_r(f) = G(f)$ so that Eqn. 2.1.20 is satisfied and the signal/noise power ratio at the output of the filter is maximized. Under these conditions,

$$H_r(f) = cH_t^*(f) \qquad 2.1.25$$

and

$$H(f) = cH_t(f)H_t^*(f) \qquad 2.1.26$$

so that $H(f)$ is real and even (symmetrical about zero frequency), and the impulse response $h(t)$ of the baseband channel is symmetrical about its central point. It can be seen from Eqn. 2.1.4 that if $H(f)$ is real and even, and if the receiver filter is matched to the received signal and so satisfies Eqn. 2.1.25, then the receiver filter also satisfies Eqn. 2.1.20 and so maximizes the signal/noise power ratio at the detector input. However, Eqn. 2.1.20 can be satisfied for any value of $H(f)$, which means that $H(f)$ need not to be real or even. When Eqn. 2.1.20 is satisfied and $H(f)$ is not real or even, Eqn. 2.1.25 cannot be satisfied, so that the receiver filter cannot now be matched to the received signal.

It is clear from the preceding discussion that when $H_t(f)$ and $H_r(f)$ satisfy Eqn. 2.1.20, $H_r(f)$ is not necessarily the complex conjugate of $H_t(f)$, so that the receiver filter is not necessarily matched to the received signal. However, when it is

matched, Eqn. 2.1.20 is necessarily satisfied, so that the matched filter is a particular case for which Eqn. 2.1.20 is satisfied.

An important case for which Eqn. 2.1.20 is satisfied is that where

$$H_r(f) = cH_t(f) \qquad 2.1.27$$

where c is any positive or negative real constant and $H_t(f)H_r(f) = H(f)$. The arrangement satisfying Eqn. 2.1.27 is more general than the case where $H_r(f) = cH_t^*(f)$, since Eqn. 2.1.27 can be satisfied for any value of $H(f)$. Furthermore, in the frequently occurring case where $H(f)$ is real, non-negative and even, and Eqn. 2.1.27 is satisfied, both $H_t(f)$ and $H_r(f)$ are real, non-negative and even, and $H_r(f) = cH_t^*(f)$ with c positive, so that the receiver filter is now matched to the received signal. Thus the condition given by Eqn. 2.1.27 ensures that the receiver filter is matched to the received signal, whenever $H(f)$ is real, non-negative and even.

2.1.2 Model of the data-transmission system [1]

Since the constant b in Eqn. 2.1.13 and 2.1.20 may be taken to have any positive real value without affecting the signal/noise power ratio at the detector input, it is convenient to set $b = 1$. Under these conditions, the signal/noise power ratio at the detector input is then maximum when

$$|H_r(f)| = |H_t(f)| \qquad 2.1.28$$

It will in fact be assumed that

$$H_r(f) = \pm H_t(f) \qquad 2.1.29$$

As before, $H_t(f)H_r(f) = H(f)$. Under these conditions,

$$\int_{-\infty}^{\infty} |H_t(f)|^2 df = \int_{-\infty}^{\infty} |H_r(f)|^2 df = \int_{-\infty}^{\infty} |H(f)| df = k \qquad 2.1.30$$

as can be seen from Eqn. 2.1.5.

The signal/noise power ratio at the input to the detector is now

$$\frac{F}{N} = \frac{E}{\frac{1}{2} N_0} \int_{-\infty}^{\infty} |H(f)|^2 df \qquad 2.1.31$$

as can be seen from Eqns. 2.1.14 and 2.1.30. From Eqn. 2.1.3, the average transmitted energy per signal element, at the input to the transmission path, is

$$E = \overline{s_i^2} \qquad 2.1.32$$

and, from Eqn. 2.1.11, the Gaussian noise waveform $v(t)$ at the output of the baseband channel has, at any time, zero mean and variance

$$N = \tfrac{1}{2} N_0 \int_{-\infty}^{\infty} |H_r(f)|^2 \, df \qquad 2.1.33a$$

$$= \tfrac{1}{2} N_0 \int_{-\infty}^{\infty} |H(f)| df \qquad 2.1.33b$$

The data-transmission system is now as shown in Fig. 2.2, which is a particular arrangement of Fig. 2.1, with $H_r(f) = \pm H_t(f)$. Clearly, $\pm H_t^2(f) = H(f)$. A sampler is included at the input to the detector. The received waveform $r(t)$ is sampled at the time instants $\{iT\}$, for all integer values of i, and the resulting sample values $\{r(iT)\}$ are fed to the detector.

The regular sequence of impulses, at the input to the baseband channel are antipodal signal elements being statistically independent and equally likely to have either of the two possible values.

The average energy per signal element at the input to the transmission path is $\overline{s_i^2}$. The transmission path introduces no signal distortion, attenuation or delay. White Gaussian noise with zero mean and a two-sided power spectral density of $\tfrac{1}{2} N_0$ is added to the data signal at the output of the transmission path. The baseband channel has a transfer function $H(f)$ and an impulse response $h(t)$. The noise waveform $v(t)$ at the output of the baseband channel is a sample function of a Gaussian random process with zero mean and variance N (Eqn. 2.1.33). Thus the received waveform at the output of the baseband channel is

$$r(t) = \sum_i s_i h(t - iT) + v(t) \qquad 2.1.34$$

$r(t)$ is sampled once per symbol, and the detector operates entirely on sample values $\{r(iT)\}$ to give the detected element values $\{\hat{s}_i\}$. The presence of the noise components in the $\{r(iT)\}$ will of course, result in occasional errors in the $\{\hat{s}_i\}$.

2.2 Baseband signal waveform shaping

Having determined the best way of sharing the linear filtering of the signal between the transmitter and receiver filters, when the transmission path introduces no signal distortion, it is necessary now to study the effect of the overall transfer function $H(f)$, of the transmitter and receiver filters, on the tolerance of the data-transmission system to white Gaussian noise.

In Fig. 2.2, $H(f)$ is the transfer function of the baseband channel. The spectrum (Fourier transform) of the individual received signal-element at the output of the baseband channel, resulting from the signal-element $s_i\delta(t)$ at the input to the baseband channel, is $s_iH(f)$. The term "signal spectrum" is taken to mean the spectrum of this individual signal-element. In describing the shape of the signal spectrum $s_iH(f)$, it is assumed that $s_i = 1$, so that the signal spectrum is equated to the transfer function $H(f)$, of the baseband channel.

2.2.1 Rectangular spectrum

By considering the receiver and transmitter filters in Fig. 2.2 which give a rectangular spectrum for an individual received signal-element at the output of the receiver filter. The transfer function of the baseband channel is now

$$H(f) = \begin{cases} T & , \quad -\dfrac{1}{2T} < f < \dfrac{1}{2T} \\ 0 & , \quad \text{elsewhere} \end{cases} \qquad 2.2.1$$

as shown in Fig. 2.3a. The impulse response of it is shown in Appendix 2.1 to be

$$h(t) = \frac{\sin(\pi t/T)}{\pi t/T} \qquad 2.2.2$$

as shown in Fig. 2.3b. These signal-elements, when spaced (delayed) relative to each other at time intervals which are multiples of T seconds, will cause zero ISI if sampled at the central positive peaks. Hence this is the signal-element rate for Nyquist-rate transmission.

Since $h(t) \neq 0$ for $t < 0$, $h(t)$ is not physically realisable, if a large delay of τ seconds is included in the filter characteristics without otherwise changing them, so that $h(t) \approx 0$ for $t < 0$, the filter then becomes physically realisable, for practical purposes, and has an impulse response approximately equal to $h(t-\tau)$, as shown in Fig. 2.3c. The error caused in $h(t-\tau)$ by setting this accurately to zero for $t < 0$, is negligible so long as $\tau >> T$, and under these conditions a practical filter can be made to approximate closely to the theoretical ideal, the approximation getting better

as τ increases. Of course, for the practical filter to have an impulse response exactly equal to $h(t-\tau)$, it is necessary that τ tends to infinity.

There are practical difficulties with this particular waveshape, however:

- The baseband channel has the characteristics of an ideal lowpass filter which is very difficult to approximate in practice because of the sharp cut-off in its frequency response at $(1/2T)$ Hz.

- This signal element rate requires extremely precise synchronization. If the timing at the receiver varies somewhat from exact synchronization, the zero ISI condition disappears. In fact, under certain signal sequences, the tails of adjacent pulses may add up as a divergent series, causing possible errors. Since some timing jitter is inevitable with most synchronization systems, this signal-element rate is obviously not the one to use.

2.2.2 Spectrum with sinusoidal roll-off

The difficulties of using a rectangular spectrum may be greatly overcome by smoothing the abrupt change in $H(f)$ at $f = \pm 1/2T$. In general, for a given bandwidth, the more smooth $H(f)$ varies with f, over the whole range of values of f for which $H(f) \neq 0$, the shorter the effective duration of $h(t)$ [1].

Nyquist's vestigial-symmetry theorem states that if $H(f)$ is real and has odd symmetry about the nominal cut-off frequencies $\pm 1/2T$ Hz, then the corresponding impulse-response $h(t)$ is an even time function, and $h(iT) = 0$ for all non zero integer values of i [4]. Under these conditions, it is possible to transmit data at $1/T$ elements per second without ISI.

The class of signal spectra most often used is that where $H(f)$ is real and has a sinusoidal roll-off centred at $\pm 1/2T$ Hz, as shown in Fig. 2.4a.

The transfer function of the baseband channel is now

$$H(f) = \begin{cases} T & 0 \le |f| < \dfrac{(1-\alpha)}{2T} \\ \dfrac{T}{2}\left[1 - \sin\dfrac{\pi T}{\alpha}\left(|f| - \dfrac{1}{2T}\right)\right] & \dfrac{(1-\alpha)}{2T} \le |f| \le \dfrac{(1+\alpha)}{2T} \\ 0 & \text{elsewhere} \end{cases} \qquad 2.2.3$$

where α is called the roll-off factor. For $\alpha = 0$, it becomes the rectangular spectrum previously described. When $\alpha = 1$, the spectrum has the shape of an one cycle of a cosine wave, between adjacent negative peaks, the latter being raised to zero. It is often known as a "raised-cosine" spectrum.

The time response $h(t)$, that is, the inverse Fourier Transfer function, of Eqn. 2.2.3 is shown in Appendix A2.2 to be

$$h(t) = \frac{\sin(\pi t/T)}{\pi t/T} \quad \frac{\cos(\alpha\pi t/T)}{1-4\alpha^2 t^2/T^2} \qquad 2.2.4$$

This function consists of products of two factors : the factor $[\sin(\pi/T)]/[(\pi/T)]$ associated with the ideal lowpass filter, and a second factor that decreases at $1/|t|^2$ for large $|t|$. The first factor ensures zero crossing of $h(t)$ at the desired sampling instants of time, $t = iT$ with i an integer. The second factor reduces the tails of the signal-element considerably below that obtained from the ideal lowpass filter, so that the pulse is relatively insensitive to sampling timing errors. In fact, the amount of ISI resulting from this timing error decreases as the roll-off factor α is increased from zero to one. Figures 2.4a and 2.4b show the spectral characteristics $H(f)$ and the impulse responses $h(t)$ for several values of α respectively. Since $h(t) \neq 0$ for $t < 0$, $h(t)$ is also not physically realisable. However, as said before, a delay of τ seconds can be included in the filter characteristics to make it physically realisable.

In this thesis, all the transmission systems are optimized by sharing the lowpass filtering equally between the transmitter and receiver filters and with a 100%, 40% or 25% sinusoidal roll-off frequency response, in order to find the best wave shape for data transmission over satellite links.

2.2.3 Probability of error performance of the data-transmission system in an AWGN environment

The data-transmission system in Fig. 2.2 is assumed, with $H_r(f) = \pm H_t(f)$ and $|H_t(f)|^2 = H(f)$. The baseband channel transfer function, $H(f)$, has a sinusoidal rolloff frequency response, as given by Eqn. 2.2.3. White Gaussian noise with zero mean and a two-sided power spectral density of $\frac{1}{2}N_0$ is added to the data signal at the output of the transmission path. The signal at the output of the baseband channel is a continuous waveform

$$r(t) = \sum_i s_i h(t - iT) + v(t) \qquad 2.2.5$$

where $h(t)$ is given by Eqn. 2.2.4. It can be seen from Eqn. 2.2.4 that $h(0) = 1$ and $h(iT) = 0$ for all values of the integer i other than $i = 0$. Thus the i th received signal-element, $s_i h(t - iT)$ may be detected from the sample value of the received waveform $r(t)$, at the time instant $t = iT$. The sample value is

$$r(iT) = s_i + v(iT) \qquad 2.2.6$$

This may be written more simply as

$$r_i = s_i + v_i \qquad 2.2.7$$

where $r_i = r(iT)$ and $v_i = v(iT)$.

It is assumed that $s_i = \pm k$. The detection process that minimizes the probability of error in the detection of s_i from r_i, under the assumed conditions, selects the possible value of s_i closest to r_i. This is achieved by comparing r_i with the decision threshold of zero. When $r_i < 0$, s_i is detected as $-k$, and when $r_i > 0$, s_i is detected as k.

An error occurs in the detection of s_i whenever the noise component v_i carries r_i onto the opposite side of the decision threshold with respect to the transmitted s_i. Since v_i is a sample value of a Gaussian random variable with zero mean and variance N (Eqn. 2.1.33), the probability of an error in the detection of s_i, when $-k$ is received and r_i is wrongly detected is

$$P_{e1} = \int_{k}^{\infty} \frac{1}{\sqrt{2N\pi}} \exp(\frac{-v^2}{2N}) dv = \int_{k/\sqrt{N}}^{\infty} \frac{1}{\sqrt{2\pi}} \exp(\frac{-v^2}{2}) dv$$

$$= Q(\frac{k}{\sqrt{N}}) \qquad 2.2.8$$

when $+k$ is received and r_i is wrongly detected, the probability of an error in the detection of s_i is

$$P_{e2} = \int_{-\infty}^{-k} \frac{1}{\sqrt{2N\pi}} \exp(\frac{-v^2}{2N}) dv = \int_{-\infty}^{-k/\sqrt{N}} \frac{1}{\sqrt{2\pi}} \exp(\frac{-v^2}{2}) dv$$

$$= Q(\frac{k}{\sqrt{N}}) \qquad 2.2.9$$

where $$Q(y) = \int_{y}^{\infty} \frac{1}{\sqrt{2\pi}} \exp(-\frac{v^2}{2}) dv$$

The integral giving $Q(y)$ cannot be evaluated directly, but $Q(y)$ has been tabulated for positive real values of y.

P_{e1} and P_{e2} are conditional probabilities with P_{e1} assuming that $-k$ was transmitted and P_{e2} assuming that k was transmitted. Thus assuming the

equiprobable case of $\pm k$, the average probability of error P_e in the receiver is given by

$$P_e = \tfrac{1}{2} P_{e1} + \tfrac{1}{2} P_{e2}$$

$$= Q(\frac{k}{\sqrt{N}}) = Q(\sqrt{\frac{k^2}{N}}) \qquad 2.2.10$$

where k is the peak voltage at time $t = iT$ and N is the noise variance.

2.2.4 Bit-energy-to-noise power spectral density ratio

Appendix A1 shows for systems in which only one signal-element (ISI free) is transmitted, the matched-filter detector is the optimum detector for the received signal-element, and the error-rate performance depends on the ratio of the received signal energy to the white Gaussian noise power spectral density at the filter input. (Note that, for a matched filter, the variance of a noise sample at the output of the filter is equal numerically to the two-sided power spectral density at the input). For this reason, the bit-energy-to-noise power spectral density ratio, $2E_b/N_0$, is frequently used in digital communication systems to enable a comparison of systems having variable transmission rates and of the performance of various modulations and coded systems in a complex interference environment. Here E_b is the energy per bit at the input to the receiver and $\frac{1}{2} N_0$ is the white Gaussian two-sided noise power spectral density measured at the same point.

Equation 2.2.10 shows, under the assumed conditions, that the error-rate performance depends on the peak voltage to average noise ratio or the peak power to the noise variance ratio, at time $t = iT$. Now it is to determine the bit-energy-to-noise spectral power density ratio, $2E_b/N_0$, at the receiver input, under the same assumed conditions.

From Eqn. 2.1.3, the average energy per signal-element at the input to the transmission path is

$$E = \overline{s_i^2} \int_{-\infty}^{\infty} |H_t(f)|^2 \, df$$

Since a binary antipodal signal, $s_i = \pm k$, is assumed, and the bit energy E_b ($= E$ in this case), can be written as

$$E_b = k^2 \int_{-\infty}^{\infty} |H_t(f)|^2 \, df \qquad 2.2.11$$

From Eqn. 2.1.33a, the average power (mean-square value) of the noise waveform at the detector input (or receiver filter output) is

$$N = \tfrac{1}{2} N_0 \int_{-\infty}^{\infty} |H_r(f)|^2 \, df$$

therefore the two-sided power spectral density of the AWGN, in terms of the noise variance N and the receiver filter transfer function $H_r(f)$, can be written as

$$\tfrac{1}{2} N_0 = \frac{N}{\int_{-\infty}^{\infty} |H_r(f)|^2 \, df} \qquad 2.2.12$$

From Eqn. 2.2.11 and 2.2.12, the ratio of the transmitted-bit-energy to noise-power-spectral-density, at the receiver input, is

$$\frac{E_b}{\tfrac{1}{2} N_0} = \frac{k^2 \int_{-\infty}^{\infty} |H_t(f)|^2 \, df \int_{-\infty}^{\infty} |H_r(f)|^2 \, df}{N}$$

$$= \frac{k^2 \int_{-\infty}^{\infty} |H(f)| \, df \int_{-\infty}^{\infty} |H(f)| \, df}{N} \qquad 2.2.13$$

as can be seen from Eqn. 2.1.30.

$H(f)$ has a sinusoidal roll-off spectrum, as given by Eqn. 2.2.3 so $\int_{-\infty}^{\infty} |H(f)| df = 1$, and Equation 2.2.13 can be simplified to

$$\frac{2E_b}{N_0} = \left(\frac{k^2}{N}\right) = \left(\frac{k}{\sqrt{N}}\right)^2 \qquad 2.2.14$$

It can be seen that, under the assumed conditions, i.e., $H_r(f) = H_t(f)$ and $|H_r(f)|^2 = |H_t(f)|^2 = |H(f)|$ with $H(f)$ a sinusoidal roll-off frequency response, the bit-energy-to-noise power spectral density ratio at the receiver input is equal to the square of the peak voltage to noise variance at the detector input. Using Eqn. 2.2.14, Eqn. 2.2.10 can be rewritten, in terms of $2E_b/N_0$, as

$$P_e = Q(\sqrt{\frac{2E_b}{N_0}}) \qquad 2.2.15$$

This is also the error-rate performance of a matched-filter detector which depends upon the value of $2E_b/N_0$ at the input of the filter, as shown in Appendix A1. The matched-filter detector is only optimum for single-shot transmission, whereas the present arrangement is optimum for even a sequence of signal-element transmissions. Note that the bit energy E_b is in Joules and the noise power spectral density $\frac{1}{2}N_0$ is in Watts per Hz, so that the ratio $2E_b/N_0$ is dimensionless.

2.3 Data-transmission system for satellite links

The simplest way to achieve multiple access at a satellite is to give different users different transponders. The trouble with this approach is that the transponders are of fixed capacity, whereas many users want a variable channel assignment. Furthermore, the transponder capacity is much too big for many users. Even when a corporation leases a whole transponder, it still has a demand assignment problem in using that transponder. Some means are needed for geographically dispersed users to share a transponder [5].

When each of many earth stations has access to the same transponder, the bandwidth of that transponder may be shared by frequency-division multiple access or time-division multiple access. These are referred to as FDMA and TDMA, respectively [5].

With FDMA, the transponder bandwidth is divided into smaller bandwidths. An earth station transmits on one or more of these frequency bands [5]. This frequency allocation makes sure that no two earth stations transmit on the same frequency band at the same time. A frequency band can be reallocated from one earth station to another as the demand for channels varies [5].

With TDMA, each earth station is allowed to transmit a high-speed burst of bits for a brief period of time. The times of the bursts are carefully controlled so that no two bursts overlap. For the period of its burst, the earth station has the entire transponder bandwidth available to it [5].

TDMA offers a number of advantages over the FDMA systems which have dominated the first generation of multiple-access satellite communication systems. Perhaps its most significant advantage is the presence of only one carrier at a time in the satellite transponder. FDMA requires simultaneous transmission of a multiplicity of carriers through a common TWTA in the satellite. It is well known that TWTAs are highly nonlinear and the intermodulation products produced by the presence of multiple carriers generate interference which degrades the individual channel

performance if left uncorrected. To avoid this, it is common practice in FDMA systems to back-off the TWTA operating point from maximum power output, consequently forcing a reduction in the amount of traffic capacity that can be realized in that TWTA. With TDMA, since only one carrier appears at a time, the intermodulation distortion is eliminated and the resulting capacity reduction due to TWTA nonlinearity is significantly reduced.

A second important advantage is the use of the time domain rather than frequency domain to achieve selectivity. In an FDMA system, an earth station must transmit and receive on a multiplicity of frequencies to achieve a desired traffic plan and must accordingly provide a large number of frequency-selective up-conversion and down-conversion chains. In a TDMA system, the needed selectivity is accomplished in time rather than frequency.

TDMA is also ideally suited to digital communications since digital signals are naturally matched to the storage, rate conversions, and time-domain processing operations used in TDMA terminal implementation. For the same reasons TDMA is ideal for accomplishing satellite on-board processing [6]. An TDMA system is assumed in this thesis.

2.3.1 Satellite earth station configuration

A typical satellite earth station configuration is shown in Fig. 2.5. Three independent channels are shown. However, note that the number of channels in an earth station may vary from one to several thousand. The filters F11, F12 and F13 bandlimit the modulated signals S_1, S_2, and S_3, respectively. Usually, for common output frequency modems, the first intermediate frequency (IF) f_{IF} may be specified to be the same for all channels [6].

The upconverters (U/Cs) translate the modulated, bandlimited signal to the desired transmitted radio frequencies. The filters F21, F22, and F23 select the required sidebands of the upconverted signals. The center frequencies of these bandpass filters are at $f_c + \Delta f + f_{IF}$, $f_c + f_{IF}$, and $f_c - \Delta f + f_{IF}$ or at $f_c + \Delta f - f_{IF}$, $f_c - f_{IF}$, and $f_c - \Delta f - f_{IF}$, depending on whether the upper or the lower sidebands of the modulated and upconverted signals are used. To obtain a high power efficiency, most transmitter high power amplifiers (HPAs) have to operate in a nonlinear mode. This mode of operation spreads the spectrum of the modulated bandlimited signal. Therefore the filters F31, F32, and F33, having the same centre frequencies as the filters F21, F22, and F23, respectively, are used to prevent spectral spillover into the adjacent channels, i.e., to suppress ACI (adjacent channel interference). Greater ACI suppression is provided by the baseband filtering at both transmitter and receiver.

The sum of the modulated signals is received and amplified by the satellite receiver antenna. They are filtered and amplified by a low-noise amplifier. A frequency translation is required to prevent, in-band interference from the high-power satellite output to the satellite input. If the satellite transponder is not equipped with a frequency translator, then a tremendously high isolation (in the range 100 to 150 dB) between the output and input would be required (practical radio-frequency systems do not even approach this requirement). The signals are then further amplified by a TWTA. The satellite input and output filters F3 and F4 have a bandwidth wide enough to accommodate the overall spectrum of the signal. These two filters are used to bandlimit the signal, and thereby reduce the unwanted out-of-band noise and spectral spreading caused by the TWTA.

The filters F41, F42 and F43 in the receiver earth station prevent excessive ACI; that is, they prevent the overloading of the downconverters, which translate the desired radio channels to common IF frequencies before the signals are demodulated. The filters F51, F52 and F53 preceding the demodulator, having a common centre frequency f_{IF}, are used to select the respective downconverted signals.

The heart of the satellite channel is the modulator and the demodulator (i.e., modem). The modulation techniques employed, the filtering strategy and demodulation method have a major impact on the performance of the system. Spectral efficiency, required power, antenna size, and overall performance are significantly influenced by the performance of the modem in both linear and nonlinear channel environments.

2.3.2 Basic assumptions on the configuration of the satellite channel

- For many applications where the radio-carrier frequency f_c is much higher than the data bit rate ($f_c / f_b > 10^5$, where f_b is the data bit rate), it is very difficult to design spectrally efficient and temperature-stable radio frequency filters. For example, in a 1.4 GHz uplink using a 64 Kbit/s QPSK signal, the filter F31 (Fig. 2.5) requires a center frequency of 1.4 GHz and a two-sided bandwidth of 32 KHz. Because of the complexity of this filter design, many satellite earth station do not utilize spectral shaping filters after the HPA. Thus the restored signal spectra created by the nonlinear amplifier causes interference in the adjacent satellite channels.

-The TWTA operating point is backed-off from maximum power output, i.e., to operate the satellite transponder in a more linear mode. F3 and F4 (Fig. 2.5) are wideband filters when compared with the filters F51, F52 and F53, so, they have insignificant effects on the signals. In most satellite systems, the value of $2E_b/N_0$ in the uplink is normally made much higher than that in the downlink. Hence it can be assumed that, for the uplink, $2E_b/N_0 = \infty$. This is equivalent to bypassing the

satellite transponder and adding the noise only at the input of the receiver at the earth station.

- At the receiver, the filters F41, F42 and F43 are used to prevent the overloading of the downconverters (D/Cs). These are also radio-frequency filters and so cannot be narrow band. In order not to introduce distortion into the signal, they should have a linear phase characteristic over the corresponding signal spectra.

- The filters F21, F22 and F23 are used to select the required sideband of the upconverted signals so that they can be made wideband with a linear phase characteristic over the corresponding signal spectra.

Hence, the basic assumptions of the satellite channel can be summarised as follows:

1) Post HPA filtering is not used.
2) The filters and TWTA in the satellite do not cause any amplitude or phase distortion in the signal.
3) $2E_b/N_0$ for the uplink is made much higher than that for the downlink.
4) The radio-frequency filters at the receiver of the earth station do not cause any amplitude or phase distortion in the signal.
5) The filters F21, F22 and F23 do not cause any amplitude or phase distortion in the signal.

Based on these assumptions, the satellite earth station configuration can be simplified as shown in Fig. 2.6, where the post HPA filters, the satellite transponder, and the radio-frequency filters F41, F42 and F43 have been removed.

Since the filters F21, F22 and F23 are assumed to be memoryless, this configuration can be further simplified by considering the linear upconverters, the HPAs and the linear downconverters, as a transmission path in an intermediate frequency band. The resultant configuration is shown in Fig. 2.7, where the upconverters, the downconverters and the filters F21, F22 and F23 are removed. The channels are still separated with a channel spacing of f_{cs} Hz. The IF filters F11 and F51, F12 and F52, and F13 and F53 still have the same characteristics, but are centered at $f_{IF} + f_{cs}$, f_{IF}, and $f_{IF} - f_{cs}$ Hz, respectively.

2.4 Filter configurations for computer simulation

2.4.1 Digital modulation and demodulation filters

Since the transmission system can be optimized by sharing the filtering equally between the transmitter and receiver filters and with a resultant sinusoidal roll-off amplitude response, the modulation and demodulation filters of the satellite system are designed to have the same characteristics and with an overall frequency response

having a sinusoidal roll-off. In order to find the best baseband wave shape for data transmission over satellite links, the sinusoidal roll-off of 100%, 40% and 25% (i.e., $\alpha = 100\%$, 40% and 25% respectively, in Eqn. 2.2.3) are used for investigations. The modulation and demodulation filters have to be digital, since it is difficult to design an analog filter which has the wanted frequency response. Provided that their finite sampled impulse responses are long enough and the quantization error is negligible, they can have frequency responses of any desired shapes. So in all the transmission systems described in this thesis, the modulation filter is a pair of digital baseband filters which determine the characteristics of the modulating signal, with the demodulation filter at the receiver also a pair of digital baseband filters which achieve the matched filtering of the baseband demodulation signal.

The finite sampled impulse responses of the transmitter and receiver filters are designed using IDFT (Inverse Discrete Fourier Transform) to derive the impulse response tap gains for the desired frequency and phase characteristics in frequency domain, as shown in Table 2.1 and plotted in Fig. 2.8. A truncation length of $12T$ has been made and sampling rate of $8/T$ samples per second has been used, where $1/T$ is the signal element-rate. A delay of $6T$ seconds is introduced to make the filters realisable for computer simulation.

In practice, a digital-to-analog (D/A) conversion process is used to obtain the required shape of the analog baseband modulating signal. This will introduce a $[\sin(x)/x]$ amplitude characteristic on the frequency response. Thus an $[x/\sin(x)]$ amplitude characteristic might be required for compensation. However if the sampling rate is several (say 4) times greater than the bandwidth of the signal, the $[\sin(x)/x]$effect is insignificant and so is neglected in the filter design described in this thesis.

2.4.2 IF bandpass filters F_{IF}

In satellite communication systems, the IF frequency (e.g. 70 MHz) is usually too high to use digital IF filters, so the IF bandpass filters have to be analog. The IF bandpass filters used in the project have the characteristics of a real surface acoustic wave (SAW) bandpass filter (Andersen No. BP-70-400-2.5-107A) centered at the frequency of 70 MHz with a 3 dB bandwidth of 625 KHz. The filters have a symmetrical amplitude response (characteristic) as shown in Fig. 2.9a, and an asymmetrical linear phase characteristic over the bandwidth. They have the baseband equivalent model which can easily be obtained by shifting the center frequency to zero frequency, as it is shown in Appendix A4. Since the phase characteristic is linear, without loss of generality, it can be set to zero across the bandwidth; this means that the impulse response will be symmetrical at time $t = 0$ and a delay must

be re-introduced in the impulse response in order to make the filter physically realizable for computer simulation. The sampled impulse response of the filter is obtained, using the inverse DFT (IDFT) on the equivalent baseband amplitude response, as shown in Table 2.2 and Fig. 2.9b, where the sampling rate of $8/T$ samples per second has been used. A truncation length of $6T$ is used to approximate to the ideal impulse responses of the IF filters in all the simulation tests, so that a delay of $3T$ seconds is re-introduced to make the filters realizable. It can be seen that the sampled impulse response shown in Table 2.2 contains only real values. This is because the filter has a symmetrical amplitude characteristic and an asymmetrical phase characteristic around the center frequency, and under these conditions, the filter does not introduce any quadrature crosstalk in the signal (Appendix A5).

2.4.3 Post D/A conversion filters

In practice, the analog baseband signal is obtained by means of a D/A conversion process, so an extra pair of analog post D/A conversion lowpass filters has to be used to reject spurious signals around multiples of the digital sampling frequency. These filters should have a linear phase characteristic over the wanted signal bandwidth. If the cutoff frequency is too low, unwanted ISI will occur. For a sampling rate of $8/T$ samples per second, an acceptable cutoff frequency may be $4/T$ [7]. Since these are wideband filters which do not have any significant effect on the wanted signal, they are not included in the baseband equivalent models of the transmission systems described in this thesis.

2.4.4 Pre A/D conversion filters

The digital baseband signal, at the input of the demodulation filter in the receiver, is obtained by means of A/D (analog-to-digital) conversion process, so that an extra pair of analog pre A/D conversion filter lowpass filters has to be used to remove any unwanted spectral components generated in the demodulation process. These filters should also have a linear phase characteristic over the wanted signal bandwidth. They are wideband filters which do not have any significant effect on the wanted signal, so they are not included in the baseband equivalent models of the transmission systems described in this thesis.

2.5 Nonlinearity

2.5.1 Introduction

In a satellite communication system, the modulated signal passes through the high power amplifier (HPA) in the earth station prior to transmission to the satellite

and through the travelling wave tube amplifier (TWTA) prior to retransmission back to an earth station. Typical input/output power and phase characteristics of an HPA and TWTA are shown in Fig. 2.10. It can be seen that the HPA or TWTA introduces nonlinear AM-AM and AM-PM conversion effects. For a low input level, the output power from either device is essentially a linear function of the input power. As the input drive increases, the output power increases nonlinearly until a point is reached at which any additional input level increase results in a decreasing output power. This point of maximum output is referred to as saturation. The operating point of an HPA (or TWTA) is usually given in terms of the input or output backoff below saturation, that is, the input or output power in decibels relative to the level at saturation.

In general, a transponder will carry a single wideband modulation (in TDMA systems) or a number of narrowband carriers (in FDMA systems) spaced in frequency over the transponder bandwidth. Once the signal level approaches the amplifier saturation region, it will cause the following effects: [5], [6], [18]

1) For a multicarrier signal, intermodulation occurs. Signals will be suppressed and there will be disproportionate power sharing.
2) For a single bandlimited signal, any envelope fluctuation will cause unwanted phase modulation and spectral spreading.

To maximize the available power of the TWTA, it is desirable to have a high input level. However, effect (1) explains why, in FDMA systems, the satellite TWTA is well backed off to avoid intermodulation effects.

Due to the presence of the HPA and TWTA, many theoretical results are presently available which describe the performance of PSK transmission over a nonlinear satellite channel [9] [10]. Several results have been calculated to show the performance of a phase-keying system through a purely amplitude limiting channel [13], [14], [15]. But the assumption, though greatly simplifying the analysis, does not include the AM-PM conversion effect, which can significantly influence the communication system's performance when angle-modulated signals are employed.

2.5.2 Modelling of HPA for computer simulation

In recent years a considerable effort [13], [15], [16] has been made in attempting to develop analytic expressions that characterise the HPA and TWTA. One technique, as originated by Kaye et al [17], entails determining approximations for the envelope nonlinearities in a quadrature model for the HPA (or TWTA), and is now developed [16] (Fig. 2.11a).

An input signal

$$S(t) = \sqrt{2}a(t)\cos\omega_c t - \sqrt{2}b(t)\sin\omega_c t \qquad 2.5.1$$

where ω_c is the carrier frequency in rad/s, can be written as

$$S(t) = B(t)\cos[\omega_c t + \theta(t)] \qquad 2.5.2$$

where $$B(t) = \{2[a^2(t) + b^2(t)]\}^{1/2} \qquad 2.5.3$$

and $$\theta(t) = \tan^{-1}\left[b(t)/a(t)\right] \qquad 2.5.4$$

So that $$\sqrt{2}a(t) = B(t)\cos\theta(t) \qquad 2.5.5a$$

and $$\sqrt{2}b(t) = B(t)\sin\theta(t) \qquad 2.5.5b$$

The HPA output signal is given by

$$Z(t) = G_p(B)B(t)\cos[\omega_c t + \theta(t)] - G_q(B)B(t)\sin[\omega_c t + \theta(t)] \qquad 2.5.6$$

$$= \left|G(B)\right|B(t)\cos[\omega_c t + \theta(t) + g(B)] \qquad 2.5.7$$

where $$\left|G(B)\right| = \{[G_p(B)]^2 + [G_q(B)]^2\}^{1/2} \qquad 2.5.8$$

and $$g(B) = \tan^{-1}\left[G_q(B)/G_p(B)\right] \qquad 2.5.9$$

with B the input signal envelope, i.e., short-hand notation for $B(t)$ given by Eqn. 2.5.3. Here $\left|G(B)\right|$ and $g(B)$ are the AM-AM and AM-PM conversion functions, respectively, of the HPA for an input signal with an envelope B. If the input signal has a constant envelope, i.e., $B(t)$ in Eqn. 2.5.3 is constant, then $\left|G(B)\right|$ and $g(B)$ in Eqns. 2.5.8 and 2.5.9, respectively, remain constant all the time. Hence, it can be seen in Eqn. 2.5.7 that the HPA will have no nonlinear distortion effect on the signal $Z(t)$.

Equation 2.5.6 can be written as

$$Z(t) = [B(t)\cos\theta(t)G_p(B) - B(t)\sin\theta(t)G_q(B)]\cos\omega_c t$$

$$-[B(t)\sin\theta(t)G_p(B) + B(t)\cos\theta(t)G_q(B)]\sin\omega_c t \qquad 2.5.10$$

$$= \sqrt{2}[a(t)G_p(B) - b(t)G_q(B)]\cos\omega_c t$$

$$-\sqrt{2}[b(t)G_p(B)+a(t)G_q(B)]\sin\omega_c t \qquad 2..5.11$$

as can be seen from Eqn. 2.5.5.

The equivalent baseband signals of $S(t)$ and $Z(t)$, in Eqns. 2.5.1 and 2.5.11 can be represented (Appendix A6) as the complex-valued signals

$$s(t) = a(t) + jb(t) \qquad 2.5.12$$

$$\text{and} \quad z(t) = [a(t)G_p(A) - b(t)G_q(A)] + j[b(t)G_p(A) + a(t)G_q(A)] \qquad 2..5.13$$

respectively, where $j = \sqrt{-1}$, A is now the envelope of the equivalent baseband signal $s(t)$, i.e., short-hand notation for $A(t)$ given by

$$A(t) = [a^2(t) + b^2(t)]^{1/2} \qquad 2.5.14$$

and the conversion functions $G_p(A)$ and $G_q(A)$ are now dependent on the signal envelope A, instead of B (the envelope of the radio-frequency signal). Equation 2.5.13 can be written as

$$z(t) = [a(t) + jb(t)][G_p(A) + jG_q(A)] \qquad 2.5.15$$

$$= s(t)G(A) \qquad 2.5.16$$

$$\text{where} \qquad G(A) = G_p(A) + jG_q(A) \qquad 2.5.17$$

and $s(t)$ and $G(A)$ have complex values. The baseband equivalent model of the HPA is shown in Fig. 2.11b, where the HPA is represented by the conversion function $G(A)$. Since the value of $G(A)$ is dependent on the input signal envelope $A(t)$, it can be varied by multiplying $A(t)$ by a constant factor M_c to give the envelope (Eqn. 2.5.14)

$$\hat{A}(t) = M_c[a^2(t) + b^2(t)]^{1/2} \qquad 2.5.18$$

This is equivalent to shifting the operating point along the HPA transfer characteristics by using the value of M_c, so M_c can be used to locate the operating point at the required backoff value. M_c is called the HPA backoff factor. From Eqns. 2.5.12 and 2.5.15, and with the use of the HPA backoff factor, the signal from the HPA output, for an input signal of

$$s(t) = a(t) + jb(t) \qquad 2.5.19$$

is given by

$$z(t) = [a(t) + jb(t)]M_c[G_p(\hat{A}) + jG_q(\hat{A})] \qquad 2.5.20$$

$$= s(t)\,M_c G(\hat{A}) \qquad 2.5.21$$

The model can be used to assess the performance of a modulation technique by means of computer simulation. The amplitude and phase characteristics of the HPA are obtained by converting its power and phase characteristics. Samples of $G(\hat{A})$, which provide sufficient resolution, can be stored and used to determine the output signal values by means of interpolation. The samples are obtained as follows.

- To represent the HPA amplitude characteristic by, say n, discrete values of $|G(A)|$, the HPA amplitude characteristic is quantized into regular intervals of λ volts along the input axis ($n\lambda$ volts will be the maximum input voltage to the HPA). The values of $|G(\lambda_m)|$, where $\lambda_m = m\lambda$, for m= 1, 2, ..., n, are obtained using the amplitude (voltage) characteristic of the HPA and the equation

$$|G(\lambda_m)| = \frac{\text{Output voltage for an input value of } m\lambda \text{ volts}}{m\lambda \text{ volts}} \qquad 2.5.22$$

- To represent the HPA phase characteristic by n discrete values of $g(A)$, the HPA phase characteristic is quantized into intervals of λ volts along the input axis. The values of $g(\lambda_m)$, where $\lambda_m = m\lambda$, for m=1, 2, ..., n, are obtained from the HPA phase characteristic. The quadrature components, $G_p(\lambda_m)$ and $G_q(\lambda_m)$, for m=1, 2, ..., n, are then obtained using the phase characteristic of the HPA and $|G(\lambda_m)|$ with the use of the following two equations

$$G_p(\lambda_m) = |G(\lambda_m)|\cos[g(\lambda_m)] \qquad 2.5.23a$$

and

$$G_q(\lambda_m) = |G(\lambda_m)|\sin[g(\lambda_m)] \qquad 2.5.23b$$

- The values of $G_p(\lambda_m)$ and $G_q(\lambda_m)$, for m=1, 2, ..., n, are then taken as real and imaginary values, respectively, such that

$$G(\lambda_m) = G_p(\lambda_m) + jG_q(\lambda_m) \qquad 2.5.24$$

Hence the $\{G(\lambda_n)\}$ are obtained.

From Eqns. 2.5.19, 2.5.20, and 2.5.21, the signal from the HPA output for an input signal of

$$s(t) = a(t) + jb(t) \qquad 2.5.25$$

is given by

$$z(t) = [a(t) + jb(t)]M_c[G_p(\hat{A}) + jG_q(\hat{A})] \qquad 2.5.26$$

$$= s(t)M_c G(\hat{A}) \qquad 2.5.27$$

where $s(t)$, $a(t)$, $b(t)$, $z(t)$ and $G(\hat{A})$ are continuous functions. In computer simulation tests, discrete signals are used, so the signals in Eqns. 2.5.25, 2.5.26, and 2.5.27 are sampled at the time instants $\{iT_s\}$, where $1/T_s$ is the sampling rate, to give the signal sample values s_i and z_i, at time $t = iT_s$, where

$$s_i = a_i + jb_i \qquad 2.5.28$$

and

$$z_i = s_i M_c[G_p(\hat{A}_i) + jG_q(\hat{A}_i)] \qquad 2.5.29$$

$$= s_i M_c G(\hat{A}_i) \qquad 2.5.30$$

respectively, $s_i = s(iT_s), a_i = a(iT_s), b_i = b(iT_s)$ and $z_i = z(iT_s)$, and $\hat{A}_i$ is the value of λ_n closest to the signal envelope $|M_c(a_i + jb_i)|$ at the input, and M_c is the HPA backoff factor. The model of the HPA for discrete signals is shown in Fig. 2.11c.

The values of $\{G(\lambda_n)\}$, for n = 1, 2, ..., 32, obtained by quantizing the assumed HPA characteristics (Fig. 2.12) into regular intervals along the input axis and using Eqns. 2.5.22, 2.5.23 and 2.5.24 are shown in Table 2.3. The 19th sample represents the 0 dB OBO(output backoff point). Since none of the samples represents 1 dB OBO, the 9th sample, representing 0.7 dB OBO and marked as 'C' in Fig. 2.12, is used instead. The 12th sample, representing the 0.315 dB OBO and is marked as 'B', is used to determine the nonlinear effects when the HPA is slightly backed off below saturation. In all simulation tests discussed in this thesis, the HPA (when present) is operating at 0 dB, 0.315 dB or 0.7 dB OBO.

2.6 The baseband equivalent models of quadrature modulation systems

In quadrature modulation, the modulated signal consists of the sum of two double sideband suppressed carrier components whose carrier signals have the same frequency but are in phase-quadrature to each other. It is shown in Chapters 3 and 4

that quadrature modulation is used in QPSK, DEQPSK, OQPSK and CE8PSK techniques, so the baseband equivalent model of a quadrature modulation system is considered here.

The model of a quadrature modulation system with a nonlinear satellite channel is shown in Fig. 2.13a, where the transmitter and receiver IF filters are assumed to be the ones described in section 2.4.2. $a(t)$ and $b(t)$ are two modulating signals in element synchronism and are obtained from two independent data-sources. They are applied to the respective multipliers. The second input to the inphase multiplier is the carrier signal, $\sqrt{2}\cos\omega_c t$ and the second input to the quadrature multiplier is the carrier signal shifted exactly by $-\pi/2$, i.e., $-\sqrt{2}\sin\omega_c t$. The multiplier outputs are added linearly to give the quadrature signal

$$S(t) = \sqrt{2}a(t)\cos\omega_c t - \sqrt{2}b(t)\sin\omega_c t \qquad 2.6.1$$

which is filtered and nonlinearly distorted by the transmitter IF filters and the HPA, respectively.

At the output of the transmitter, the signal is

$$\hat{S}(t) = \sqrt{2}\hat{a}(t)\cos\omega_c t - \sqrt{2}\hat{b}(t)\sin\omega_c t \qquad 2.6.2$$

where $\sqrt{2}\hat{a}(t)$ and $\sqrt{2}\hat{b}(t)$ are the inphase and quadrature signal waveforms that have been nonlinearly distorted by the HPA.

The equivalent baseband signal of the quadrature modulated signal, expressed by Eqn. 2.6.1, can be represented (Appendix A6) as the complex-valued signal

$$s(t) = a(t) + jb(t) \qquad 2.6.3$$

where $j = \sqrt{-1}$. Likewise, the signal $\hat{S}(t)$, at the output of the transmitter, given by Eqn. 2.6.2, can be represented as the complex-valued signal

$$\hat{s}(t) = \hat{a}(t) + j\hat{b}(t) \qquad 2.6.4$$

The noise waveform $N(t)$, at the input of the receiver, is a sample function of a Gaussian random process with zero mean and a two-sided power spectral density of $\frac{1}{2}N_0$ over the signal frequency band. Assume $N(t)$ is a narrowband bandpass noise, so that it can be expanded (Appendix A7) into

$$N(t) = N_c(t)\cos\omega_c t - N_s(t)\sin\omega_c t \qquad 2.6.5$$

where $N_c(t)$ and $N_s(t)$ are sample functions of Gaussian random processes with zero mean, and the two-sided power spectral density of each of them is twice that of $N(t)$ (Appendix A7). The equivalent baseband form of $N(t)$ can be represented as the complex-valued signal

$$n(t) = n_c(t) + jn_s(t) \qquad 2.6.6$$

where $n_c(t)$ and $n_s(t)$ all have the same variance and are sample functions of Gaussian random processes with zero mean and a two-sided spectral power density of $\frac{1}{2} N_0$ over the frequency band of the baseband data signal $s(t)$.

So in the model of the quadrature modulation system, since the transmitter and receiver IF filters F_{IF} and the HPA can be represented by their baseband equivalent models, and the bandpass signals $N(t)$, $S(t)$, and $\hat{S}(t)$ can be represented by their equivalent baseband signals $n(t)$, $s(t)$, and $\hat{s}(t)$, respectively, the model of the quadrature modulation system can be simplified by assigning real values to the signals in one of the two parallel channels (that associated with $\sqrt{2}\cos\omega_c t$) and imaginary values to the signals in the other channel (that associated with $\sqrt{2}\sin\omega_c t$), and then considering the linear modulator, the transmitter IF filter, the HPA, the receiver IF filter, the linear demodulator, as a baseband transmission path carrying complex-valued signals. The resultant system is shown in Fig. 2.13b.

In this thesis, three baseband equivalent models of different bandpass channels are used for computer simulation tests. They are (a) linear and memoryless, (b) linear and bandlimited and, (c) nonlinear and bandlimited channels, as shown in Fig. 2.14, which are obtained from Fig. 2.13a by removing the appropriate blocks. The baseband equivalent model of the system under two conditions are considered in this thesis. They are (1) when the transmitter operates the HPA in a linear mode and, (2) when the transmitter operates the HPA in a nonlinear mode.

m (unit of *T*/8 *sec*)	sampled impulse responses of			*m* (unit of *T*/8 *sec*)	sampled impulse responses of		
	α =100%	α=40%	α=25%		α=100%	α=40%	α=25%
0	1	1	1	±25	-0.0060	0.0140	-0.0048
±1	0.942	0.963	0.9662	±26	-0.0010	0.0180	-0.0440
±2	0.785	0.858	0.8694	±27	0.0039	0.0160	-0.0350
±3	0.565	0.72	0.7420	±28	0.0051	0.0130	-0.0200
±4	0.333	0.511	0.5570	±29	0.0033	0.0050	-0.0040
±5	0.134	0.316	0.3959	±29	-0.00099	-0.0060	0.0110
±6	0.0005	0.139	0.1802	±30	-0.00393	-0.0120	0.0210
±7	-0.0628	-0.001	0.0549	±31	-0.0050	-0.0140	0.0250
±8	-0.0666	-0.0844	-0.0582	±32	-0.00393	-0.0100	0.0210
±9	-0.0367	-0.0130	-0.1440	±33	0.00032	-0.0060	0.0150
±10	-0.0011	-0.1400	-0.1880	±34	0.0033	0.0009	0.0040
±11	0.0241	-0.112	-0.1920	±35	0.0041	0.0060	-0.0050
±12	0.0285	-0.066	-0.1630	±36	0.00203	0.0099	-0.0124
±13	0.0171	-0.026	-0.1160	±37	0.00087	0.0080	-0.0164
±14	0.00013	0.035	-0.0560	±38	-0.00298	0.0040	-0.0155
±15	-0.0140	0.040	0.0020	±39	-0.0040	-0.0009	-0.0140
±16	-0.0170	0.035	0.0490	±40	-0.00304	-0.0070	-0.0040
±17	-0.0099	0.016	0.0806	±41	-0.00154	-0.0087	0.0030
±18	-0.0011	0.014	0.0100	±42	0.002	-0.0080	0.0090
±19	0.0079	0.0016	0.0830	±43	0.003	-0.0070	0.0131
±20	0.0101	-0.0098	0.0640	±44	0.002	-0.0035	0.0131
±21	0.0069	-0.0230	0.0360	±45	0.0009	0.0035	0.0110
±22	0.00002	-0.0180	0.0060	±46	-0.0031	0.0060	0.0050
±23	-0.0071	-0.0090	-0.0210	±47	-0.0031	0.0070	-0.0020
±24	-0.0090	-0.0001	-0.0390				

Table 2.1 Sample impulse response of the modulator (or demodulator) filters, with different values of α. The truncation lengths have been made to be $\pm 8T$ with sampling rate of $8/T$.

m (unit of $T/8$ sec)	sample impulse response	m (unit of $T/8$ sec)	sample impulse response
0	1	±13	0.054
±1	0.936	±14	0.039
±2	0.76	±15	0.017
±3	0.512	±16	-0.005
±4	0.254	±17	-0.017
±5	0.041	±18	-0.021
±6	-0.099	±19	-0.017
±7	-0.156	±20	-0.008
±8	-0.146	±21	0.002
±9	-0.095	±22	0.009
±10	-0.031	±23	0.011
±11	0.022	±24	0.008
±12	0.049		

Table 2.2 Sampled impulse response of the equivalent baseband model of the transmitter (or receiver) IF filter. The truncation length has been made to be $\pm 3T$ with sampling rate of $8/T$ samples per second.

m	$G(\lambda_m) = G_p(\lambda_m) + jG_q(\lambda_m)$		m	$G(\lambda_m) = G_p(\lambda_m) + jG_q(\lambda_m)$	
1	3.397	0.118	17	0.85	0.778
2	2.69	0.230	18	0.787	0.760
3	2.5	0.352	19	0.723	0.749
4	2.396	0.509	20	0.675	0.737
5	2.212	0.551	21	0.624	0.706
6	2	0.613	22	0.569	0.690
7	1.933	0.703	23	0.524	0.671
8	1.801	0.746	24	0.483	0.653
9	1.644	0.732	25	0.458	0.626
10	1.514	0.771	26	0.436	0.601
11	1.4	0.809	27	0.4	0.583
12	1.3	0.812	28	0.375	0.567
13	1.186	0.800	29	0.352	0.552
14	1.092	0.793	30	0.332	0.525
15	1.019	0.796	31	0.328	0.506
16	0.922	0.793	32	0.31	0.487

Table 2.3 Sampled representation of HPA transfer characteristics shown in Fig. 2.12

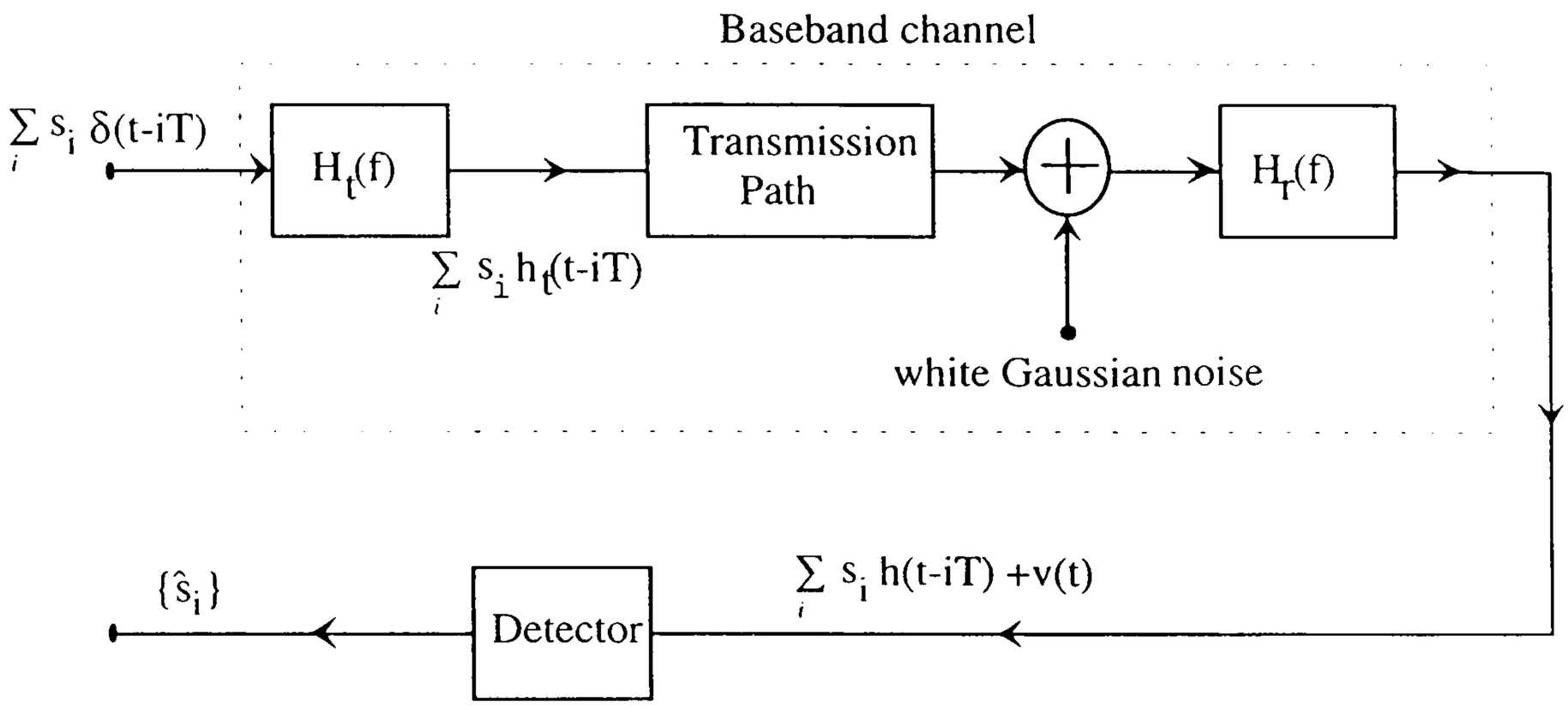

Figure 2.1 Baseband model of the data-transmission system

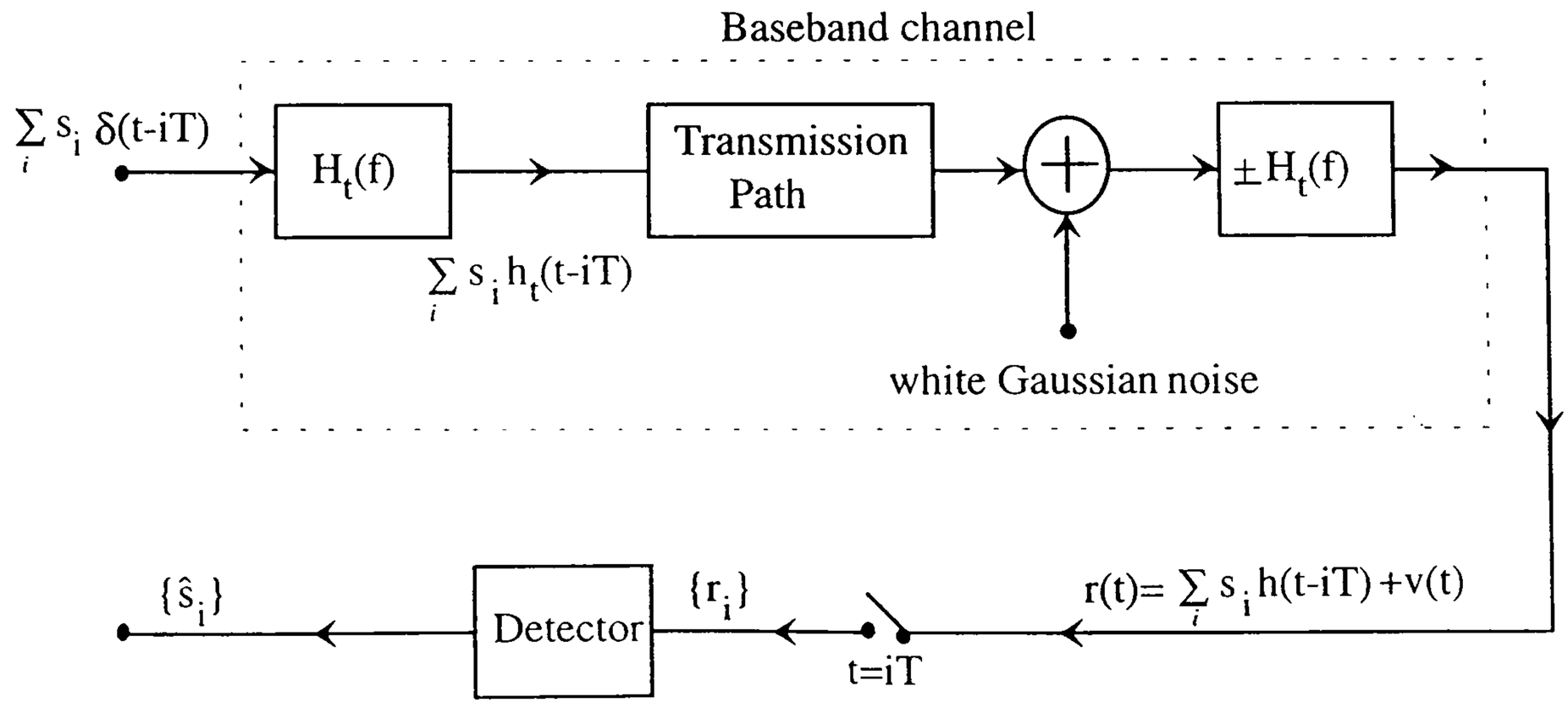

Figure 2.2 Assumed model of the data-transmission system

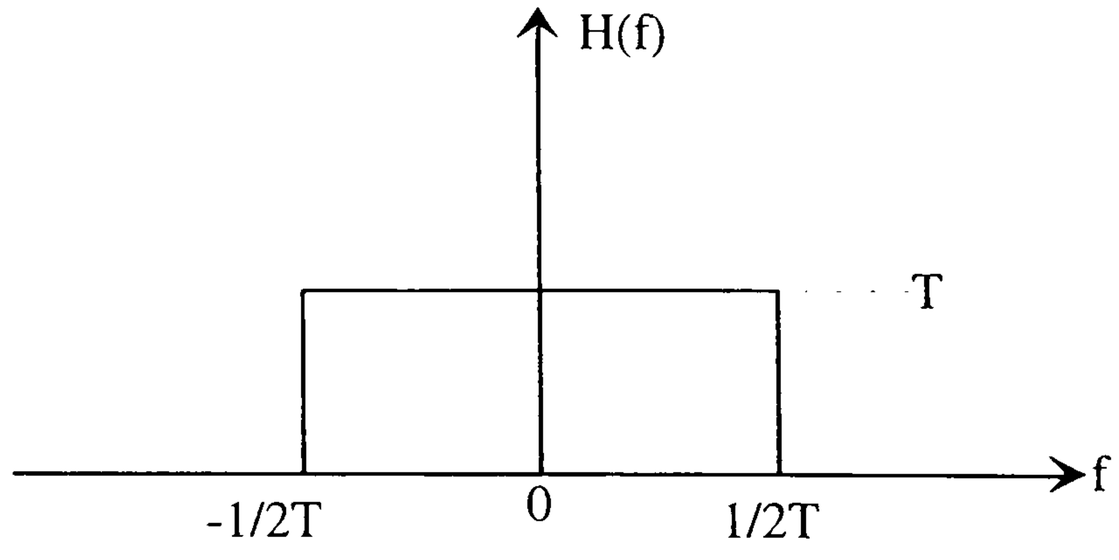

Figure 2.3a Channel transfer-function giving a rectangular signal-spectrum

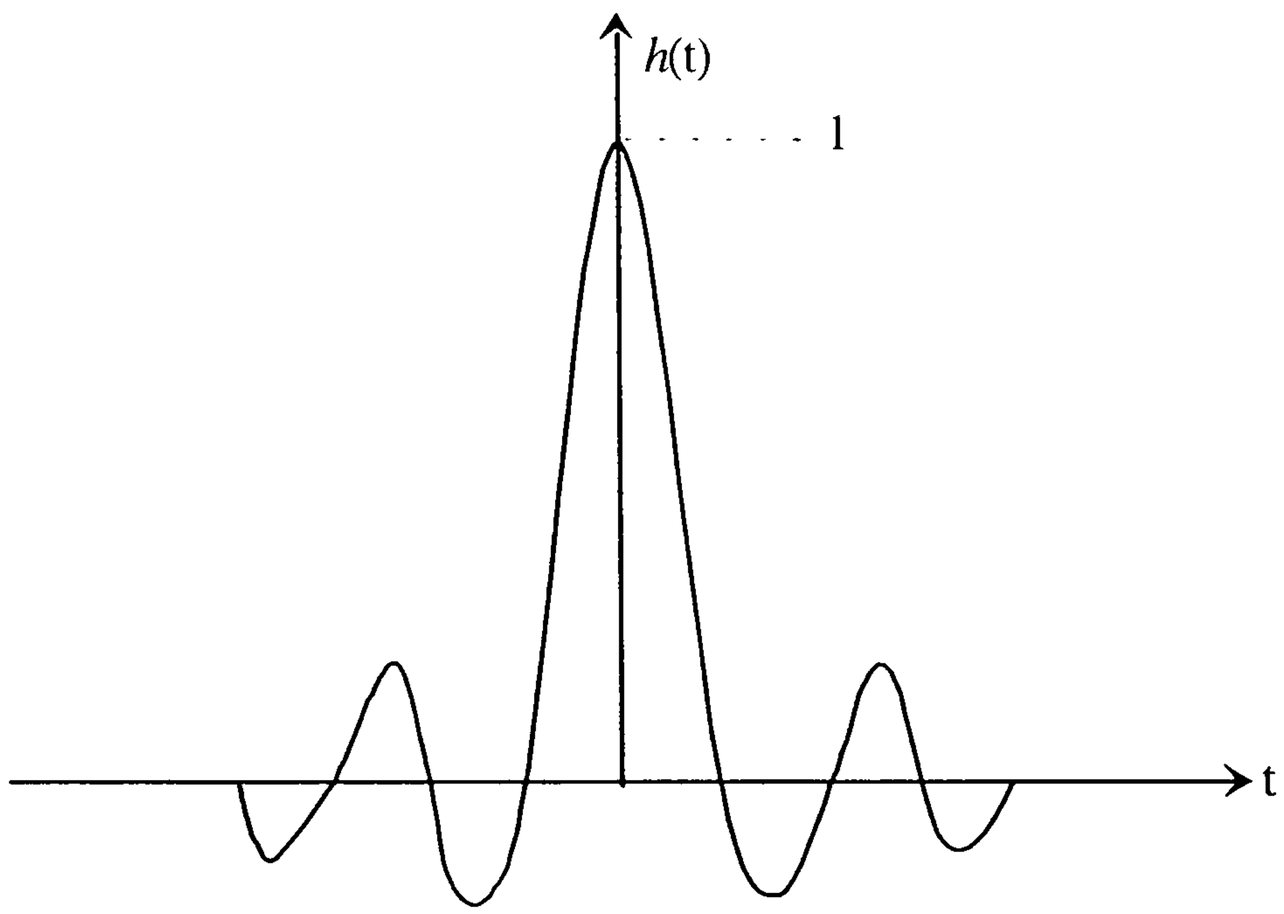

Figure 2.3b Impulse response of baseband channel.

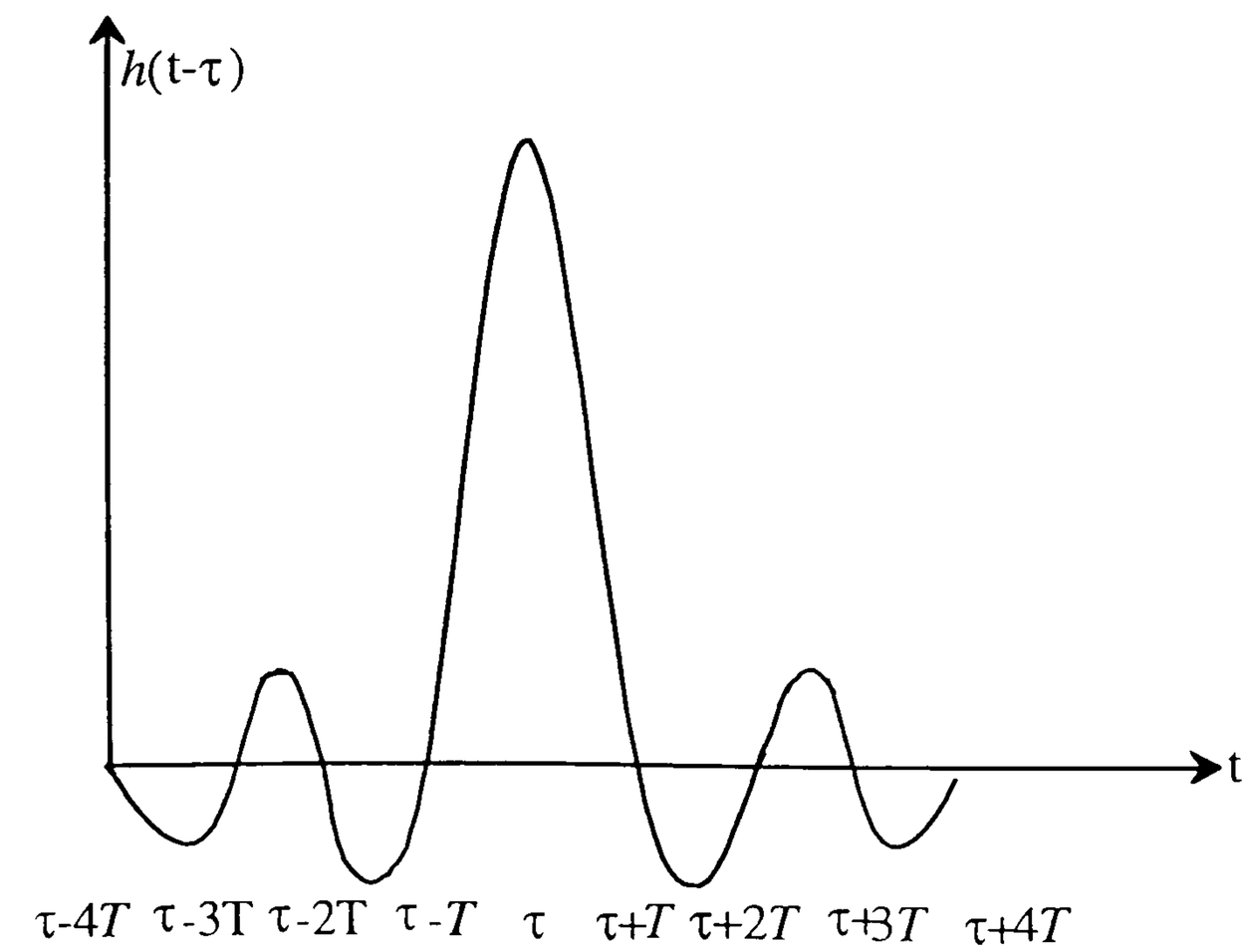

Figure 2.3c Physically realisable impulse response.

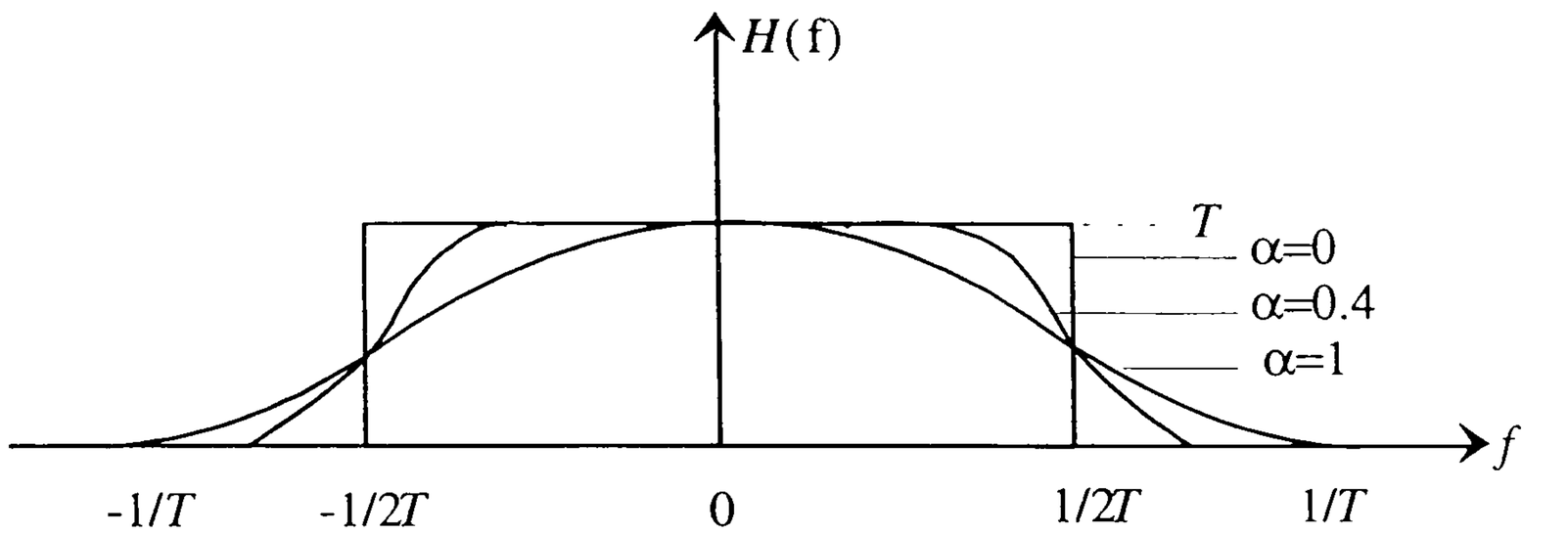

(a)

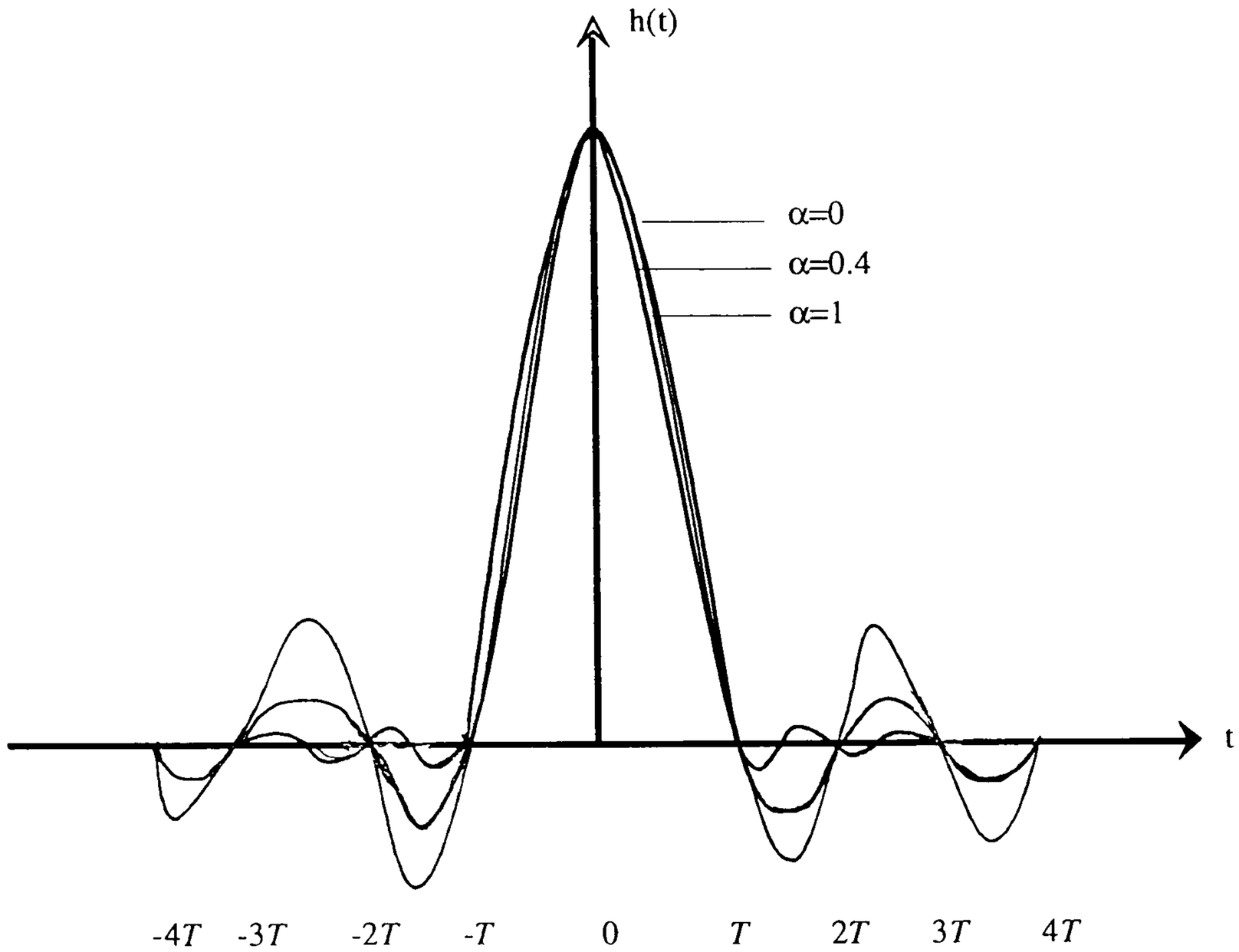

(b)

Figure 2.4 Response of different rolloff factor. a) Frequency response
b) Time response

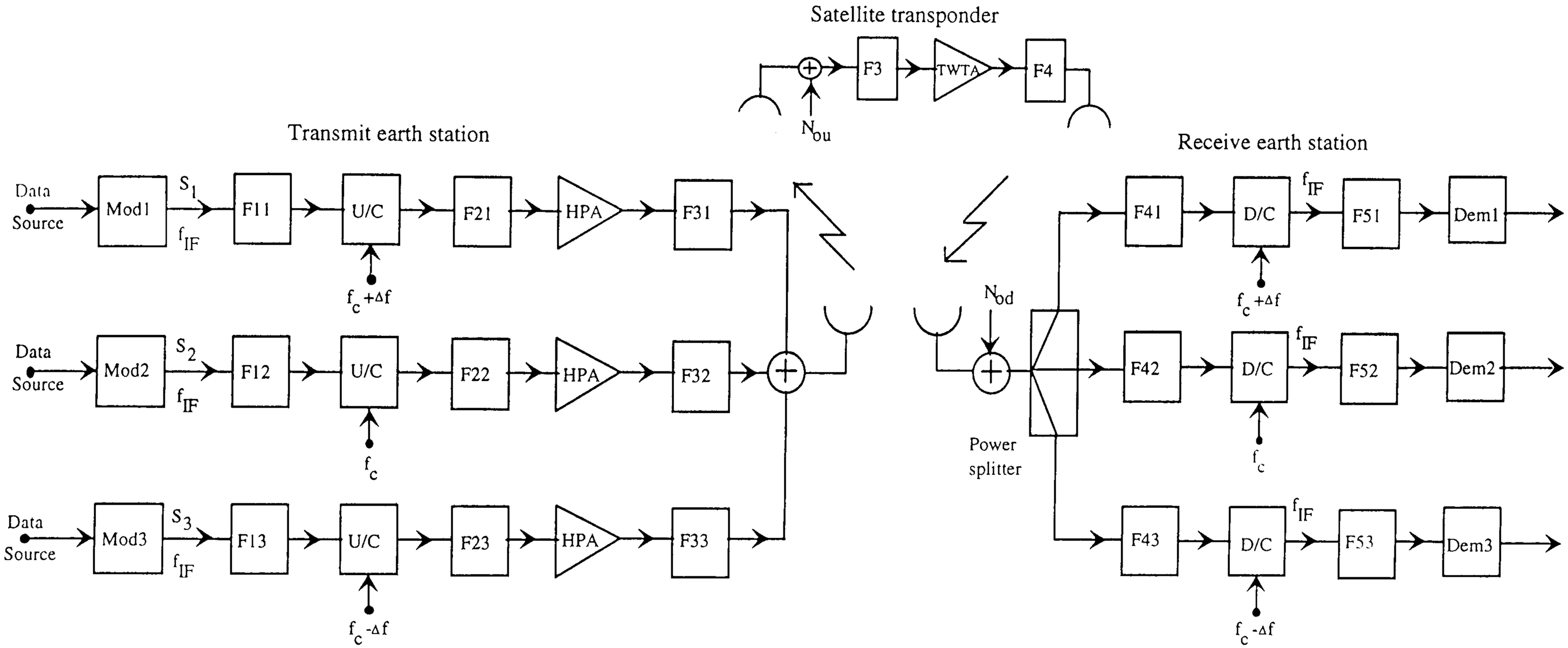

Figure 2.5 Typical satellite earth station configuration. Mod, modulator; Dem, demodulator; U/C, up-converter; D/C, down-converter, and Nou, uplink noise; Nod, downlink noise.

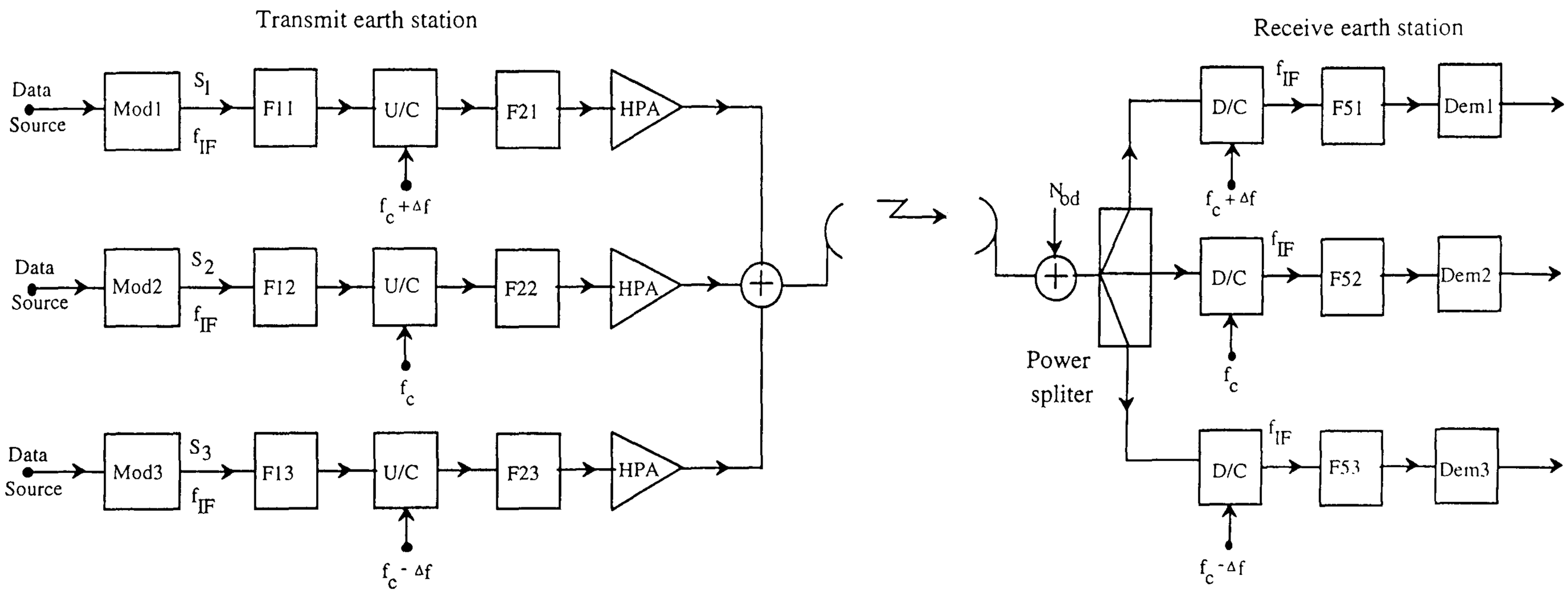

Figure 2.6 Satellite earth station system.

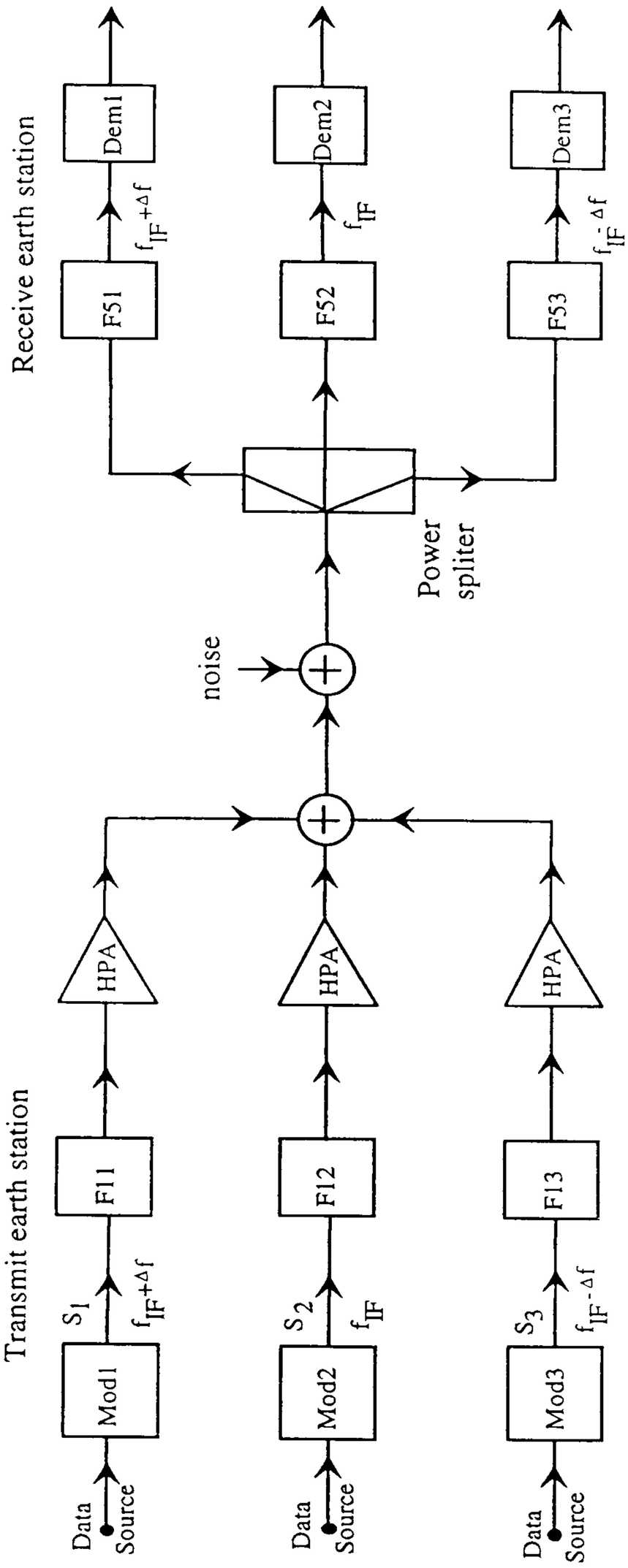

Figure 2.7 Simplified model of the satellite earth station system at IF frequency band.

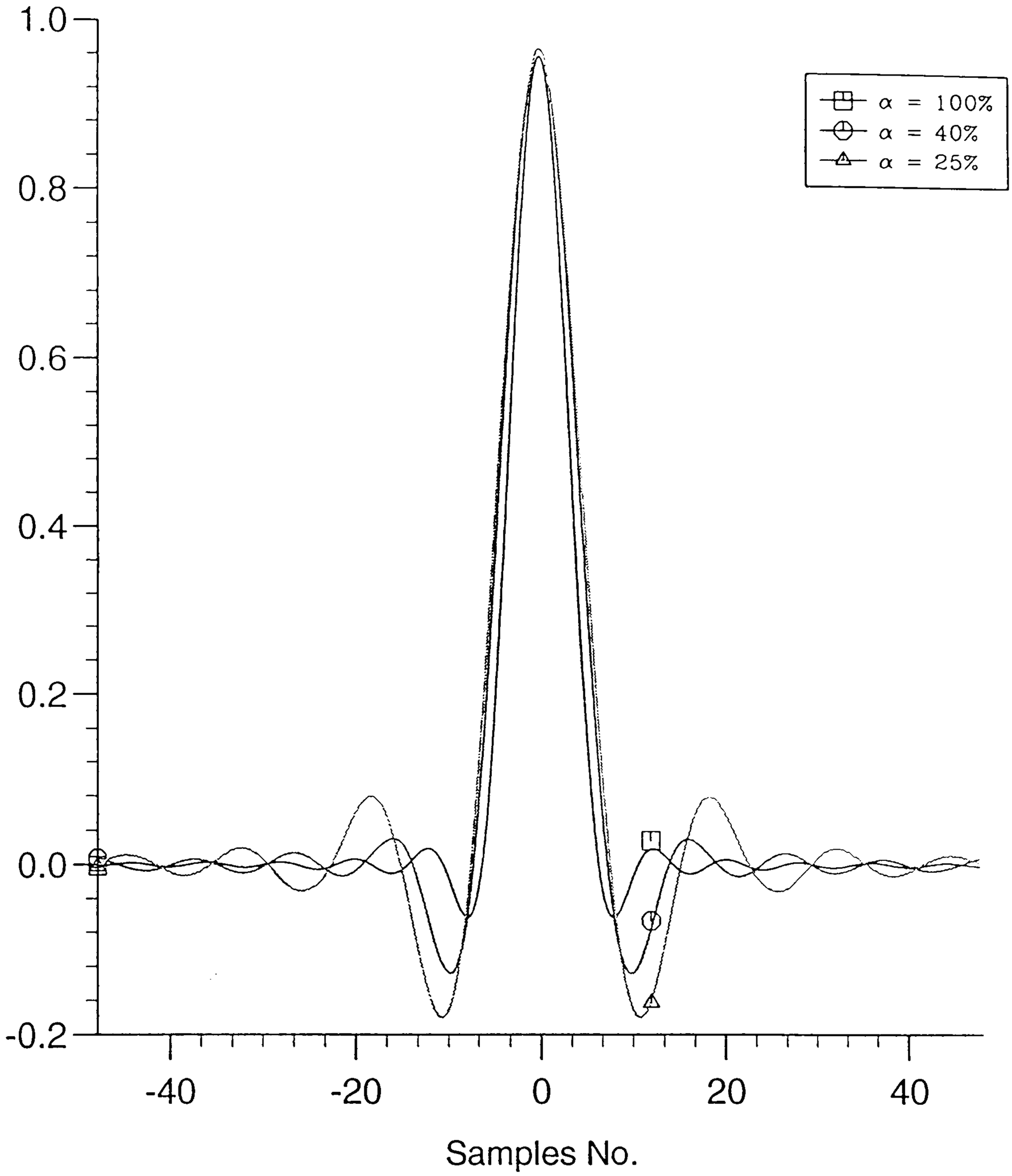

Figure 2.8 Impulse response of the modulation and demodulation filters with $\alpha = 100\%$, 40% and 25%

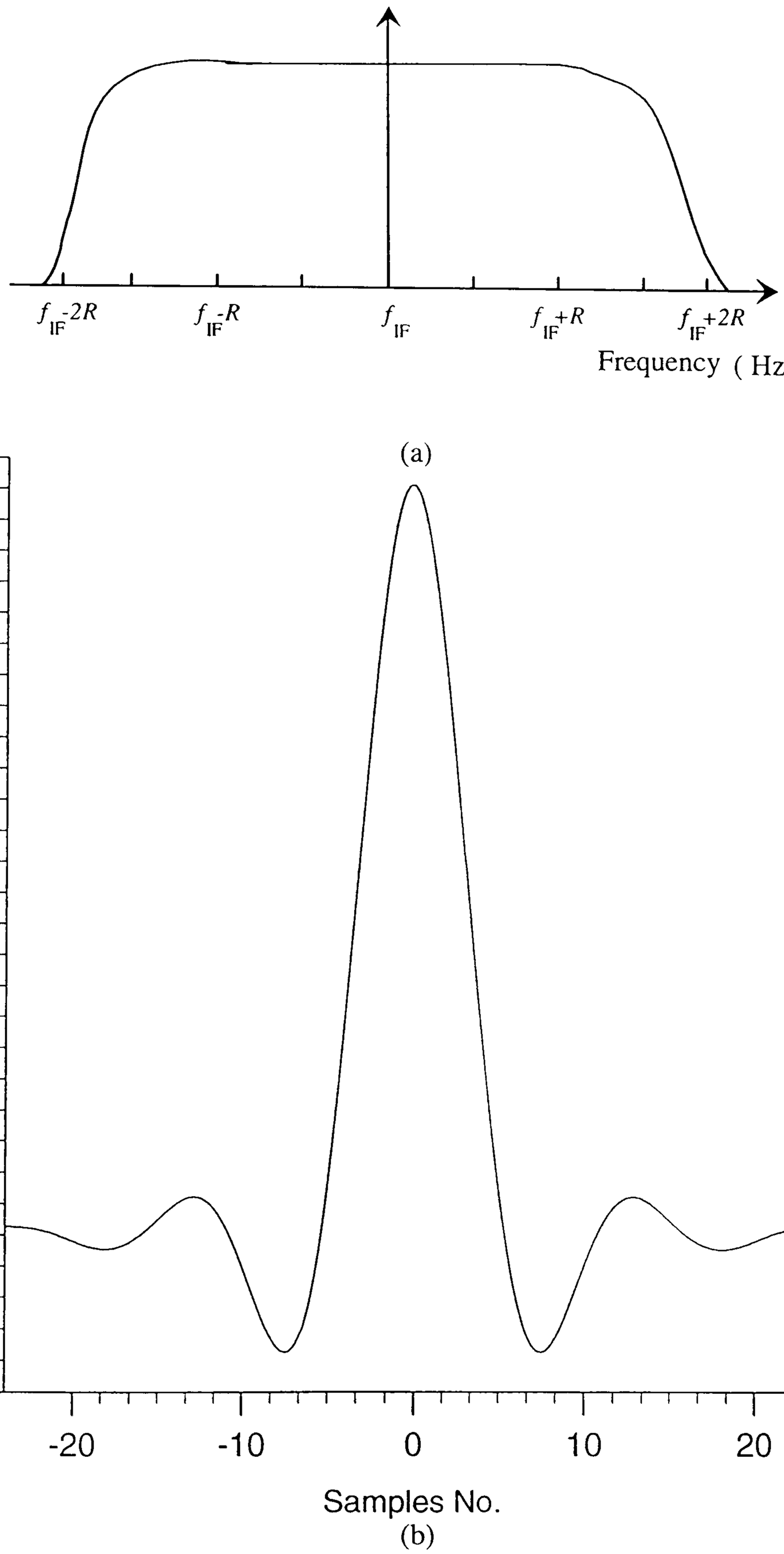

Figure 2.9 Characteristics of the assumed IF filter. a) The actual frequency responses. b) The impulse response of the baseband equivalent model.

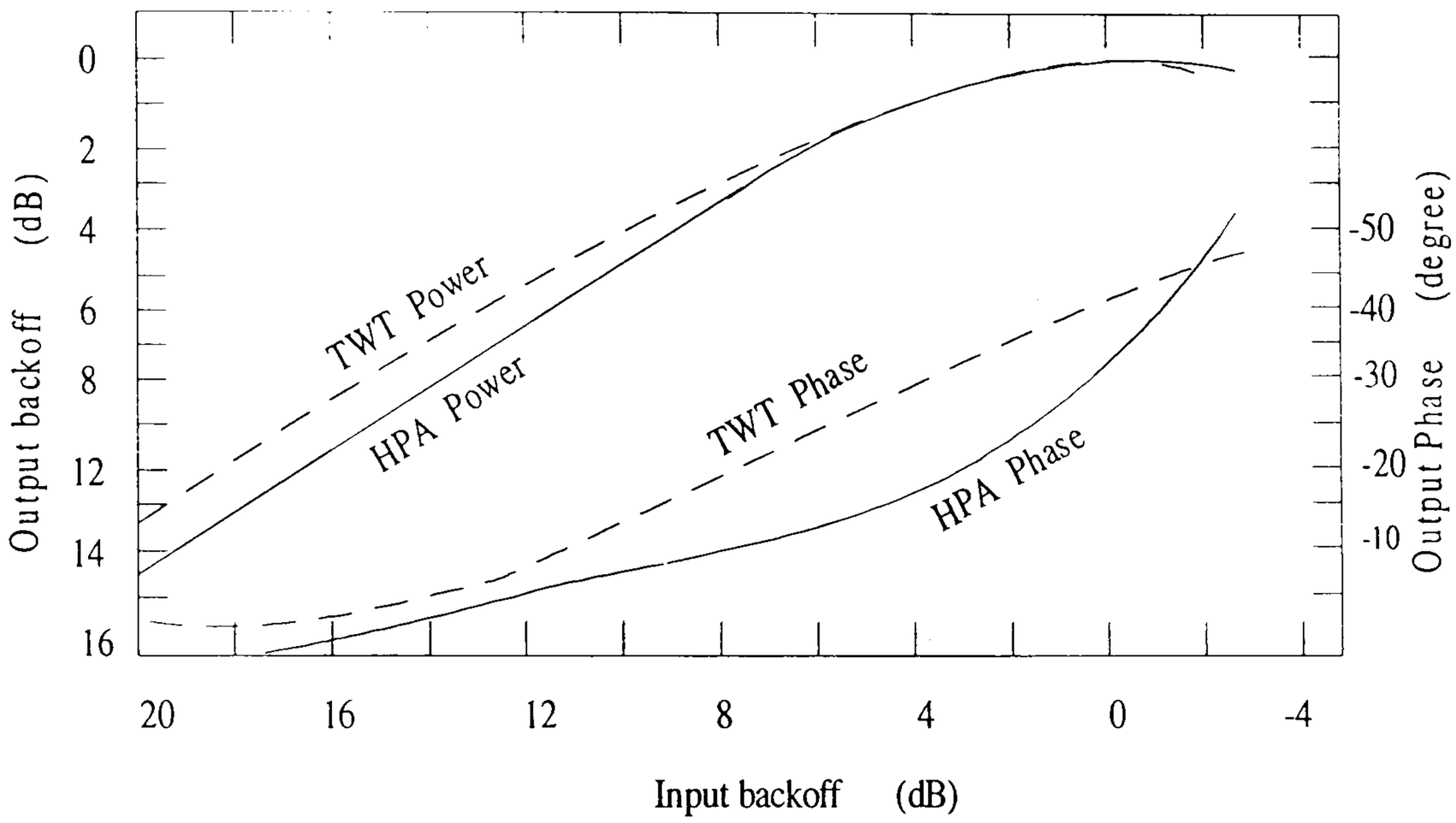

Figure 2.10 Typical input/output power and phase characteristics of an HPA and TWTA- used in the INTELSAT-V TDMA 6/4 GHz system.

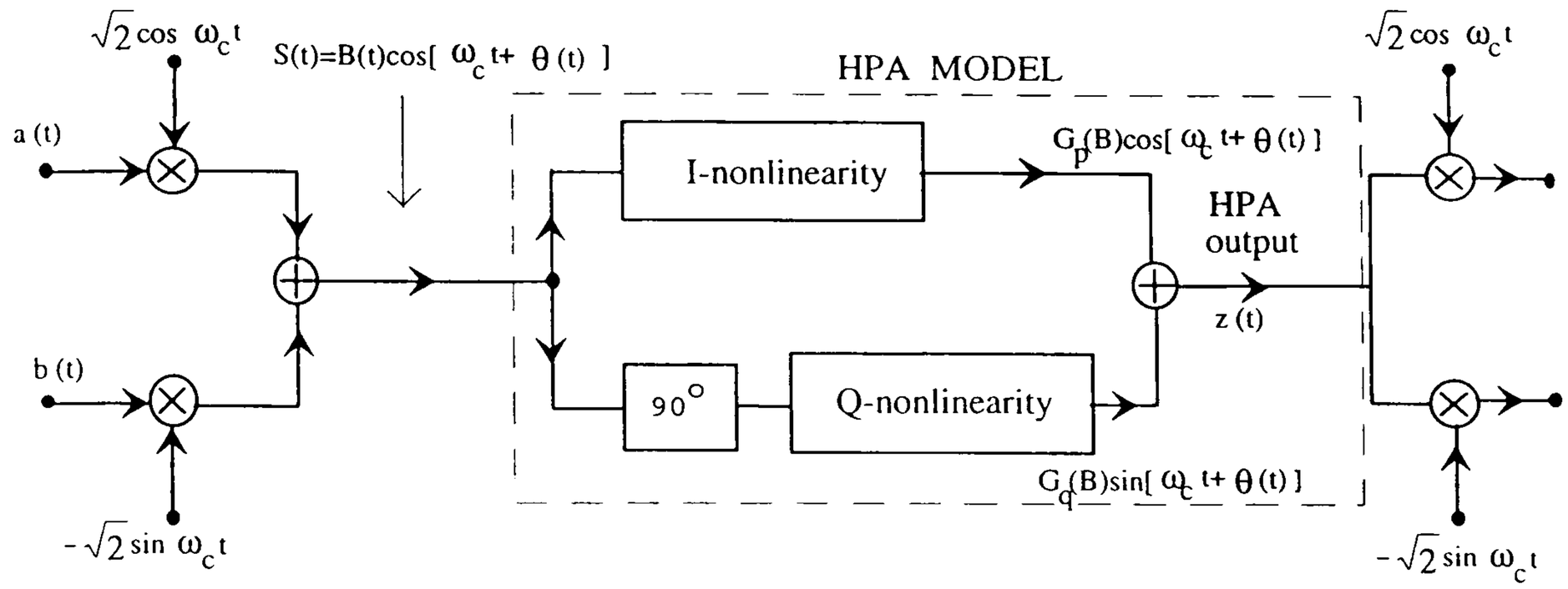

Figure 2.11a Quadrature model of HPA in a quadrature modulation system.

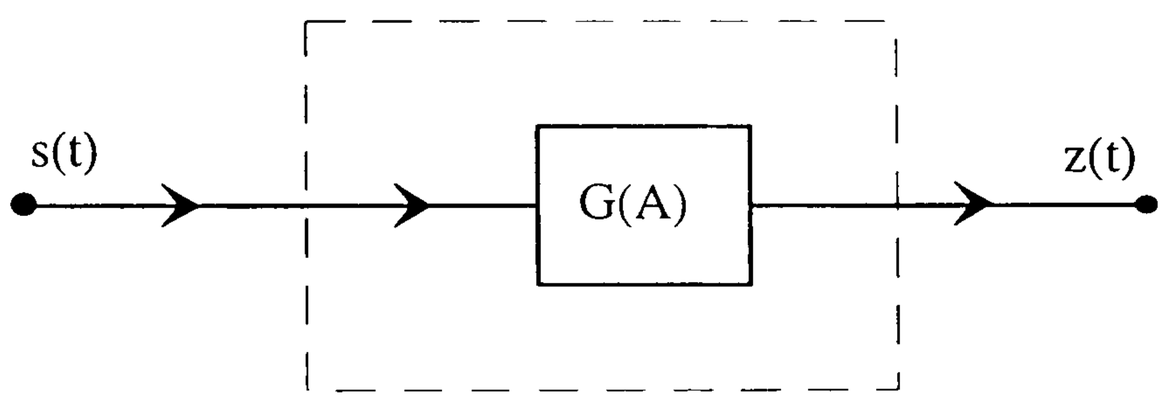

Figure 2.11b Baseband equivalent model of HPA.

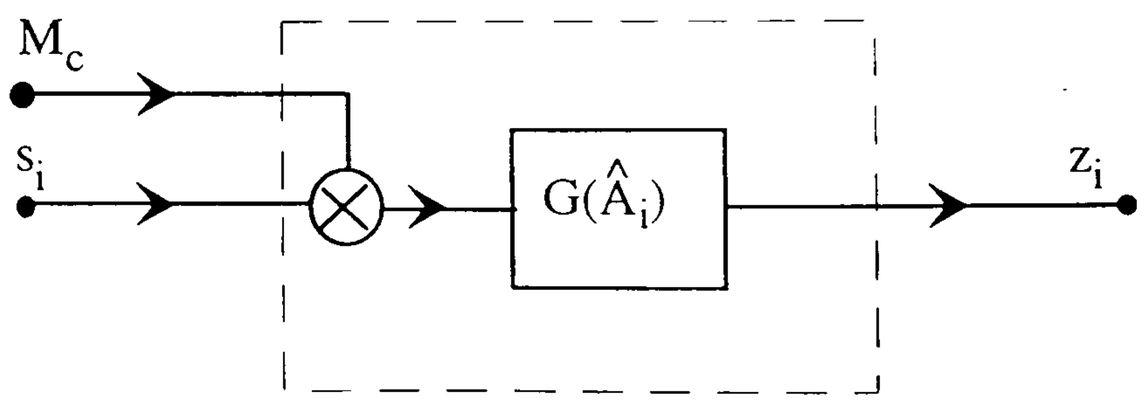

Figure 2.11c Baseband equivalent model of HPA for discrete signals.

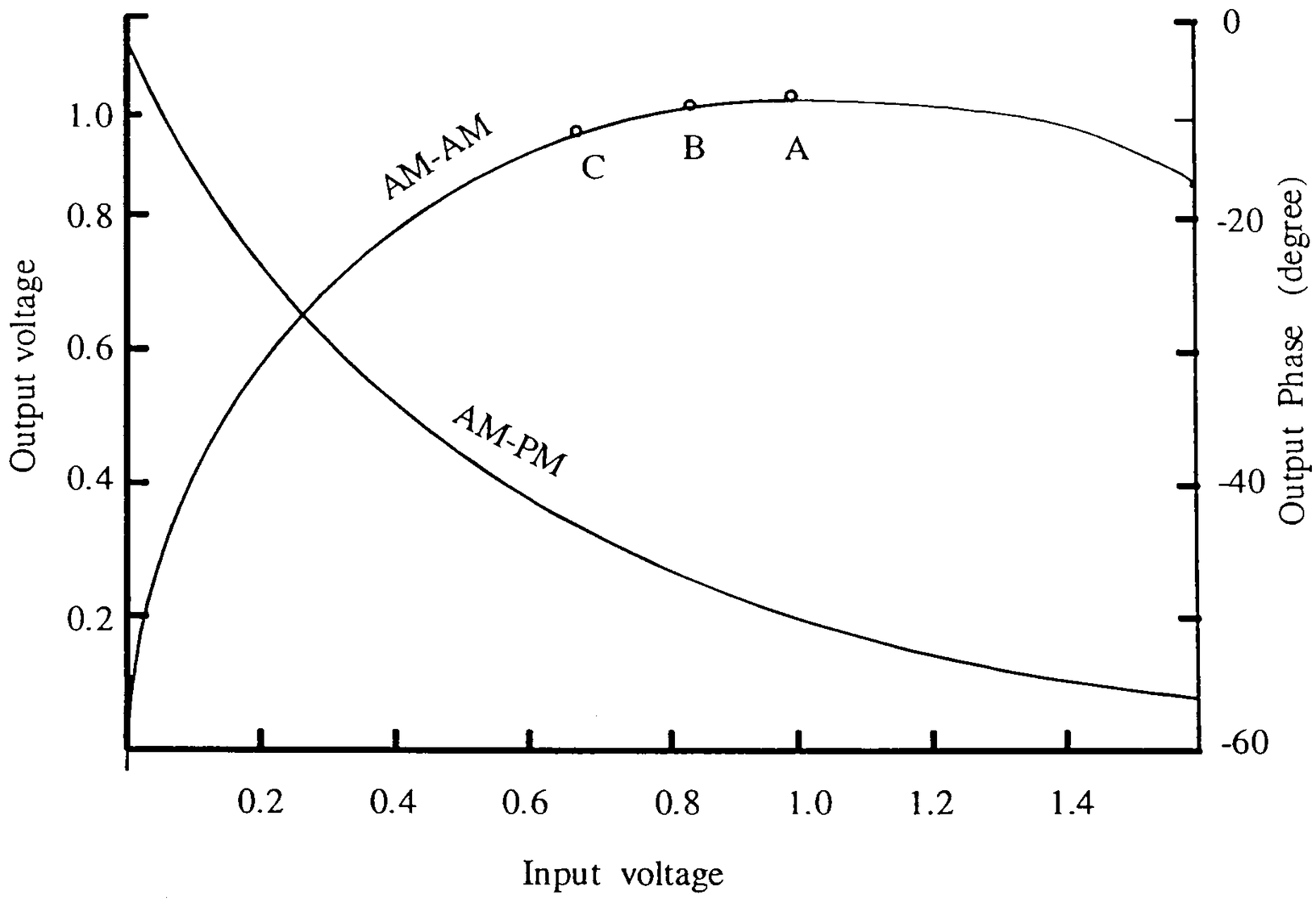

Figure 2.12 Assumed HPA characteristics.

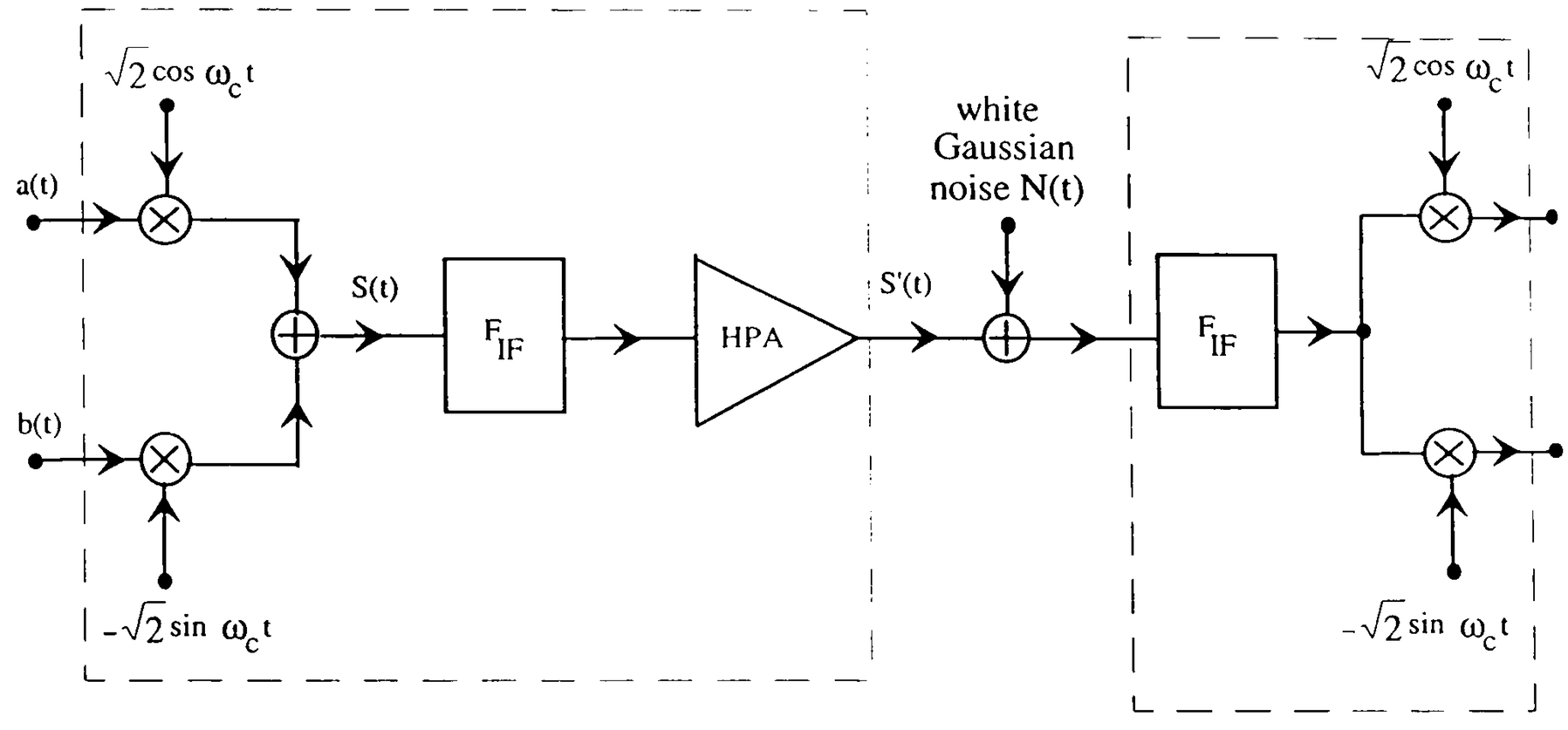

Figure 2.13a Model of a quadrature modulation system over a nonlinear satellite channel. F_{IF}, IF filter.

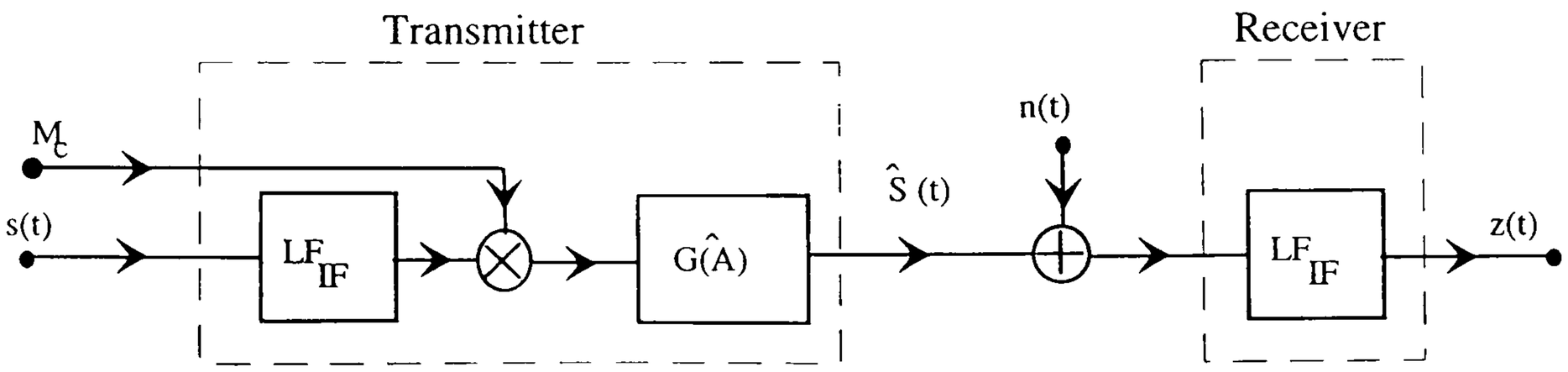

Figure 2.13b The equivalent baseband model of the system shown in Fig. 2.13a. LF_{IF} is the baseband equivalent model of the IF filter F_{IF}.

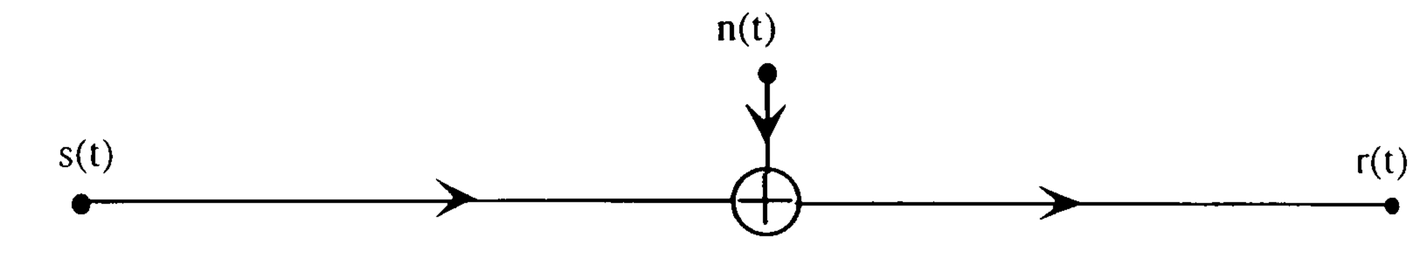

(a)

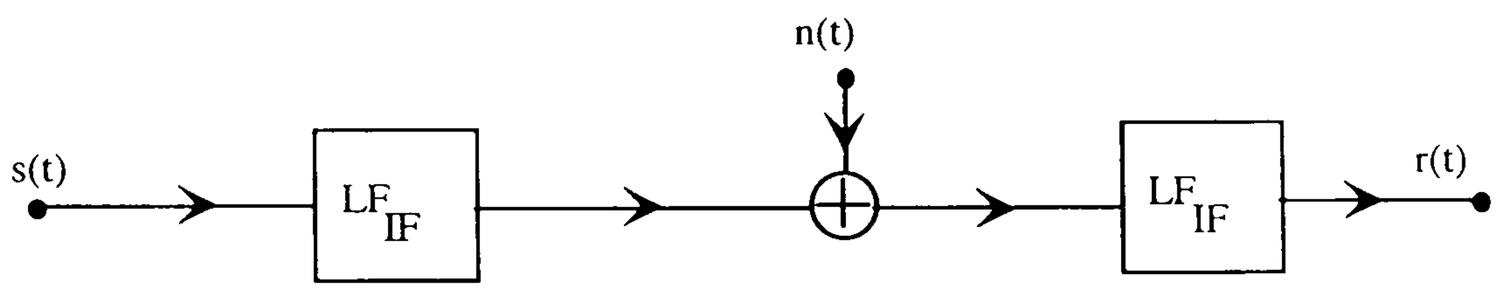

(b)

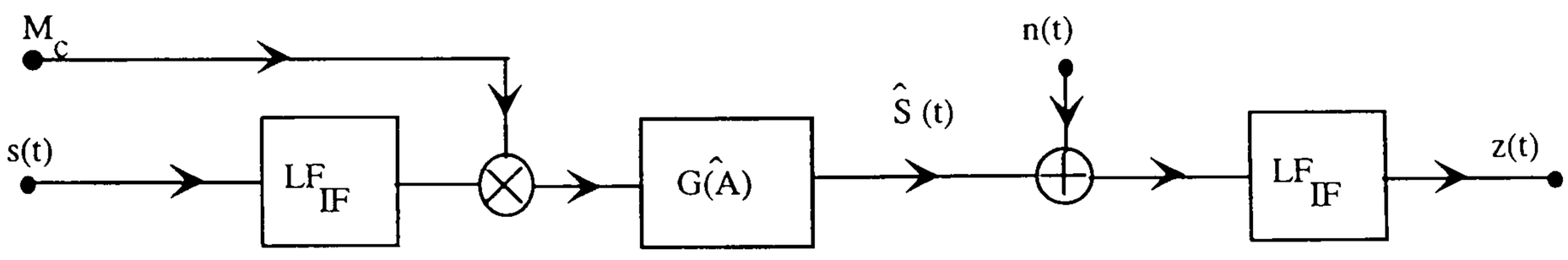

(c)

Figure 2.14 Baseband equivalent models of the bandpass channels. a) A linear and memoryless channel. b) A linear and bandlimited channel. c) A nonlinear and bandlimited channel.

CHAPTER 3

COHERENT QUATERNARY PSK SYSTEMS OVER A LINEAR OR NONLINEAR SATELLITE CHANNEL

3.1 Description of coherent QPSK, DEQPSK and OQPSK systems

3.1.1 Coherent quaternary phase-shift keying (QPSK) systems

In QPSK systems the modulated signal has four distinct states. These states are generated by a unique mapping scheme of consecutive pairs of bits into symbols. The symbol intervals has a two-bit duration. The four possible pairs of bits are frequently mapped in accordance with the Gray code. An important property of this code is that adjacent symbols differ by only one bit (Fig. 3.2). In transmission systems corrupted by noise and interference, the most frequent errors are introduced by making a decision error between two adjacent states. In this case, the Gray code assures that a single symbol error corresponds to one bit error.

A rectangular baseband modulating waveform is usually used to describe QPSK systems. However, it is not a practical waveform, so that a rounded baseband modulating waveform is used here to describe the QPSK systems instead.

A block diagram of a conventional QPSK system is shown in Fig. 3.1. The information to be transmitted is carried by the sequence of binary data-symbols $\{s_i\}$. Each data symbol therefore carries one bit of information. The S/P (serial-to-parallel) converter converts the sequence $\{s_i\}$ into two sequences of binary symbols $\{u_{1,i}\}$ and $\{u_{2,i}\}$, where $u_{j,i} = 0$ or 1 for $j = 1,2$. The relationship between the input data sequence $\{s_i\}$ and the two binary sequences $\{u_{1,i}\}$ and $\{u_{2,i}\}$ is shown in Fig. 3.2. The Gray coder, in Fig. 3.1 codes these two sequences of symbols according to Table 3.1, and gives two output sequences $\{q_{1,i}\}$ and $\{q_{2,i}\}$, where $q_{j,i} = \pm 1$ for $j = 1,2$. These two sequences are converted into the corresponding sequences of impulses

$\{\sum_i q_{1,i}\delta(t-iT)\}$ and $\{\sum_i q_{2,i}\delta(t-iT)\}$, which are fed into the modulation filter and hence to produce two baseband modulating waveforms

$$a(t)=\sum_i q_{1,i}h_t(t-iT) \qquad 3.1.1a$$

and

$$b(t)=\sum_i q_{2,i}h_t(t-iT) \qquad 3.1.1b$$

where $h_t(t)$ is the impulse response of the modulation filter with the transfer function of $H_t(f)$. $a(t)$ and $b(t)$ are called the inphase and quadrature baseband signals, respectively. These two baseband signals are quadrature modulated, as described in Section 2.6, and then added linearly to give the QPSK signal

$$S(t)=\sqrt{2}a(t)\cos\omega_c t-\sqrt{2}b(t)\sin\omega_c t \qquad 3.1.2$$

with ω_c the carrier frequency in rad/s. The resultant signal is fed into the bandpass transmission channel. Assume that the bandpass transmission channel introduces no attenuation, delay or distortion, but adds a Gaussian noise waveform, $N(t)$, to the transmitted signal. So at the receiver, the signal input to the demodulation filter is

$$r(t)=\sqrt{2}[a(t)\cos\omega_c t-b(t)\sin\omega_c t]+N(t) \qquad 3.1.3$$

where $N(t)$ is a sample function of a Gaussian random process with zero mean and a two-sided power spectral density of $\frac{1}{2}N_0$ over the signal frequency band. Assume that the bandwidth of $N(t)$ is small compared with ω_c, so it can be expanded [19] into

$$N(t)=N_c(t)\cos\omega_c t-N_s(t)\sin\omega_c t \qquad 3.1.4$$

where $N_c(t)$ and $N_s(t)$ are sample functions of Gaussian random processes with zero mean and a two-sided power spectral density twice that of $N(t)$ (Appendix A7). Hence Eqn. 3.1.3 can be written as

$$r(t)=[\sqrt{2}a(t)+N_c(t)]\cos\omega_c t-[\sqrt{2}b(t)+N_s(t)]\sin\omega_c t \qquad 3.1.5$$

Since the inphase and quadrature signal components are orthogonal [1], [20], the receiver is able to demodulate them independently of each other. The inphase and quadrature data signal components plus noise just prior to the demodulation filter are

$$r(t)\sqrt{2}\cos\omega_c t = \{[\sqrt{2}a(t)+N_c(t)]\cos\omega_c t - [\sqrt{2}b(t)+N_s(t)]\sin\omega_c t\}\sqrt{2}\cos\omega_c t$$

$$= [\sqrt{2}a(t)+N_c(t)]\sqrt{½}(1+\cos 2\omega_c t) - [\sqrt{2}b(t)+N_s(t)]\sqrt{½}\sin 2\omega_c t$$

$$= a(t)+\sqrt{½}N_c(t)+[a(t)+\sqrt{½}N_c(t)]\cos 2\omega_c t - [b(t)+\sqrt{½}N_s(t)]\sin 2\omega_c t$$

$$= a(t)+\sqrt{½}N_c(t)+\text{h.f.c} \qquad 3.1.6a$$

and

$$-r(t)\sqrt{2}\sin\omega_c t = -\{[\sqrt{2}a(t)+N_c(t)]\cos\omega_c t - [\sqrt{2}b(t)+N_s(t)]\sin\omega_c t\}\sqrt{2}\sin\omega_c t$$

$$= -[\sqrt{2}a(t)+\sqrt{½}N_c(t)]\sin 2\omega_c t + [\sqrt{2}b(t)+N_s(t)]\sqrt{½}(1-\cos 2\omega_c t)$$

$$= -[a(t)+\sqrt{½}N_c(t)]\sin 2\omega_c t + b(t)+\sqrt{½}N_s(t) - [b(t)+\sqrt{½}N_s(t)]\cos 2\omega_c t$$

$$= b(t)+\sqrt{½}N_s(t)+\text{h.f.c} \qquad 3.1.6b$$

respectively, where h.f.c means high frequency components. The demodulation filter blocks the h.f.c in the signals and produces the wanted noisy inphase and quadrature baseband signal components, $a(t)+\sqrt{½}N_c(t)$ and $b(t)+\sqrt{½}N_s(t)$, respectively. When comparing with the inphase and quadrature baseband components of the signals in Eqn. 3.1.5, it can be seen that the demodulation process has reduced both the signal and noise powers by the same factor of $\sqrt{½}$ and so retained the signal/noise power ratio.

At the demodulation filter output, the inphase and quadrature baseband signal components are

$$r_1(t) = \sum_i q_{1,i}h(t-iT) + v_1(t) \qquad 3.1.7a$$

and

$$r_2(t) = \sum_i q_{2,i}h(t-iT) + v_2(t) \qquad 3.1.7b$$

respectively, where $h(t)$ is the inverse Fourier transform of $H(f)$ which is the transfer function of the modulation and demodulation filters in cascade.

$v_1(t)$ and $v_2(t)$ are filtered Gaussian noise waveforms. Bearing in mind that the bandpass transmission channel introduces no attenuation, delay or distortion.

Assume that the modulation and demodulation filters have the same characteristics, i.e., $H_t(f) = H_r(f)$ in Fig. 3.1, and the combined transfer function, $H(f) = H_t(f)H_r(f)$, is a sinusoidal roll-off frequency response (Eqn. 2.2.3) with a linear phase characteristic, such that $h(0) = 1$ and $h(iT) = 0$, for all values of the integer i other than $i = 0$. The signals $r_1(t)$ and $r_2(t)$ have no ISI at the time $\{iT\}$. Assume also that the receiver provides the ideal required timing signal, so that the two baseband waveforms, $r_1(t)$ and $r_2(t)$, at the demodulation filter output, are sampled at the time instants $\{iT\}$, to give two sequences of sample values $\{r_{1,i}\}$ and $\{r_{2,i}\}$ which are fed into the detector. Since there is no ISI at the sampling instants $\{iT\}$, which implies that $r_{1,i}$ and $r_{2,i}$ depend only on $q_{1,i}$ and $q_{2,i}$, respectively, but not any $\{q_{1,j}\}$ and $\{q_{2,j}\}$ for $j \neq i$. The resultant operation of the channel is to add to the input symbols $q_{1,i}$ and $q_{2,i}$ the noise components $v_{1,i}$ and $v_{2,i}$, respectively, to give at its output the samples, at time $t = iT$,

$$r_{1,i} = q_{1,i} + v_{1,i} \qquad 3.1.8a$$

and

$$r_{2,i} = q_{2,i} + v_{2,i} \qquad 3.1.8b$$

where $v_{1,i}$ and $v_{2,i}$ are sample values of Gaussian random variables with zero mean and fixed variance σ^2, the $\{v_{1,i}\}$ and $\{v_{2,i}\}$ being statistically independent and independent also of the $\{s_i\}$.

It is shown, in Section 2.2, that under these assumed conditions, the optimum detection process for $\{r_{1,i}\}$ and $\{r_{2,i}\}$ is by comparing each of them with a decision threshold of zero, therefore two separate threshold detectors are used to detect these two sequences of sample values $\{r_{1,i}\}$ and $\{r_{2,i}\}$, according to Table 3.3. The detected symbols are Gray decoded to produce the sequences $\{\hat{u}_{1,i}\}$ and $\{\hat{u}_{2,i}\}$. The sequence of decoded binary data symbols $\{\hat{s}_i\}$ is obtained by using a P/S (parallel-to-serial) converter. In the absence of noise, the $\{\hat{s}_i\}$ are the same as the $\{s_i\}$.

In the absence of noise, Eqn. 3.1.8 becomes

$$r_{1,i} = q_{1,i} = \pm 1 \qquad 3.1.9a$$

and

$$r_{2,i} = q_{2,i} = \pm 1 \qquad 3.1.9b$$

The four possible received signal vectors are shown in Fig. 3.3. The signal points are said to represent a signal constellation. It can be seen that QPSK signals have 4 distinct phases, $\pm\pi/4$ and $\pm 3\pi/4$ radians.

3.1.2 Differentially encoded coherent quaternary phase-shift keying (DEQPSK) systems

In the coherent QPSK system just described, each pair of binary symbols, $(u_{1,i}\ \ u_{2,i})$, is Gray coded linearly to one of the four possible symbols and then transmitted. At the receiver, one of the 4 possible phases, $\pm\pi/4$ and $\pm 3\pi/4$ radians, is received (Fig. 3.3) at the input of the detector. They are detected and Gray decoded linearly to obtain the corresponding pair of binary symbols (Table 3.3). However at the receiver, most carrier recovery circuits will introduce a fourfold ambiguity. This means that the carrier may shift the received signal vector (Fig. 3.3) by a phase of 0, $\pi/2$, π, or $3\pi/2$. To resolve this ambiguity, differential encoding is commonly used.

Differential encoding encodes the pair of binary symbols, $(u_{1,i}\ \ u_{2,i})$, so that the phase change rather than the absolute phase carries the data, thus eliminating the need for a reference phase at the receiver. A block diagram of a conventional DEQPSK system is shown in Fig. 3.4. Each pair of binary symbols $(u_{1,i}\ \ u_{2,i})$, at time $t = iT$ seconds, represents a 2-bit binary value. In generation of a differential encoded pair of binary symbols, $(d_{1,i}\ \ d_{2,i})$, i.e. $d_{j,i} = 0$ or 1 for $j = 1,2$, the 2-bit binary value of the present pair of symbols, $(u_{1,i}\ \ u_{2,i})$, is added to the 2-bit binary value of the previous differential encoded pair of symbols, $(d_{1,i-1}\ \ d_{2,i-1})$, to form the present differential encoded pair of binary symbols, $(d_{1,i}\ \ d_{2,i})$. This process produces two sequences $\{d_{1,i}\}$ and $\{d_{2,i}\}$ which are Gray coded (Table 3.1) to give two output sequences $\{q_{1,i}\}$ and $\{q_{2,i}\}$, where $q_{j,i} = \pm 1$ for $j = 1,2$. Since each pair of the transmitted symbols represents a possible phase value received at the detector (Eqn. 3.1.9), this process actually produces the transmitted symbols which are the phase changes, rather than the absolute phases, of the data symbols to be received at the detector. The sampling, filtering and modulation processes following this are exactly the same as they are described in the QPSK system.

Assume that the transmission channel is the same as the one used in the QPSK system described before. Assume also that the receiver provides the ideal required timing signal, so that the baseband signal components at the demodulator output are sampled, at time instants $\{iT\}$, to give two sequences $\{r_{1,i}\}$ and $\{r_{2,i}\}$ which are threshold detected and Gray decoded to produce two binary sequences $(\hat{d}_{1,i}\ \ \hat{d}_{2,i})$. At the time instants $\{iT\}$, each pair of symbols $(\hat{d}_{1,i}\ \ \hat{d}_{2,i})$ represents a 2-bit binary value. The differential decoded pair of binary symbols, $(\hat{u}_{1,i}\ \ \hat{u}_{2,i})$ is obtained by subtracting from the binary values of the present pair of symbols $(\hat{d}_{1,i}\ \ \hat{d}_{2,i})$ the

binary values of the previous pair, $(\hat{d}_{1,i-1} \quad \hat{d}_{2,i-1})$, and the difference is expressed modulo-4. (An arbitrary initial pair of binary symbols may be assumed). The sequence of the binary-data symbols $\{\hat{s}_i\}$ is obtained using a P/S (parallel-to-serial) converter.

3.1.3 Coherent offset quaternary phase-shift keying (OQPSK) systems

A block diagram of an offset quaternary phase-shift keying (OQPSK) system is shown in Fig. 3.5. The block diagram of this system is very similar to conventional QPSK just described. The difference lies in the two binary sequences $\{u_{1,i}\}$ and $\{u_{2,i}\}$, as they enter the Gray coder. The incoming data stream is applied to a S/P (serial-to-parallel) converter. The S/P converts the incoming sequence $\{s_i\}$ into two sequences of binary symbols $\{u_{1,i}\}$ and $\{u_{2,i}\}$, one of them, the binary sequence $\{u_{2,i}\}$ in the case shown in Fig. 3.5, is then offset with respect to the other by delaying it by an amount equal to the incoming signal bit duration, $T_b = T_s/2$. This results in the relationship between the $\{u_{1,i}\}$ and $\{u_{2,i}\}$ and the input data $\{s_i\}$ shown in Fig. 3.6. The resulting instantaneous phase states at the modulator output are the same as for QPSK [28] [29]. As for QPSK these two sequences are Gray coded according to Table 3.1, and the resulting sequences are fed into the modulation filter and then into quadrature modulator. However, because both data streams applied to the quadrature modulator can never be in transition simultaneously, only one of the vectors that comprise the offset quadriphase modulator output signal can change at any one time. The result is that only $\pi/2$ phase transitions occur in the modulator output signals.

Like QPSK, an unfiltered offset QPSK signal has a constant-amplitude. However for filtered OQPSK signals, the result is a maximum amplitude variation of 3 dB (70%) compared to the 100% amplitude variation for conventional QPSK. This low-amplitude envelope variation imparts certain advantage to OQPSK as compared to QPSK [25]. Offset QPSK has been studied intensively over the last years for applications in digital satellite communications. Though OQPSK shows a better performance over nonlinear channels than QPSK [27].

The receiver shown in Fig. 3.5 is identical to that shown in Fig. 3.1 for QPSK, with the exception that the regenerated binary sequence $\{\hat{u}_{1,i}\}$ is delayed by a unit bit duration $T_b = T_s/2$, so that when combined with the regenerated $\{\hat{u}_{2,i}\}$, the data sequence $\{\hat{s}_i\}$ is recreated by using a P/S (parallel-to-serial) converter. Of course, this is subject to error because of the effects of noise and filtering. In the absence of noise, the $\{\hat{s}_i\}$ are the same as the $\{s_i\}$.

3.2 Error probability performances of coherent QPSK, DEQPSK and OQPSK signals

3.2.1 QPSK signals

In Section 2.2, it is shown that, the optimum filtering arrangement of a baseband data-transmission system is the filtering which is shared equally between the transmitter and the receiver filters and with a sinusoidal roll-off frequency response. Under these conditions and if binary antipodal signals are used, the bit error probability is given by $Q(\sqrt{2E_b/N_0})$ (Eqn. 2.2.15), where $2E_b/N_0$ is the ratio of the average transmitted energy per bit to the two-sided noise power spectral density at the input to the receiver.

The QPSK system, described in Section 3.1.1, has the filtering shared equally between the transmitter and receiver filters and with a sinusoidal roll-off frequency response, and so is the optimum filtering arrangement for baseband data transmission. However since the demodulation process does not alter the signal/noise power ratio (Section 3.1.1), the filtering arrangement is also optimum for a bandpass data transmission system; the inphase and quadrature channels, each carrying binary antipodal signals, are orthogonal and they can be demodulated independently of each other, so each of the two channels can be treated independently; hence, the bit error probability of each of the inphase and quadrature channels should also be equal to $Q(\sqrt{2E_b/N_0})$.

Denoting the bit error probability in the inphase channel as P_{eI} and in the quadrature channel as P_{eQ}, the symbol error probability is therefore

$$P_{eS} = 1-(1-P_{eI})(1-P_{eQ})$$

$$= P_{eI} + P_{eQ} - P_{eI}P_{eQ} \qquad 3.2.1$$

Since $P_{eI} = P_{eQ}$, and they are typical small quantities ($< 10^{-2}$) in practice, a good approximation for the overall symbol error probability is

$$P_{eS} \approx P_{eI} + P_{eQ} = 2P_{eI} = 2P_{eQ} \qquad 3.2.2$$

The bit error probability of an individual channel is

$$P_{eI} = P_{eQ} = Q(\sqrt{2E_b/N_0}) \qquad 3.2.3$$

so the symbol error probability is

$$P_{eS} = 2P_{el} = 2Q(\sqrt{2E_b/N_0}) \qquad 3.2.4$$

The Gray-coded and non-Gray-coded cases are shown in Table 3.2. In the Gray-coded constellation case, adjacent symbols differs by only one bit, whereas in the non-Gray-coded case, the adjacent symbols differs by one or by two bits. With AWGN, by far the most likely error in the detection of a symbol is that which involves the crossing of the nearest decision threshold. Thus the bit error rate of an ideal Gray-coded QPSK system approximately equals to one-half of its symbol error rate, i.e.,

$$P_e = \frac{1}{2} P_{eS} = Q(\sqrt{2E_b/N_0}) \qquad 3.2.5$$

A more vigorous analysis of the P_e and P_{eS} relationship is presented in [16].

3.2.2 DEQPSK and OQPSK signals

In a differentially encoded coherent QPSK system (DEQPSK), the differentially decoding process at the receiver is carried out after the detection process. During differential decoding, error multiplication by a factor of 2 occurs. Thus the bit error rate of the Gray-coded DEQPSK signal is (Eqn. 3.2.5)

$$P_{e(DEQPSK)} = 2P_{e(QPSK)} = 2Q(\sqrt{2E_b/N_0}) \qquad 3.2.6$$

The fundamental difference between coherent QPSK and OQPSK systems lies in the presence or absence of the T_b-second offset delay element (Fig. 3.5 and Fig. 3.6). As the inphase and quadrature channels are orthogonal and independent at the sampling instant, the insertion of a delay element into the offset QPSK system does not affect the performance of the coherent QPSK system. Thus the P_e performance of the OQPSK system is described by

$$P_{e(OQPSK)} = Q(\sqrt{2E_b/N_0}) \qquad 3.2.7$$

Equations 3.2.5, 3.2.6, and 3.2.7 are the theoretical error-rate performances of the QPSK, DEQPSK, and OQPSK systems transmitting signals over an optimum data-transmission channel where only AWGN is added. In any practical satellite links, there are many other factors, such as HPA distortion, etc., which affect the performances of the systems. Since these factors are too difficult to use mathematical

expressions to analyse, their effects on error-rate performances require complex computer simulations. Because computer simulations are more easily carried out on the baseband models with the use of a digital computer, the baseband equivalent models of the different systems are modelled digitally as described in the following sections.

3.3 Baseband equivalent model of DEQPSK system, for computer simulation

The DEQPSK system considered here operates at a speed of 64, 128 or 256 Kbit/s over a satellite link. Since DEQPSK signals use a quadrature modulation technique (Section 2.6), the system can be greatly simplified by assigning real values to the signal in one of the two parallel channels (that associated with $\sqrt{2}\cos\omega_c t$) and imaginary values to the signals in the other channel (that associated with $-\sqrt{2}\sin\omega_c t$), and then considering the linear modulator, the transmitter IF filter, the HPA, the receiver IF filter and the linear demodulator, as a baseband transmission path carrying complex-valued signals (Section 2.6). The resultant baseband equivalent model of the DEQPSK system, with the baseband equivalent model of the bandpass channel will be either (as shown in Fig. 2.14) a linear and memoryless, a linear and bandlimited, or a nonlinear and bandlimited satellite channel. For computer simulation used in this thesis, the baseband equivalent model of the bandpass channel will be a nonlinear and bandlimited channel and is shown in Fig. 3.8. The information to be transmitted is carried by the sequence of binary data-symbols $\{s_i\}$, where the $\{s_i\}$ are taken to be statistically independent and equally likely to be either 0 or 1. The encoded symbols $\{q_i\}$ are obtained from the $\{s_i\}$, by the encoder, after being differentially encoded and Gray-code. The i^{th} symbol has the value $q_i = \pm 1 \pm j$, where $j = \sqrt{-1}$, the $\{q_i\}$, of course, being statistically independent and equally likely to have any of the four possible values. Each q_i is a quaternary signal element. The sequence $\{q_i\}$ is used to form the sequence of impulses $\{\sum_i q_i \delta(t - iT)\}$, at the input of the modulation filter. The signal waveform at the output of the filter is the complex-valued baseband signal

$$u(t) = \sum_i q_i h_t(t - iT) \qquad 3.3.1$$

where $h_t(t)$ is the impulse response of the modulation filter, and at any given value of t, is real (Section 2.4.1).

Since a digital computer is used to do the simulation tests, the transmission system is modelled digitally for simulation. The continuous waveforms in the system are modelled as discrete waveforms. So the complex-valued waveform $u(t)$ is sampled, at the time instants $\{mT_s\}$ (8 times per symbol), where $T = 8T_s$, to give the sequence $\{u_m\}$, where $u_m = u(mT_s)$ has a complex value. The $\{u_m\}$ are then fed to a baseband equivalent model of the bandpass channel. Three different bandpass channels, as shown in Fig. 2.14, are considered here. They are linear and memoryless, linear and bandlimited and nonlinear and bandlimited channels.

The linear and memoryless channel does not distort the signal, but only adds the Gaussian noise samples to the signal samples. So at time $t = mT_s$, the signal sample at the channel output is

$$w_m = u_m + n_m \qquad 3.3.2$$

where w_m, u_m and n_m all have complex values. The real and imaginary parts of all noise samples are taken to be statistically independent Gaussian random variables with zero mean and fixed variance σ^2 (which will be discussed later).

In a linear and bandlimited channel the signal is filtered by the baseband equivalent model of the transmitter IF filter. The sampled impulse responses of the baseband equivalent models of the transmitter and receiver IF filters, sampled at $1/T_s$ samples per second, are given by the $(g+1)$-component vector

$$F = [f_0 \ f_1 \ f_2 \ \ldots\ldots \ f_g] \qquad 3.3.3$$

where the $\{f_m\}$, for $0 \le m \le g$, have real valued components, as shown in Table 2.2, and $f_m = f(mT_s)$. The signal at the output of the filter is sampled at the time instants $\{mT_s\}$. So at time $t = mT_s$, the signal sample is

$$e_m = \sum_{h=0}^{g} u_{m-h} f_h \qquad 3.3.4$$

where e_m has a complex value. After adding the noise component, the sample becomes

$$y_m = e_m + n_m \qquad 3.3.5$$

where y_m also has a complex value. The sequence of $\{y_m\}$ is fed into the receiver IF filter which is modelled as a digital filter, with a sampling rate $1/T_s$ samples per second, and which produces at the output, at time $t = mT_s$, the sample

$$w_m = \sum_{h=0}^{g} y_{m-h} f_h \qquad 3.3.6$$

where w_m has a complex value.

For a nonlinear and bandlimited channel the $\{u_m\}$ are first filtered by the transmitter IF filter, as described before, to produce at its output, at time $t = mT_s$, the signal sample (Eqn. 3.3.4)

$$e_m = \sum_{h=0}^{g} u_{m-h} f_h \qquad 3.3.7$$

where e_m has a complex value, which is then nonlinearly distorted by the HPA. After adding the noise sample, the sample at the input of the receiver IF filter becomes (Eqn. 2.5.30)

$$z_m = e_m M_c G(\hat{A}_m) + n_m \qquad 3.3.8$$

where z_m, e_m and n_m all have complex values, $G(\hat{A}_m)$ is the conversion function of the baseband equivalent model of the HPA, M_c is the HPA backoff factor, and $\hat{A}_m$ is the one of the values $\{\lambda_n\}$ (Table 2.3) closest to the input signal envelope $|e_m M_c|$. The $\{z_m\}$ are fed into the receiver IF filter, at time $t = mT_s$, which produces the signal sample

$$w_m = \sum_{h=0}^{g} z_{m-h} f_h \qquad 3.3.9$$

In all these three cases, the sampled signal $\{w_m\}$ (given by Eqn. 3.3.2, 3.3.6 and 3.3.9) from the baseband equivalent models of the bandpass channels are filtered by the demodulation filter, sampled at the rate of $1/T_s$ samples per second, is given by the $(n+1)$-component vector

$$p = [\ p_0\ \ p_1\ \ p_2\ \ \ldots\ldots\ p_n\ ] \qquad 3.3.10$$

where the $\{p_m\}$, for $0 \le m \le n$, have real-valued components (Table 2.1), and $p_m = p(mT_s)$. Thus, at time $t = mT_s$, the signal sample at the output of the demodulation filter is

$$r_m = \sum_{h=0}^{n} w_{m-h} p_h \qquad 3.3.11$$

where r_m has a complex value. Assume that the receiver provides the required ideal timing signal. So that the sequence $\{r_m\}$ is sampled once per symbol, at time instants $\{iT\}$, to give the sequence $\{r_i\}$ which are detected and then decoded into the sequence of binary data-symbols $\{\hat{s}_i\}$.

Since the bit-energy-to-noise power spectral density ratio at the input to the receiver is always used for comparison of performances of different systems, we must now determine the two-sided power spectral density at the input to the receiver under the assumed conditions. The noise samples $\{n_m\}$ in Eqns. 3.3.2, 3.3.5 and 3.3.8 are assumed to have variance σ^2. It is shown in Appendix A8 that, under these assumed conditions, the two-sided noise power spectral density at the input to the receiver is (Eqn. A8.10 or A8.11)

$$\frac{N_0}{2} = \frac{\sigma^2 T}{k} \qquad 3.3.12$$

where k/T is the sampling rate used in the simulation tests. Equation 3.3.12 relates the two-sided noise power spectral density to the sampling rate used in the simulation tests. The sampling rate must be greater than twice the signal bandwidth to prevent alaising.

To calculate $2E_b/N_0$ value, i.e., signal/noise power ratio or bit energy-to-noise power spectral density ratio value, in a simulation test, the average energy per sample of the transmitted signal is first measured (bearing in mind that the channel introduces no attenuation) by transmitting a few thousand symbols and using the equation (Eqn. A8.15)

$$\text{Average energy/sample} \qquad P_a = \frac{1}{kL} \sum_{m=1}^{kL} |S_m|^2 \qquad 3.3.13$$

where k: number of samples taken per T seconds in the simulation test (i.e., k=8 for the present case).

L: number of transmitted symbols in the test,

and $|S_m|$: amplitude of the m^{th} sample in the transmitted signal, i.e., $|u_m|$, $|e_m|$, or $|e_m M_c G(\hat{A}_m)|$, as can be seen in Eqns. 3.3.2, 3.3.4 and 3.3.8, respectively, depending on which of the bandpass channels is used.

The value of the noise variance σ^2 for any required value of $2E_b/N_0$, under the assumed conditions, is then computed using equation (Eqn. A8.21)

$$\sigma^2 = \frac{N_0 P_a k}{4E_b} \qquad 3.3.14$$

The Gaussian random number generator in the computer is used to generate the inphase and quadrature noise samples with zero mean and fixed variance σ^2.

After computing the value of σ^2 for the required value of $2E_b/N_0$, the test is then carried out again with a large number of symbols to find the probability of error, P_e, at the given value of $2E_b/N_0$. At the end of the test, the value of P_a (average energy per sample) is computed again, and the value of $2E_b/N_0$ are checked using the equation (Eqn. A8.20)

$$\frac{2E_b}{N_0} = \frac{P_a k}{2\sigma^2} \qquad 3.3.15$$

to make sure it has the correct value.

Therefore, all the simulation tests, discussed in this thesis, are carried out in the sampled time domain by generating large numbers of binary data-symbols, encoding them, convolving them with the sampled impulse responses of the various filters in the baseband equivalent model, detecting and decoding them. The sampling rate is 8 samples per symbol.

It is shown in Appendix 8 that, when a continuous waveform is sampled at $1/T_s$ samples per second to produce the sampled signal, the latter must be scaled by the sampling interval T_s, in order to have the same signal energy level. However, the scaling factor is, for convenience, omitted here. This does not affect the signal/noise power ratio of the systems tested, because the signal and noise energy levels are measured at the same point, thus the scaling factors cancel each other.

3.4 Power spectra of QPSK, DEQPSK and OQPSK signals

In the QPSK system described in Section 3.1.1, the lowpass filtering is shared equally between the transmitter and receiver filters and with a sinusoidal roll-off frequency response. If the input data are random and equiprobable, the power spectra of the inphase and quadrature baseband signals at the modulation filter output have

the same shape as the transfer function of the modulation filter. The modulation process, (i.e., multiplying the inphase and quadrature baseband signals by the carrier signal components $\sqrt{2}\cos\omega_c t$ and $-\sqrt{2}\sin\omega_c t$, respectively) shifts the spectra by ω_c rad/s in the frequency domain from baseband to bandpass. When these signals are added linearly in the time domain to form the QPSK signal, the shapes of the individual spectra are not altered (this can be seen from the linearity property of the Fourier transform). So if the bandpass channel is linear and memoryless (i.e., it does not distort the signals) and the carrier frequency is high enough to prevent aliasing, the power spectrum of the transmitted bandpass signal (i.e., the sum of the inphase and quadrature signals) has the shape same as the baseband signals power spectra which are shaped solely by the modulation filter.

The differential encoding process in DEQPSK systems and offset QPSK systems do not alter the shapes of the spectra, so if the same transmitter filtering is used, DEQPSK and OQPSK signals will have the same signal power spectra as those of QPSK signals.

3.5 Spectral estimation of QPSK, DEQPSK and OQPSK signals by computer simulation

A good method of estimating the power spectral density of a modulated signal is by computer simulation. This method is quite straightforward and general [22]. A pseudorandom data sequence is generated, and the modulation process is produced digitally. Since the signal has a certain bandwidth, the sampling rate must be high in order to prevent alaising. Suppose there are k samples and the DFT (Discrete Fourier Transform) of sampled signal is $X_k(f)$. The power spectrum of the latter is estimated as [22]

$$S(f)=\frac{1}{k}\left|X_k(f)\right|^2 \qquad 3.5.1$$

The shape of the spectrum is concerned here, so the factor $1/k$ can be neglected. Provided the sequence is suitably long and random, $S(f)$ will approach the exact signal spectrum. In order to get a good smooth estimation, it is need to average over a number of data sequence of several hundred symbols. Even so, considerable spectral variance remains, and small bias may remain. The variance can be reduced by a smoothing window, e.g., Turkey or Barttett, though this will increase the bias and spectrum resolution [23], [24], [30].

The baseband equivalent model, used for spectral estimation of the transmitted QPSK signal, is shown in Fig. 3.9. The spectra of the sampled signals are estimated at the output of the HPA with the effects of the modulation filter, the transmitter IF

filter and the spectral spreading of the sampled caused by the HPA, for systems operating over a nonlinear satellite channel. The spectral estimation methods for this signal is described as follows.

The spectrum at the output of the modulation filter can be estimated as follows, a sequence of L quaternary data-symbols $\{q_i\}$ are generated where $q_i = \pm 1 \pm j$ and $j = \sqrt{-1}$. The $\{q_i\}$ being statistically independent and equally likely to have any of the four possible values. The sequence $\{q_i\}$ is sampled at the time instants $\{iT\}$ and used to form the sequence of impulses $\{\sum_i q_i \delta(t - iT)\}$ which are fed into the modulation filter. The signal at the filter output is the complex-valued waveform

$$u(t) = \sum_{i}^{L} q_i h_t (t - iT) \qquad 3.5.2$$

with $h_t(t)$ the impulse response of the modulation filter. The waveform $u(t)$ is sampled, at time instants $\{mT_s\}$ (8 times per symbol), where $T_s = T/8$ and T is the symbol duration, to give the signal sequence $\{u_m\}$, with $u_m = u(mT_s)$.

The sample values $\{u_m\}$ are further filtered by the baseband equivalent model of the transmitter IF filter. The sampled impulse response of the baseband equivalent model of the transmitter IF filter, sampled at the rate of $1/T_s$ samples per second, is given by the $(g+1)$-component vector

$$F = [f_0 \; f_1 \; f_2 \; ..... \; f_g] \qquad 3.5.3$$

where the $\{f_m\}$, for $0 \le m \le g$, have real-valued components (Table 2.2), so that at time $t = mT_s$, the signal sample at the IF filter output is

$$e_m = \sum_{h=0}^{g} u_{m-h} f_h \qquad 3.5.4$$

The sample values $\{e_m\}$ are nonlinearly distorted by the HPA, so that at time $t = mT_s$, the signal sample at the output of the HPA is (Eqn. 2.5.30)

$$z_m = e_m M_c G(\hat{A}_m) \qquad 3.5.5$$

where $G(\hat{A}_m)$ is the conversion function of the baseband equivalent model of the HPA, M_c is the HPA backoff factor, and $\hat{A}_m$ is the one of the values $\{\lambda_n\}$ (Table 2.3) closest to the input signal envelope $|e_m M_c|$.

The FFT (Fast Fourier Transform) routine in the computer is used to evaluate the Fourier transform. Since the routine runs faster if the number of samples is a power of 2 (NAGF computer manual), the number of elements, in the resultant sequence $\{z_m\}$, is arranged to be $2^{10} = 1024$. Since the $\{u_m\}$, $\{e_m\}$ and $\{z_m\}$ have complex values, the amplitude spectra of the real and imaginary components of these signals, representing the spectra of the inphase and quadrature signals, respectively, are computed spearately by means of FFT and then added to form the amplitude spectrum of the QPSK signals. The 1024 samples are reduced to 128 samples by averaging every 8 samples. In order to obtain a good estimate of the amplitude spectrum of the sampled signal, the same procedure is repeated for 100 different sequence of data-symbols $\{q_i\}$ and then averaged. The signal power spectral density of the sampled signal in dB is then obtained by taking the function $20\log_{10}(*)$ on each of these 128 sample values.

Since if the same filtering are used, DEQPSK and OQPSK signals will have the same spectra as those of QPSK signals and do not modify the power spectral density.

3.6 Simulation results and discussion

Computer simulation tests have been carried out on different systems, using DEQPSK and OQPSK signals, to assess the error-rate performances, under different conditions, with the equipment filters and HPA described in Section 2.5. The simulation model and methods are described in Sections 3.3, 3.4 and 3.5. In all simulation tests, it is assumed that the receiver provides the required ideal carrier and timing signals, and the data-transmission systems are optimised by sharing the overall filtering equally between the transmitter and receiver filters.

3.6.1 Performances of DEQPSK signals, with different truncation lengths of the sampled impulse responses of the modulation and demodulation filters

This section studies the minimum truncation length (number of taps) of the sampled impulse responses of the modulation and demodulation filters (Section 2.4.1) required to approximate to the ideal error-rate performances of the signals in the practical region, i.e., $P_e = 10^{-3} - 10^{-4}$. The simulation model used to evaluate the error-rate performance is shown in Fig. 3.8, where the nonlinear and bandlimited channel is used. Different truncation lengths (number of taps) of sampled impulse responses for different values of α (roll-off factor) are used as the sampled impulse responses of the modulation and demodulation filters. The effects of different values of α (roll-off factor) on the performance are shown in Fig. 3.10.

With $\alpha = 25\%$, Fig. 3.10a shows that, the minimum truncation length of the sampled impulse responses required for the modulation and demodulation filters to

approximate to the theoretical ideal error-rate performance, at $P_e \leq 10^{-4}$, is $8T$ (64 taps). With $\alpha = 40\%$, the results in Fig. 3.10b show that, the required minimum truncation length to approximate to the theoretical ideal error-rate performance, at $P_e \leq 10^{-4}$, is $5T$ (40 taps). Whereas, with $\alpha = 100\%$, Fig. 3.10c shows that the required minimum truncation length is $5T$ (40 taps).

Table 3.4 shows that the degradation in tolerance to noise of DEQPSK signals with different truncation lengths, at $P_e = 10^{-4}$, in comparison with that of an ideal DEQPSK system. This degradation is due to ISI caused by not using enough of the sampled impulse responses of the modulation and demodulation filters, and the effect of nonlinearity of the HPA. It can be seen, in Fig. 3.10, that these degradations get larger at low error rates where ISI is the dominated factor causing errors.

The results indicate that the minimum truncation lengths of the sampled impulse responses of the modulation and demodulation filters, with $\alpha = 100\%$, 40% and 25% required to approximate to the theoretical ideal error-rate performance at $P_e = 10^{-4}$ are 5T, 5T and 8T, respectively.

3.6.2 Performances of DEQPSK signals over a nonlinear and bandlimited channel

In any practical satellite system, the signal from the modulator at the transmitter is always further bandlimited by the IF filter before being up-converted to a microwave frequency, and at the receiver, a receiver IF filter, having the same characteristics as the transmitter IF filter, is always used to select the lower sideband of the desired down-converted signal. Since these IF filters are narrowband, they may also introduce ISI into the signal.

In a nonlinear and bandlimited bandpass channel, the HPA at the earth station is operating in the nonlinear mode for high power efficiency. This introduces AM-AM and AM-PM conversion effects of the transmitted signal. These effects degrade the tolerance to noise of the system, because the signal is nonlinearly distorted.

When the signal is nonlinearly distorted, the receiver filters no longer match the received signal, and inevitably degrade the performance. The simulation model, used to evaluate the effects of nonlinear distortion on the error-rate performance, is shown in Fig. 3.8, where the nonlinear and bandlimited bandpass channel is used.

The DEQPSK signal, with $\alpha = 100\%$ and a truncation length of $5T$ (40 taps) has been chosen for the evaluation, and is known here as signal 1A. With $\alpha = 40\%$, a signal with a truncation length of $5T$ (40 taps) is long enough to bandlimit the signal. This signal, is known here as signal 2A. With $\alpha = 25\%$ the signal with a truncation length of $8T$ (64 taps) has been chosen. This signal, is known here as signal 3A.

The error-rate performances for signals 1A, 2A and 3A transmitted over the nonlinear and bandlimited channel, are shown in Figs. 3.11, 3.12 and 3.13, with the HPA here operates at 0, 0.315 or 0.7 dB output backoff respectively.

With the HPA operating at 0 dB OBO (output backoff) (i.e., at saturation point), Fig. 3.11 shows that, of these signals, signal 3A ($\alpha = 25\%$) suffers the largest degradation in tolerance to noise (about 2.6 dB at $P_e = 10^{-4}$) because of its relatively narrow bandwidth, which causes more severe fluctuations in the timing waveform (Fig. 2.8). Thus more nonlinear distortion is caused by the HPA.

With the HPA operating at 0.315 dB OBO (i.e., slightly below saturation), Fig. 3.12 shows that the degradation in tolerance to noise of signals 1A, 2A and 3A remains the same as those with 0 dB HPA OBO, at $P_e \geq 10^{-4}$, whereas signal 3A has reduced the degradation to about 2.3 dB (i.e., 0.3 dB improvement is achieved).

Figure 3.13 shows that, with the HPA OBO value further increased to 0.7 dB, the degradation in tolerance to noise of signals 1A, 2A and 3A, at $P_e \geq 10^{-4}$ little improvement in error-rate performances of signals 1A and 2A has been achieved in comparison with those with the HPA operating at 0 dB OBO, and the further improvement in error-rate performance of signal 3A is insignificant.

Figures 3.14, 3.15 and 3.16 show the error-rate performances for signals 1A, 2A and 3A respectively, with the HPA OBO operating at 0, 0.315 or 0.7 dB for each of the signals. The results show that the degradations in tolerance to noise of the signals decreases when the HPA operating point is further below saturation (i.e., 0.7 dB OBO).

Figures 3.17, 3.18 and 3.19 show the power spectral densities of signals 1A, 2A and 3A, at the output of the HPA, with the HPA operating point at 0, 0.315 or 0.7 dB OBO.

The degradation in tolerance to noise of the signals, at $P_e = 10^{-4}$, is given in Table 3.5. It can be seen that, with the HPA operating at 0, 0.315 or 0.7 dB OBO, the P_e degradation of signals 1A and 2A, due to the nonlinear distortion effects, is insignificant (≤ 0.75 dB), at $P_e \geq 10^{-4}$, whereas, for signal 3A with 0 dB HPA OBO, the degradation in tolerance to noise is about 2.6 dB, at $P_e = 10^{-4}$, which can be reduced to about 2.3 dB by increasing the HPA OBO value from 0 dB to 0.315 dB. However, a further increase in the HPA OBO value does not give any signifficant improvement for signal 3A.

These results have shown that, under these conditions, for the present filters and HPA, the most cost effective arrangement is to use signal 1A ($\alpha = 100\%$) or 2A ($\alpha = 40\%$) and to operate the HPA slightly (say, e.g. 0.315 dB) below saturation. The degradation in tolerance to noise is about 0.6 dB, at $P_e = 10^{-4}$, in comparison with that of an ideal DEQPSK system.

3.6.3 Performances of OQPSK signals over a nonlinear and bandlimited channel

The simulation model, used to evaluate the effects of nonlinear distortion on the error-rate performance, is the same as the one used for DEQPSK signal and is shown in Fig. 3.8. The same signals 1A, 2A and 3A have been used for OQPSK system for the simulation tests.

The error-rate performances for signals 1A, 2A and 3A with OQPSK system, transmitted over the a nonlinear and bandlimited channel, are shown in Figs. 3.20, 3.21 and 3.22, respectively. The HPA here operates at 0, 0.315 or 0.7 dB OBO.

By comparing the results of OQPSK system with those of DEQPSK system when the HPA operating at 0, 0.315 or 0.7 dB OBO, it is shown that the same degradation in tolerance to noise can be seen for signals 1A and 2A, and signal 3A suffers the largest degradation in tolerance to noise.

The power spectral densities of signals 1A, 2A and 3A, at the output of the HPA for OQPSK system, and as it has been stated before is the same as for DEQPSK signal.

From these results and under these conditions, for the present filters and HPA, and as DEQPSK system, the most cost effective arrangement for OQPSK system is to use signal 1A or 2A and to operate the HPA slightly below saturation. As for DEQPSK system the degradation in tolerance to noise is about 0.6 dB, at $P_e = 10^{-4}$, in comparison with that of an ideal DEQPSK system.

$u_{1,i}$	$u_{2,i}$	$q_{1,i}$	$q_{2,i}$
0	0	+1	+1
0	1	+1	-1
1	0	-1	+1
1	1	-1	-1

Table 3.1 Gray coding.

Input data		Gray coded		Non-Gray coded	
$u_{1,i}$	$u_{2,i}$	$q_{1,i}$	$q_{2,i}$	$q_{1,i}$	$q_{2,i}$
0	0	+1	+1	+1	+1
0	1	+1	-1	-1	-1
1	0	-1	**+1**	**+1**	**-1**
1	1	-1	**-1**	**-1**	**+1**

Table 3.2 Comparison of Gray coded and non-Gray coded.

Received sample values		Detected sample values		Gray decoded values	
$r_{1,i}$	$r_{2,i}$	$\hat{r}_{1,i}$	$\hat{r}_{2,i}$	$u_{1,i}$	$u_{2,i}$
>0	>0	+1	+1	0	0
>0	<0	+1	-1	0	1
<0	>0	-1	+1	1	0
<0	<0	-1	-1	1	1

Table 3.3 Threshold detection and Gray decoding.

α =	Truncation length of			
	$4T$	$5T$	$6T$	$8T$
25%	-	-	2.3	1.4
40%	2.2	0.4	-	-
100%	0.2	0.1	-	-

Table 3.4 Degradations in tolerance to noise of DEQPSK signals, with different truncation lengths of the sampled impulse responses (Table 2.1) of the modulation and demodulation filters, with $\alpha = 100\%$, 40% and 25%, at $P_e = 10^{-4}$, expressed in dB, measured in comparison with that of an ideal DEQPSK system (from Fig. 3.10).

HPA OBO (in dB)	signal		
	1A	2A	3A
0	0.75	0.75	2.6
0.315	0.5	0.65	2.3
0.7	0.35	0.5	2.2

Table 3.5 Degradations in tolerance to noise of signals 1A, 2A and 3A over a nonlinear and bandlimited channel, with the HPA operating at 0, 0.315 and 0.7 dB OBO, at $P_e = 10^{-4}$, expressed in dB, measured in comparison with that of an ideal DEQPSK system (from Figs. 3.11, 3.12 and 3.13).

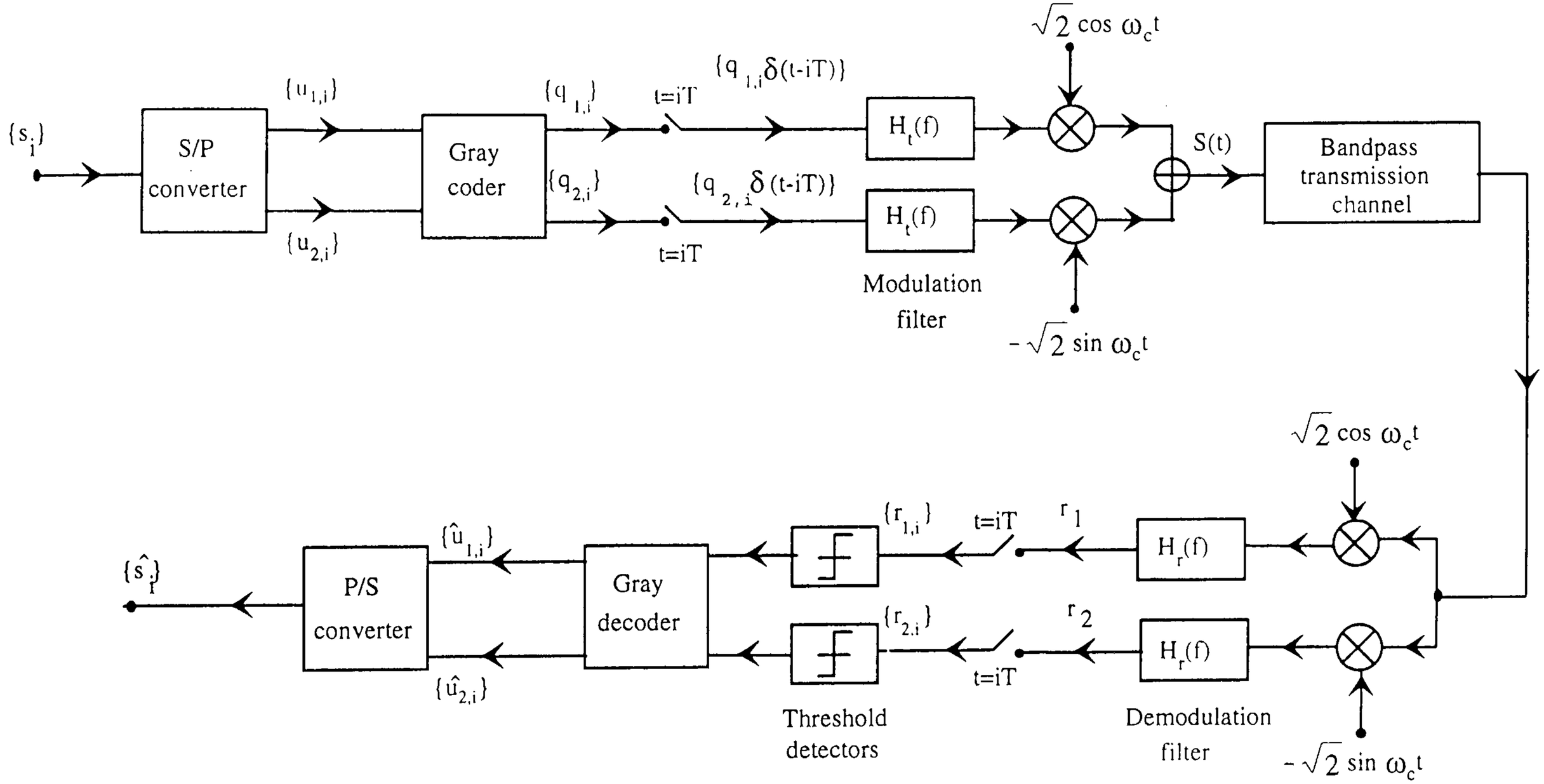

Figure 3.1 Block diagram of a conventional QPSK system representation.

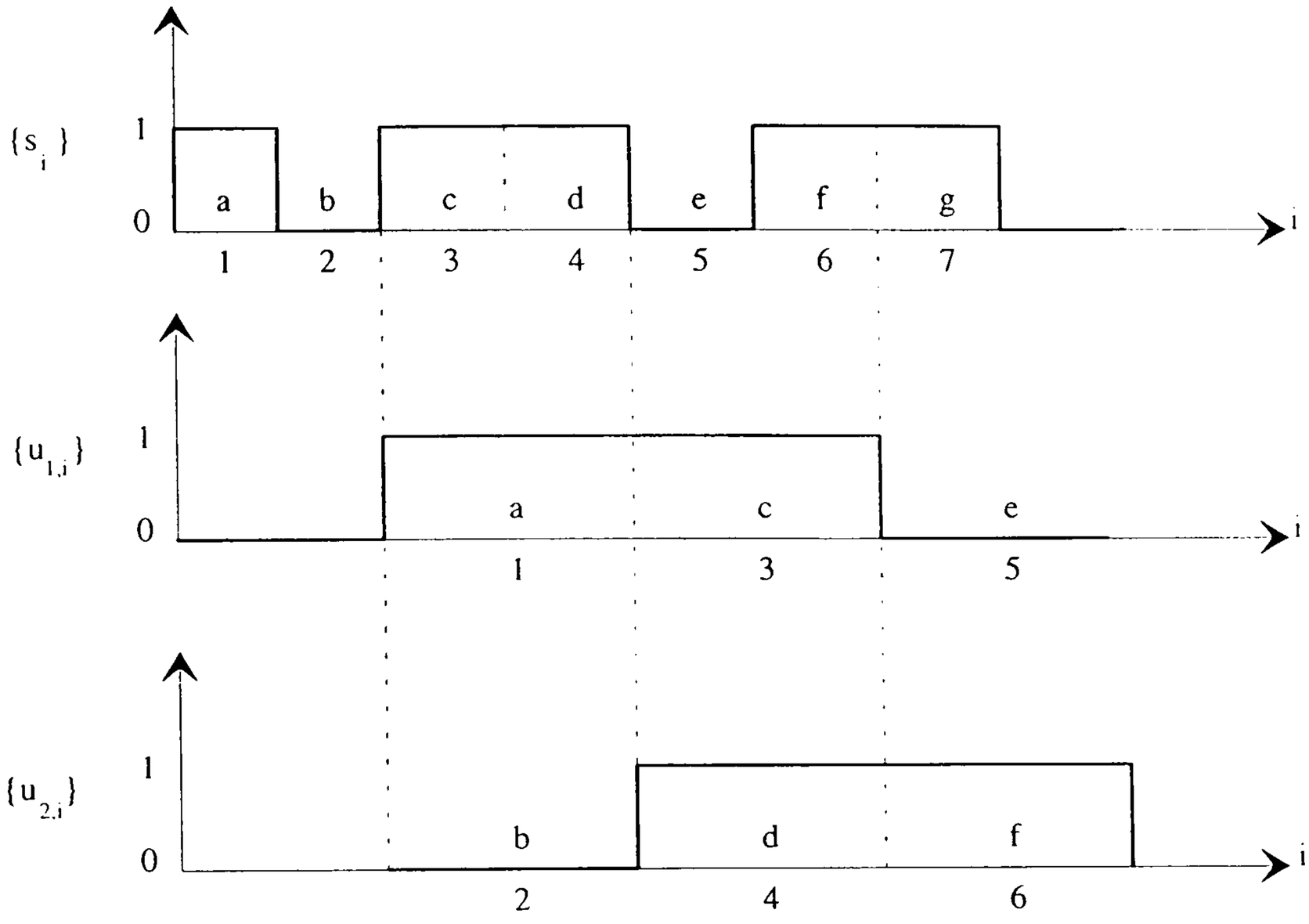

Figure 3.2 Relationship between input data sequence $\{s_i\}$ and the two binary sequences $\{u_{1,i}\}$ and $\{u_{2,i}\}$ for QPSK system.

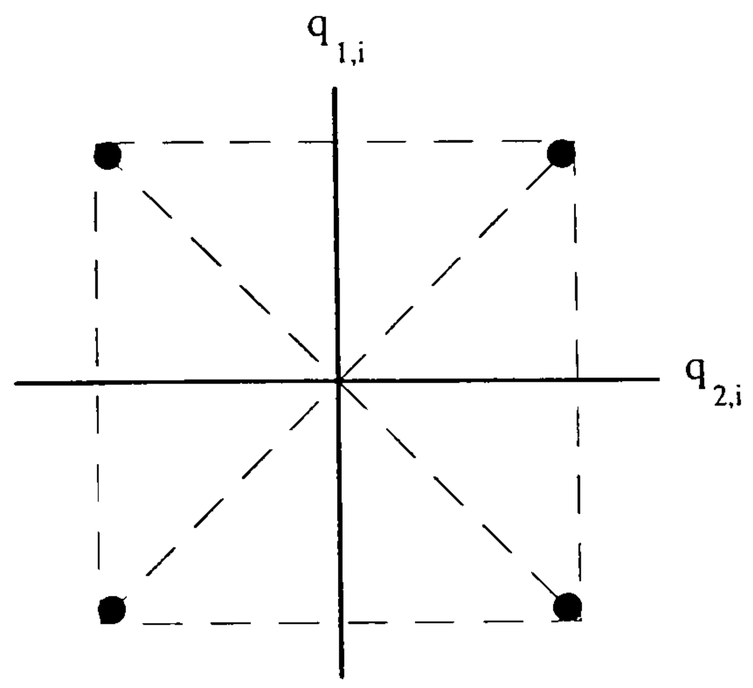

Figure 3.3 QPSK (or DEQPSK) signal constellation.

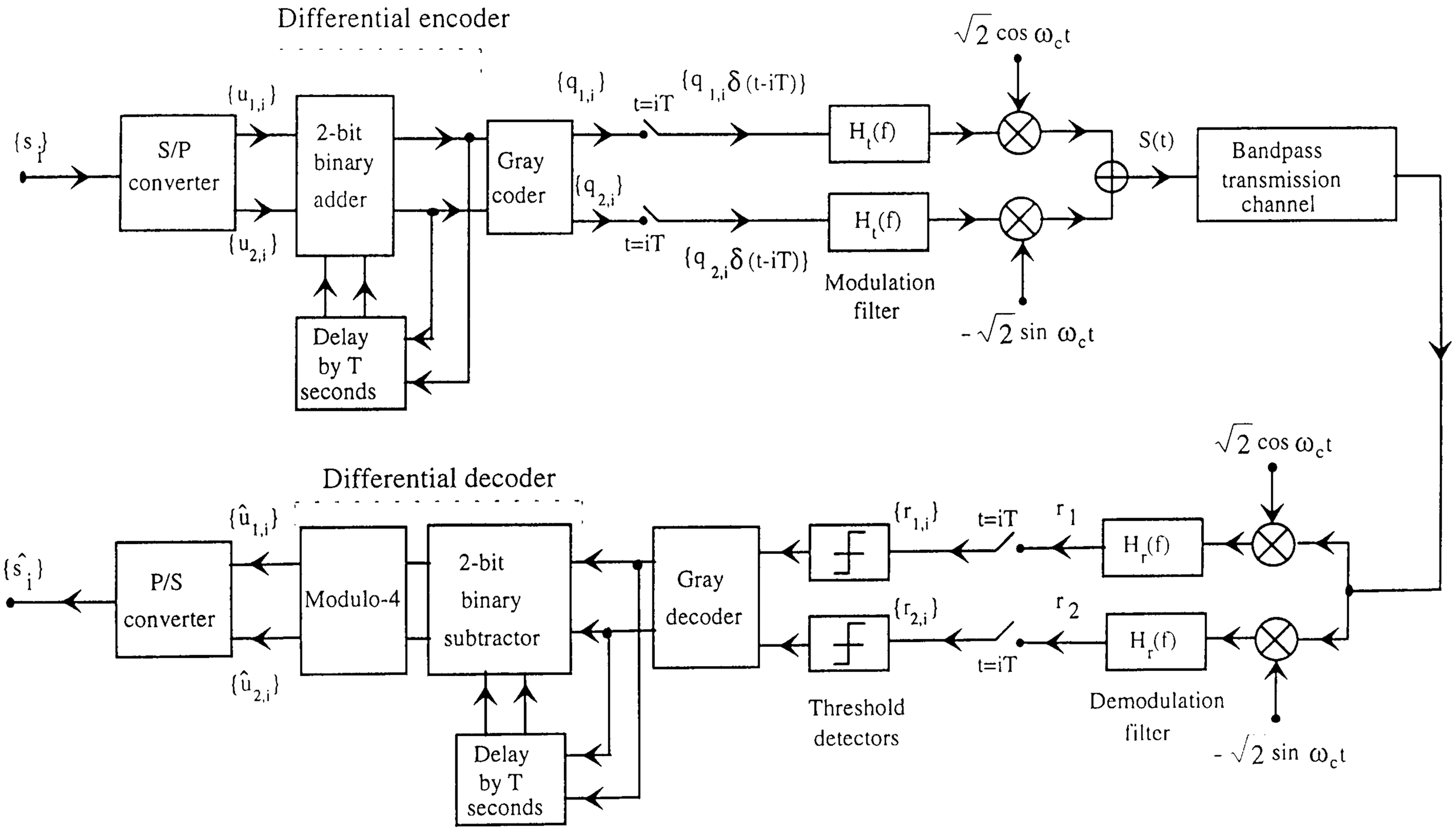

Figure 3.4 Block diagram of a conventional DEQPSK system representation.

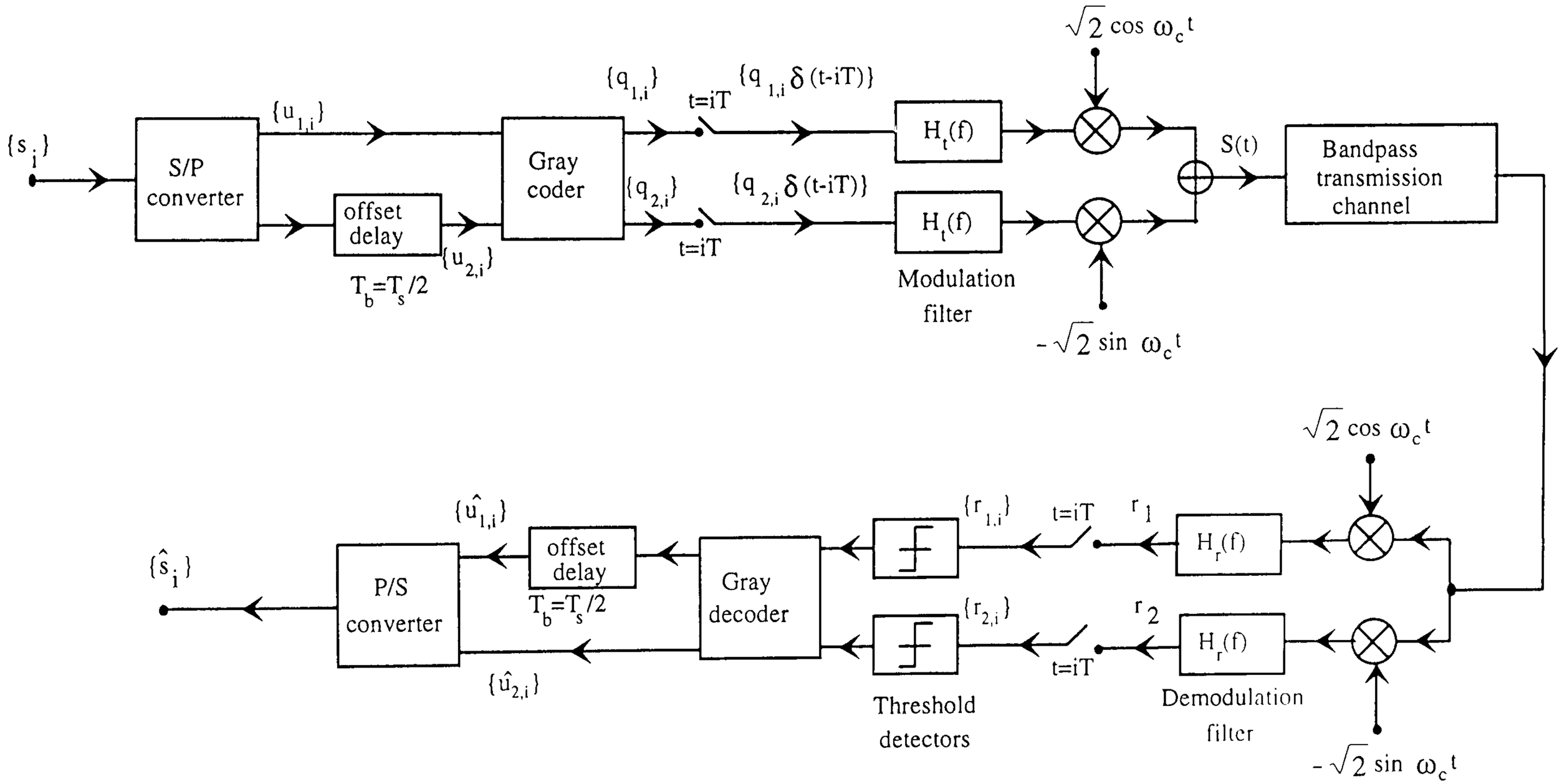

Figure 3.5 Block diagram of Offset QPSK system representation.

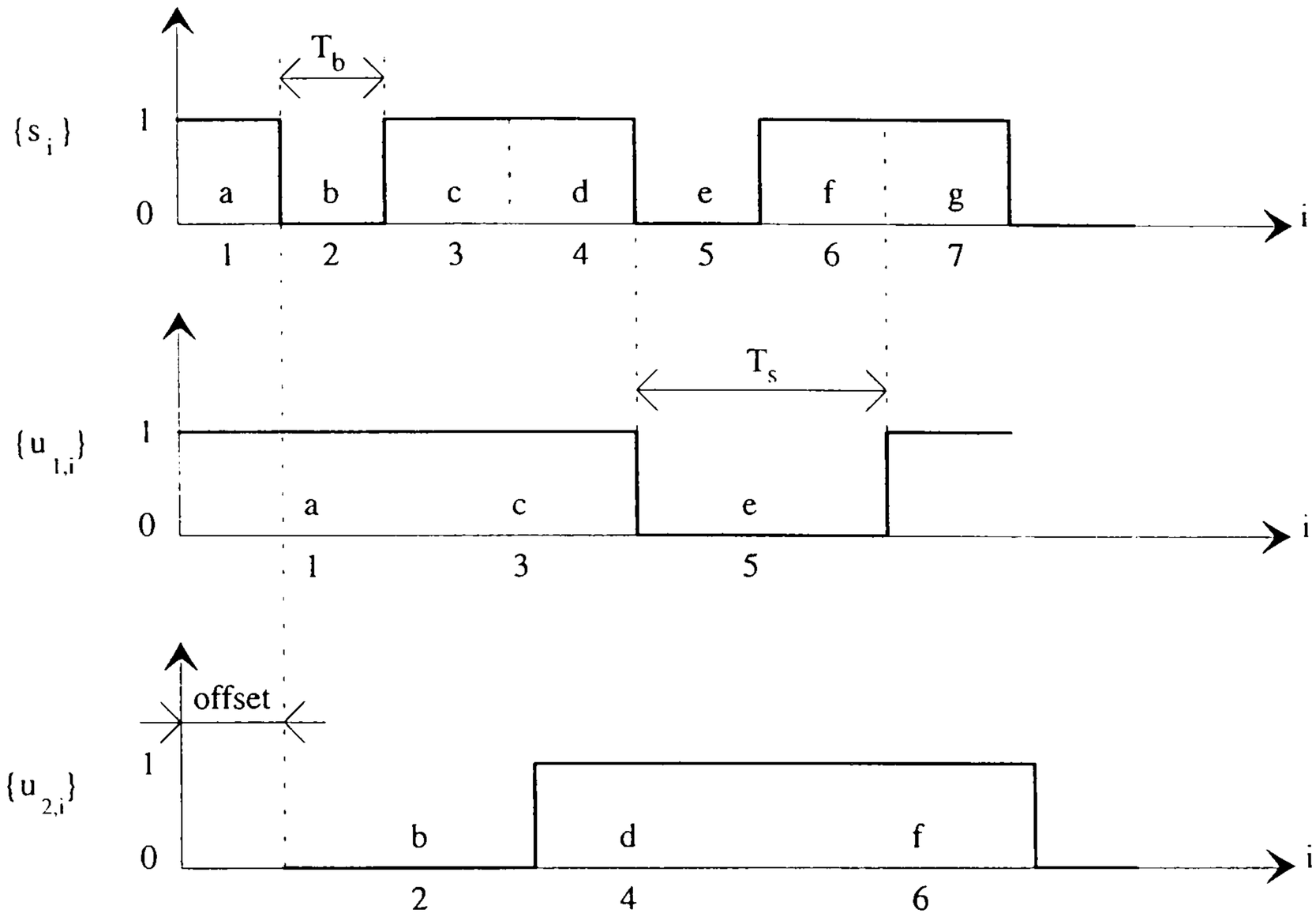

Figure 3.6 Relationship between input data sequence $\{s_i\}$ and the two binary sequences $\{u_{1,i}\}$ and $\{u_{2,i}\}$ for OQPSK system.

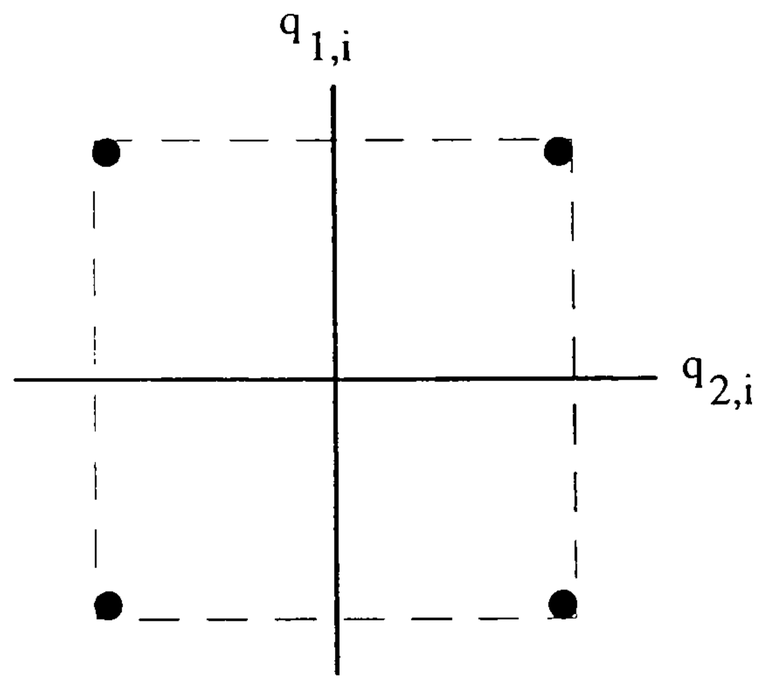

Figure 3.7 OQPSK signal constellation.

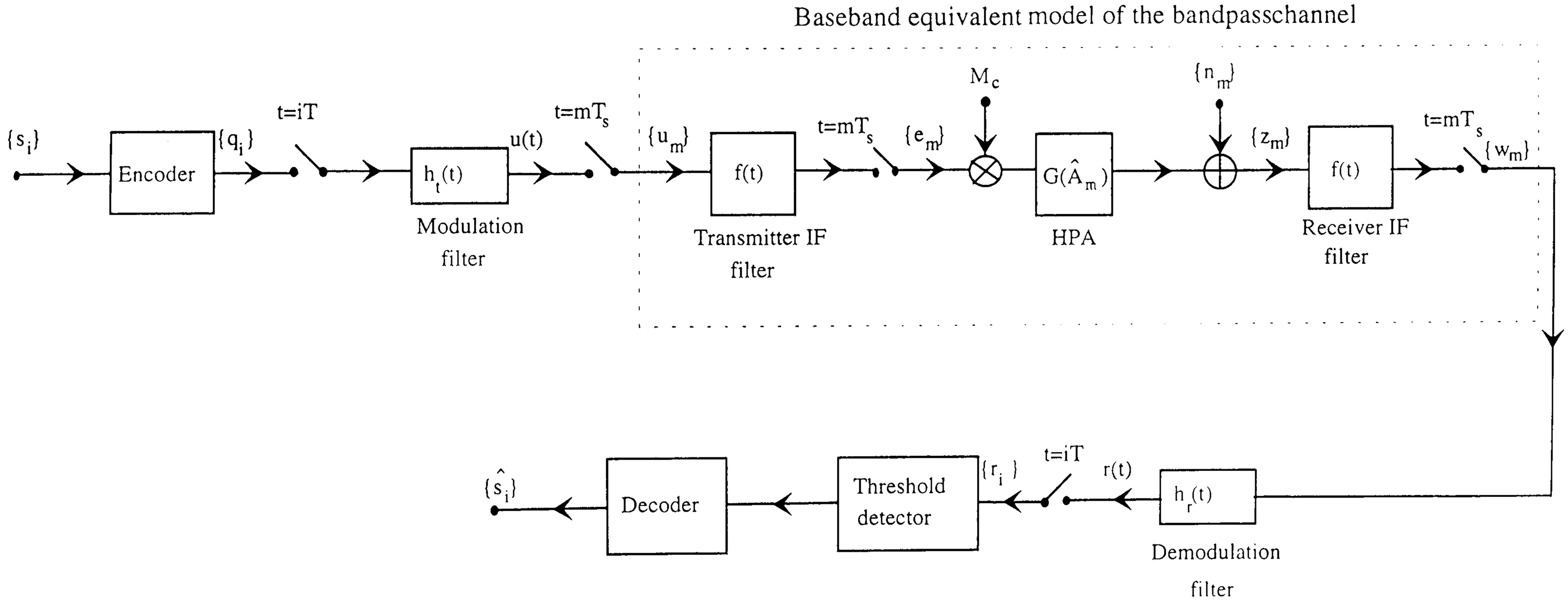

Figure 3.8 Baseband equivalent model of the DEQPSK system, with the bandpass channel as a nonlinear and bandlimited satellite channel, for computer simulation.

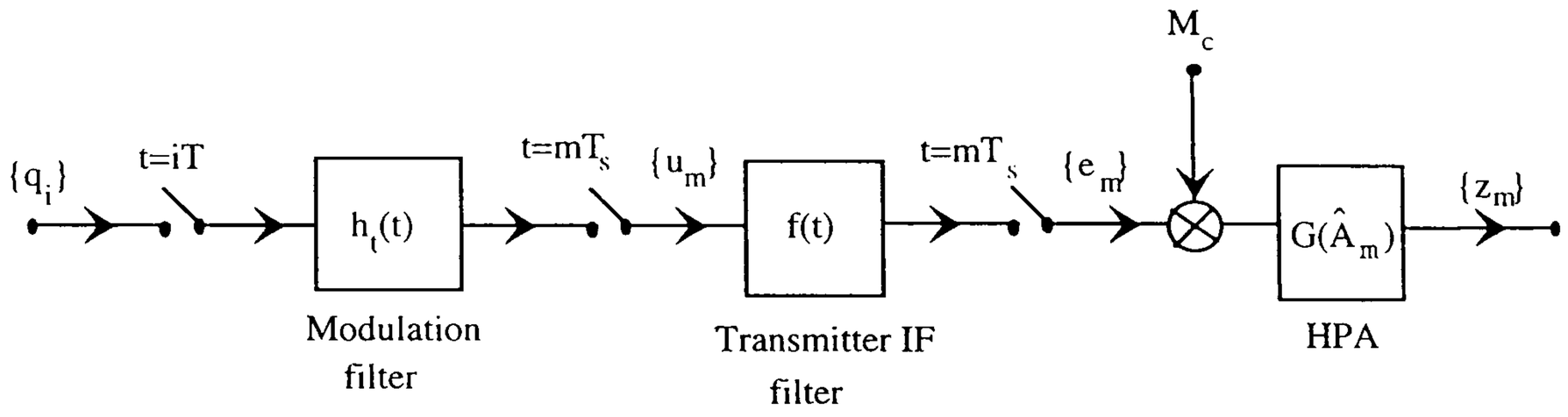

Figure 3.9 Baseband equivalent model for spectral estimation of DEQPSK signals.

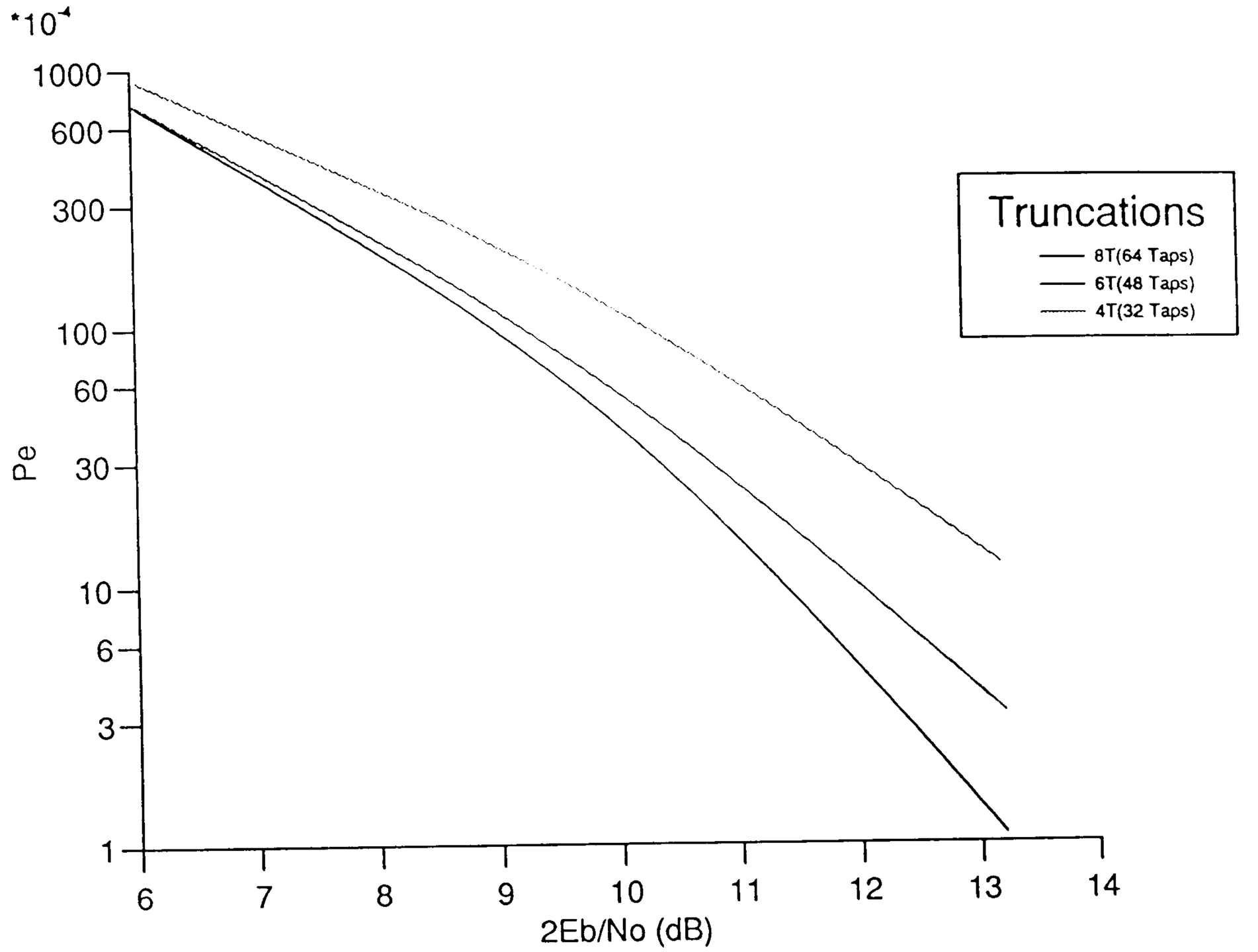

Figure 3.10a Error-rate performances of DEQPSK signals for different truncation lengths of the sampled impulse responses (Table 2.1) of the modulation and demodulation filters with $\alpha = 25\%$.

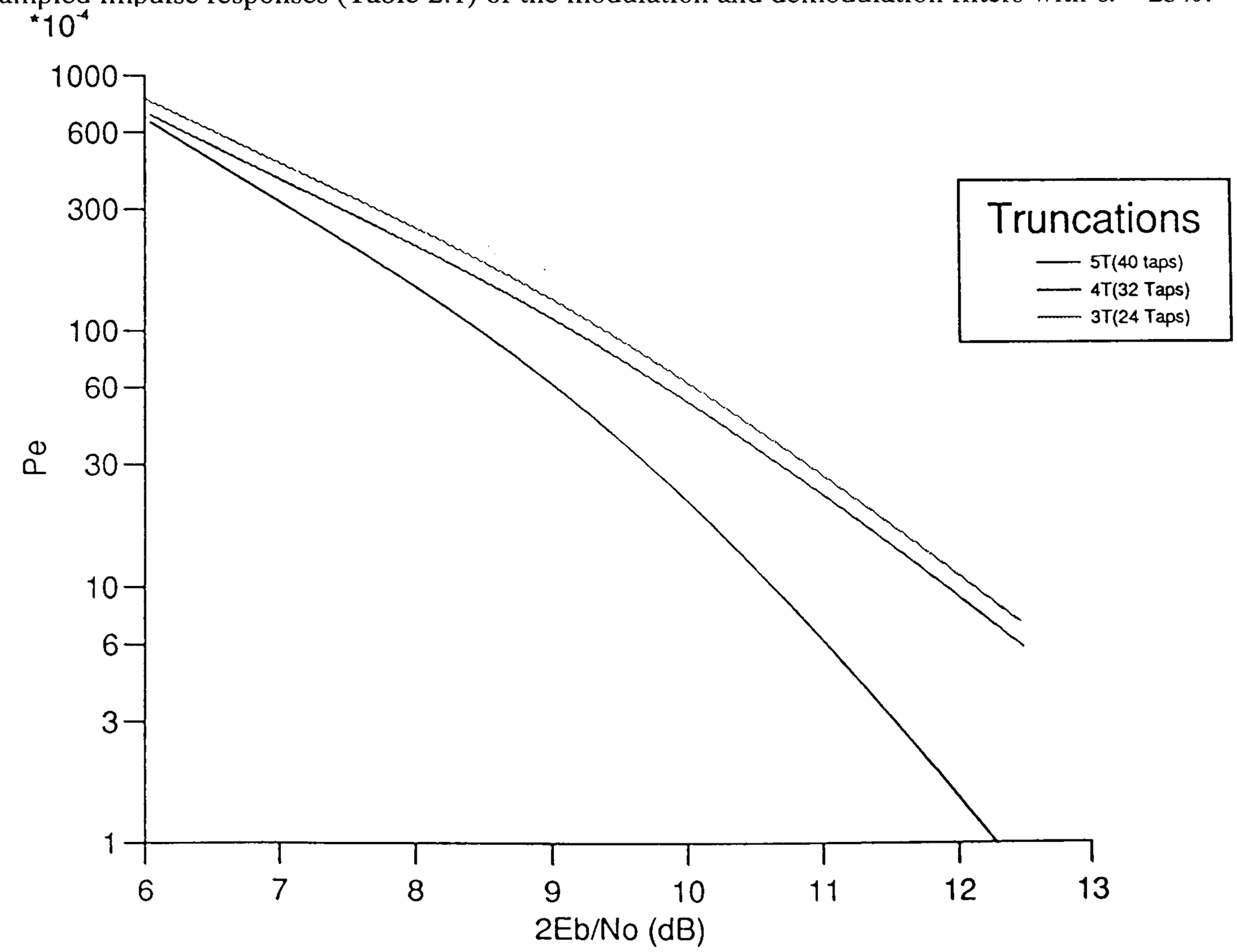

Figure 3.10b Error-rate performances of DEQPSK signals for different truncation lengths of the sampled impulse responses (Table 2.1) of the modulation and demodulation filters with $\alpha = 40\%$.

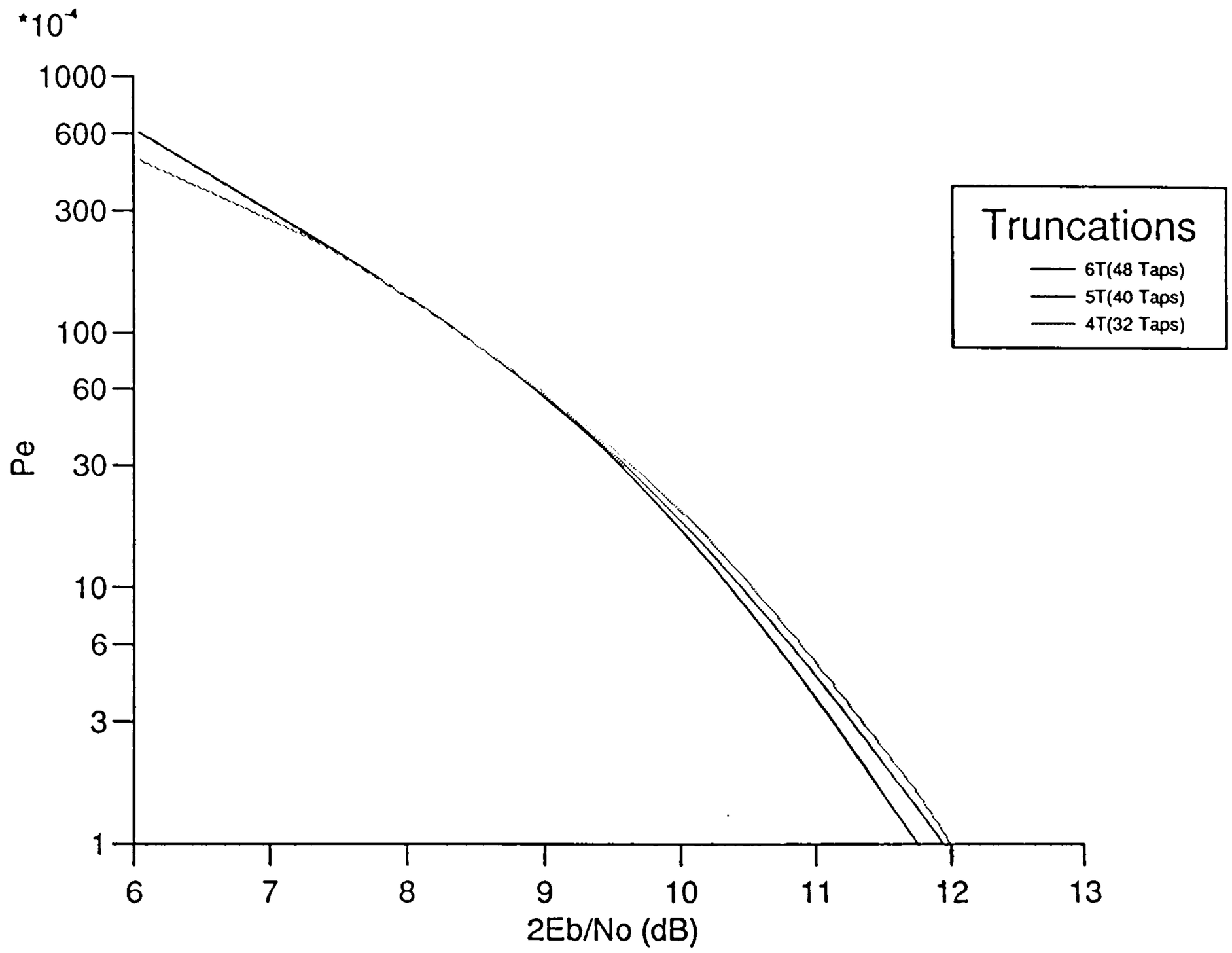

Figure 3.10c Error-rate performances of DEQPSK signals for different truncation lengths of the sampled impulse responses (Table 2.1) of the modulation and demodulation filters with $\alpha = 100\%$.

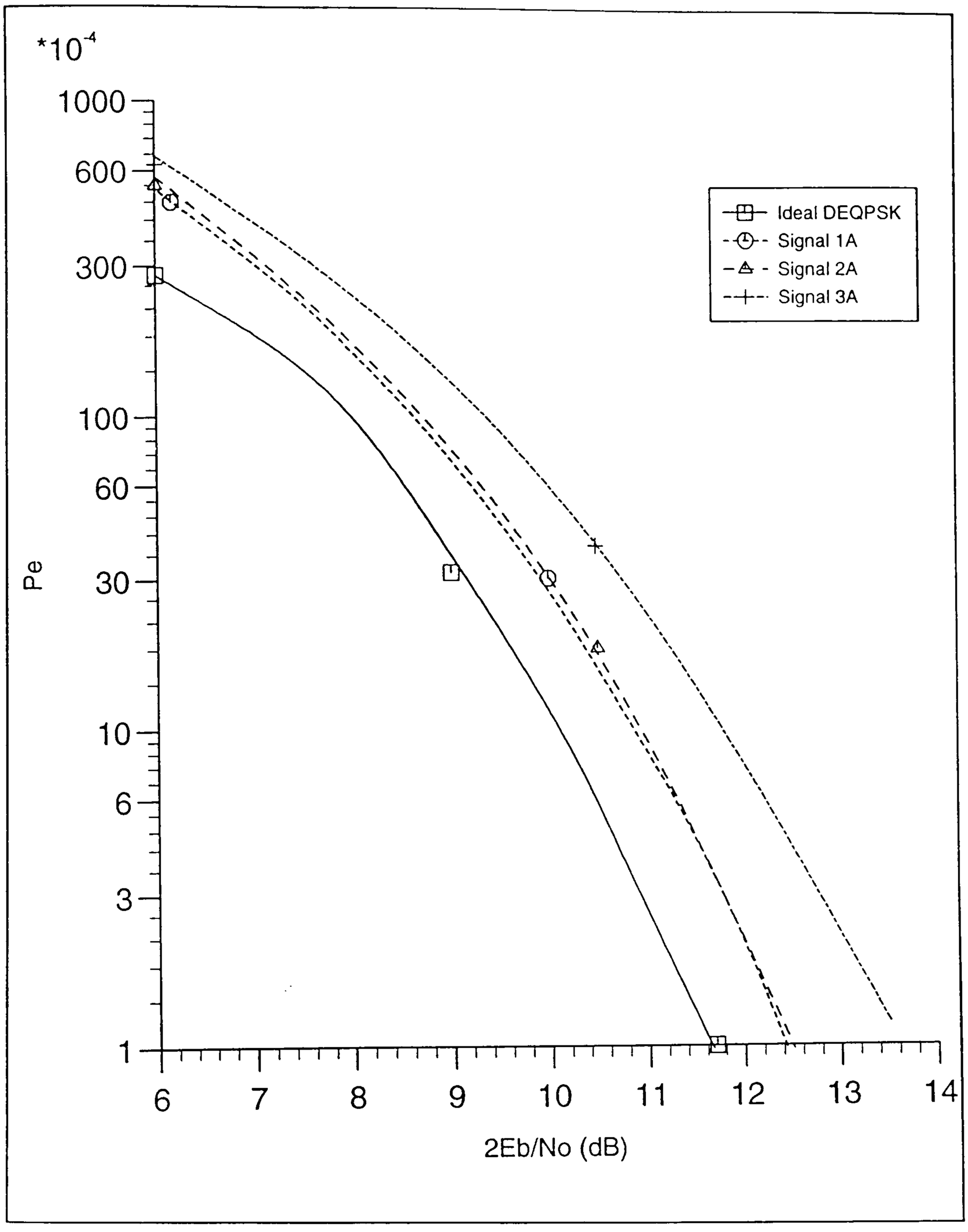

Figure 3.11 Error-rate performances of signals 1A, 2A and 3A, for DEQPSK system over a nonlinear and bandlimited channel, with the HPA operating at 0 dB OBO.

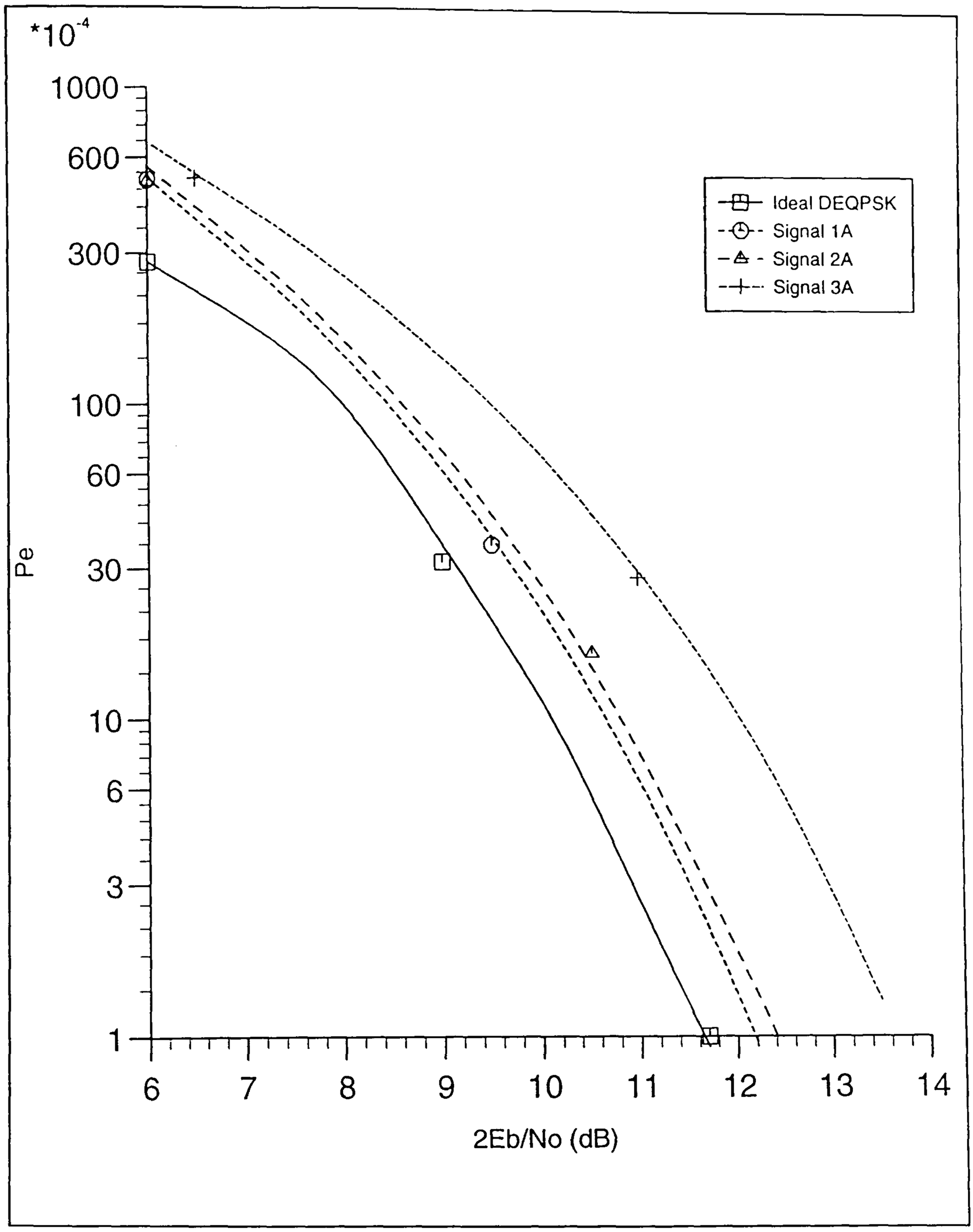

Figure 3.12 Error-rate performances of signals 1A, 2A and 3A, for DEQPSK system over a nonlinear and bandlimited channel, with the HPA operating at 0.315 dB OBO.

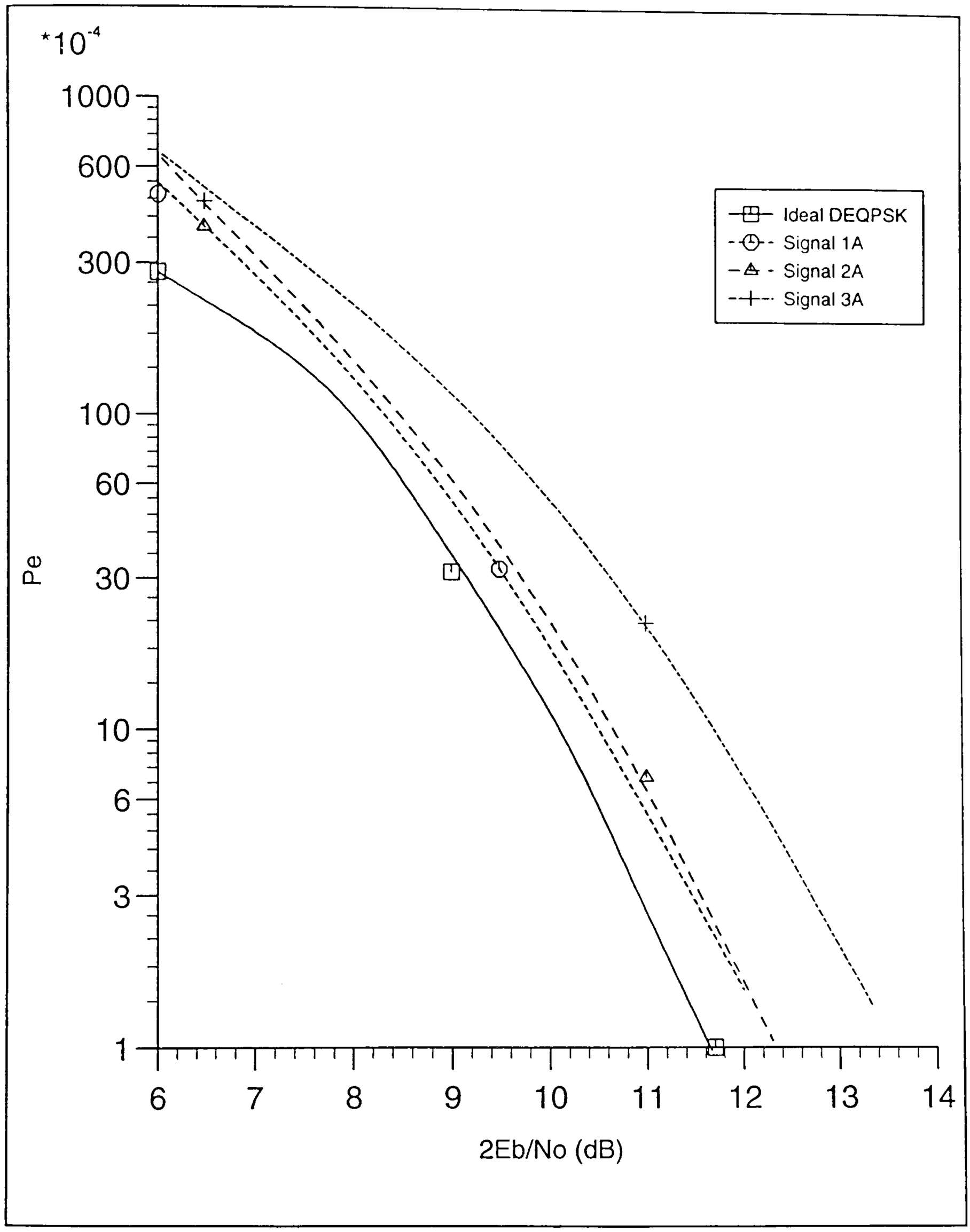

Figure 3.13 Error-rate performances of signals 1A, 2A and 3A, for DEQPSK system over a nonlinear and bandlimited channel, with the HPA operating at 0.7 dB OBO.

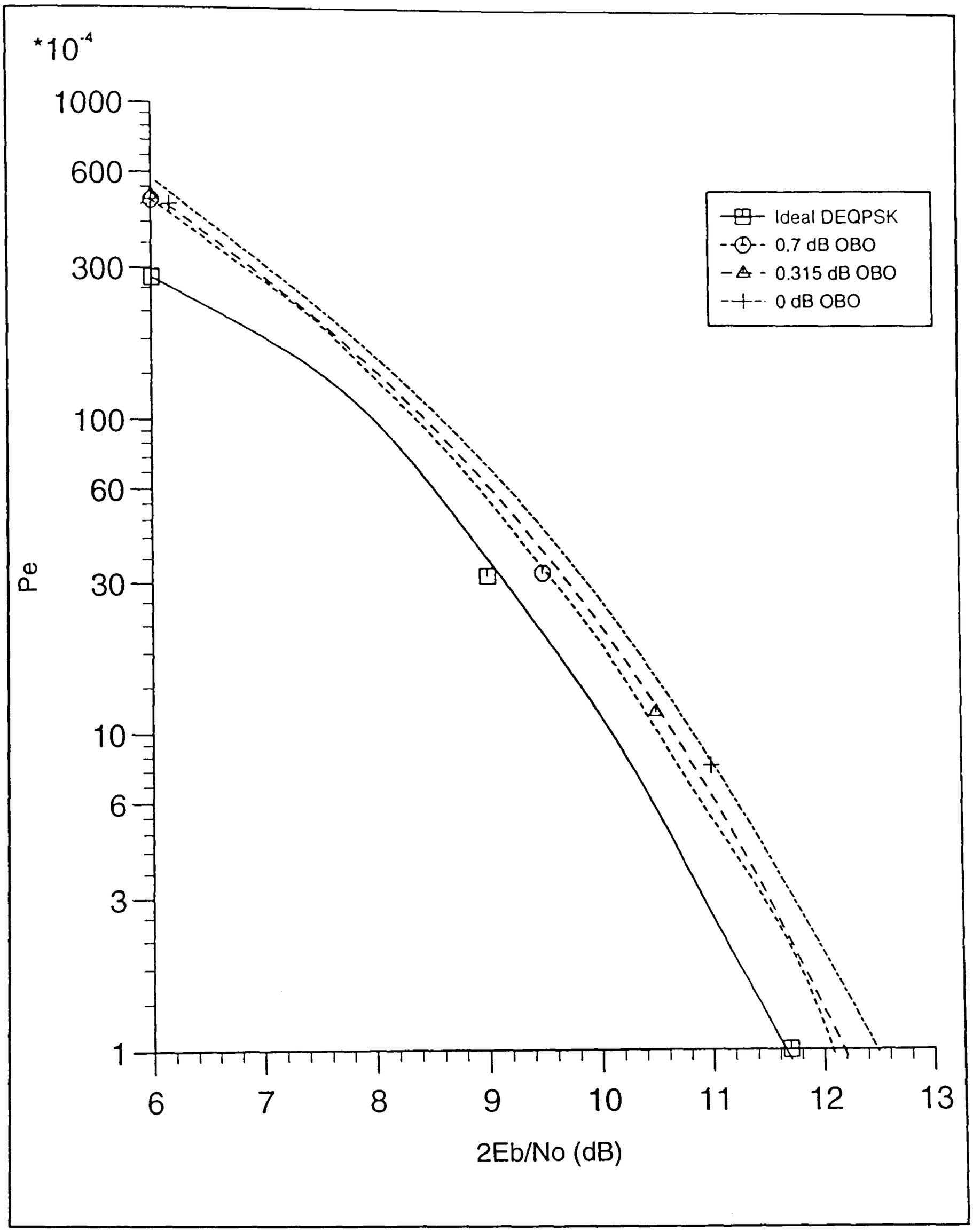

Figure 3.14 Error-rate performances of signal 1A, for DEQPSK system over a nonlinear and bandlimited channel, with the HPA operating at 0, 0.315 or 0.7 dB OBO.

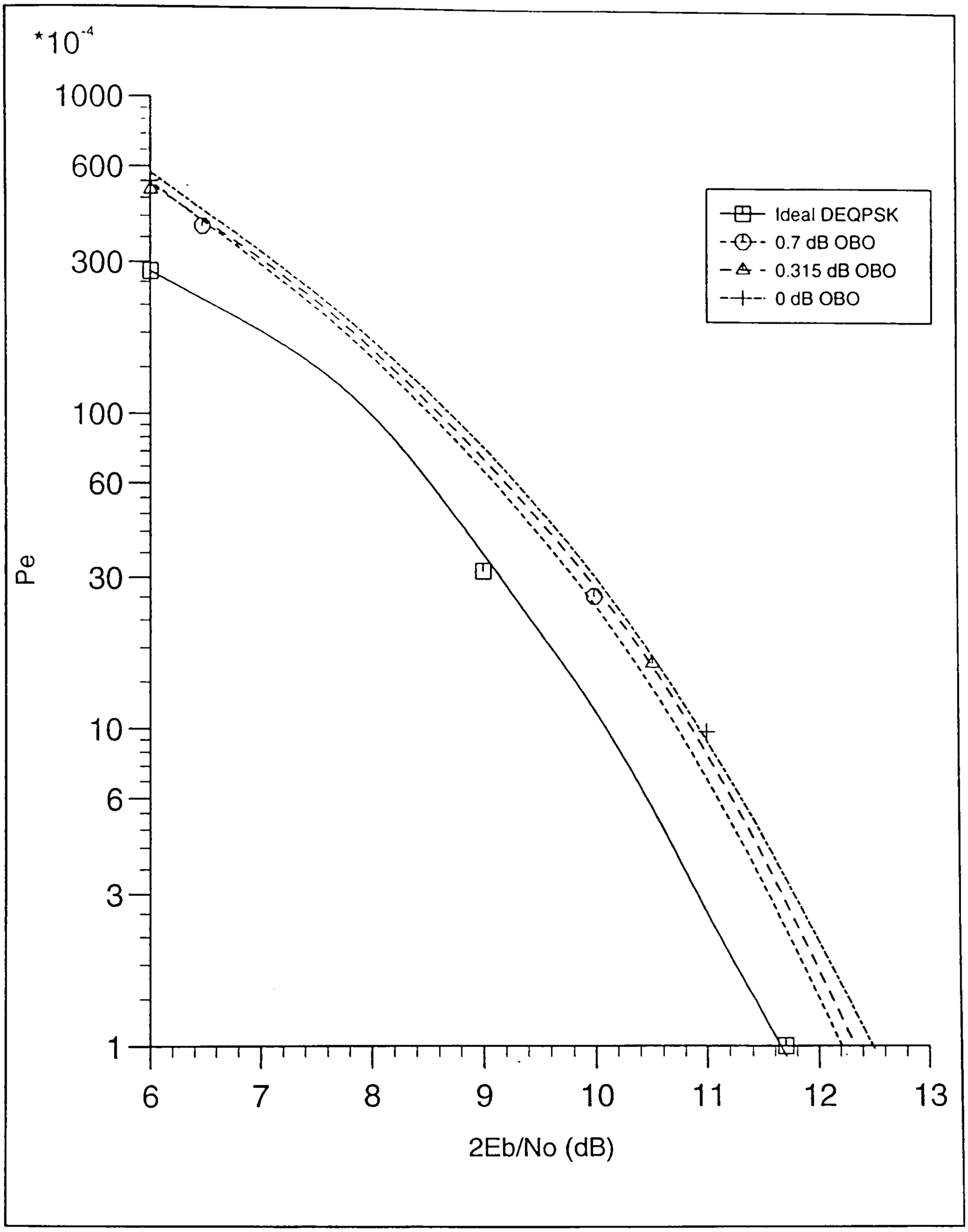

Figure 3.15 Error-rate performances of signal 2A, for DEQPSK system over a nonlinear and bandlimited channel, with the HPA operating at 0, 0.315 or 0.7 dB OBO.

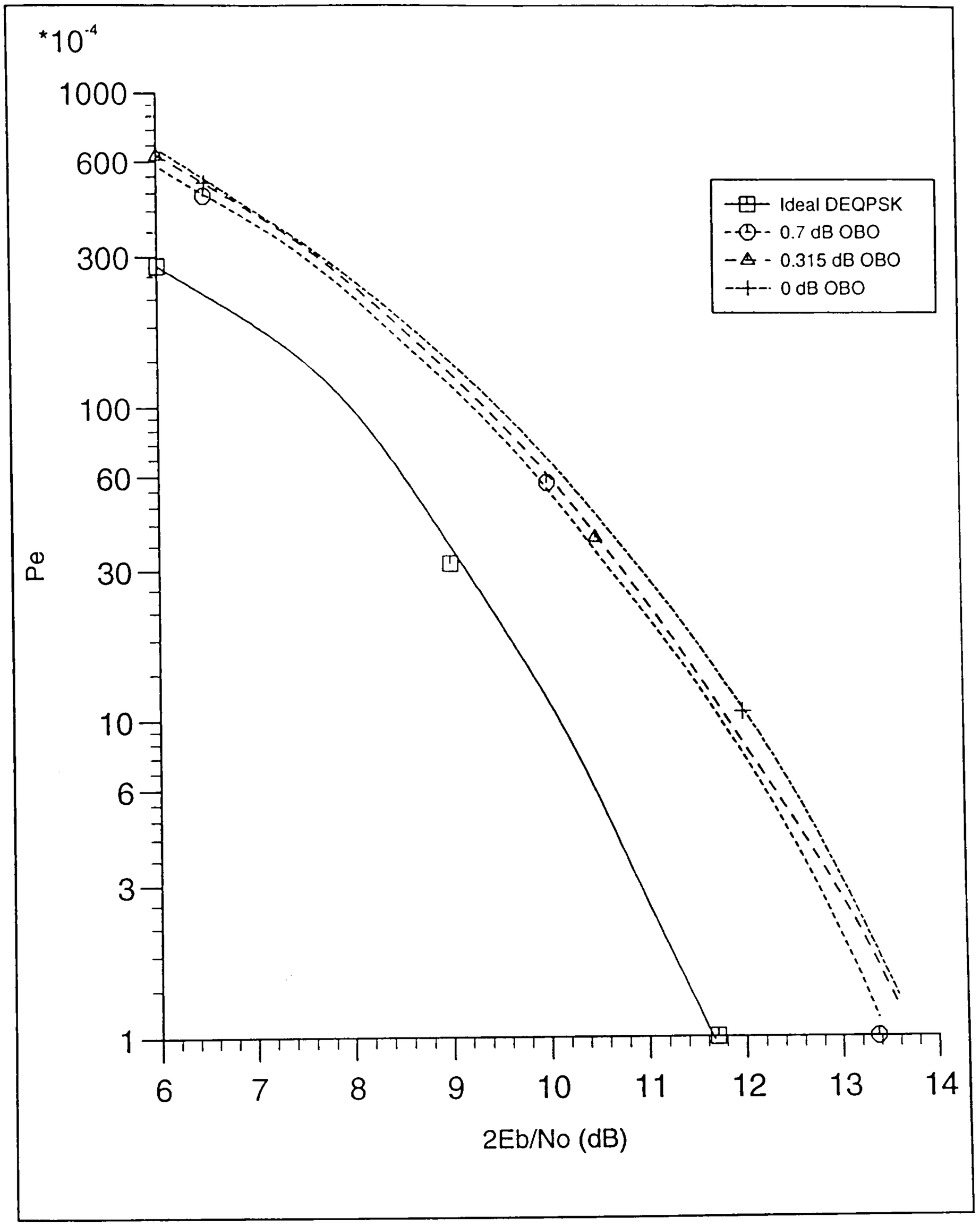

Figure 3.16 Error-rate performances of signal 3A, for DEQPSK system over a nonlinear and bandlimited channel, with the HPA operating at 0, 0.315 or 0.7 dB OBO.

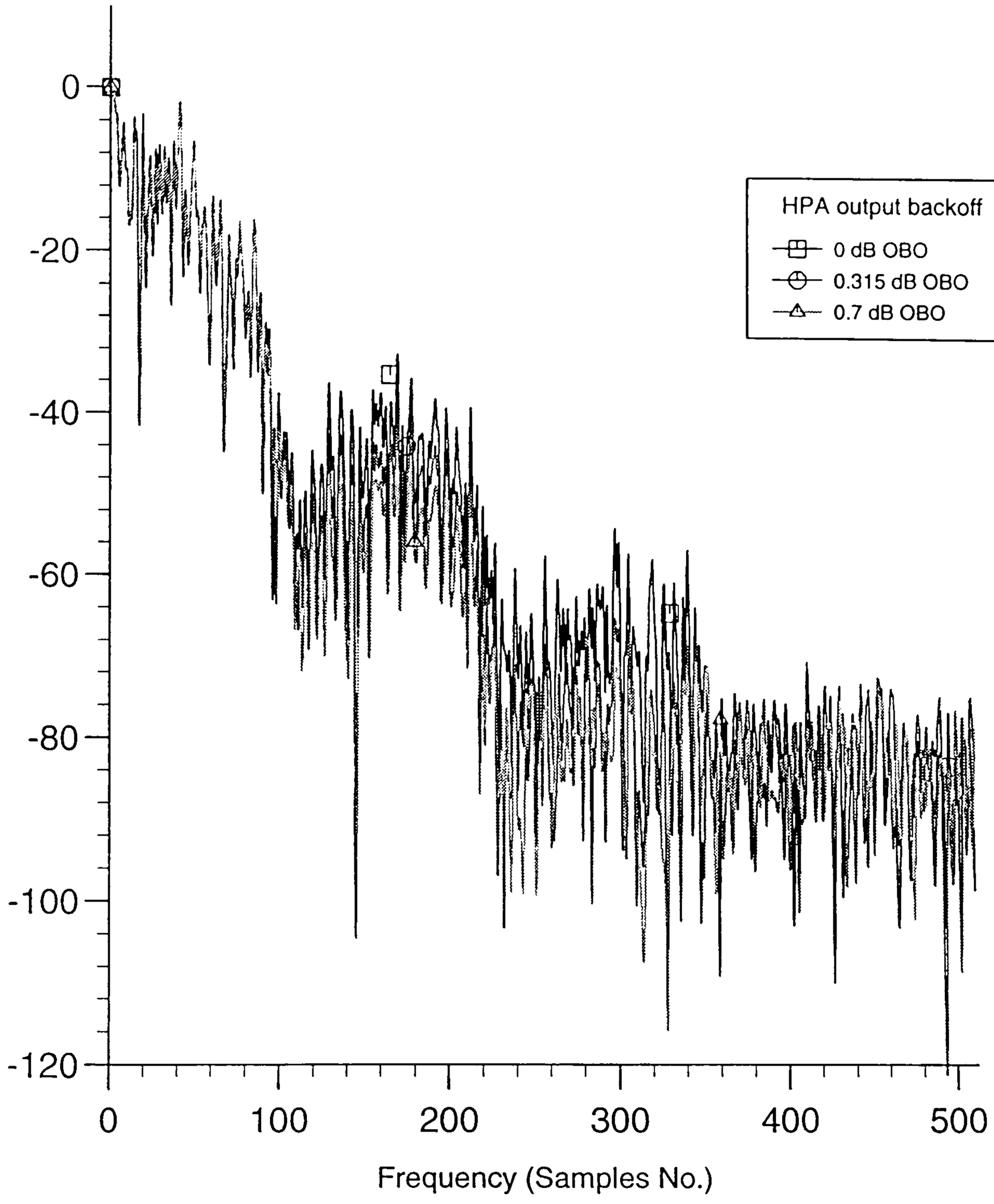

Figure 3.17 Power spectral densities of signal 1A, at the output of the HPA operating at 0, 0.315 or 0.7 dB OBO.

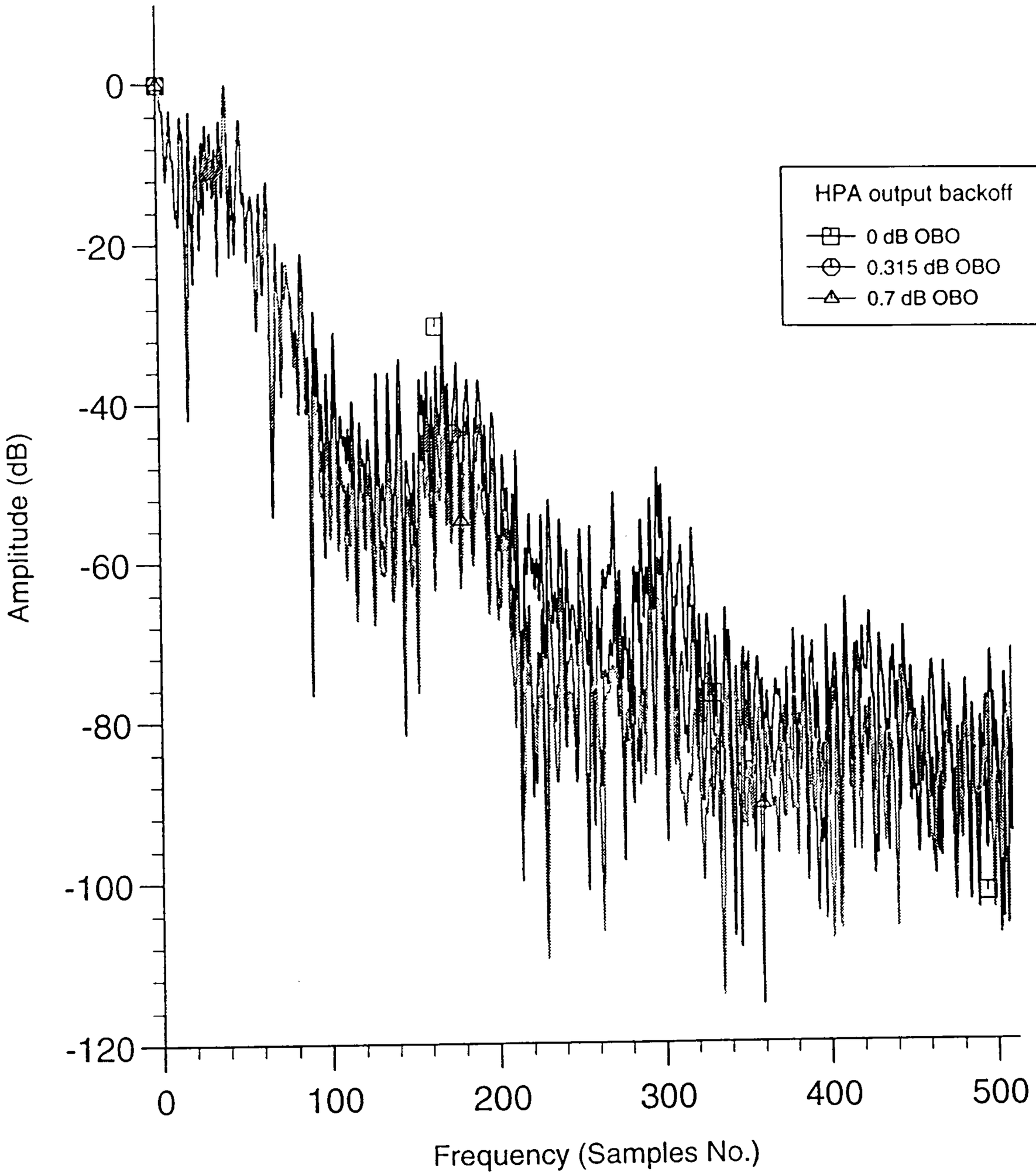

Figure 3.18 Power spectral densities of signal 2A, at the output of the HPA operating at 0, 0.315 or 0.7 dB OBO.

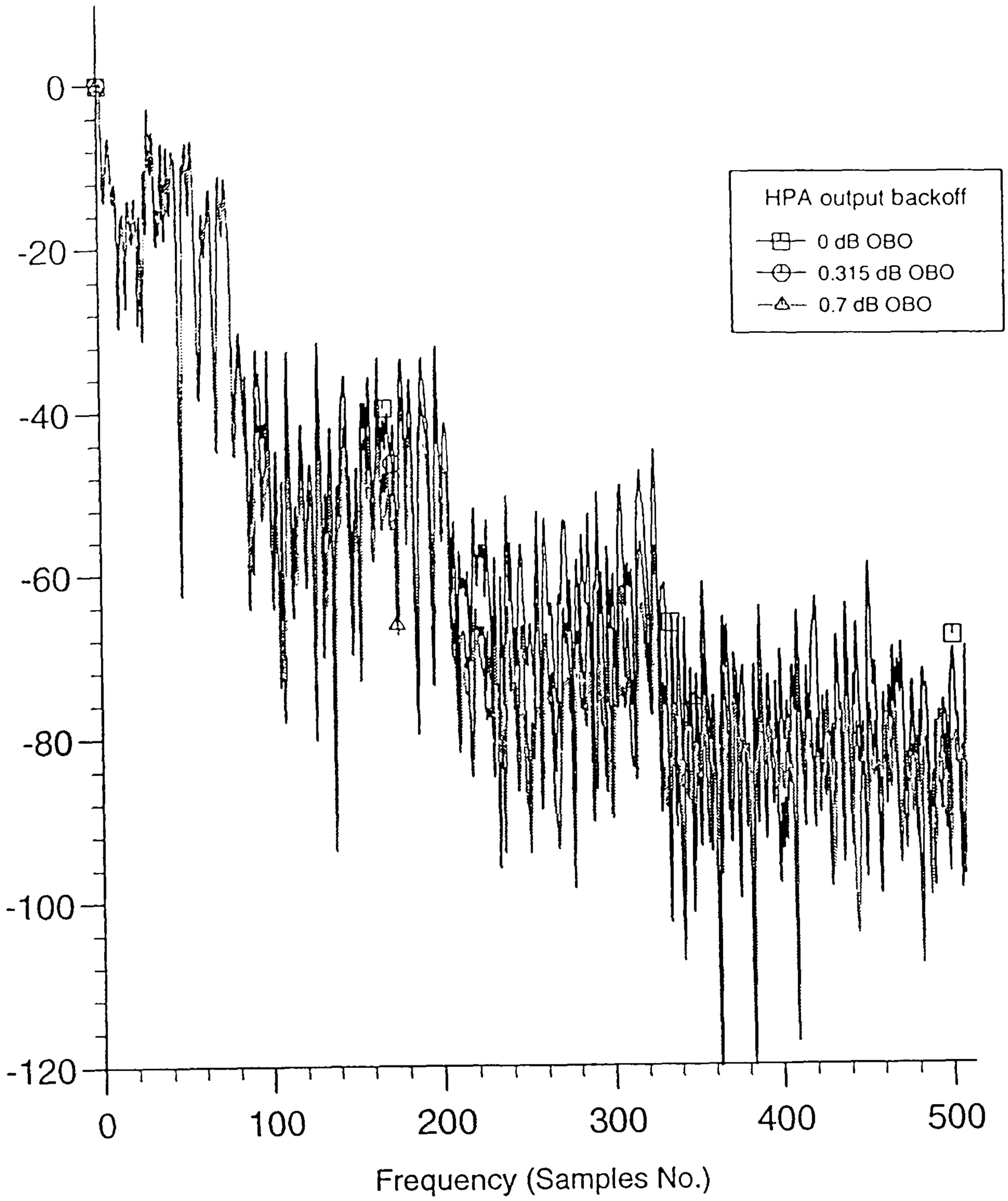

Figure 3.19 Power spectral densities of signal 3A, at the output of the HPA operating at 0, 0.315 or 0.7 dB OBO.

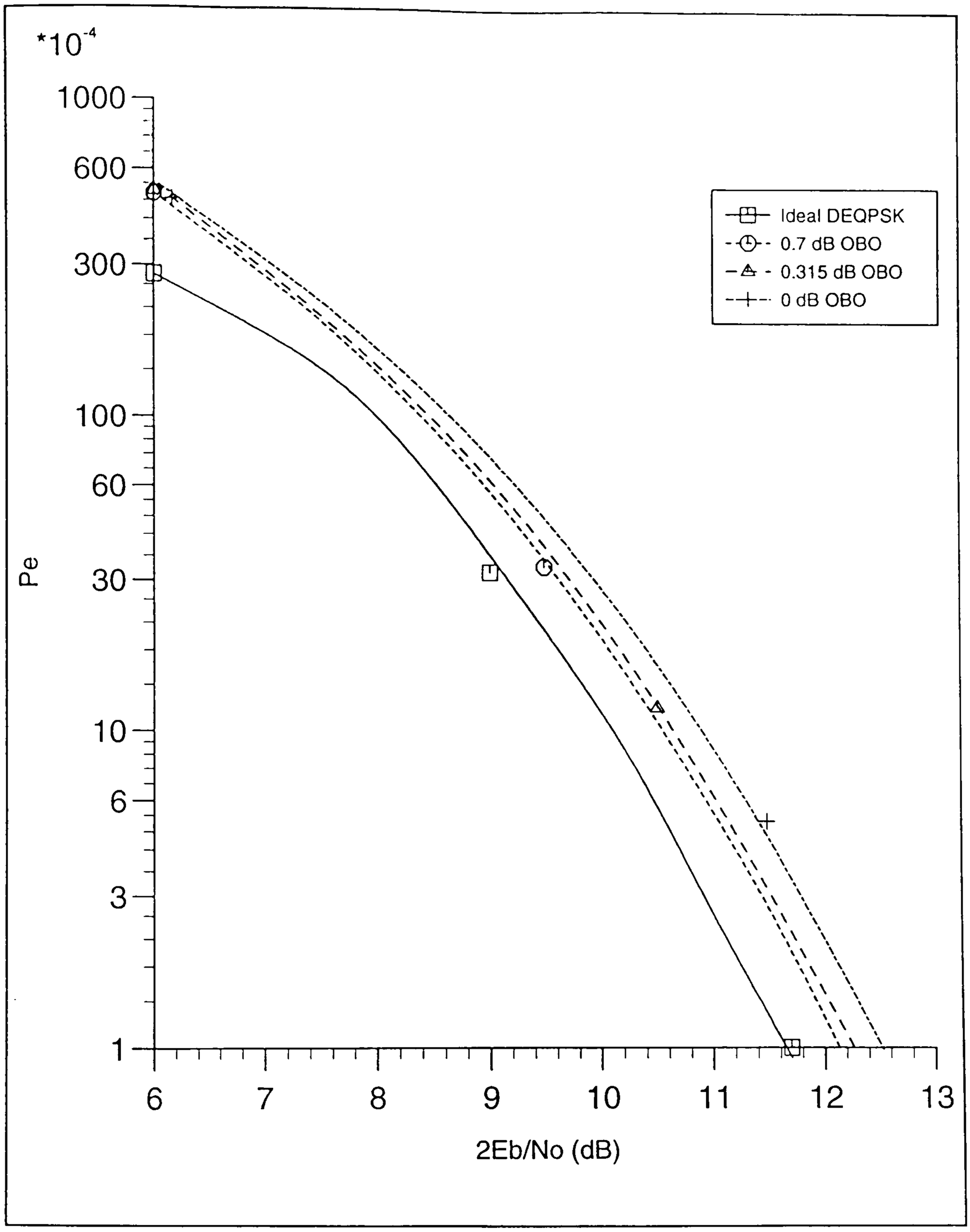

Figure 3.20 Error-rate performances of signal 1A, for OQPSK system, over a nonlinear and bandlimited channel, with the HPA operating at 0, 0.315 or 0.7 dB OBO.

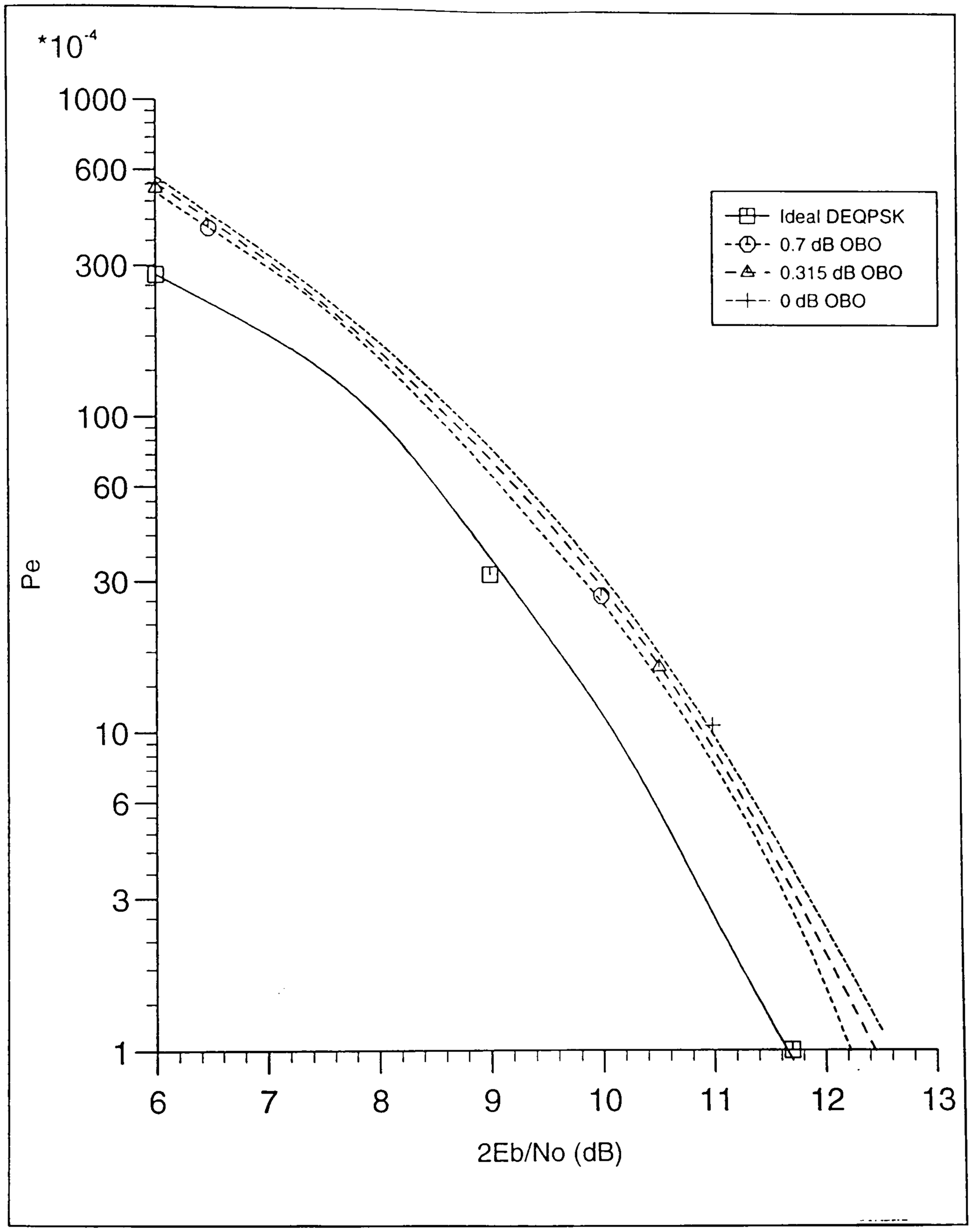

Figure 3.21 Error-rate performances of signal 2A, for OQPSK system, over a nonlinear and bandlimited channel, with the HPA operating at 0, 0.315 or 0.7 dB OBO.

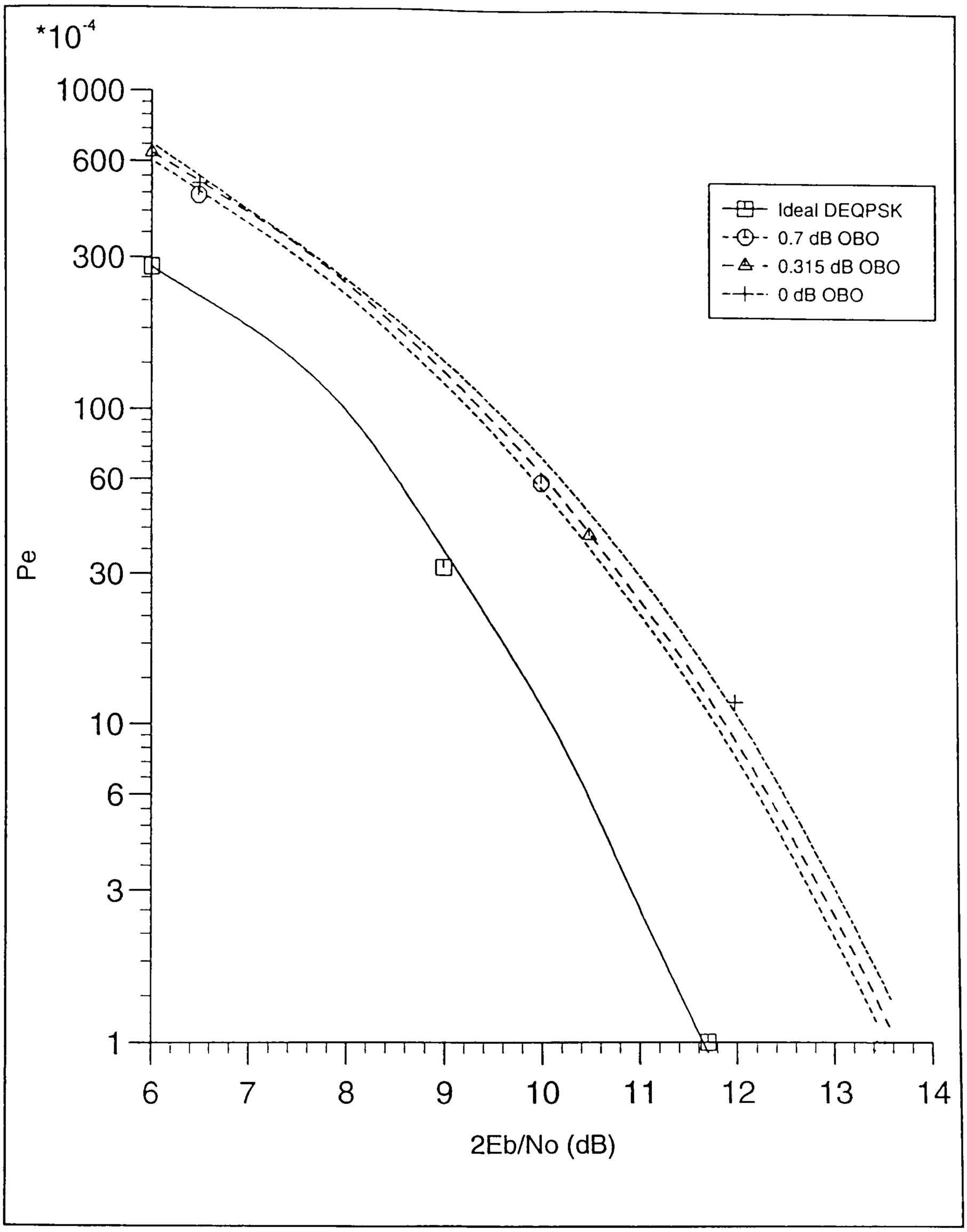

Figure 3.22 Error-rate performances of signal 3A, for OQPSK system, over a nonlinear and bandlimited channel, with the HPA operating at 0, 0.315 or 0.7 dB OBO.

CHAPTER 4

CONVOLUTIONAL ENCODING AND COHERENT 8PSK SYSTEMS OVER A NONLINEAR SATELLITE CHANNEL

4.1 Introduction

In satellite technology, multiple access means the shared use of a satellite transponder. TDMA may be defined as the sharing of a satellite transponder by many earth stations by virtue of bursts of transmissions which are timed and interleaved so as not to overlap each other.

In a TDMA system, each user is allocated a time slot in which information can be transmitted. The information bursts for each user, together with reference bursts which provide synchronisation information, make up a multiplexed TDMA frame [38]. Only one TDMA carrier accesses the satellite transponder at a given time, and the full downlink power is avialable for that access. The length of a TDMA frame depends on the type of traffic being carried [6] [38].

Differentially encoded coherent quaternary phase-shift keying (DEQPSK) is currently the prevalent modulation technique proposed for digital satellite communications. When the information bit rate is limited by power considerations, forward-error-correction (FEC) coding may be used to decrease the power requirement necessary to achieve a desired tolerance to noise. The coded redundancy needed for error correction represents a bandwidth sacrifice in that the ratio of required bandwidth to information bit rate is increased by the use of FEC coding. Hence, the trade off is reduced bandwidth efficiency for increasing power efficiency.

Since modulation and FEC coding are intimately related, bandwidth and power can be utilised more effectively by combining these two functions. Correlative phase-shift keying (CORPSK) [34] is an example of this, and is sometimes referred to as coded trellis signalling [35]. For M-ary PSK communications, the signal trellis is a phase trellis. and the unified signalling technique is categorised as coded phase

modulation (CPM). Convolutionally encoded 8 phase-shift keying (CE8PSK) [31], [32], [33] is an example of the latter. With CPM, the number M of phase positions may be increased to provide the redundancy for FEC coding without sacrificing bandwidth efficiency. With CE8PSK techniques, the phase is constrained to allow only four possible phase changes during each symbol interval.

4.1.1 Convolutional code [6], [49], [18], [69]

A convolutional encoder is shown in Fig. 4.1, generally consists of a K-stage shift register, n modulo-2 adders, a commutator, and a set of connections between the shift register and the adders. The input data to the encoder is shifted into and along the shift register, k bits at a time. The outputs of the modulo-2 adders, determined by the connections to the shift register, are then sampled in turn by the commutator to produce n output bits. Consequently, the code rate is defined as k/n. The parameter K is called the constraint length of the convolutional code.

Coding gain is the reduction in signal/noise power ratio required for providing a specified error-rate performance. It is used as the main performance measure for FEC coding. In the case of CE8PSK signals, coding gain can be expressed relative to signal/noise power ratio requirement of an uncoded QPSK signal. As $P_e \rightarrow 0$ at high signal/noise power ratio, the reduction in required signal/noise power ratio is referred to as the asymptotic coding gain. The coding gain for practical values of P_e (e.g., at $P_e = 10^{-3}$) is smaller than the asymptotic value.

Table 4.1 lists the two best codes discovered [31], [32] so far with 4 and 6-bits memory for CE8PSK signals, with asymptotic coding gain of 4.1 dB and 5 dB, respectively, for an AWGN channel. Hui et al [32] carried out a computer simulation study to evaluate the performances of these two codes over an AWGN channel using Viterbi-algorithm decoding. The results, as shown in Fig. 4.2, show that Code 2 gains the advantage of only 0.5 dB in tolerance to AWGN over Code 1, for practical values of P_e (i.e., $P_e = 10^{-3} - 10^{-4}$). Since Code 1 requires 16 vectors of storage in the Viterbi decoder, whereas Code 2 requires 64 vectors, Code 1 is more cost effective and so is studied here.

4.2 TDMA frame structure

TDMA traffic bursts are organized in a TDMA frame so that overlap at the satellite does not occur between bursts from different earth stations. The frame begins with a reference burst transmitted by one earth station acting as a reference station, and this reference burst used by all the other stations to acieve timing synchronisation. After this initial reference burst, each earth station transmits its own traffic bursts, which together comprise the frame. A guard time between bursts is

organized to prevent further overlap. This takes into account the different distances between the satellite and the earth stations, as well as variations in the timing accuracies of the earth stations [6] [38].

A typical frame organisation is shown in Fig. 4.3. The reference burst (RB1) is emitted by a reference station and, as previously indicated, constitute the basis for synchronising all other stations in a network, the second reference burst (RB2) is optional. The structure of a typical reference burst is shown in Fig. 4.3b. This burst consist of a carrier and bit timing recovery period to help the earth station to perform coherent demodulation and to optimally sample the received bit stream. The burst continues with a unique word, possessing a good impulsive autocorrelation function, to provide a timing reference. It is followed by a signalling channel, comprising control data for each earth station. The traffic bursts are emitted by the traffic stations and are synchronised relative to the reference burst to occupy assigned positions in the TDMA frame. The structure of a typical traffic is shown in Fig. 4.3c. The first two parts of a traffic burst are similar to the reference burst, and consist of a carrier and bit timing recovery sequence and a unique word. Following the unique word, the traffic burst may also contain a service channel (SC) and order wires which are used for supporting system operating protocols and for utility teletype (TTY) and voice (VOW) communications among the stations [6] [38].

The traffic data section of the traffic burst carries the payload of customer service, this includes both digital speech interpolated data and digital non-interpolated traffic sub-bursts.

The traffic burst used for computer simulation to evaluate the performances of the convolutionally encoded 8PSK (CE8PSK) system in a TDMA environment is shown in Fig. 4.4. It consists of a preamble and data burst, the preamble consists of 128 symbols for carrier and bit timing recovery and unique word, the data burst consists of 1280 symbols which are convolutionally encoded and 8PSK modulated before being transmitted through the HPA at the earth station.

4.3 Convolutional code and coherent 8PSK (CE8PSK) system

The block diagram of a convolutionally encoded coherent 8PSK system is shown in Fig 4.5. The information to be transmitted is carried by the sequence of binary data-symbols $\{s_i\}$. Each data symbol therefore carries one bit of information. The S/P (serial-to-parallel) converter converts the sequence $\{s_i\}$ into two sequences of binary symbols $\{u_{1,i}\}$ and $\{u_{2,i}\}$, where $u_{j,i} = 0$ or 1 for j=1, 2. The relationship between the input data sequence $\{s_i\}$ and the binary sequences $\{u_{1,i}\}$ and $\{u_{2,i}\}$ is exactly the same as that in the case of the QPSK system described in Section 3.1.1 (Figure 3.2). The

two sequences $\{u_{1,i}\}$ and $\{u_{2,i}\}$ are input to the convolutional encoder in pairs with a code rate 2/3.

The representation of the code generator for Code 1 as shown in Fig 4.6 which consists of a pair of sub-generators. One of the pair, associated with the input sequence $\{u_{1,i}\}$ has been labelled G_1, while the other one, associated with the input sequence $\{u_{2,i}\}$, has been labelled as G_2. There are three pairs of binary symbols $(u_{1,i}\ \ u_{2,i})$, $(u_{1,i-1}\ \ u_{2,i-1})$ and $(u_{1,i-2}\ \ u_{2,i-2})$ used in the generator at the time $t = iT$, and each pair associated with one or more of the outputs $(e_{j,i})$, where $j = 1,2,3$. The convolutional coder operates such that the coded vector e_i, at time $t=iT$, is a function of the current input vectors $u_{j,i-1}$, $u_{j,i-2}$, ..., $u_{j,i-k}$ of the storage elements in the shift register.

The pair of sub-generators G_1 and G_2 each have a K-stage shift register (K=3 for Code 1), so the code generator has a memory of (K-1) symbols and the code has a constraint length of K symbols. One method for describing a convolutional code is to give its generator pairs, which are defined as follows,

$$G_1(j) = [g_1(1,j)\ g_2(1,j)\ g_3(1,j)\ \ldots g_k(1,j)] \qquad 4.3.1a$$

and

$$G_2(j) = [g_1(2,j)\ g_2(2,j)\ g_3(2,j)\ \ldots g_k(2,j)] \qquad 4.3.1b$$

specify the connection between a stage of the shift register and the j^{th} modulo-2 adder, both of which are associated with output $e_{j,i}$ at time $t = iT$. For the present case, there are 3 modulo-2 adders, so $j = 1,\ 2$ or 3. The component $g_h(1,j)$ is equal to 1 if the j^{th} modulo-2 adder is connected to stage h of the shift register in G_1, otherwise, it is equal to 0. Again the component $g_h(2,j)$ is equal to 1 if the j^{th} modulo-2 adder is connected to stage h of the shift register in G_2, otherwise, it is equal to 0, as it is illustrated in Table 4.1. The encoder determines the following quantities $\{e_{j,i}\}$, for $j = 1,\ 2,\ 3$.

$$e_{j,i} = \sum_{h=1}^{k} u_{1,i-h+1} g_h(1,j) + \sum_{h=1}^{k} u_{2,i-h+1} g_h(2,j) \qquad 4.3.2$$

for $j = 1,\ 2,\ 3$, the summations are modulo-2 addition, so that $e_{j,i} = 0$ or 1. Hence, the sequences $\{u_{1,i}\}$ and $\{u_{2,i}\}$ are encoded to give a sequence $\{e_i\}$ which is a 3-component vector given by

$$e_i = [e_i(1)\ \ e_i(2)\ \ e_i(3)] \qquad 4.3.3$$

where $e_i(j) = 0$ or 1 for $j = 1,\ 2,\ 3$, at time $t = iT$, e_i has one of eight possible values 0, 1, 2, 3, 4, 5, 6 or 7 given by

$$e_i = 2^2 e_i(1) + 2^1 e_i(2) + 2^0 e_i(3) \qquad 4.3.4$$

The Gray encoder, in Fig. 4.5, encodes each of the vectors in $\{e_i\}$ according to Table 4.2, the phase angle of the corresponding transmitted symbol $q_{j,i}$, in the complex number plane, is determined by

$$\phi_i = \frac{2\pi e_i}{M} + \frac{\pi}{8} \qquad \text{(radians)} \qquad 4.3.5$$

for $M = 2^n$, in our case $M = 8$, and gives two sequences $\{q_{1,i}\}$ and $\{q_{2,i}\}$, where $q_{j,i} = \pm 0.924$ or ± 0.383 for $j = 1,2$. These two sequences are used to form the corresponding sequences of impulses $\{\sum_i q_{1,i}\delta(t - iT)\}$ and $\{\sum_i q_{2,i}\delta(t - iT)\}$, at the input of the modulation filter, and hence to produce two baseband modulating waveforms

$$a(t) = \sum_i q_{1,i} h_t(t - iT) \qquad 4.3.6a$$

$$b(t) = \sum_i q_{2,i} h_t(t - iT) \qquad 4.3.6b$$

where $h_t(t)$ is the impulse response of the modulation filter with the transfer function of $H_t(f)$. $a(t)$ and $b(t)$ are called the inphase and quadrature baseband signals respectively. These signals are then quadrature modulated, as described in Section 2.6, and added to give the convolutionally encoded 8PSK (CE8PSK) signal

$$S(t) = \sqrt{2}a(t)\cos\omega_c t - \sqrt{2}b(t)\sin\omega_c t \qquad 4.3.7$$

with ω_c the carrier frequency in rad/s. The resultant signal is then fed into the bandpass transmission channel. Assume that the bandpass transmission channel introduces no attenuation, delay or distortion, but that it only adds a Gaussian noise waveform, $N(t)$, to the transmitted signal, so that the channel is exactly the same as the one used in the QPSK system described in Section 3.1.1. At the input of the demodulator, the signal is

$$r(t) = \sqrt{2}[a(t)\cos\omega_c t - b(t)\sin\omega_c t] + N(t) \qquad 4.3.8$$

where $N(t)$ is a sample function of a Gaussian random process with zero mean and a two-sided power spectral density of $\frac{1}{2}N_0$ over the signal frequency band. Assume that the bandwidth of $N(t)$ is small compared with its carrier frequency ω_c rad/s, so Eqn. 4.3.8 can be written [19] as

$$r(t) = [\sqrt{2}a(t) + N_c(t)]\cos\omega_c t - [\sqrt{2}b(t) + N_s(t)]\sin\omega_c t \qquad 4.3.9$$

as can be seen from Eqn. 3.1.4, where $N_c(t)$ and $N_s(t)$ are sample functions of Gaussian random processes, with zero mean and a two-sided power spectral density twice that of $N(t)$ [Appendix A7].

It is shown, in Section 3.1.1, that under these conditions, the inphase and quadrature baseband signal components plus noise, at the demodulation filter output, are

$$r_1(t) = \sum_i q_{1,i}h(t - iT) + v_1(t) \qquad 4.3.10a$$

and

$$r_2(t) = \sum_i q_{2,i}h(t - iT) + v_2(t) \qquad 4.3.10b$$

respectively, where $h(t)$ is the inverse Fourier transform of $H(f)$, which is the transfer function of the modulation and demodulation filters in cascade. Also $v_1(t)$ and $v_2(t)$ are filtered Gaussian noise waveforms. Bear in mind that the bandpass channel introduces no attenuation, delay or distortion.

Assume that the modulation and demodulation filters have the same characteristics, and the combined transfer function is a sinusoidal roll-off frequency response (Eqn. 2.2.3) with a linear phase characteristic, so that $h(0) = 1$ and $h(iT) = 0$, for all values of the integer i other than $i = 0$. The signals $r_1(t)$ and $r_2(t)$ have no ISI at the time instants $\{iT\}$. Assume also that the receiver provides the ideal required timing signal, so that the two baseband waveforms, $r_1(t)$ and $r_2(t)$, at the demodulation filter output are sampled at time instants $\{iT\}$, to give two sequences of sample values $\{r_{1,i}\}$ and $\{r_{2,i}\}$ to the decoder. At time $t = iT$, the samples are (Eqn. 3.1.8)

$$r_{1,i} = q_{1,i} + v_{1,i} \qquad 4.3.11a$$

and

$$r_{2,i} = q_{2,i} + v_{2,i} \qquad 4.3.11b$$

where $v_{1,i}$ and $v_{2,i}$ are sample values of Gaussian random variables with zero mean and fixed variance σ^2, the $\{v_{1,i}\}$ and $\{v_{2,i}\}$ being statistically independent and independent also of the $\{s_i\}$.

The received samples $\{r_{1,i}\}$ and $\{r_{2,i}\}$ are fed to the decoder which produces at its output the sequence of symbols $\{\hat{s}_i\}$ which forms the sequence of decoded data symbols. In the absence of noise, the $\{\hat{s}_i\}$ are the same as the transmitted symbol $\{s_i\}$. The aim of the decoder is to generate the sequence $\{\hat{s}_i\}$ such that the corresponding sequences $\{q_{1,i}\}$ and $\{q_{2,i}\}$, which would have been transmitted in response to the given $\{s_i\}$ at the transmitter input, are at the minimum resultant (total) unitary distance from the received sequences $\{r_{1,i}\}$ and $\{r_{2,i}\}$ [37].

In the absence of noise, Eqn. 4.2.11 becomes

$$r_{1,i} = q_{1,i} = \pm 0.924 \text{ or } \pm 0.383 \qquad 4.3.12a$$

and

$$r_{2,i} = q_{2,i} = \pm 0.924 \text{ or } \pm 0.383 \qquad 4.3.12b$$

The eight possible received signals vectors (signal constellation) are shown in Fig. 4.7. It can be seen that CE8PSK signals have eight distinct possible phases, $\pm\pi/8$, $\pm 3\pi/8$, $\pm 5\pi/8$, and $\pm 7\pi/8$ radians.

The minimum distance properties of convolutional codes play a very important role in determining the error-correction capability of the codes [18]. Two minimum distance parameters, each has its own importance, are now defined for rate-k/n binary convolutional codes. Let

$$u = [u_0 \;\; u_1 \;\; u_2 \;\; .....] \qquad 4.3.13a$$

and

$$u' = [u'_0 \;\; u'_1 \;\; u'_2 \;\; .....] \qquad 4.3.13b$$

be any two possible messages that differ in their first vectors (data symbols) $\{u_0\}$, and let

$$e = [e_0 \;\; e_1 \;\; e_2 \;\; .....] \qquad 4.3.14a$$

$$e' = [e'_0 \;\; e'_1 \;\; e'_2 \;\; .....] \qquad 4.3.14b$$

be the corresponding code sequences of the messages u and u', respectively. Now, consider

$$e(l) = [e_0 \;\; e_1 \;\; e_2 \;\; .....e_{l-1}] \qquad 4.3.15a$$

and $$e'(l) = [e'_0 \;\; e'_1 \;\; e'_2 \;\; .....e'_{l-1}] \qquad 4.3.15b$$

where $e(l)$ and $e'(l)$ take on the first l components of the code sequences e and e' respectively.

The Hamming distance between the two binary-valued code sequences $e(l)$ and $e'(l)$ is denoted by $d_{\mathrm{H}}[\, e(l), e'(l)]$, and it is defined as the total number of positions (binary digits) where $e(l)$ and $e'(l)$ differ.

The l^{th} column distance function η_l of the code is the minimum Hamming distance between all pairs of code sequences of length l symbols that differ in their first coded vectors $\{e_0\}$. This is given by

$$\eta_l = \min\{d_{\mathrm{H}}[\, e(l), e'(l)]\} \qquad 4.3.16$$

The most important distance parameter for binary convolutional codes is the minimum free Hamming distance, $d_{\mathrm{H}}(\text{free})$, defined as follows,

$$\begin{aligned} d_{\mathrm{H}}(\text{free}) &= \lim_{l \to \infty} (\eta_l) \\ &= \min\{d_{\mathrm{H}}[\, e, e']\} \end{aligned} \qquad 4.3.17$$

The minimization is carried out over all valid code sequences $\{e\}$ and $\{e'\}$ of arbitrary length that differ in their first code symbols. The second most important distance parameter of the convolutional codes is the distance profile Ω, where Ω is the $(g+L)$-tuple column distance function

$$\Omega = \{\eta_1, \eta_2, ..., \eta_{g+L}\} \qquad 4.3.18$$

η_l, for $l=1, 2, ..., (g+L)$, is defined by Eqn. 4.3.16. g is the code memory in bits. Clearly, the distance profile of the code is a measure of the rate of the growth in the column distance function.

The minimum free unitary distance squared, d^2_{free}, of the convolutionally coded signal is now defined. Let $\{q_i\}$ and $\{q'_i\}$ be any two possible (valid) sequences of complex-valued code symbols of arbitrary length that differ in their first symbols, then

$$d^2_{\text{free}} = \min\{\sum_{i=0}^{\infty} |q_i - q'_i|^2\} \qquad 4.3.19$$

The minimization is carried out over all valid coded signal sequences.

It is appropriate here to examine the potential gains available in terms of channel capacity. The well known channel capacity equation for a memoryless AWGN channel with a discrete input and a continuous-valued output, as the channel assumed here, may be given as [27,28]

$$C^* = \max \sum_{h=0}^{M-1} p(h) \int_{-\infty}^{\infty} f(r/q(h)) \log_2 \left(\frac{f(r/q(h))}{\sum_{k=0}^{M-1} p(k) f(r/q(k))} \right) dr \qquad 4.3.20$$

where

C^* = number of information bits per signal interval (bits/T), or equivalently, the number of bits per transmitted signal element.

M = number of discrete signal elements at the input of the channel.

$q(h)$ = a possible value of q_i, for h= 0, 1, ...(M-1).

r = continuous-variable received sample.

$f(r/q(h))$ = conditional probability density function of r, for a given value of $q(h)$,

$p(h)$ = probability that code symbol $q(h)$ is transmitted.

In an AWGN channel

$$f(r/q(h)) = \frac{1}{2\pi\sigma^2} \exp\{-\frac{|r-q(h)|^2}{2\sigma^2}\} \qquad 4.3.21$$

bearing in mind that both r and $q(h)$ are complex-valued.

If all code symbols $\{q_i\}$ are equally likely to have any of the M different possible values, the maximization over $\{p(h)\}$ can be omitted. Now,

$$C^* = \log_2 M - \frac{1}{M} \sum_{h=0}^{M-1} \mathrm{E}\{\log_2 \sum_{k=0}^{M-1} \exp(-\frac{|q(h)+N-q(k)|^2 - |N|^2}{2\sigma^2})\} \qquad 4.3.22$$

where the integration is replaced by the expectation over the Gaussian distribution complex-valued noise variable N [39], [40], [42].

In Fig. 4.8, C^*(bits/T) is plotted against the signal/noise ratio, defined here as $2E_b/N_0$, for different MPSK signals[27], [28], [30], the value of $2E_b/N_0$ at which a symbol error rate of 10^{-5} is achieved for uncoded transmission is also indicated (marked as a small circle on each curve). E_b is the average energy per bit and $\frac{1}{2} N_0$ is the two-sided power spectral density of the white Gaussian noise.

It can be seen from Fig. 4.8 that the 8PSK system theoretically achieves an information rate of 3 bits/T at a sufficient large $2E_b/N_0$. For instance, a symbol error rate of 10^{-5} is achieved at $2E_b/N_0 = 18.2$ dB, as can be seen in Fig. 4.6. But below 12 dB, C^* decreases rapidly, and at $2E_b/N_0 = 5.7$ dB, C^* falls to 2 bits/T. On the other hand, The QPSK system achieves the symbol error rate of 10^{-5} only if $2E_b/N_0 > 13.1$ dB. The evidence here suggests that, instead of employing a QPSK signal to transmit two information bits per symbol interval at $2E_b/N_0 = 13.1$ dB, the same error can be achieved by employing an 8PSK signal to carry the two information bits together with one redundant bit (that is generated by FEC coding). In the latter case, however, $2E_b/N_0 = 5.7$ dB is sufficient. It follows that, while maintaining the information rate of 2 bits/T, a gain in tolerance to noise of up to 7.4 dB may be obtained in this way, at a BER of 10^{-5}, as a net result of extensive coding and decoding.

The second interesting point from Fig. 4.8 is that almost all that is to be gained in terms of achievable channel capacity could be obtained by doubling the total number of possible transmitted symbol values, relative to that for the uncoded system. Any further increase in the number of signal levels will only yield a small (if any) additional gain in tolerance to noise. Take the example at the information rate of 2 bits/T, in Fig. 4.8. The step from QPSK to 8PSK signals can yield a theoretical advantage of 7.4 dB, whereas an additional gain of only 1.2 dB may be achieved by going to an infinitely large signal set. The conclusion here is that, the majority of available gains obtained by going from QPSK to 8PSK signals can be achieved with a corresponding rate-2/3 convolutional code.

4.4 Baseband equivalent model of CE8PSK system, with a nonlinear satellite channel, for computer simulation.

The CE8PSK system considered here operates at 64, 128 or 256 kbits/s over a satellite link. Since CE8PSK signals use a quadrature modulation techniques, the system can be greatly simplified by assigning real values to the signals in one of the two parallel channels (that associated with $\sqrt{2}\cos\omega_c t$) and imaginary values to the signals in the other channel (that associated with $-\sqrt{2}\sin\omega_c t$), and then considering the linear modulator, the transmitter IF filter, the HPA, the receiver IF filter and the linear demodulator, as a baseband transmission path carrying complex-valued signals. The resultant system is shown in Fig. 4.7. The information to be transmitted is carried by the sequence of binary data-symbols $\{s_i\}$, where the $\{s_i\}$ are taken to be statistically independent and equally likely to have any of the possible values of 0 or 1. The encoded symbols $\{q_i\}$ are obtained from the $\{s_i\}$, by the encoder, after being S/P converted, convolutionally encoded and then Gray encoded (Section 4.3). The i^{th} symbol has the value

$$q_i = (\pm 0.924 \pm j0.383) \text{ or } (\pm 0.383 \pm j0.924) \qquad 4.4.1$$

where $j = \sqrt{-1}$, the $\{q_i\}$, of course, being statistically independent and equally likely to have any of the eight possible values. The sequence $\{q_i\}$ is used to form the corresponding sequence of impulses $\{\sum_i q_i \delta(t - iT)\}$ at the input of the modulation filter. The signal waveform at the output of the modulation filter is the complex-valued baseband signal

$$u(t) = \sum_i q_i h_t(t - iT) \qquad 4.4.2$$

where $h_t(t)$ is the impulse response of the modulation filter and, at any given of t, is real (Section 2.4.1).

Similar to the system described in Section 3.3, the system is modelled digitally for computer simulation. The continuous waveforms are modelled as discrete waveforms. The waveform $u(t)$ is sampled 8 samples per symbol, at the time instants $\{mT_s\}$, where $T = 8T_s$, to give the sequence $\{u_m\}$, where $u_m = u(mT_s)$. The $\{u_m\}$ are then fed to a baseband equivalent model of the bandpass channel, as shown in Fig. 4.9. As with the DEQPSK system.

The sampled signal $\{w_m\}$ (given by Eqn. 3.3.9), from the baseband equivalent model of the bandpass channel, are filtered by the demodulation filter. The sampled impulse response of the demodulation filter, sampled at the rate of $1/T_s$ samples per second, is given by the $(n+1)$-component vector

$$p = [p_0 \;\; p_1 \;\; p_2 \;\; \ldots\ldots p_n] \qquad 4.4.3$$

where the $\{p_m\}$, for $0 \le m \le n$, have real-valued components (Table 2.1), and $p_m = p(mT_s)$. Thus, at time $t = mT_s$, the signal sample at the filter output is

$$r_m = \sum_{h=0}^{n} w_{m-h} p_h \qquad 4.4.4$$

where r_m has a complex value.

Assume that the receiver provides the required ideal timing signal, so the signal is sampled once per symbol, at the time instants $\{iT\}$, to give the sequence $\{r_i\}$, where r_i has a complex value. The $\{r_i\}$ are fed to the decoder which produces at its output the sequence of symbols $\{\hat{s}_i\}$ which form the sequence of decoded binary-data symbols. These decoded symbols $\{\hat{s}_i\}$, having the minimum probability of being

incorrect, form the possible sequence data symbols at the input to the transmitter for which there is minimum mean-square difference (minimum unitary distance squared) [50-52] between the corresponding received sequence of $\{q_i\}$ in the absence of noise and the samples $\{r_i\}$ actually received [41]. Thus, under these conditions, minimum-distance decoding minimizes the probability of error in decoding the received signal. In the absence of noise, the $\{\hat{s}_i\}$ are the same as the $\{s_i\}$ at the input to the encoder at the transmitter.

When the $\{r_i\}$ are fed to the decoder, the decoder forms and stores a set of $m = 2^L$ vectors (sequences) $\{X_L\}$, where

$$X_L = [x_1 \;\; x_2 \;\; x_3 \;\; \ldots\ldots x_L] \qquad 4.4.5$$

and $x_h = 0$ or 1, for $h = 1, 2, \ldots, L$. x_h here represents a possible value of s_h. For each stored vector X_L the decoder forms the vector

$$Y_i = [y_1 \;\; y_2 \;\; y_3 \;\; \ldots\ldots y_i] \qquad 4.4.6$$

where $i = L/2$ (because a coded-symbol is transmitted for each pair of data symbols). The $\{y_h\}$, for $h = 1, 2, \ldots, i$, have complex values, and Y_i, would have been transmitted in place of the sequence of the $\{q_i\}$ had the vector X_L been fed to the encoder at the transmitter in place of the vector

$$S_L = [s_1 \;\; s_2 \;\; s_3 \;\; \ldots\ldots s_L] \qquad 4.4.7$$

that was actually sent. The ISI introduced by the channel is neglected in the decoding process in order to reduce the equipment complexity of the decoder (This assumption is valid because the IF filters only introduce a low level of ISI). The decoder then forms and stores together with each X_L, the corresponding cost measure

$$C_i = c_1 + c_2 + c_3 + \ldots\ldots + c_i \qquad 4.4.8$$

where for $h = 1, 2, \ldots, i$, $c_h = |r_h - y_h|^2$, $|r_h - y_h|$ is the absolute value of the complex value $(r_h - y_h)$. C_i is the square of the unitary distance between the corresponding sequences (vectors) $\{r_i\}$ and $\{y_i\}$. Whether the square of the unitary distance or the unitary distance itself is used, does not affect the basic operation of the system, so that this distance measure will be considered simply as the cost [14]. The m vectors with the minimum costs, subject to any constraints that may be applied to the possible values of some of the $\{x_h\}$.

In practice, each time a new set of m costs $\{C_i\}$ are stored, together with the corresponding m vectors $\{X_L\}$, the values of the smallest cost is subtracted from each C_i, thus setting the smallest C_i to zero. This prevents overflow in the stored values of the $\{C_i\}$, which would otherwise inevitably occur during the reception of a long message. However, to avoid unnecessarily complicating the description of the Viterbi-algorithm decoder, this modification will be neglected. Furthermore, although the cost C_i is that between the $\{r_i\}$ and the $\{y_i\}$, it will, for simplicity, be referred to as the cost of the corresponding X_L.

Ideally, no firm decision is reached as to the value of any s_h until the whole sequence $\{r_i\}$ has been received, when all $\{s_h\}$ are decoded simultaneously from the received $\{r_i\}$, the decoded values $\{\hat{s}_h\}$ being the values of the $\{x_h\}$ in the stored vector X_L having the smallest cost C_i. In practice, as much delay as possible is introduced before decoding (reaching a firm decision on) the value of any s_h, and now $(\hat{s}_{L-2n+1}\ \hat{s}_{L-2n+2})$ taken as the values of $(x_{L-2n+1}\ x_{L-2n+2})$, respectively, in the stored vector X_L having the smallest cost C_i. The integer n is, preferably, several times greater than K (the constraint length of the code) in order to avoid a significant increase in the error probability due to taking firm decisions on the $\{s_h\}$ before the whole message is received [36]. In the determination of $(\hat{s}_{L-2n+1}\ \hat{s}_{L-2n+2})$ the decoder does not need to consider the values of x_{L-2n}, x_{L-2n-1}, ... Thus, instead of storing m L-component vectors $\{X_L\}$, the decoder stores the corresponding $2n$-component vector $\{Z_L\}$, where

$$Z_L = [x_{L-2n+1}\ \ x_{L-2n+2}\ \ x_{L-2n+3}\ \ .....x_L] \qquad 4.4.9$$

so that Z_L is formed by the last $2n$ components of the corresponding vector X_L. The cost C_i of this vector X_L is now said to be the cost of Z_L.

4.5 Viterbi-algorithm decoder for CE8PSK signals

In this section, the Viterbi-algorithm decoding scheme is described for the rate-2/3 convolutionally encoded 8PSK signals. This decoding algorithm, invented by Viterbi, A. J. in 1967 [43], utilises the structural and distance properties of convolutional codes systematically, and it selects the decoded message, the possible sequence of data symbols that has the maximum likelihood function conditioned upon the received signal.

The decoder is described in terms of its output, a set of stored vectors and costs. The algorithm repeated during each symbol interval, which uses the stored values to generate the decoded data symbol $\{\hat{s}_i\}$.

In the Viterbi-algorithm decoder the receiver holds in store the $m = 4^{K-1}$ vectors $\{Z_L\}$ with the minimum costs corresponding to the 4^{K-1} different possible combinations of values of $x_{L-2n+3}, x_{L-2n+4}, \ldots\ldots x_L$. Thus each stored vector Z_L forms the last $2n$ component of the vector X_L that minimizes C_i subject to the constraint that $x_{L-2n+3}, x_{L-2n+4}, \ldots\ldots x_L$ have the given values. It is assumed for convenience here that L>K. Associated with each stored vector Z_L is stored the corresponding C_i. The decoded binary data-symbol $(\hat{s}_{L-2n+3}\ \hat{s}_{L-2n+4})$ are taken to be the values of $(x_{L-2n+3}\ x_{L-2n+4})$, respectively, in the vector Z_L associated with the smallest C_i.

Following the receipt of the sample r_{i+1}, each of the stored vectors $\{Z_L\}$ forms a common part of 4 vectors $\{X_{L+2}\}$, having the 4 possible values of $(x_{L+1}\ x_{L+2})$. Each of these 4 possible vectors is associated with the corresponding cost

$$C_{i+1} = C_i + c_{i+1} \qquad 4.5.1$$

where

$$c_{i+1} = \left| r_{i+1} - y_{i+1} \right|^2 \qquad 4.5.2$$

and C_i is the cost of the original vector Z_L. For each of the 4^{K-1} possible combinations of values $x_{L-2n+5}, x_{L-2n+6}, \ldots\ldots x_{L+1}, x_{L+2}$, the decoder now selects the vector Z_{L+2} and C_{i+1}. $(\hat{s}_{L-2n+3}\ \hat{s}_{L-2n+4})$ are taken to be the values of $(x_{L-2n+3}\ x_{L-2n+4})$, respectively, in the stored vector Z_{L+2} associated with the smallest C_{i+1}. Finally the lowest cost C_i is subtracted from each cost, setting the smallest cost to zero, and the process continues in this way.

r_{i+1} and y_{i+1} in Eqn. 4.5.2 are complex-valued:

$$c_{i+1} = (\mathrm{Re}(r_{i+1} - y_{i+1}))^2 + (\mathrm{Im}(r_{i+1} - y_{i+1}))^2 \qquad 4.5.3$$

and so it requires two operations of squaring or multiplication to determine each value of c_{i+1} (i.e., the unitary distance of two complex numbers). There are 4 different values of c_{i+1} to be computed for each of the m vector $\{Z_L\}$. So that it requires altogether $8m$ operations of squaring or multiplication to determine all the possible values $\{c_{i+1}\}$. However, y_{i+1}, in Eqn. 4.5.2, has only 8 different values because it is one of the possible received complex-valued samples (Fig. 4.7). Thus, of these $4m$ values of c_{i+1}, many have the same values. Therefore there are only 8 possible values of c_{i+1}, and each of them requires 2 operations of squaring or multiplication to be determine. Therefore, following the receipt of the sample r_{i+1}, the decoder has to carry out 16 operations of squaring or multiplication to compute the 8 different values of c_{i+1} which are used to form the $4m$ values of $\{C_{i+1}\}$.

Theoretically, the final choice of the decoded message is not reached until the entire sequence $\{r_i\}$ has been received. But this usually means an unacceptable delay in detection. A good starting up procedure at the beginning of a transmission is to send a known sequence of $\{s_i\}$, immediately correct synchronisation has been achieved at the receiver, and then to set one of the m stored vectors $\{Z_L\}$ in the decoder to the correct sequence and its associated C_i to zero. The remaining vectors $\{Z_L\}$ may be set to any values, and their associated $\{C_i\}$ are set to some very high value. After a few decoding operations, that is after a few received samples $\{r_i\}$, all the stored vectors $\{Z_L\}$ will have been derived from the original correct vector. It is not, in fact, absolutely necessary that this vector to be correct, so that when the decoder has no prior knowledge of the transmitted $\{s_i\}$, the vector Z_L associated with zero may be selected arbitrarily. Correct operation will now be achieved after an initial burst of errors. However, it is absolutely necessary that the receiver provides the required carrier signal with no ambiguity at the beginning of the transmission in order to decode the CE8PSK signal, otherwise, if the recovered carrier has a phase shift of $h\pi/4$, where h=1, 2, 3, 4, 5, 6 or 7, then the decoder is not able to decode the receiving signal.

In general, the Viterbi decoder must process 4^K vectors and 4^K values of costs, following by the storage of 4^{K-1} $2n$-component vectors $\{Z_L\}$ and 4^{K-1} values $\{C_i\}$, are involved in the decoding of each received pair of data (s_{L+1} s_{L+2}). In the present case, K=3, it requires 16 vectors which expand into 64 vectors (i.e., each vector expands 4 ways, for 4 possible values of (x_{L+1} x_{L+2})) to form a Viterbi-algorithm decoder at the receiver. In receiving each sample r_{i+1} the decoder carries out two operations of squaring or multiplication to determine a value of c_{i+1} (Eqn. 4.5.2). Since there are 8 possible values of y_{i+1} the decoder has to carry out altogether 16 operations of squaring or multiplication to compute the 8 different values of c_{i+1} which are used to form the 64 values $\{C_{i+1}\}$.

4.6 Frame synchronisation in TDMA

Digital satellite communication systems require a precise method of communication network synchronisation to ensure that communication integrity is preserved. In TDMA systems the signals from each participating ground station are compressed into high-bit-rate bursts, which are transmitted in assigned nonoverlapping transmission time slots within a periodic time frame. Each transmitting ground station is required to synchronise its access to the communication network so that its burst signals pass through the satellite network without overlapping with burst signals from any other ground station. Furthermore, each receiving ground station must synchronise its access to the communication

network to demultiplex the desired burst signals. Reference bursts are transmitted at the frame rate by one station designated as the regular master reference station. These short bursts are modulated by a reference unique word.

Unique word detection is an important function in frame synchronisation and has been reported in many references [45] [46] [6] [48]. Each station transmits a unique word which has the purpose of establishing burst synchronisation. After carrier recovery and bit timing recovery, the unique word (UW) pattern is recovered by correlation to establish frame synchronisation. By using the last bit of the unique word as a frame marker to indicate the start of a frame, the ground station establishes the time reference for timing its burst signal transmission and for demultiplexing of the received burst signals.

There are two possible forms of error in frame synchronisation: false alarms and misdetection. A 'false alarm' occurs when the frame synchroniser accepts a random data sequence as the recognisable unique word. 'Misdetection' occurs when the frame synchroniser fails to recognise a corrupted unique word. The window technique has been used in some systems to suppress false alarms by taking advantage of the approximate periodicity of the occurrence of the unique word and random distribution of false alarms. In some systems a threshold method has been used to reduce misdetection by allowing a limited predetermined level of errors in the unique word.

Figure 4.10 shows a block diagram of a typical frame synchroniser. The unique word (UW) is supplied to a UW correlator, where it is correlated with a stored pattern of itself. If all bits of the received pattern correspond to those of the stored pattern, the output of the adder yield a binary value I, which correspond to number of differences detected. This value is then compared with a correlation threshold level E, and the output of the comparator (bit c) is set to logic 1 for $I \leq E$, indicating the receipt of a unique word; otherwise bit c is set to logic 0. The mode control logic ensures that the frame synchroniser operates in the right mode, on receipt of a recognisable unique word a detection bit is generated (bit c=1); this is passed through the control block which then generates the appropriate frame marker pulse.

Successful detection of the UW is necessary to mark the time of occurrence of the start of receive frame and to establish the time reference for decoding the received channels. Two types of errors, miss and false alarm, which can influence UW performance. A miss refers to the failure of the UW detector to produce a correlation spike that attains or exceeds a preassigned correlation threshold. If the correlation threshold is set to zero, the UW must be received perfectly before it is recognised. If it is set to a value of I, then I errors anywhere in the UW are allowed in recognising the UW.

The probability of a miss in detecting the UW is the probability of more than E errors in the UW. This probability is a function of the number of bits N in the UW, the bit error probability P_e of the received data, and the threshold value E. For any given number of errors, the number of combinations of a sequence of N bits out of which I bits are in error ($I \leq E$) and N-I are correct is given by [6] [48]

$$C_I^N = \frac{N!}{I!(N-I)!} \qquad 4.6.1$$

then the probability of the unique word miss, is given by [6] [48]

$$Q = \sum_{I=E+1}^{N} C_I^N P_e^I (1-P_e)^{N-I} \qquad 4.6.2$$

Miss probability versus bit-error probability for different unique word length and different correlation threshold level has been evaluated for the system and is shown in Fig. 4.12, also miss probability versus UW length and different correlation threshold level is shown in Fig. 4.13.

Unique word false alarm refers to the occurrence of a UW hit from the correlator when the UW is not actually present. If allowed to occur, it may be very disruptive to TDMA terminal performance because it will result in storage of a garbled message in the TDMA expansion buffer. If all bits, except those in the carrier and bit timing recovery sequence and in the unique word, are assumed to be randomly generated, such that each bit has a 50% probability of being a 1 or a 0, then the probability of a false alarm at any time in the random data bits slot is given by [6] [48]

$$F = \frac{1}{2^N} \sum_{I=0}^{E} C_I^N \qquad 4.6.3$$

where $\frac{1}{2^N}$ is the probability of a particular N-bit sequence in the random data bits slot. False alarm probability versus UW length for random data signal has been evaluated for the system and is shown in Fig. 4.14.

From Eqns. 4.6.2 and 4.6.3 and Figs. 4.12-4.14 it may be deduced that, by raising the error threshold (to reduce the probability of unique word miss), the probability of false alarms occurring correspondingly increases, but alternatively by lowering the error threshold (to reduce the probability of false alarms) the probability of unique word miss is increased.

4.7 Carrier recovery scheme for CE8PSK signals

Coherent demodulation of a PSK signal requires knowledge of the received frequency and phase the PSK carrier. A further requirement in burst format PSK modems is that this knowledge is obtained as quickly as possible after the start of the burst in order that receiver training does not consume a large proportion of the time available for transmission of the data burst.

Conventional methods of carrier recovery suffer from various problems. For example, schemes based on phase-locked loops can exhibit 'hang-up' effects [55] and routinely require a long and variable time to acquire lock, much longer than the minimum time required for a suitable degree of phase estimation. There has been a tremendous amount of work done in carrier recovery schemes and some of them mentioned in [57-60] for modems operating in a burst mode.

A method described in [56] for fast carrier phase estimation appears to have none of the problems associated with the conventional methods. The phase estimator forms part of a feedforward carrier phase recovery scheme in the modem receiver. A block diagram of the phase estimator for carrier synchronisation of CE8PSK signals is given in Fig. 4.11. The estimator operates on received symbol samples which contain an unknown residual frequency offset. These samples are produced by the modem receiver 'front-end' which has performed band-pass (receiver IF filter) filtering, demodulation by a nominally correct, free running carrier frequency oscillator, receiver baseband shaping (demodulation filter) and finally sampling of the resulting signal at the optimum timing phase, Fig. 4.5 and Fig. 4.9.

The signal at the input of the receiver is given by:

$$\begin{aligned} r(t) = &[\sqrt{2}a(t) + N_c(t)]\cos[\omega_c t + \phi(t)] \\ &-[\sqrt{2}b(t) + N_s(t)]\sin[\omega_c t + \phi(t)] \end{aligned} \qquad 4.7.1$$

with $N_c(t)$ and $N_s(t)$ are the noise component, $\phi(t)$ is an arbitrary phase angle.
The inphase and quadrature data signal components plus noise just prior to the demodulation filter are

$$\begin{aligned} r(t)\sqrt{2}\cos\omega_c t &= [\sqrt{2}a(t) + N_c(t)]\cos[\omega_c t + \phi(t)]\sqrt{2}\cos\omega_c t \\ &\quad -[\sqrt{2}b(t) + N_s(t)]\sin[\omega_c t + \phi(t)]\sqrt{2}\cos\omega_c t \\ &= [a(t) + \sqrt{\tfrac{1}{2}}N_c(t)]\cos[\phi(t)] - [b(t) + \sqrt{\tfrac{1}{2}}N_s(t)]\sin[\phi(t)] + \text{h.f.c} \end{aligned} \qquad 4.7.2a$$

and the quadrature component

$$-r(t)\sqrt{2}\sin\omega_c t = [\sqrt{2}a(t)+N_c(t)]\cos[\omega_c t+\phi(t)]\sqrt{2}\sin\omega_c t$$
$$+[\sqrt{2}b(t)+N_s(t)]\sin[\omega_c t+\phi(t)]\sqrt{2}\sin\omega_c t$$
$$=[a(t)+\sqrt{½}N_c(t)]\sin[\phi(t)]+[b(t)+\sqrt{½}N_s(t)]\cos[\phi(t)]+\text{h.f.c} \qquad 4.7.2b$$

The demodulation filter blocks the high frequency components in the signals and produces the inphase and quadrature baseband signal components

$$r_1(t)=[a(t)+n_c(t)]\cos[\phi(t)]-[b(t)+n_s(t)]\sin[\phi(t)] \qquad 4.7.3a$$

$$r_2(t)=[a(t)+n_c(t)]\sin[\phi(t)]+[b(t)+n_s(t)]\cos[\phi(t)] \qquad 4.7.3b$$

The inphase and quadrature baseband signal components at the demodulator filter output can be written as

$$r_1(t)=[\sum_i q_{1,i}h(t-iT)+v_1(t)]\cos[\phi(t)]-[\sum_i q_{2,i}h(t-iT)+v_2(t)]\sin[\phi(t)] \qquad 4.7.4a$$

$$r_2(t)=[\sum_i q_{1,i}h(t-iT)+v_1(t)]\sin[\phi(t)]-[\sum_i q_{2,i}h(t-iT)+v_2(t)]\cos[\phi(t)] \qquad 4.7.4b$$

respectively, where $h(t)$ is the inverse Fourier transform of the transfer function of the overall channel, $v_1(t)$ and $v_2(t)$ are filtered Gaussian noise waveforms. $q_{1,i}$ and $q_{2,i}$ are the transmitted symbols.

The signals are sampled at the demodulator output, at time instants (iT), the signal samples at the output of the demodulation filter are

$$r_{1,i}=[q_{1,i-M}+v_{1,i-M}]\cos(\phi_{i-M})-[q_{2,i-M}+v_{2,i-M}]\sin(\phi_{i-M}) \qquad 4.7.5a$$

$$r_{2,i}=[q_{1,i-M}+v_{1,i-M}]\sin(\phi_{i-M})+[q_{2,i-M}+v_{2,i-M}]\cos(\phi_{i-M}) \qquad 4.7.5b$$

where M is dependent on the lengths of the sampled impulse responses of the digital filters. The estimator operates on these received symbol samples which contain an unknown residual frequency offset.

The first stage of the estimator inputs the symbol samples to a nonlinearity which has an output (Fig. 4.11) given by

$$r'_{1,i-M}+jr'_{2,i-M}=e^{j8\theta_{i-M}} \qquad 4.7.6$$

where $$\theta_{i-M}=\tan^{-1}\left(\frac{r_{2,i-M}}{r_{1,i-M}}\right)$$

$$\theta_{i-M} = \tan^{-1}\left(\frac{[q_{1,i-M} + v_{1,i-M}]\sin(\phi_{i-M}) + [q_{2,i-M} + v_{2,i-M}]\cos(\phi_{i-M})}{[q_{1,i-M} + v_{1,i-M}]\cos(\phi_{i-M}) - [q_{2,i-M} + v_{2,i-M}]\sin(\phi_{i-M})}\right)$$

$$= \tan^{-1}\left(\frac{\tan(\phi_{i-M}) + \dfrac{[q_{2,i-M} + v_{2,i-M}]}{[q_{1,i-M} + v_{1,i-M}]}}{1 - \dfrac{[q_{2,i-M} + v_{2,i-M}]}{[q_{1,i-M} + v_{1,i-M}]}\tan(\phi_{i-M})}\right) \qquad 4.7.7$$

but $\dfrac{q_{2,i-M}}{q_{1,i-M}} = \tan\psi_{i-M}$, where ψ_{i-M} is the phase angle received at time $t=(i\text{-}M)T$ in the absence of noise and of (phase and frequency) offsets, so the phase angle can be written as

$$\theta_{i-M} = \tan^{-1}\left(\frac{\tan(\phi_{i-M}) + \tan\psi_{i-M}}{1 - \tan\psi_{i-M}\tan(\phi_{i-M})}\right) \qquad 4.7.8$$

$$\theta_{i-M} = \tan^{-1}(\tan(\phi_{i-M} + \psi_{i-M}) \qquad 4.7.9$$

$$\theta_{i-M} = (\phi_{i-M} + \psi_{i-M}) \qquad 4.7.10$$

The nonlinearity therefore obtains the phase angle θ_{i-M} for the $(i\text{-}M)$th symbol sample, multiplies this angle by 8, then converts the resulting angle back to a rectangular form.

The complex output from the nonlinearity are then averaged over $2N+1$ symbol intervals and the resulting average value is then converted to a phase angle and divided by 8 to provide an unbiased estimate of the carrier phase angle present on the symbol sample $r_{1,i} + jr_{2,i}$. That is:

$$\hat{\theta}_{i-M} = \frac{1}{8}\tan^{-1}\left[\frac{\sum_{j=-N}^{N} r'_{2,i-M-j}}{\sum_{j=-N}^{N} r'_{1,i-M-j}}\right] \qquad 4.7.11$$

After the phase estimate $\hat{\theta}_{i-M}$ has been obtained it is used to correct the symbol sample $r_{1,i} + jr_{2,i}$. However, before the correction can be made, it is necessary to know the possible symbol values. If, as is normal for CE8PSK signals, these have the values $\pm 0.924 \pm j0.383$ or $\pm 0.0.383 \pm j0.924$, then $\pi/8$ must be subtracted from $\hat{\theta}_{i-M}$ to obtain the actual carrier phase error. The correct value of $\hat{\theta}_{i-M}$ therefore lies in the range $-\pi/8 \le \hat{\theta}_{i-M} \le \pi/8$. The phase corrector must be capable of phase correction in the range $-\pi$ to π, otherwise errors will occur at regular intervals in the

presence of frequency offset. Thus, a circuit could be employed which senses when $\left|\hat{\theta}_{i-M}-\hat{\theta}_{i-M-1}\right|>\pi/8$ and increments or decrements the additional phase circuit by $\pi/4$ depending on the sign of $(\hat{\theta}_{i-M}-\hat{\theta}_{i-M-1})$. A sine and cosine for phase error can be obtain to give $\sin(-\hat{\theta}_{i-M})$ and $\cos(-\hat{\theta}_{i-M})$. These are used to remove the residual carrier frequency from $r_{1,i}+jr_{2,i}$ as follows,

$$(r_{1,i}+jr_{2,i})_{\text{correct}}=(r_{1,i}+jr_{2,i})[\cos(-\hat{\theta}_{i-M})+j\sin(-\hat{\theta}_{i-M})] \qquad 4.7.12$$

Finally, the additional phase correction is applied by performing the appropriate $n\pi/4$ phase shift on $r_{1,i}+jr_{2,i}$.

The carrier phase estimator described has been tested by the computer simulations for CE8PSK system with a carrier frequency offset Δf = 1, 2 or 3 KHz and the receiver operating over a bandlimited, nonlinear satellite channel when the HPA operates at 0 dB saturation point which introduces both AM/AM and AM/PM conversion on the transmitted signal.

4.8 Performances of CE8PSK signal

An analysis method generally applicable to the derivation of the error probability for convolutional codes is not available. Most authors use lower and upper bounds for error probability as performance criteria.

In the presence of AWGN the probability of detecting a modulated signal $m_j(t)$ when a modulated $m_i(t)$ has been sent, is given by (Appendix A10)

$$P_E=Q(\frac{d_{ij}}{\sqrt{2N_0}}) \qquad 4.8.1$$

where $\frac{1}{2}N_0$ is the two-sided noise spectral density and d_{ij} is the Euclidean distance between the modulated signals $m_j(t)$ and $m_i(t)$ given by

$$d_{i,j}^2=\int_t[m_i(t)-m_j(t)]^2dt \qquad 4.8.2$$

It is well known that for low probability of error this probability is almost completly determined by the minimum Euclidean distance $d_{\min}$ between two signals corresponding to different values of the data symbols [54], [61], [62]. Hence, at a large signal/noise power ratio, the symbol error rate probability of a CE8PSK signal can be written as

$$P_s \cong \mathrm{Q}\left(\sqrt{\frac{d_{\min}^2}{2N_0}}\right) \qquad 4.8.3$$

where $d_{\min}$ here is the minimum Euclidean distance between any two received signals corresponding to different data-symbol values. Thus the symbol error rate probability P_s is asymptotically determined by the minimum Euclidean distance $d_{\min}$.

The coding gain of CE8PSK signals can be expressed as the tolerance to noise relative to that of an uncoded QPSK signal. At large signal/noise power ratio, the reduction in required signal/noise power ratio is referred to as the asymptotic coding gain, which is completely determined by the minimum Euclidean distance, as can be seen in Eqn. 4.8.3. So, if an uncoded QPSK signal has a minimum Euclidean distance of d_0, then the asymptotic coding gain for a CE8PSK signal is equal to the square of the ratio of the minimum Euclidean distance, $d_{\min}$ of CE8PSK signal to d_0, i.e., $d_{\min}^2/d_0^2$. (Note that both QPSK and CE8PSK signals carry 2 information bits per symbol).

For the CE8PSK signal considered herein (i.e., using Code 1 in Table 4.1), the value $d_{\min}^2/d_0^2$ of the signal has been found to be 2.586 [32], and so the asymptotic coding gain is 4.1 dB. In many cases, the performance in the nonasymptotic region (e.g., $P_e = 10^{-3} - 10^{-4}$) is more important, so computer simulation tests are usually used to evaluate the performances of CE8PSK signals. For the present case, the performance of the CE8PSK signal, using Code 1 shown in Table 4.2, over AWGN channel, has been evaluated by computer simulation [31] and is shown in Fig. 4.2. This indicates that a coding gain of 2.6 dB, relative to an uncoded QPSK signal, can be obtained at $P_e = 10^{-4}$. At sufficiently low error rates the coding gain would approach the asymptotic value.

4.9 Distance measure for minimum-distance decoding of CE8PSK signals

In the CE8PSK system described in Section 4.3, the binary symbols in the original data signal are statistically independent and equally likely to be either 0 or 1. The decoding process that minimizes the probability of error in the decoding of the whole received sequence selects the possible sequence of data symbols fed to the encoder at the transmitter that maximizes the corresponding conditional probability density function of the received signal [41]. The received signal is sampled once per received encoded symbol and the decoding operation is carried out on the resultant sample values. In the presence of additive Gaussian noise, giving noise samples that are statistically independent Gaussian random variables with zero mean and fixed variance (referred to as 'white' Gaussian noise), the decoded message having the

minimum probability of being incorrect, is the possible sequence of data symbols at the input to the encoder at the transmitter for which there is the minimum unitary distance between the corresponding received sequence of samples in the absence of noise and the samples actually received [41]. Thus, under these coditions, minimum-distance decoding, using the unitary distance, minimizes the probability of error in the decoding signal at the receiver. The minimum-distance decoding of CE8PSK signal can be achieved in practice by means of the Viterbi-algorithm [41] which is described in Section 4.5.

Let the $(i+1)$ sample values r_1 to r_i used for decoding the $\{s_i\}$, Eqn. 4.4.7 in Section 4.4, be given by the i-component row vector

$$R_i = [r_1 \;\; r_2 \;\; r_3 \;\; \ldots\ldots \;\; r_i] \qquad 4.9.1$$

where the $\{r_h\}$, for $h = 1, 2, \ldots\ldots, i$, have complex values. R_i is the vector formed by the received samples. The Viterbi decoder forms and stores a set of $m = 2^L$ vectors (sequences) $\{X_L\}$, where

$$X_L = [x_1 \;\; x_2 \;\; x_3 \;\; \ldots\ldots \;\; x_L] \qquad 4.9.2$$

and $x_h = 0$ or 1, for $h = 1, 2, \ldots\ldots, L$, x_h here represents a possible value of s_h. For each stored vector X_L the decoder forms the vector

$$Y_i = [y_1 \;\; y_2 \;\; y_3 \;\; \ldots\ldots \;\; y_i] \qquad 4.9.3$$

where $i = L/2$, $\{y_h\}$, for $h = 1, 2, \ldots\ldots, i$, have complex values, and Y_i would have been transmitted in place of the sequence of the $\{q_i\}$ (the convolutionally encoded symbols), had the vector X_L been fed to the encoder at the transmitter in place of the vector

$$S_L = [s_1 \;\; s_2 \;\; s_3 \;\; \ldots\ldots \;\; s_L] \qquad 4.9.4$$

that was actually sent. The decoder forms and stores together with each X_L, the corresponding cost (Eqn. 4.4.8)

$$C_i = c_1 + c_2 + c_3 + \ldots\ldots + c_i \qquad 4.9.5$$

$$= \sum_{h=1}^{i} c_h \qquad 4.9.6$$

where, for h = 1, 2, ..., i, $c_h = |r_h - y_h|^2$ if the square of the unitary distance [50] is used as the distance measure.

The maximum likelihood sequence of possible data symbols, determined from the received vector R_i, is given by the possible vector X_L associated with the smallest value of C_i, which is the square of the unitary distance [50] between the vectors R_i and Y_i. As mentioned in Section 4.4, whether the square of the unitary distance or the unitary distance itself is used, does not affect the basic operation of the system, so that the square of the unitary distance will be considered simply as the cost. Since the encoded data symbols $\{q_i\}$ are statistically independent and equally likely to have any of their 8 possible values, the maximum likelihood vector X_L is the most likely to be correct, given the received vector R_i [50], [65].

4.10 Simulation results and discussion

To assess the error-rate performances for different systems, using CE8PSK and CDE8PSK signals, computer simulation tests have been carried out , under different conditions, with the equipment filters and HPA described in Section 2.4 and 2.5. The simulation models and methods used to obtain the results in this section are described in Sections 4.4, 4.5 and 4.7. In all simulation tests, it is assumed that the receiver provides the required ideal carrier and timing signals unless it is specified, and the data-transmission systems are optimized by sharing the overall filtering equally between the transmitter and receiver filters, and the Viterbi decoder (for CE8PSK) at the receiver uses 16 stored vectors with a delay of 32 symbols in decoding.

For DEQPSK signals, it is shown in Section 3.6.1 that, the minimum truncation lengths of the sampled impulse responses of the modulation and demodulation filters, with $\alpha = 100\%$, 40% and 25% required to approximate to the theoretical ideal error-rate performance at $P_e \geq 10^{-4}$, are 5T, 5T and 8T, respectively, and they are denoted as signals 1A, 2A and 3A, respectively. Now for CE8PSK signals, the same wave shapes of the modulating signals are used in the simulation tests, but they are known here as signals 1B, 2B and 3B, instead of signals 1A, 2A and 3A, respectively. Thus signals 1B, 2B and 3B apply to CE8PSK signals, with $\alpha = 100\%$, 40% and 25%, and with truncation lengths of the sampled impulse responses of 5T, 5T and 8T respectively.

4.10.1 Performances of signals 1B, 2B and 3B over a nonlinear and bandlimited channel

It is mentioned in Section 3.6.2, that the degradation in tolerance to noise caused by the HPA are due to nonlinear distortion. The model used to evaluate the effects of

nonlinear distortion on error-rate performance is shown in Fig. 4.9, where the nonlinear and bandlimited bandpass channel is used. The results for signals 1B, 2B and 3B, with the HPA operating at 0, 0.315 and 0.7 dB OBO, are shown in Figs. 4.15-4.17.

When the HPA operating at 0 dB OBO (output backoff) (i.e., at saturation point), Fig. 4.15 shows that signal 1B has little degradations in tolerance to noise at $P_e \geq 10^{-4}$, signal 2B has a degradation of about 0.65 dB, while signal 3B, because of its relatively narrow bandwidth, which causes more severe fluctuations in the timing waveform (Fig. 2.8), thus more nonlinear distortion is caused by the HPA, has a degradation of about 0.9 dB at $P_e = 10^{-4}$, in comparison with that of an ideal CE8PSK system.

With the HPA operating at 0.315 dB OBO (i.e., slightly below saturation), Fig. 4.16 shows that the degradations in tolerance to noise of signals 1B, 2B and 3B have little improvements in performance when compared with those with 0 dB HPA OBO, at $P_e \geq 10^{-4}$, signal 2B has improvement of about 0.25 dB, whereas signal 3B has reduced the degradation to about 0.7 dB (i.e., 0.2 dB improvement is achieved).

Figure 4.13 shows that, with the HPA OBO value further increased from 0.315 dB to 0.7 dB, the degradations in tolerance to noise of signals 1B, 2B and 3B, at $P_e \geq 10^{-4}$ have improved in comparison with 0 dB HPA OBO, and the improvement for signal 2B is about 0.3 dB and for signal 3B is about 0.4 dB.

Figures 4.18, 4.19 and 4.20 shows the error-rate performances for signals 1B, 2B and 3B respectively, with the HPA OBO operating at 0, 0.315 or 0.7 dB for each of the signals, the results show that the degradations in tolerance to noise of the signals decreases when the HPA operating point is further below saturation (i.e., 0.7 dB OBO).

The degradation in tolerance to noise of the CE8PSK signals, at $P_e = 10^{-4}$, with the HPA operating at 0, 0.315 and 0.7 dB OBO, measured in comparison with that of an ideal CE8PSK system, are shown in Table 4.3a. It can be seen that, with the HPA operating in the nonlinear mode at the earth station, the degradations in tolerance to noise of CE8PSK signals due to nonlinear distortion are insignificant. The worst case is when signal 3B is used with the HPA operating at 0 dB OBO, and the degradation is about 0.9 dB at $P_e = 10^{-4}$, in comparison with that of an ideal CE8PSK system. In all the other cases, the degradations are in the range 0.2-0.65 dB at $P_e = 10^{-4}$. Hence, with the HPA operating at 0, 0.315 and 0.7 dB OBO, the error-rate performances for the CE8PSK signals, when transmitted over the nonlinear and bandlimited bandpass channel are about the same.

Table 4.3b (reproduced from Table 3.5) shows the degradations in tolerance to noise of the DEQPSK signals, under the same assumed conditions. It can be seen that

the nonlinear distortion effects on degradations of all the CE8PSK and DEQPSK signals tested are about the same. However when the HPA is operating at 0 dB OBO, signal 3B has a degradation of about 0.9 dB at $P_e = 10^{-4}$, while signal 3A loses 2.6 dB.

4.10.2 Performances of signals 1B, 2B and 3B over a nonlinear and bandlimited channel with the use of carrier synchronisation scheme

To evaluate the error-rate performances of CE8PSK signals, over a nonlinear and bandlimited channel with the use of carrier synchronisation scheme proposed in section 4.7, the same model as shown in Fig.4.9 is used. Here the encoder at the transmitter carries out convolutional and Gray encoding of the input data, as described in Section 4.4, while the decoder at the receiver is that described in Section 4.5 and the carrier synchronisation scheme described in section 4.7 with frequency offset $\Delta f = 0$, 1, 2 and 3 KHz. As mentioned before, the CE8PSK signals here called signals 1B, 2B and 3B, respectively. Thus signals 1B, 2B and 3B are referred to CE8PSK signals with $\alpha = 100\%$, 40% and 25%, respectivelly, and with truncation lengths of the sampled impulse responses of 5T, 5T and 8T respectively. The HPA operating at 0 dB OBO.

When the frequency offset Δf =3KHz signal 1B in Fig. 4.21 has a degradation in tolerance to noise about 0.9 dB at $P_e = 10^{-4}$ in comparison with that of an ideal CE8PSK system, while when the frequency offset is further decreased from 3 to 2 KHz, the degradations in tolerance to noise of signal 1B has decreased to be 0.6 dB at $P_e = 10^{-4}$, in comparison with that of an ideal CE8PSK system and a further decrease in frequency offset to 1 KHz, the degradation is about 0.4 dB at $P_e = 10^{-4}$.

Figure 4.22 shows the error-rate performances of signal 2B when the frequency offset is 3 KHz, the degradation in tolerance to noise at $P_e = 10^{-4}$ is 1.2 dB, a further decrease in frequency offset to 2 KHz the degradation is 0.8 dB, an 0.4 dB improvements. When the frequency offset decreased to 1 KHz the degradation in tolerance to noise , is 0.6 dB at $P_e = 10^{-4}$, in comparison with that of an ideal CE8PSK signal.

Figure 4.23 shows the error-rate performances of signal 3B, which suffers the most degradation in comparison with signals 1B and 2B, because of its relatively narrow bandwidth, which causes more severe fluctuations in the timing waveform (Fig. 2.8), thus more nonlinear distortion is caused by the HPA when operating at saturation point. The degradation in tolerance to noise at $P_e = 10^{-4}$ when the frequency offset is 3 KHz is 1.6 dB and further decrease in frequency offset to 2 KHz reduce the degradation to 1.3 dB, and when it is 1 KHz the degradation decreased to about 0.9 dB in comparison to that of an ideal CE8PSK signal at $P_e = 10^{-4}$.

The degradation in tolerance to noise of the CE8PSK signals, at $P_e = 10^{-4}$, with the HPA operating at 0 dB OBO, and for different values of frequency offset, measured in comparison with that of an ideal CE8PSK system, are shown in Table 4.4. The worst case is when signal 3B is used with the HPA operating at 0 dB OBO and frequency offset is 3 KHz, and the degradation is about 1.6 dB at $P_e = 10^{-4}$, in comparison with tthat of an ideal CE8PSK system. In all other cases the degradations are in the range 0.4-1.2 dB at $P_e = 10^{-4}$. When the CE8PSK system compared eith an ideal uncoded QPSK system, there is a significant improvement for CE8PSK system and the improvement are in the range 2-2.4 dB.

Code	Code Memory (K-1) bit	Sub-genarator $G_1(j)$	Sub-genarator $G_2(j)$	j	Asymptotic gain gains (dB)
1	4	010	101	1	4.1
		111	001	2	
		000	010	3	
2	6	0110	1011	1	5
		1101	1001	2	
		0000	0110	3	

Table 4.1 Rate 2/3 binary codes for CE8PSK signals.

Octal symbol			Phase (degrees)	Magnitude of quadrature components	
$e_i(1)$	$e_i(2)$	$e_i(3)$		$q_{1,i}$	$q_{2,i}$
0	0	0	+ 22.5	+ 0.924	+ 0.383
0	0	1	+ 67.5	+ 0.383	+ 0.924
0	1	0	+ 112.5	- 0.383	+ 0.924
0	1	1	+ 157.5	- 0.924	+ 0.383
1	0	0	- 157.5	- 0.924	- 0.383
1	0	1	-112.5	- 0.383	- 0.924
1	1	0	- 67.5	+ 0.383	- 0.924
1	1	1	- 22.5	+ 0.924	- 0.383

Table 4.2 Gray encoding for CE8PSK signals.

HPA OBO (in dB)	Signal		
	1B	2B	3B
0	0.45	1	1.2
0.315	0.25	0.65	0.9
0.7	0.2	0.45	0.8

(a)

HPA OBO (in dB)	Signal		
	1A	2A	3A
0	0.75	0.75	2.6
0.315	0.5	0.65	2.3
0.7	0.35	0.5	2.2

(b)

Table 4.3 Degradations in tolerance to noise of signals (a) 1B, 2B and 3B, and (b) 1A, 2A and 3A, over a nonlinear and bandlimited channel, with the HPA operating at 0, 0.315 and 0.7 dB OBO, at $P_e = 10^{-4}$, expressed in dB, measured in comparison with that of the corresponding ideal systems (from Figs. 4.15, 4.16 and 4.17).

Frequency offset Δf (KHz)	Signal		
	1B	2B	3B
1	0.4	0.6	0.9
2	0.6	0.8	1.3
3	0.9	1.2	1.6

Table 4.4 Degradations in tolerance to noise of signals 1B, 2B and 3B, due to different frequency offset values, over a nonlinear and bandlimited channel, with the use of phase estimator, the HPA operating at 0 dB OBO, at $P_e = 10^{-4}$, expressed in dB, measured in comparison with that of the ideal CE8PSK system (from Figs. 4.21, 4.22 and 4.23).

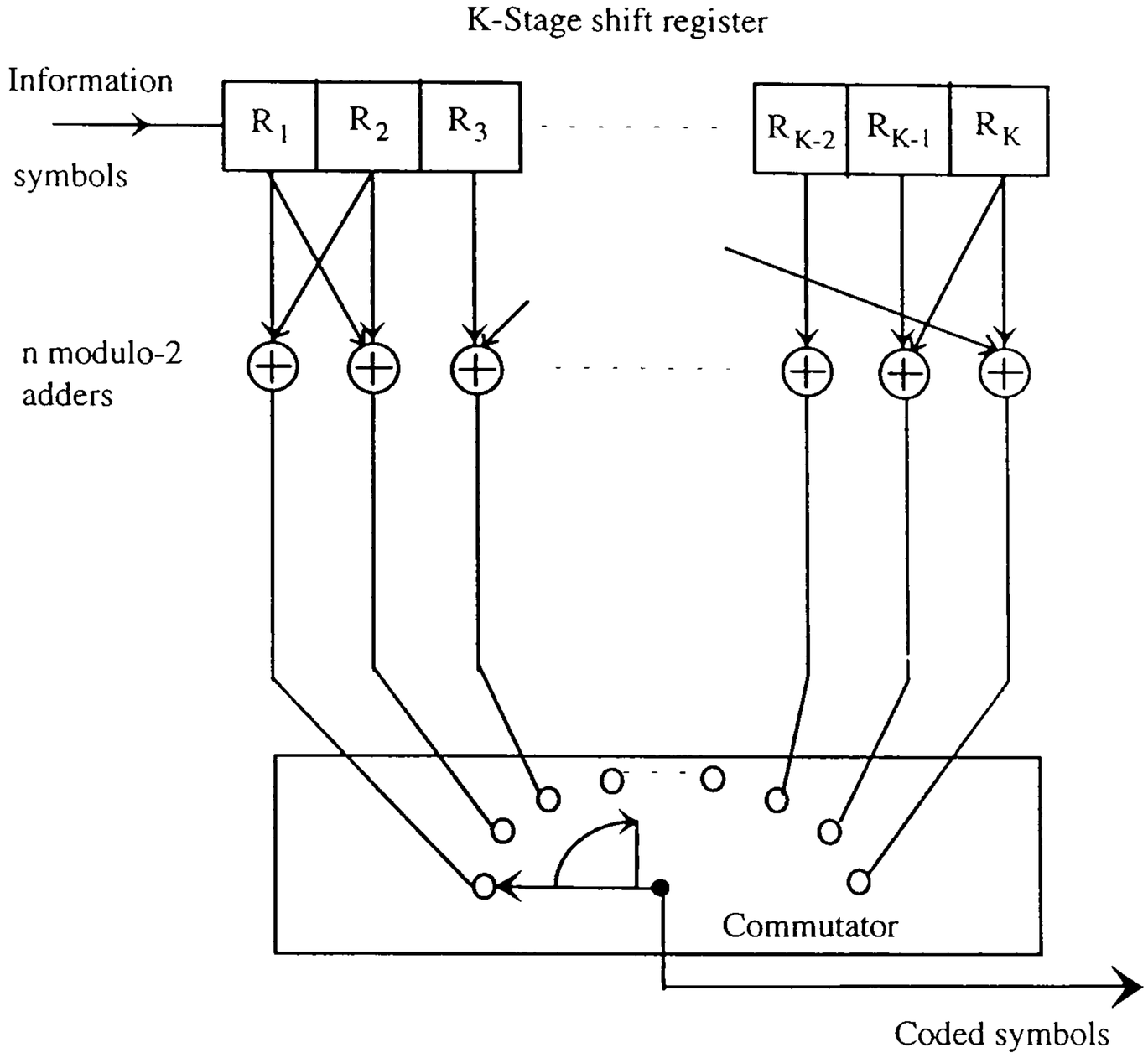

Figure 4.1 General convolutional encoder.

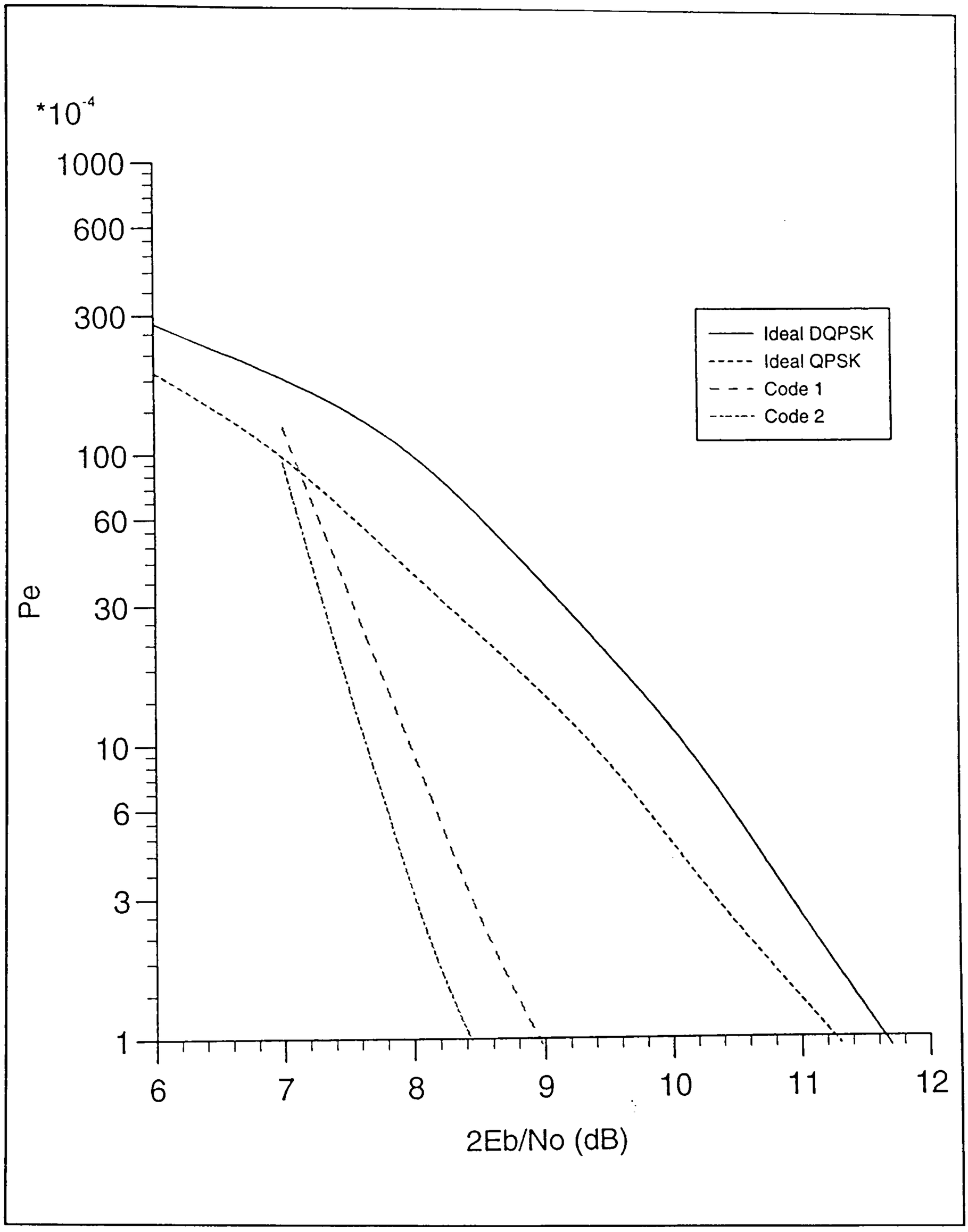

Figure 4.2 Error-rate performances of Code 1 and 2 in Table 4.1, over an AWGN channel using Viterbi decoding.

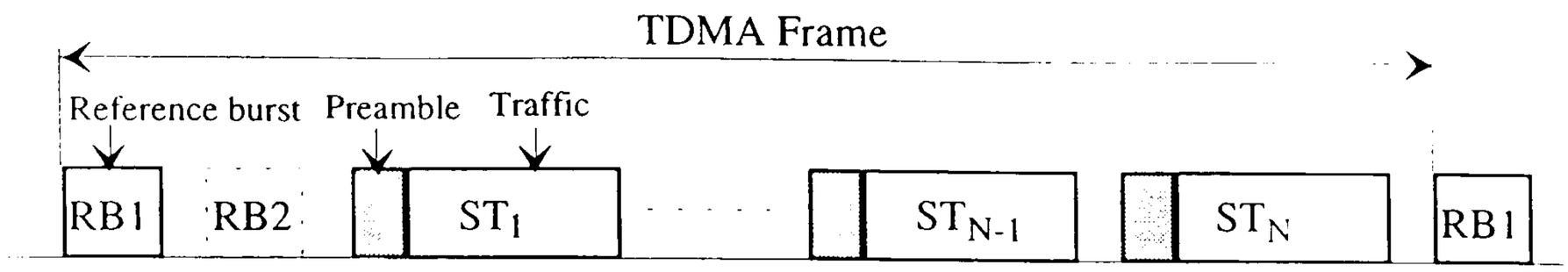

a) Frame structure.

Carrier & bit timing recovery	Unique word	TTY	SC	VOW	VOW	CDC

b) Reference burst structure.

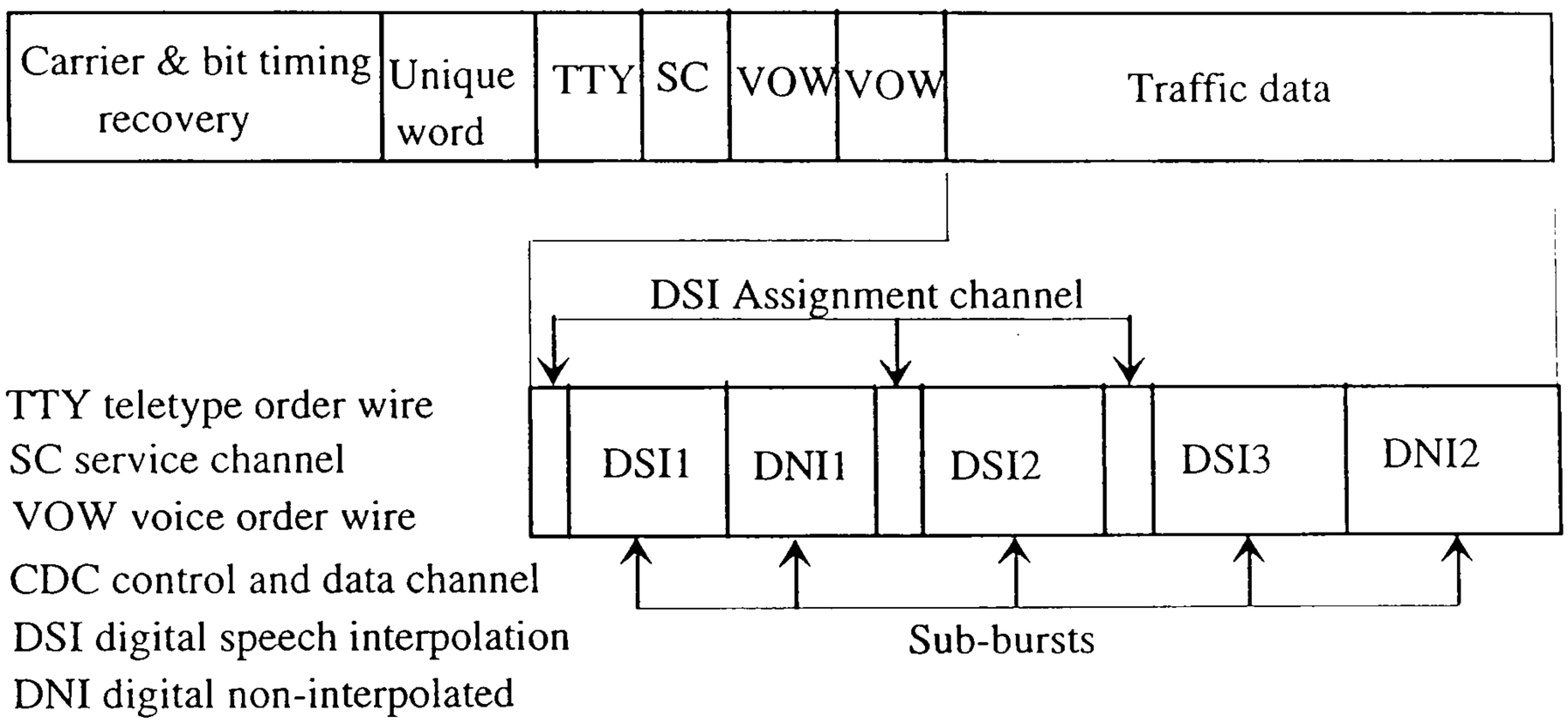

c) Traffic burst structure.

Figure 4.3 General TDMA frame organisation.

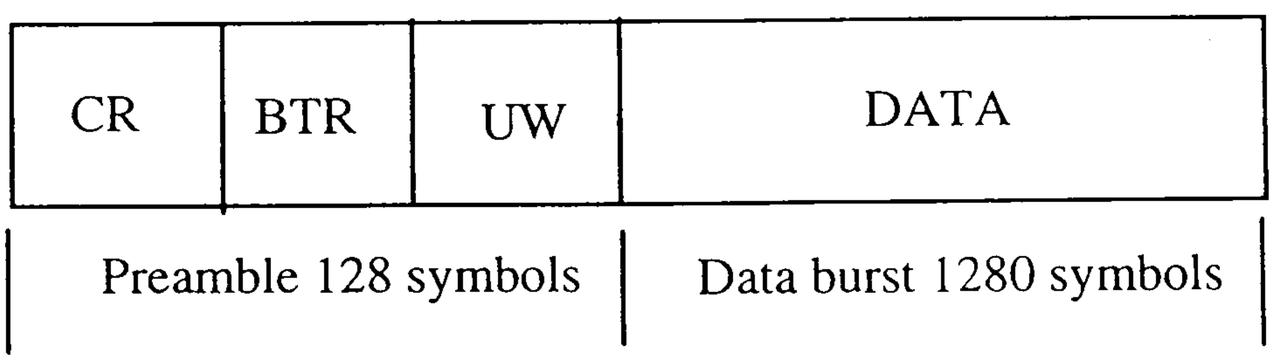

CR carrier recivery

BTR bit timing recivery

UW unique word

Figure 4.4 Traffic burst used in computer simulation.

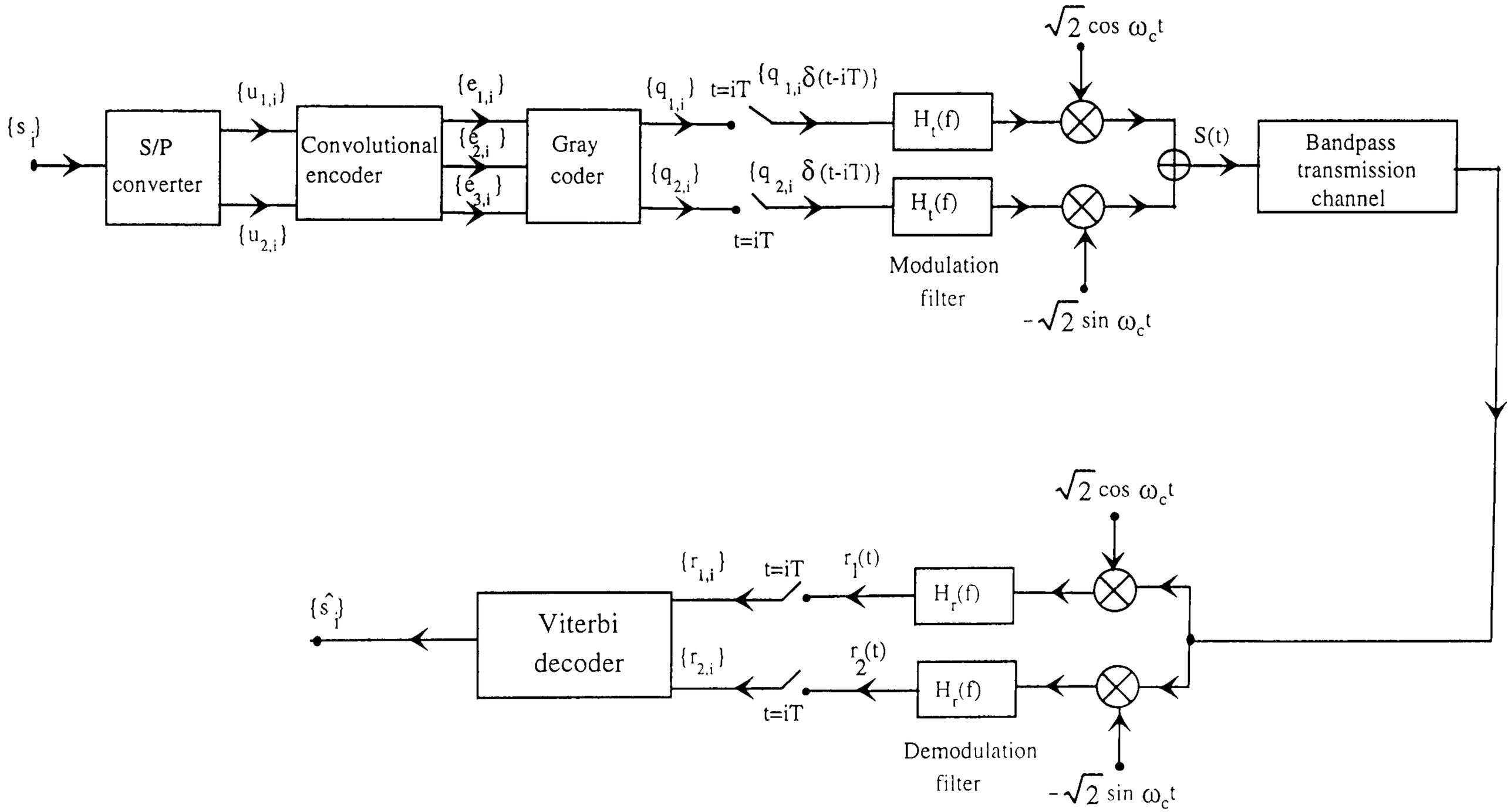

Figure 4.5 Block diagram of a convolutional encoder 8PSK (CE8PSK) system representation. S/P means serial-to-parallel.

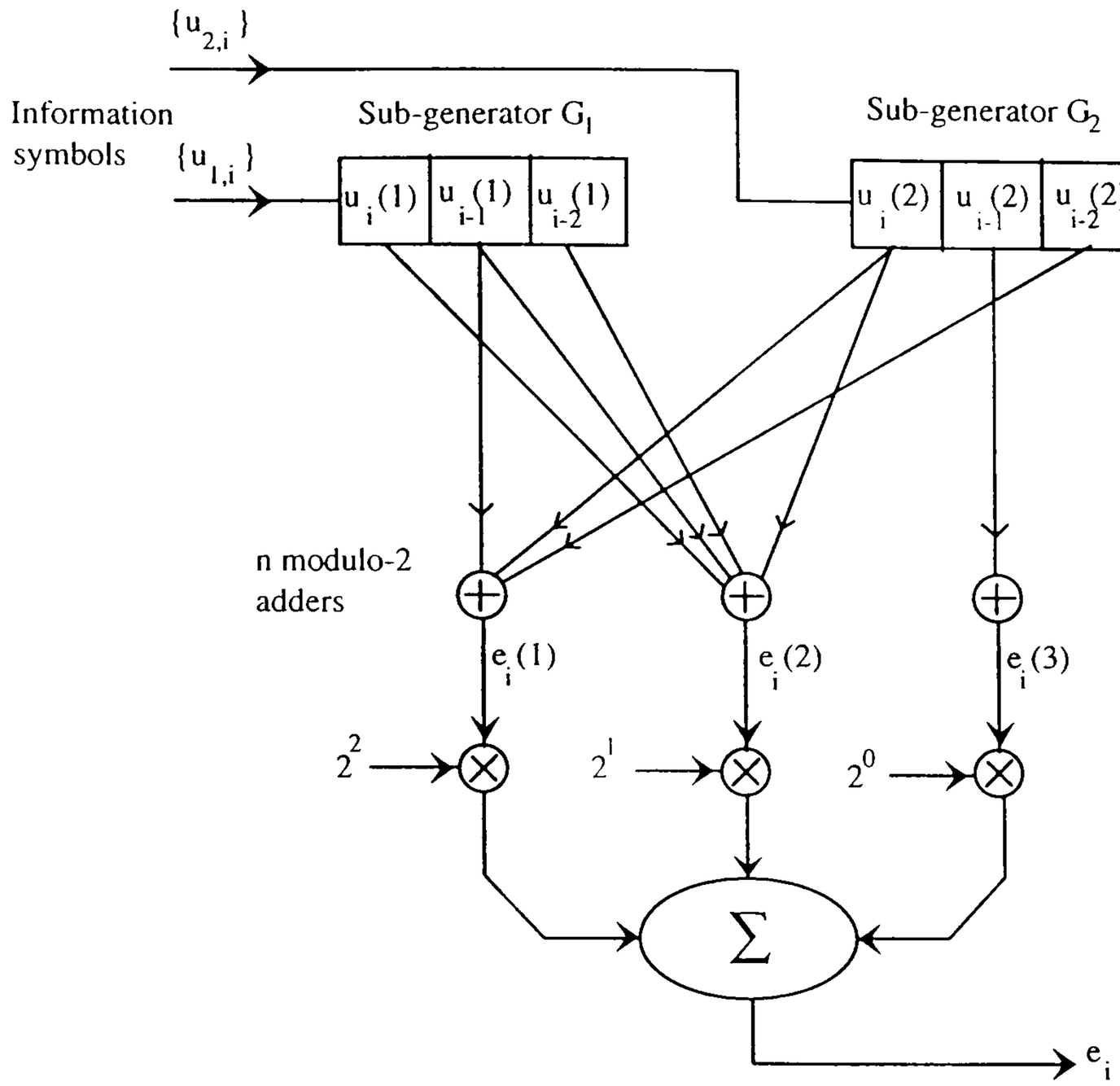

Figure 4.6 Encoder configuration for Code 1.

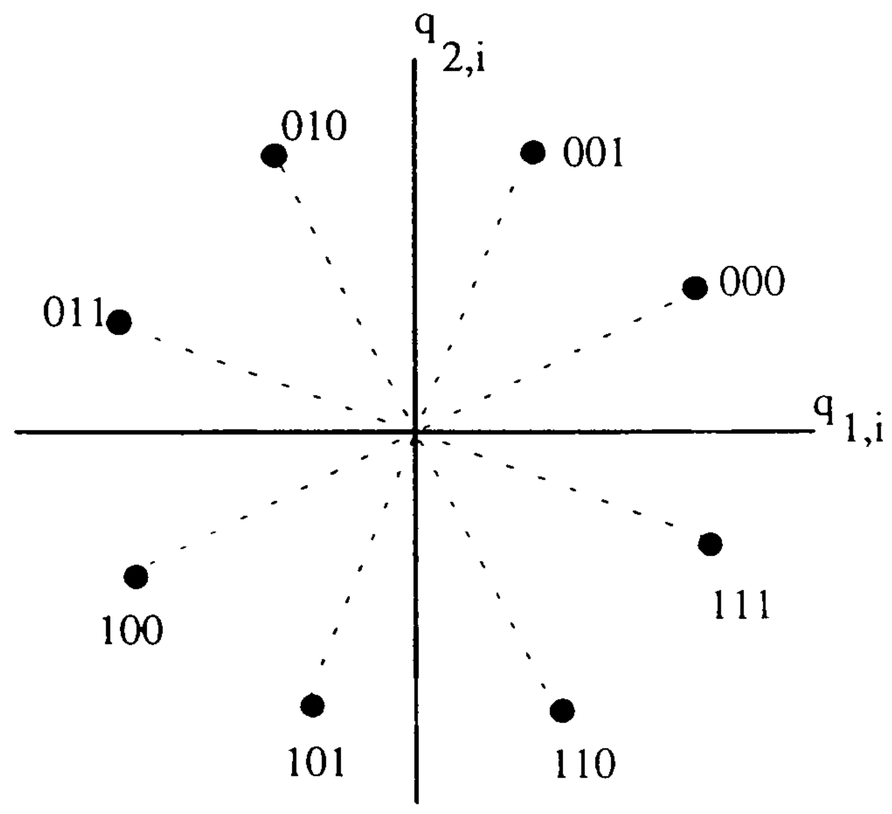

Figure 4.7 CE8PSK signal constellation (possible received signal vectors).

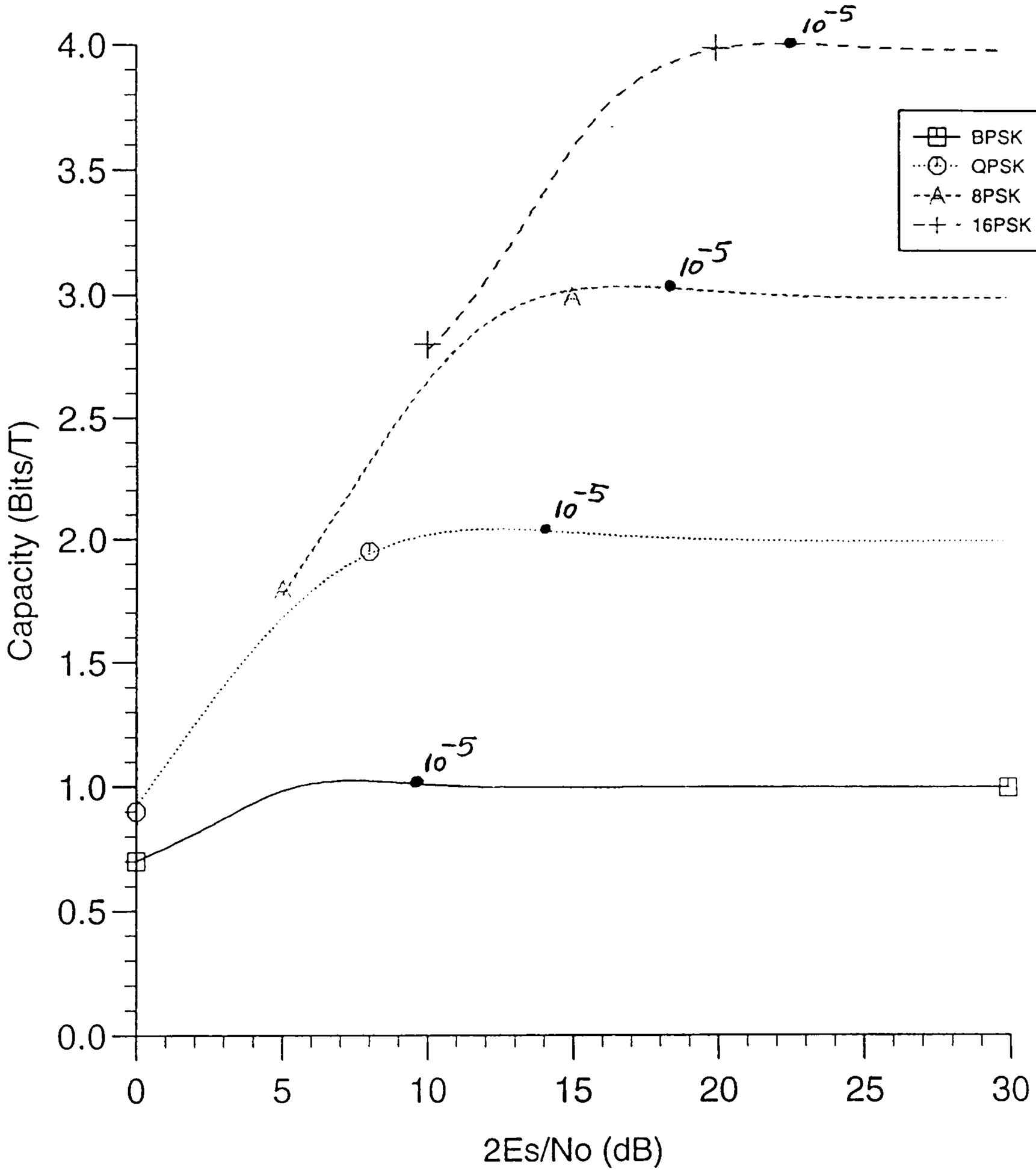

Figure 4.8 Variation of channel capacity with $2E_b/N_0$.

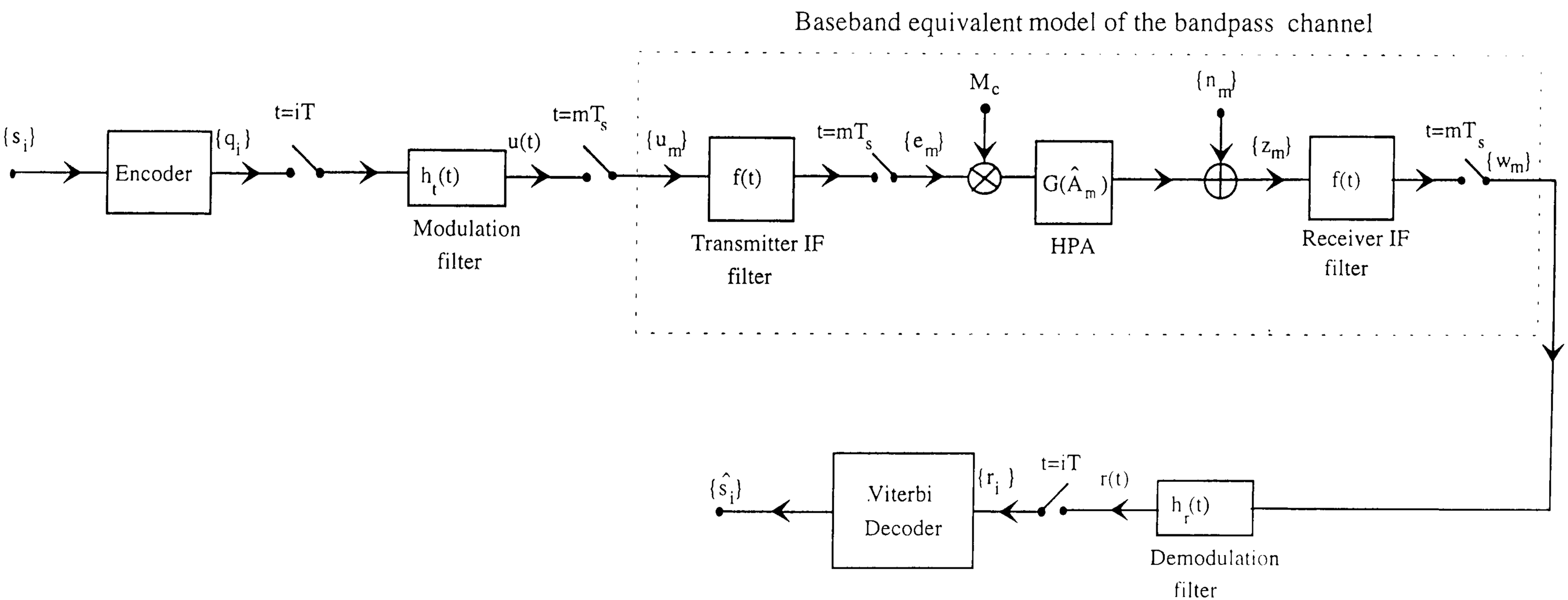

Figure 4.9 Baseband equivalent model of the CE8PSK system with a nonlinear and bandlimited satellite channel, for computer simulation.

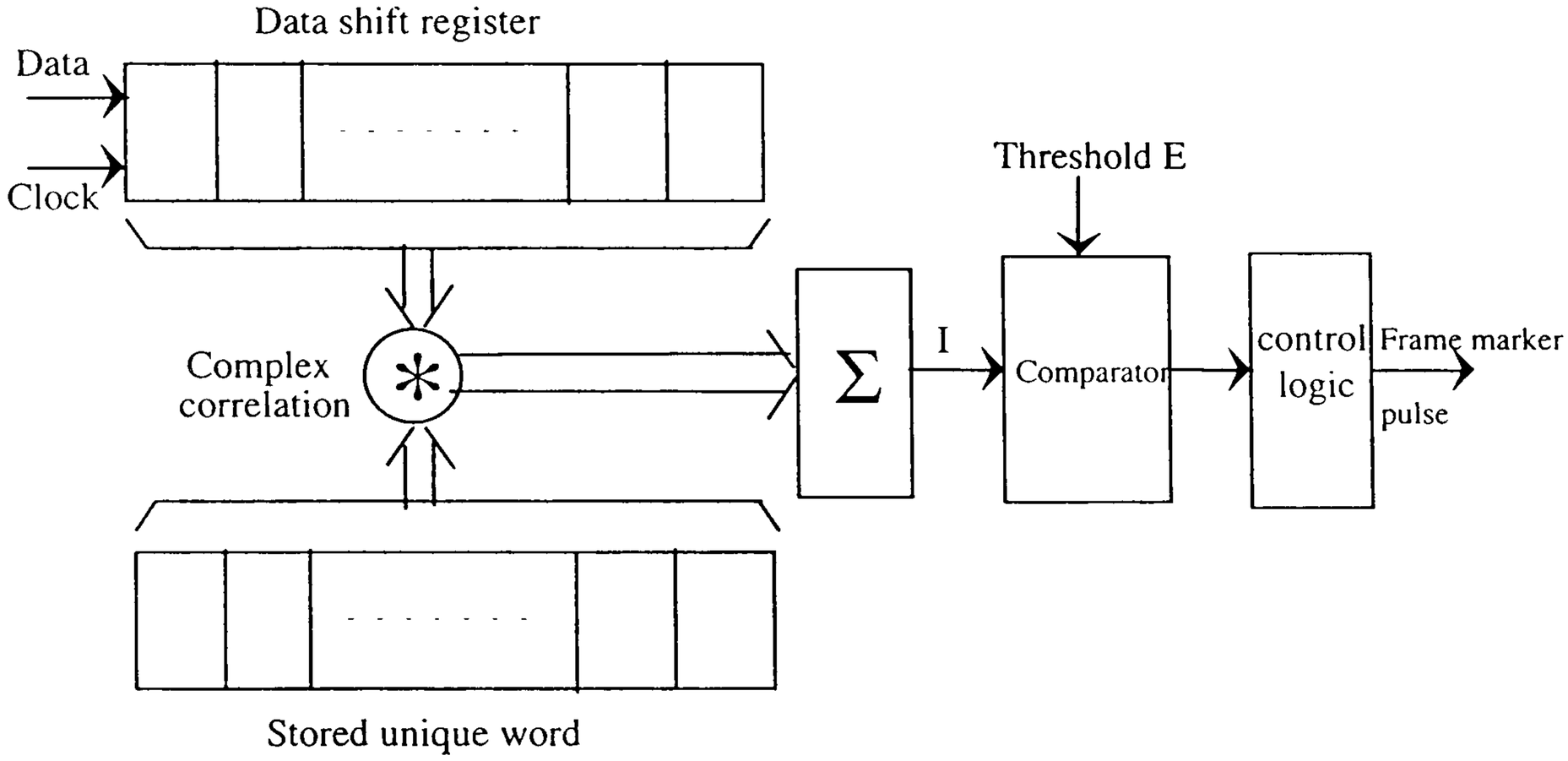

Figure 4.10 A typical digram of frame synchroniser.

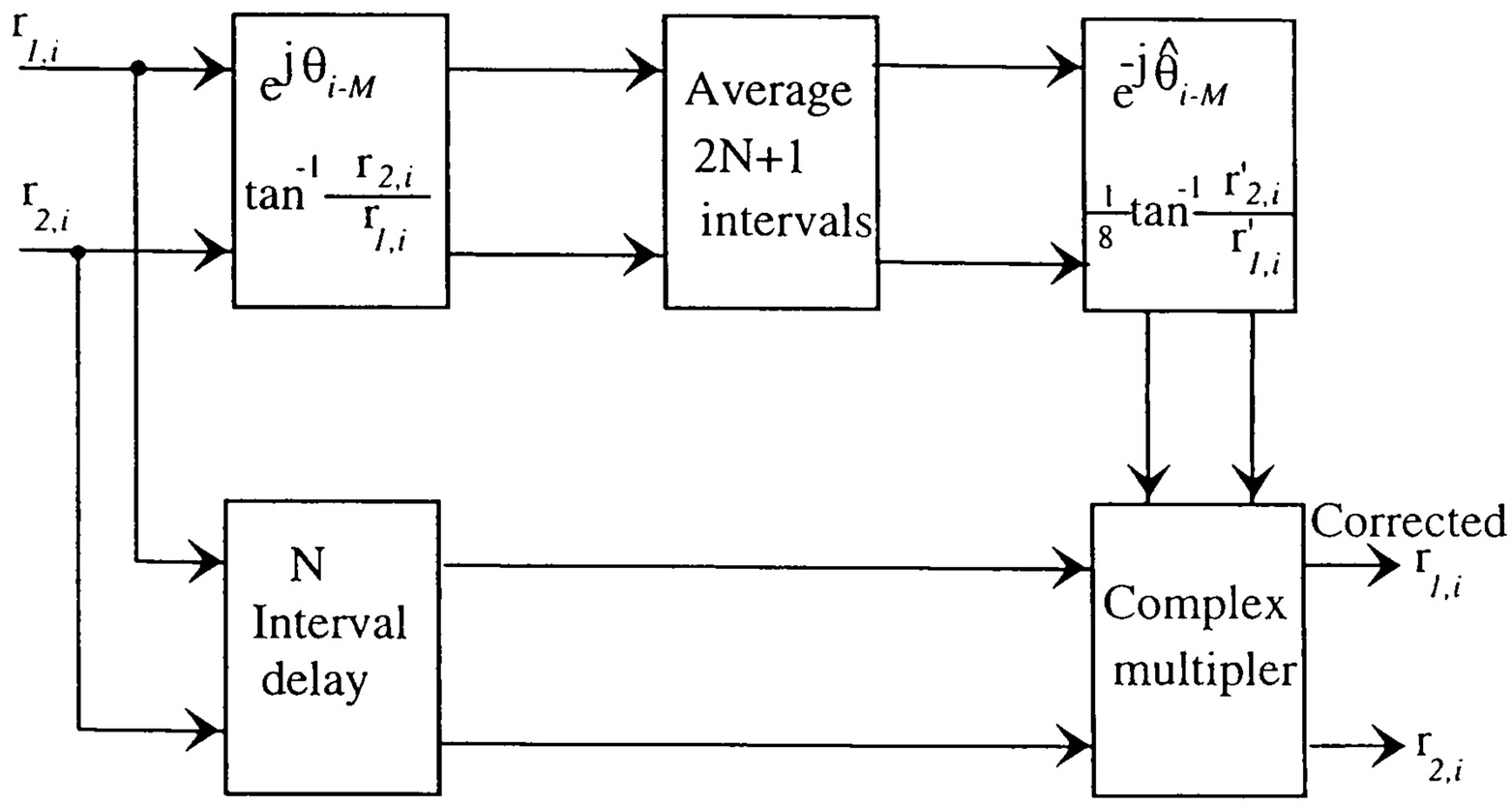

Figure 4.11 Phase estimator for carrier synchronisation of CE8PSK system.

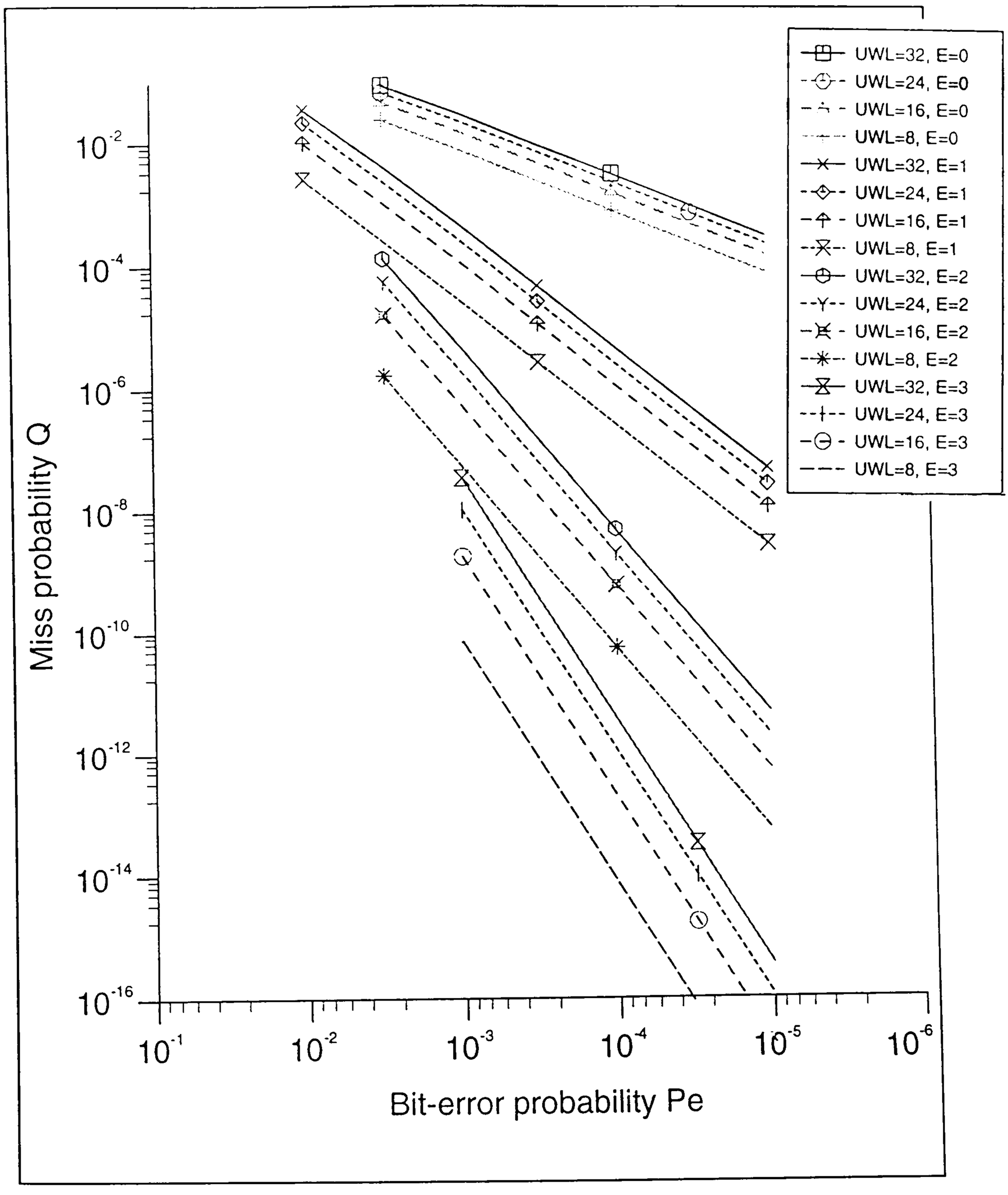

Figure 4.12 Miss probability versus bit error probability for different unique word length.

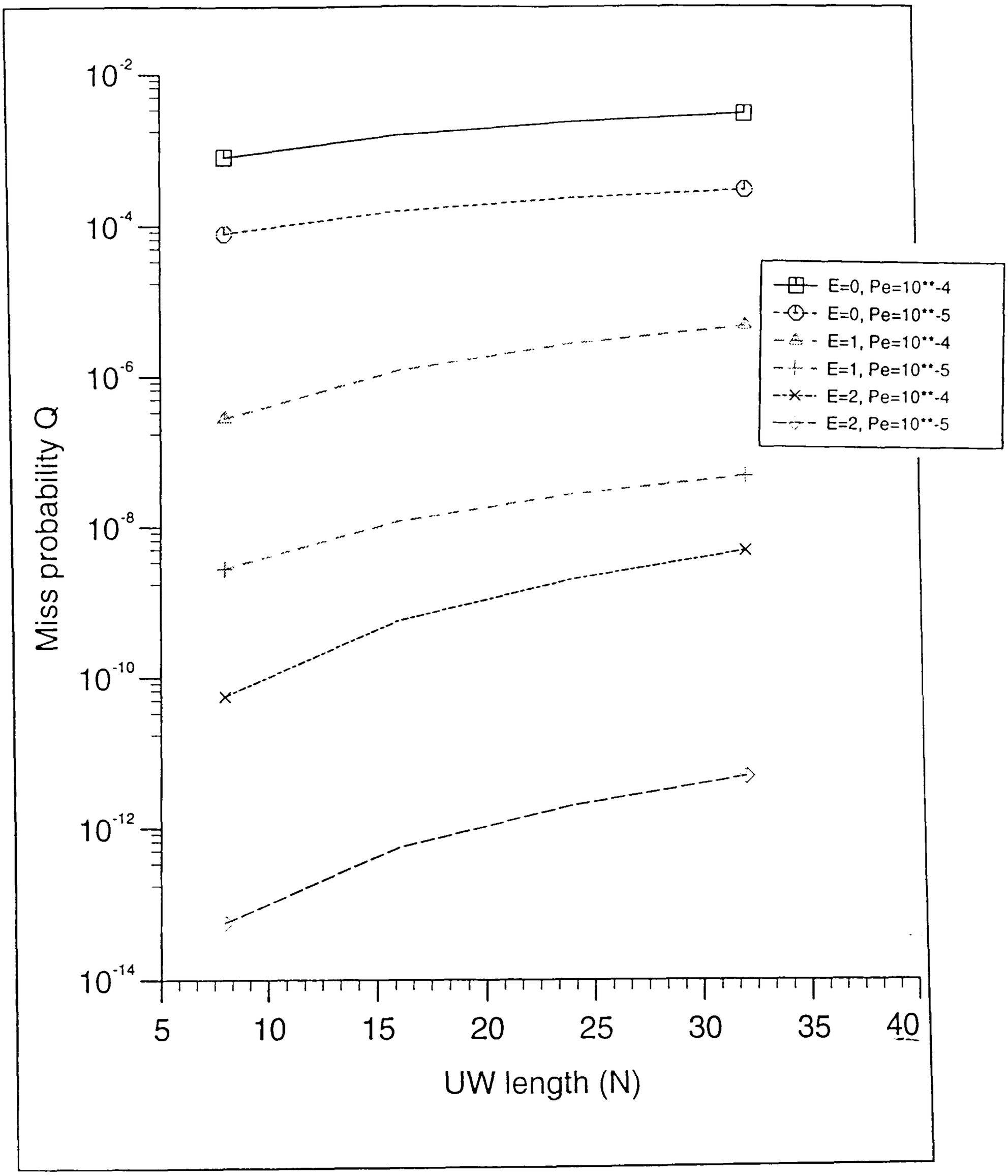

Figure 4.13 Miss probability versus unique word length.

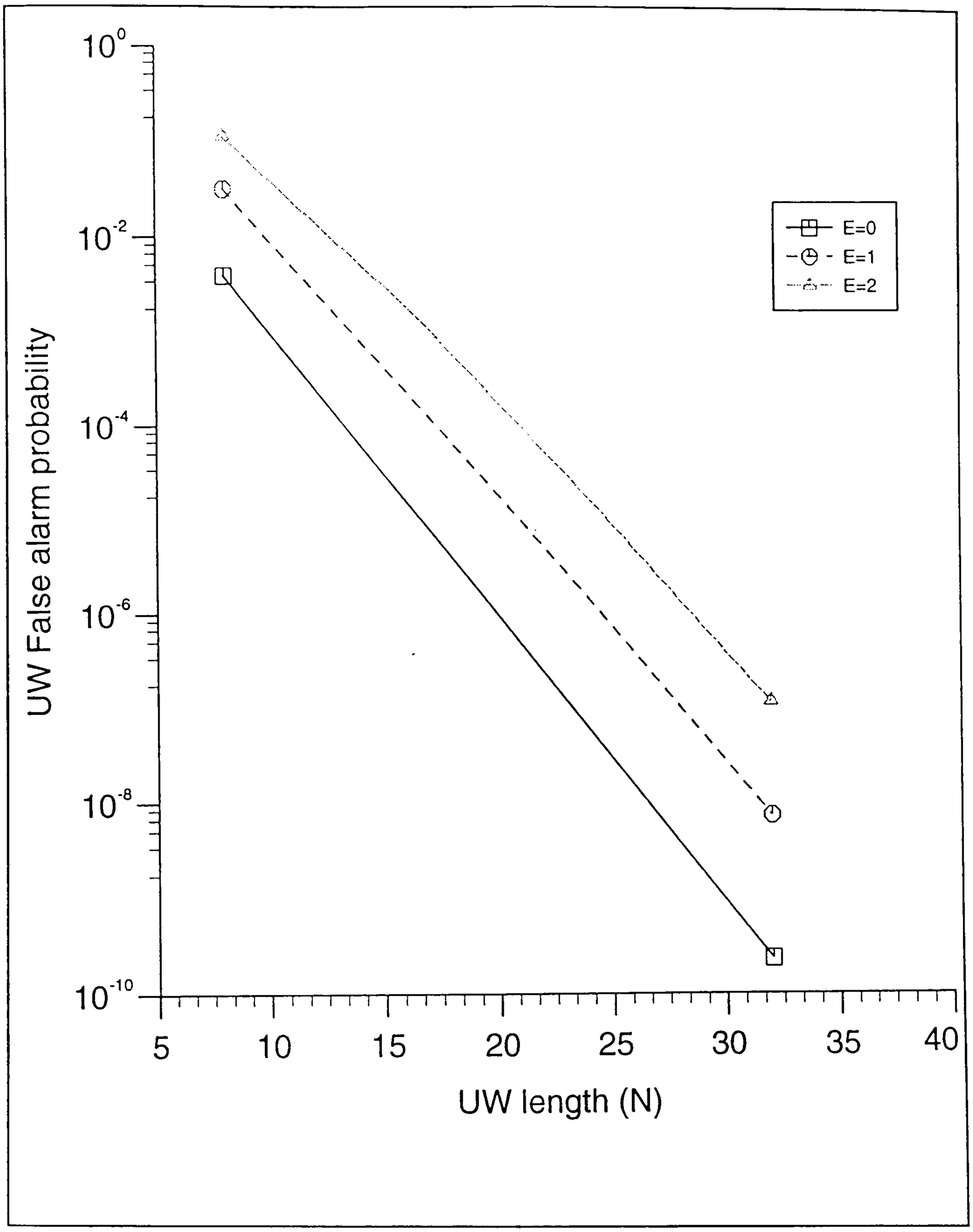

Figure 4.14 Unique word false alarm for random data signal.

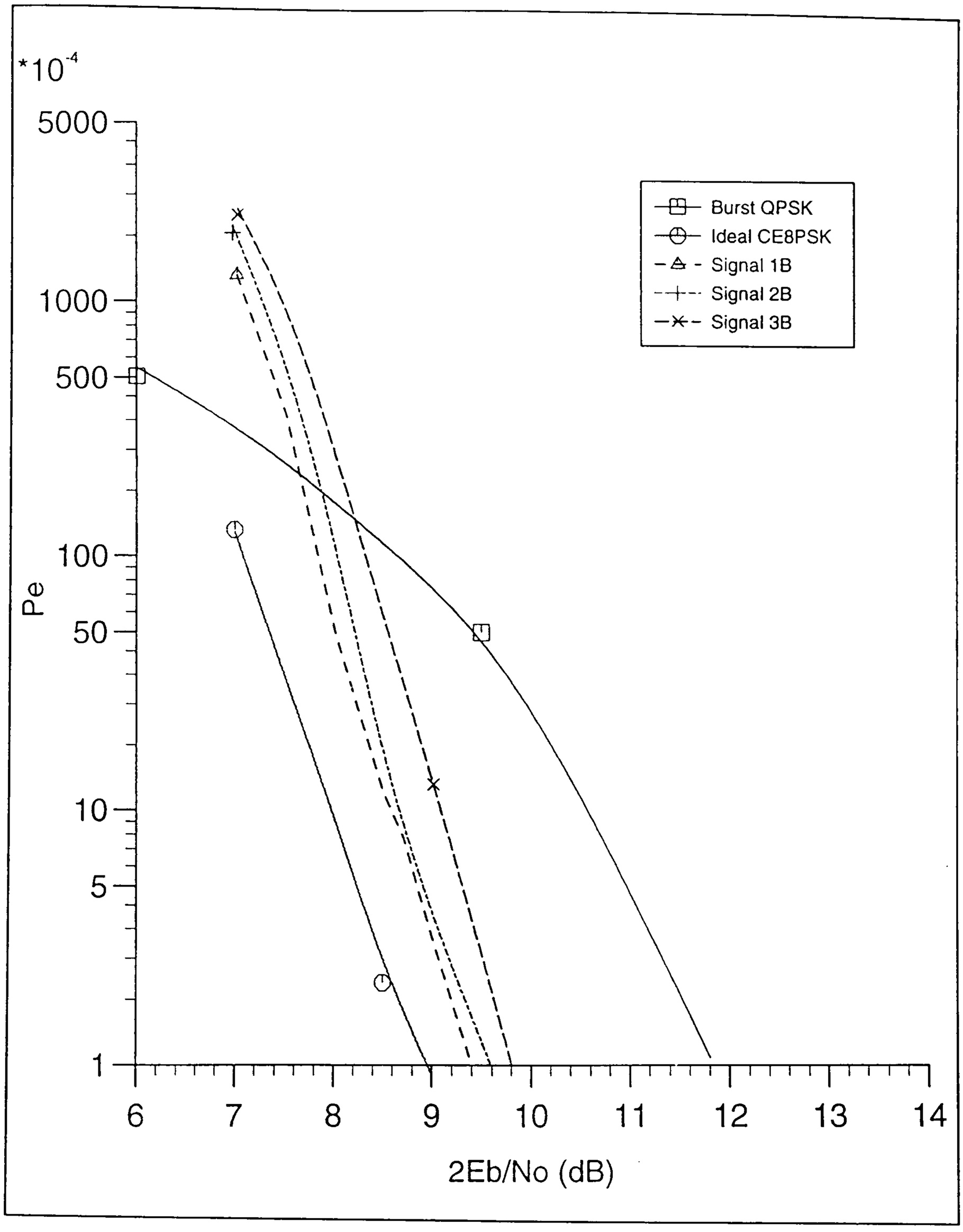

Figure 4.15 Error-rate performances of signals 1B, 2B and 3B, over a nonlinear and bandlimited channel, with the HPA operating at 0 dB OBO.

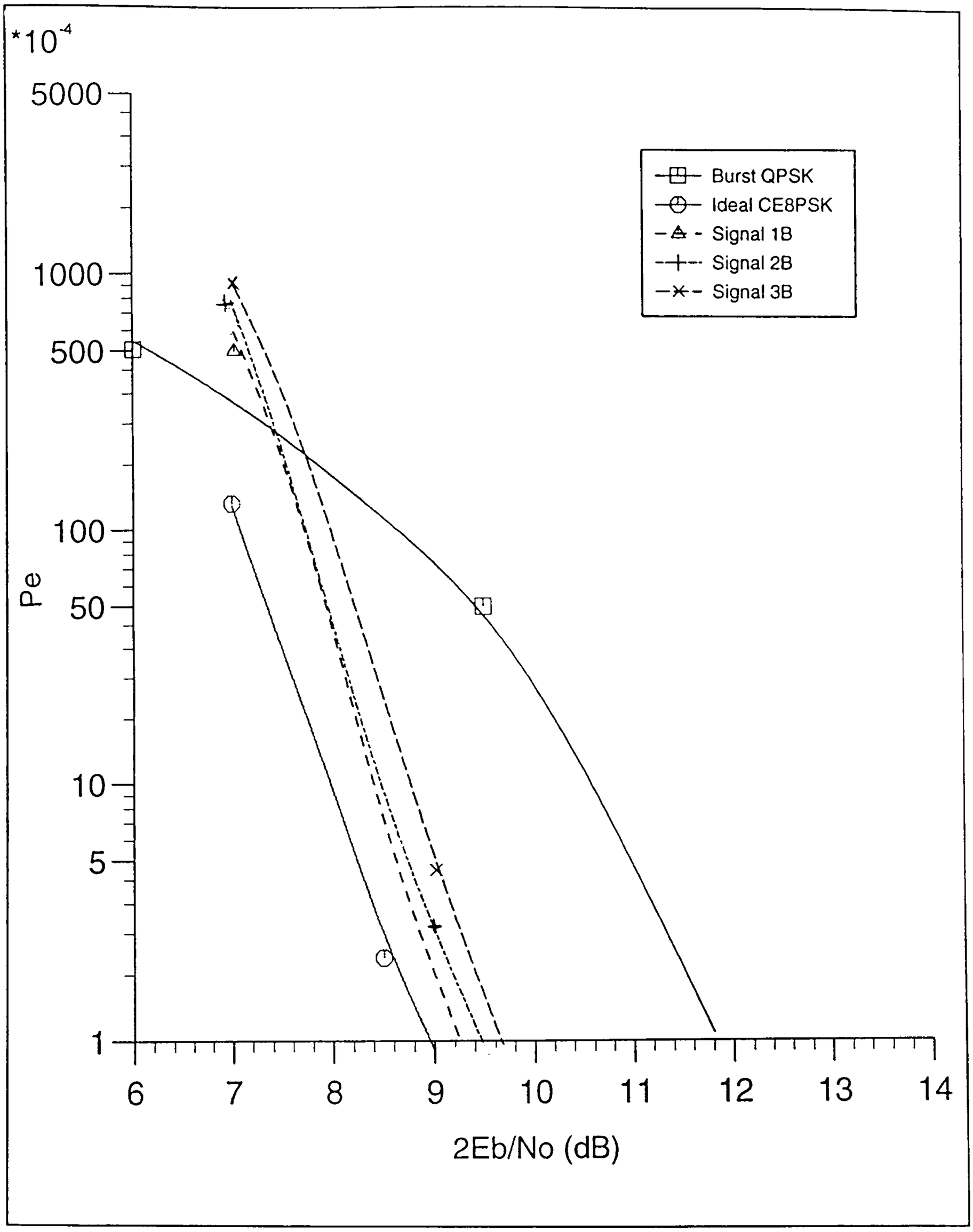

Figure 4.16 Error-rate performances of signals 1B, 2B and 3B, over a nonlinear and bandlimited channel, with the HPA operating at 0.315 dB OBO.

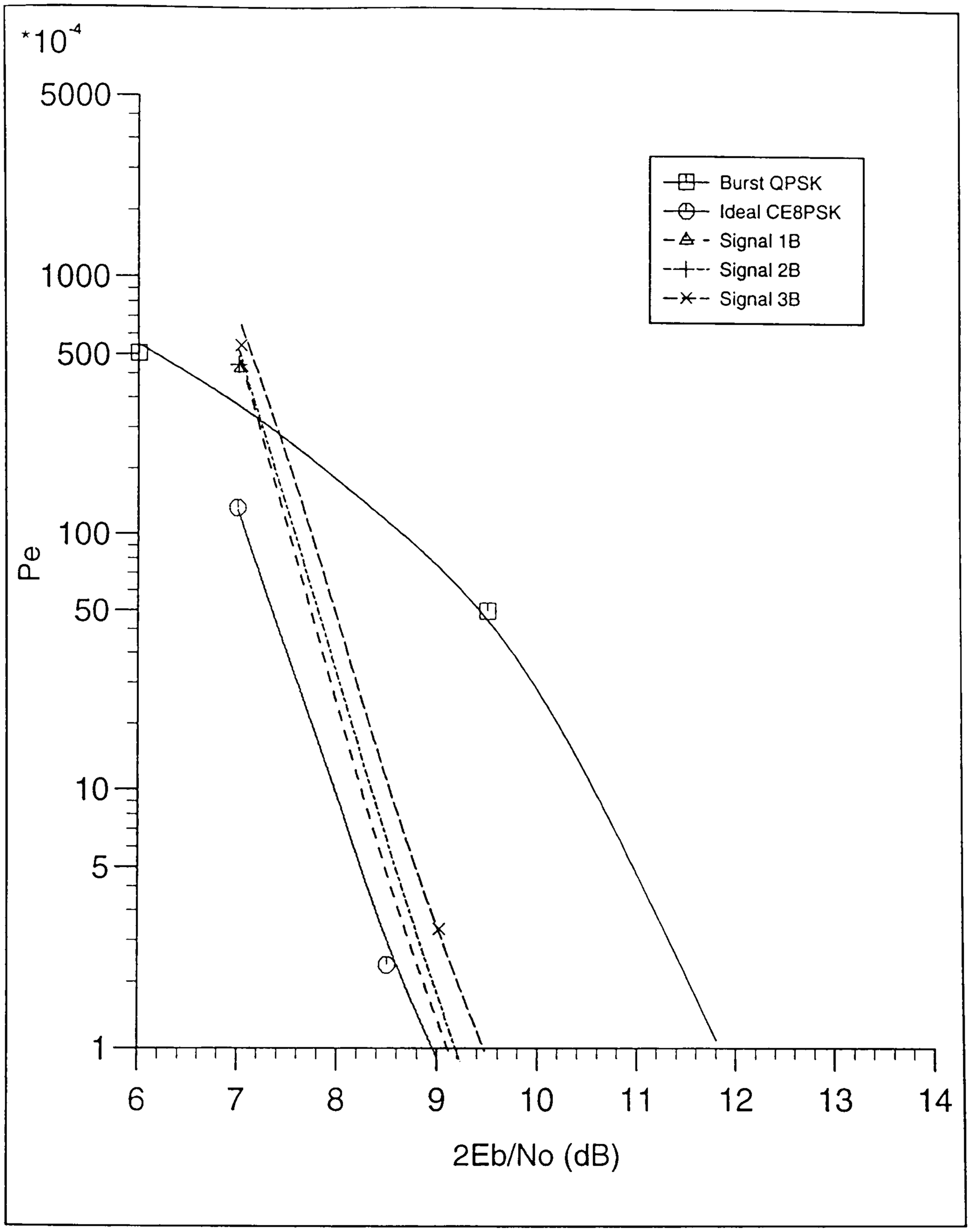

Figure 4.17 Error-rate performances of signals 1B, 2B and 3B, over a nonlinear and bandlimited channel, with the HPA operating at 0.7 dB OBO.

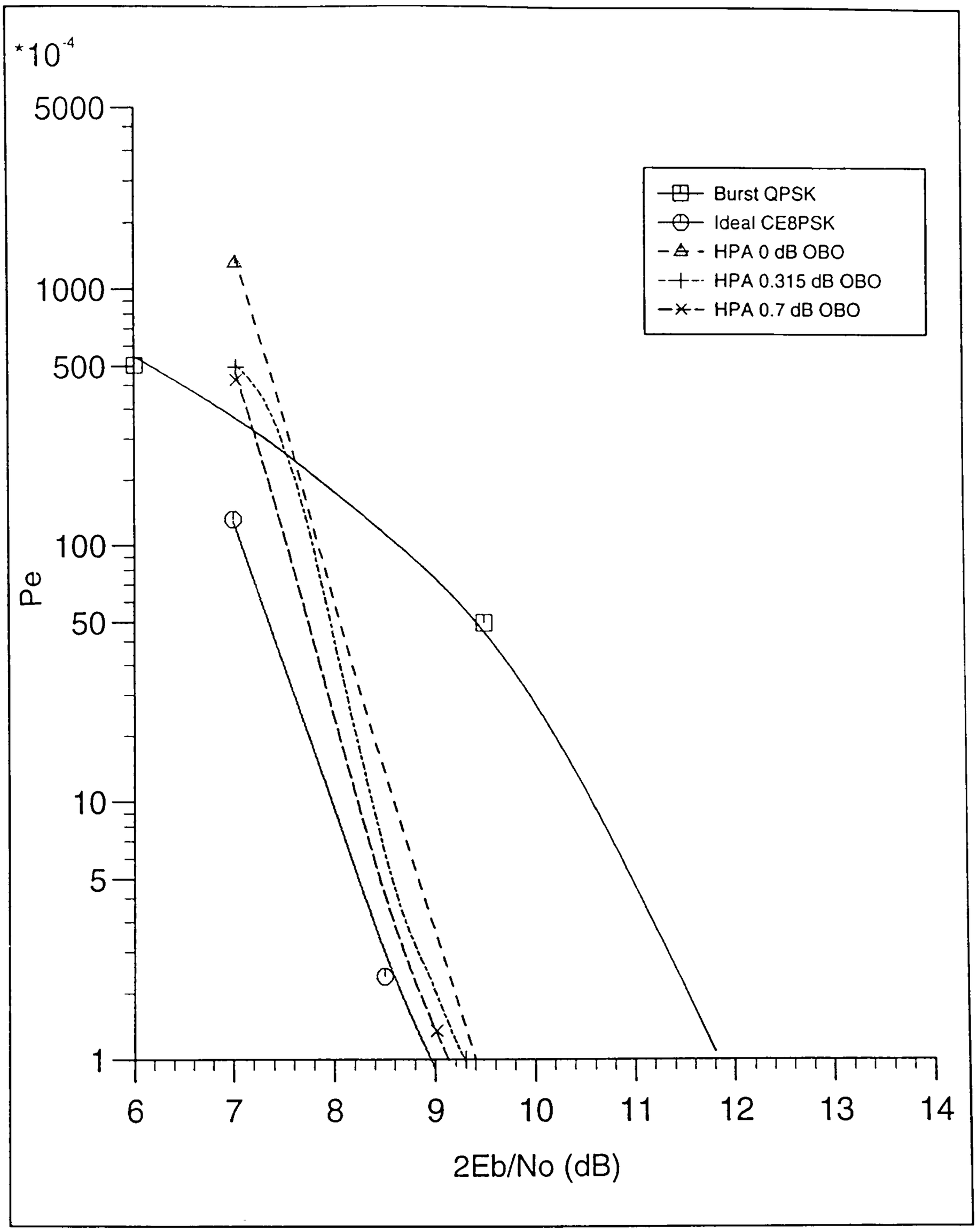

Figure 4.18 Error-rate performances of signal 1B over a nonlinear and bandlimited channel, with the HPA operating at 0, 0.315 or 0.7 dB OBO.

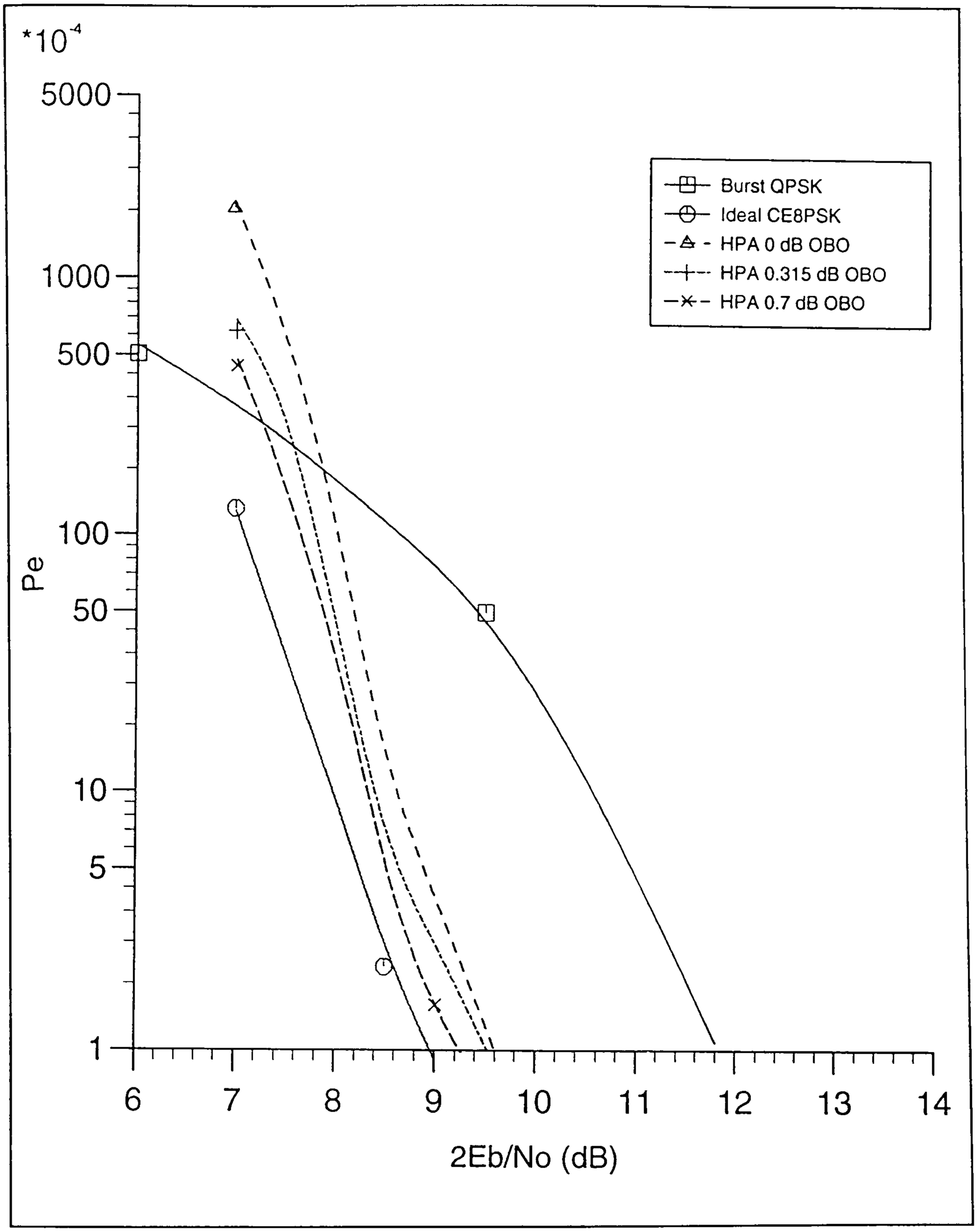

Figure 4.19 Error-rate performances of signal 2B over a nonlinear and bandlimited channel, with the HPA operating at 0, 0.315 or 0.7 dB OBO.

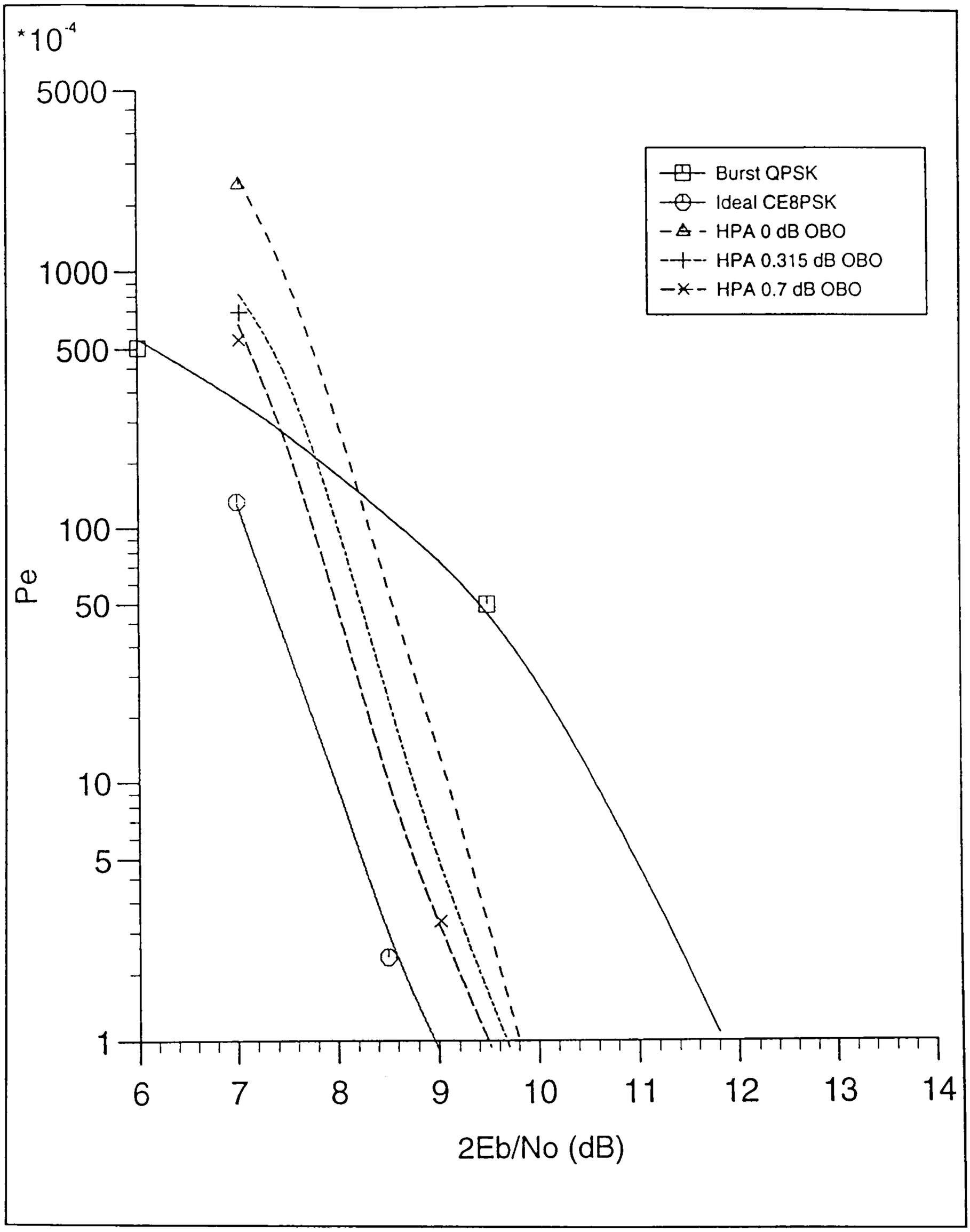

Figure 4.20 Error-rate performances of signal 3B over a nonlinear and bandlimited channel, with the HPA operating at 0, 0.315 or 0.7 dB OBO.

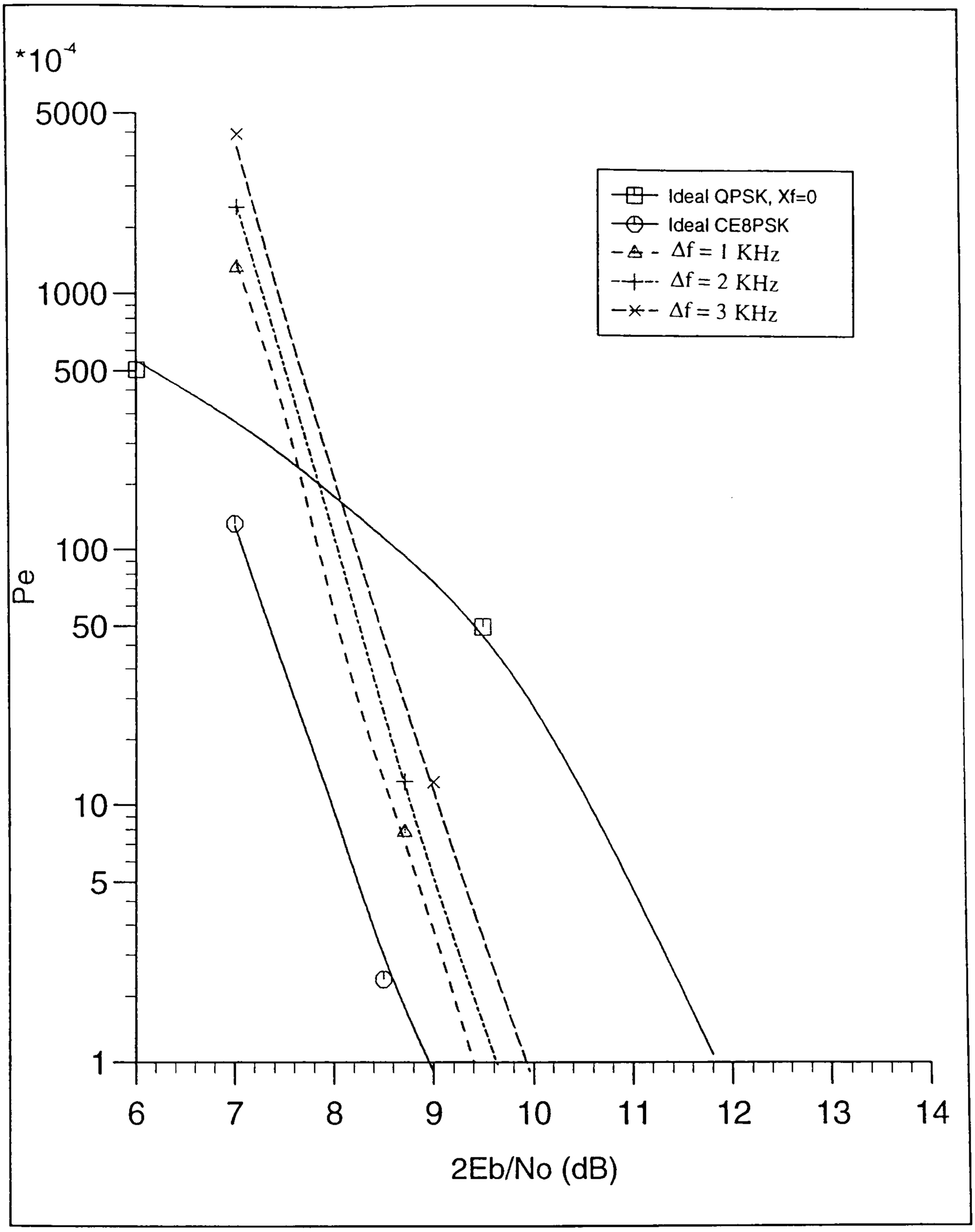

Figure 4.21 Error-rate performances of signal 1B over a nonlinear and bandlimited channel, with the HPA operating at 0 dB OBO and input carrier frequency offset is 1, 2 or 3 KHz.

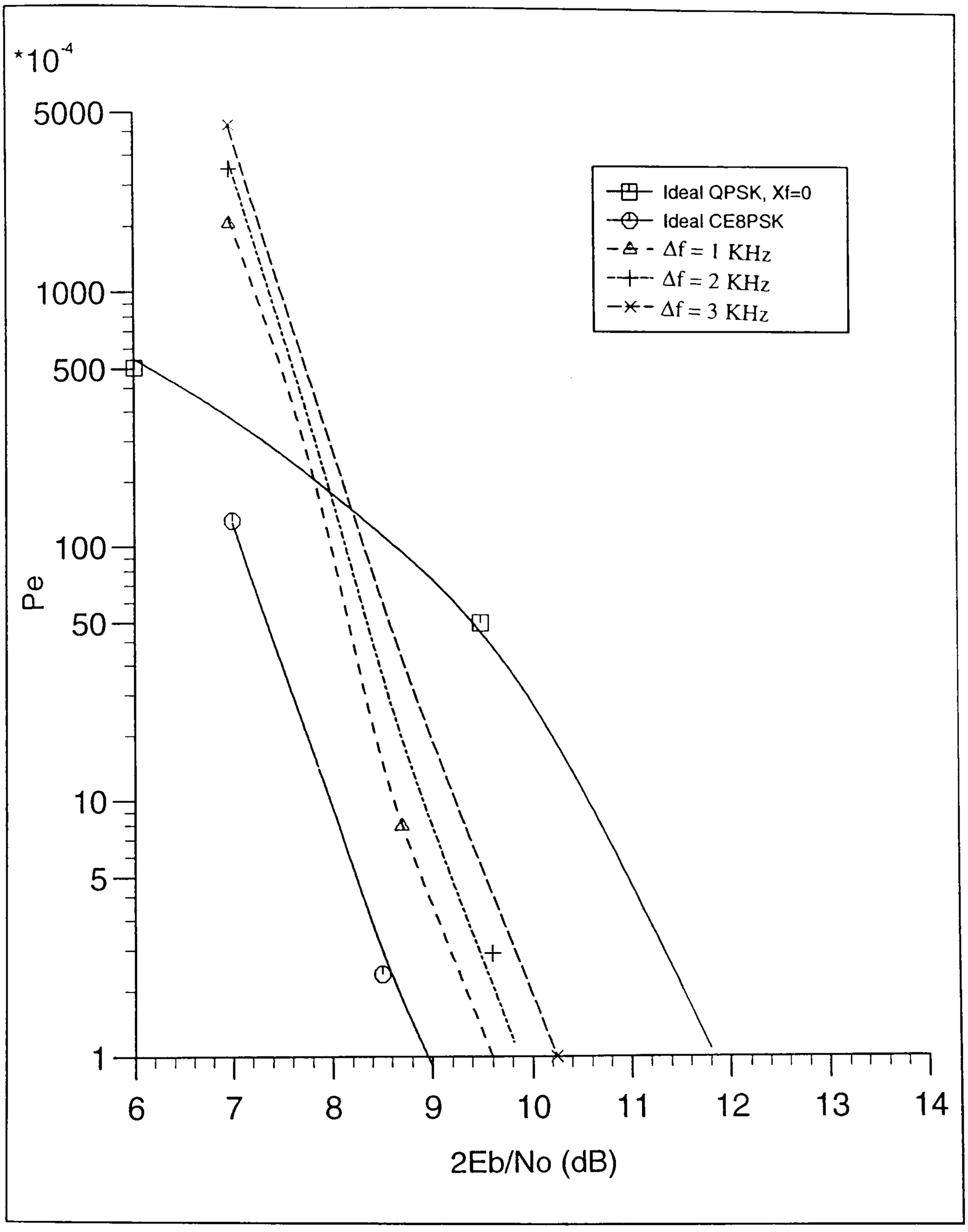

Figure 4.22 Error-rate performances of signal 2B over a nonlinear and bandlimited channel, with the HPA operating at 0 dB OBO and input carrier frequency offset is 1, 2 or 3 KHz.

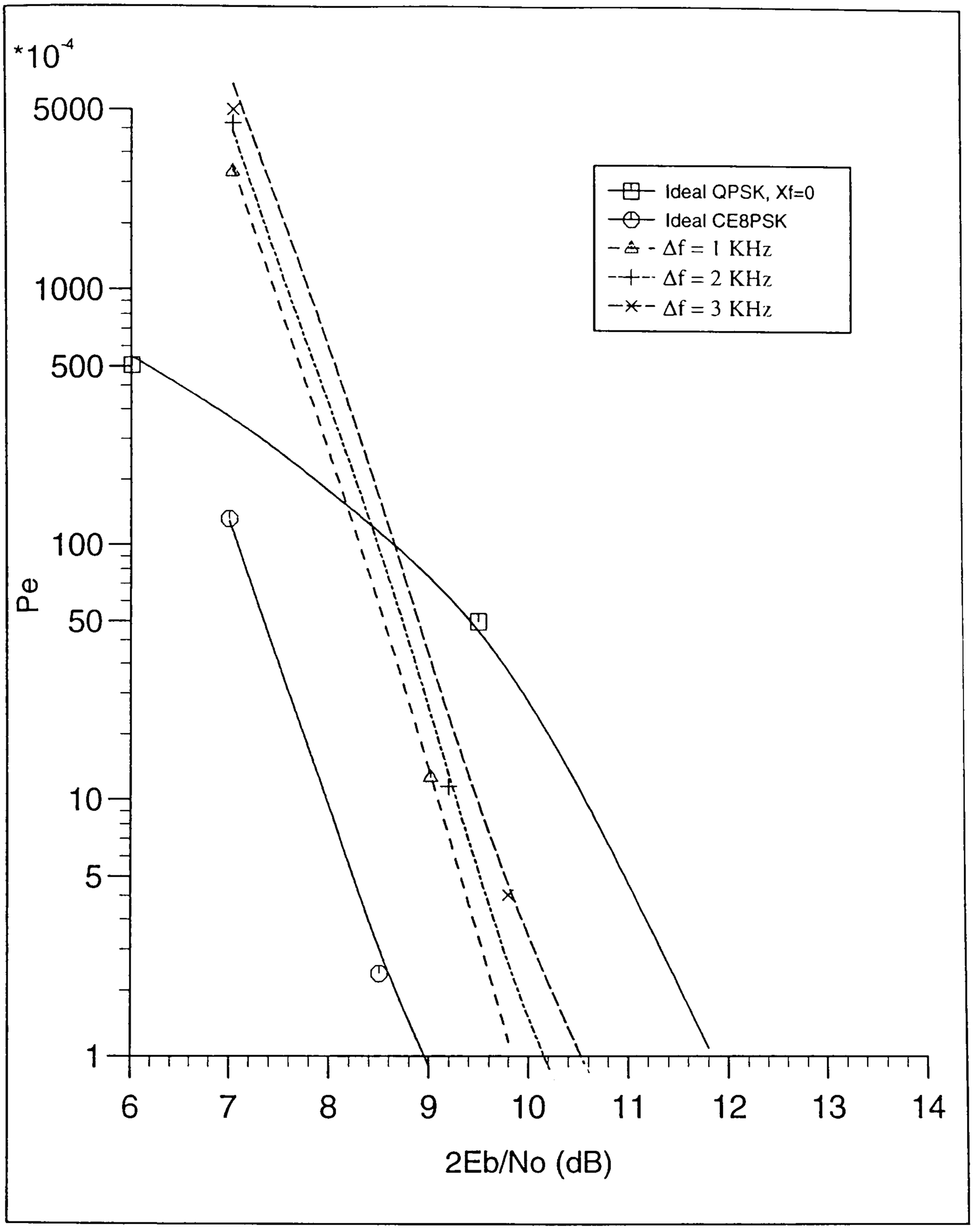

Figure 4.23 Error-rate performances of signal 3B over a nonlinear and bandlimited channel, with the HPA operating at 0 dB OBO and input carrier frequency offset is 1, 2 or 3 KHz.

CHAPTER 5

CONVOLUTIONAL ENCODING AND COHERENT DIFFERENTIALLY 8PSK SYSTEMS OVER A NONLINEAR SATELLITE CHANNEL

5.1 Introduction

In any modulation technique, if the information is transmitted in M different phases, there is an M-fold ambiguity in the data recovery. The ambiguity is not a defect of the carrier recovery circuit, but is inherent to suppressed-carrier, phase-shift keying [63]. It can only be resolved by special encoding or other information carried in the message.

In QPSK signals (Section 3.1.1), since the information is carried in 4 different phases, the carrier recovery circuit has a four-fold ambiguity, and so differential encoding is used to resolve the ambiguity. In the CE8PSK system described in Section 4.2, each pair of data bits, together with the previous two pair of dat bits, are used to determine one of the eight possible carrier phases by means of the convolutional encoder. So when the carrier is recovered, there is an eight-fold ambiguity. In CE8PSK signal if the recovered carrier has a wrong reference phase, the decoder is not able to decode the received signal, i.e., catastrophic failure results. So, the eight-fold ambiguity in carrier recovery must be resolved.

The simplest method of resolving the ambiguity is to send a training sequence of data, at the start of any transmission, to locate the phase of the reference carrier. The advantage of the method is that no special coding is required. However, the disadvantage is that, during the transmission, if there is a sudden phase change or fading in the signal, the carrier may lose the reference phase and catastrophic failure results.

5.2 Convolutional code and differentially encoded 8 phase-shift keying (CDE8PSK) technique

Another method to resolve the ambiguity is to use a differential encoding technique. In the DEQPSK system described in Section 3.1.2, the differential encoder at the transmitter encodes each pair of binary symbols, so that the phase change rather than the absolute phase carries the data, thus eliminating the need for a reference phase at the receiver. The same principle, in fact, can be applied to CE8PSK signals which then become convolutionally and differentially encoded 8PSK (CDE8PSK) signals. The block diagram of a CDE8PSK system is shown in Fig. 5.1. The information to be transmitted is carried by the sequence of binary data-symbols $\{s_i\}$. The $\{s_i\}$, after being serial-to-parallel converted and convolutionally encoded (Section 4.3), produce a sequence of $\{e_i\}$, where e_i is a 3-component vector. At time $t=iT$, e_i has one of 8 possible values given by (Eqn. 4.3.3 in Section 4.3)

$$e_i = [e_i(1)\ \ e_i(2)\ \ e_i(3)] \qquad 5.2.1$$

where $e_i(j) = 0$ or 1 for $j = 1,2,3$. Each vector e_i represents a 3-bit binary sequence. In the generation of a differential encoded vector d_i is also a 3-component vector with 8 possible values given by

$$d_i = [d_i(1)\ \ d_i(2)\ \ d_i(3)] \qquad 5.2.2$$

where $d_i(j) = 0$ or 1 for $j = 1,2,3$, the present vector, e_i, is added to the previous differential encoded vector, d_{i-1} to form the present differential encoded vector d_i. This process produces a sequence $\{d_i\}$ is then Gray encoded, according to Table 5.1 (which is similar to Table 4.2), to give two output sequences $\{q_{1,i}\}$ and $\{q_{2,i}\}$, where $q_{j,i} = \pm 0.924$ or ± 0.383 for $j = 1,2$. The sampling, filtering and modulation processes, etc., following this are exactly the same as described in the CE8PSK system in Section 4.3.

Assume that, in Fig. 5.1, the bandpass transmission channel introduces no attenuation, delay or distortion, but that it only adds a Gaussian noise waveform, $N(t)$, to the transmitted signal, so that the channel is exactly the same as the one used in the QPSK or CE8PSK systems described in Sections 3.1.1 or 4.3, respectively. At the input of the demodulator, the signal is (Eqn. 4.3.8)

$$r(t) = \sqrt{2}[a(t)\cos\omega_c t - b(t)\sin\omega_c t] + N(t) \qquad 5.2.3$$

where $N(t)$ is a sample function of a Gaussian random process with zero mean and a two-sided power spectral density of $\frac{1}{2} N_0$ over the signal frequency band. Assume that the bandwidth of $N(t)$ is small compared with its carrier frequency ω_c rad/s, so Eqn. 5.2.3 can be written [19] as

$$r(t) = [\sqrt{2}a(t) + N_c(t)]\cos\omega_c t - [\sqrt{2}b(t) + N_s(t)]\sin\omega_c t \qquad 5.2.4$$

as can be seen from Eqn. 3.1.4, where $N_c(t)$ and $N_s(t)$ are sample functions of Gaussian random processes, with zero mean and a two-sided power spectral density twice that of $N(t)$ (Appendix A7).

It has been shown, in Section 3.1.1, that under these conditions, the inphase and quadrature baseband signal components plus noise, at the demodulation filter output, are

$$r_1(t) = \sum_i q_{1,i} h(t - iT) + v_1(t) \qquad 5.2.5a$$

and

$$r_2(t) = \sum_i q_{2,i} h(t - iT) + v_2(t) \qquad 5.2.5b$$

respectively, where $h(t)$ is the inverse Fourier transform of $H(f)$, which is the transfer function of the modulation and demodulation filters in cascade. $v_1(t)$ and $v_2(t)$ are filtered Gaussian noise waveforms. Bearing in mined that the bandpass channel introduces no attenuation, delay or distortion.

Assume that the modulation and demodulation filters have the same characteristics, and the combined transfer function is a sinusoidal roll-off frequency response (Eqn. 2.2.3) with a linear phase characteristic, so that $h(0) = 1$ and $h(iT) = 0$, for all values of the integer i other than $i = 0$. The signals $r_1(t)$ and $r_2(t)$ have no ISI at the time instants $\{iT\}$. Assume also that the receiver provides the ideal required timing signal, so the two baseband waveforms, $r_1(t)$ and $r_2(t)$, at the demodulation filter output are sampled at time instants $\{iT\}$, to give two sequences of sample values $\{r_{1,i}\}$ and $\{r_{2,i}\}$ to the decoder. At time $t = iT$, the samples are (Eqn. 3.1.8)

$$r_{1,i} = q_{1,i} + v_{1,i} \qquad 5.2.6a$$

and

$$r_{2,i} = q_{2,i} + v_{2,i} \qquad 5.2.6b$$

where $v_{1,i}$ and $v_{2,i}$ are sample values of Gaussian random variables with zero mean and fixed variance σ^2, the $\{v_{1,i}\}$ and $\{v_{2,i}\}$ being statistically independent and independent also of the $\{s_i\}$.

The received samples $\{r_{1,i}\}$ and $\{r_{2,i}\}$ are fed to the decoder which produces at its output the sequence of symbols $\{\hat{s}_i\}$ which forms the sequence of decoded data symbols. In the absence of noise, the $\{\hat{s}_i\}$ are the same as the $\{s_i\}$. The aim of the decoder is to generate the sequence $\{\hat{s}_i\}$ such that the corresponding sequences $\{q_{1,i}\}$ and $\{q_{2,i}\}$, which would have been transmitted in response to the given $\{s_i\}$ at the transmitter input, are at the minimum (total) unitary distance from the received sequences $\{r_{1,i}\}$ and $\{r_{2,i}\}$ [37].

5.3 Baseband equivalent model of CDE8PSK system, with a nonlinear satellite channel, for computer simulation.

The CDE8PSK system here operates at a speed of 64, 128 or 256 kbits/s over a satellite link. Since CDE8PSK signals, as for CE8PSK signals, use a quadrature modulation techniques, the system can be greatly simplified by assigning real values to the signals in one of the two parallel channels (that associated with $\sqrt{2}\cos\omega_c t$) and imaginary values to the signals in the other channel (that associated with $-\sqrt{2}\sin\omega_c t$), and then considering the linear modulator, the transmitter IF filter, the HPA, the receiver IF filter and the linear demodulator, as a baseband transmission path carrying complex-valued signals, as it has been done for the CE8PSK system shown in Section 4.4. In fact apart from the differentially encoding process used at the transmitter and the decoding process used at the receiver, a CDE8PSK system is exactly the same as a CE8PSK system, thus the model shown in Fig. 4.9 is used here to describe the CDE8PSK system over a nonlinear satellite channel. The information to be transmitted is carried by the sequence of binary data-symbols $\{s_i\}$, where the $\{s_i\}$ have the possible values 0 or 1. The coded symbols $\{q_i\}$ are obtained from the $\{s_i\}$, by S/P converter, convolutionally and differentially and Gray encoder (Section 4.3), The i^{th} symbol has the value

$$q_i = (\pm 0.924 \pm j0.383) \text{ or } (\pm 0.383 \pm j0.924) \qquad 5.3.1$$

where $j = \sqrt{-1}$, the $\{q_i\}$, of course, being statistically independent and equally likely to have any of the eight possible values. The $\{q_i\}$ are used to form the sequence of impulses $\{\sum_i q_i \delta(t - iT)\}$ at the input of the modulation filter. The signal waveform at the output of the modulation filter is the complex-valued baseband signal

$$u(t) = \sum_i q_i h_t(t - iT) \qquad 5.3.2$$

where $h_t(t)$ is the impulse response of the modulation filter and, at any given of t, is real (Section 2.4.1).

Similar to the DEQPSK and CE8PSK system described in Section 3.3 and 4.4, respectively, the system is modelled digitally for computer simulation. The continuous waveforms are modelled as discrete waveforms.

The waveform $u(t)$ is sampled 8 samples per symbol, at the time instants $\{mT_s\}$, where $T = 8T_s$, to give the sequence $\{u_m\}$, where $u_m = u(mT_s)$. The $\{u_m\}$ are then fed to the baseband equivalent model of the bandpass channel, as shown in Fig. 4.9.

The sampled signal $\{w_m\}$ (given by Eqn. 3.3.9), from the baseband equivalent model of the bandpass channel, are filtered by the demodulation filter. The sampled impulse response of the demodulation filter, sampled at the rate of $1/T_s$ samples per second, is given by the $(n+1)$-component vector

$$p = [p_0 \;\; p_1 \;\; p_2 \;\; \ldots\ldots p_n] \qquad 5.3.3$$

where the $\{p_m\}$, for $0 \le m \le n$, have real-valued components (Table 2.1), and $p_m = p(mT_s)$. Thus, at time $t = mT_s$, the signal sample at the filter output is

$$r_m = \sum_{h=0}^{n} w_{m-h} p_h \qquad 5.3.4$$

where r_m has a complex value.

Assume that the receiver provides the required ideal timing signal, so the sequence $\{r_m\}$ is sampled once per symbol, at the time instants $\{iT\}$, to give the sequence $\{r_i\}$, where r_i has a complex value. The $\{r_i\}$ are fed to the decoder which produces at its output the sequence of symbols $\{\hat{s}_i\}$ which form the sequence of decoded binary-data symbols.

5.4 Suboptimum decoder for CDE8PSK signals

In the CDE8PSK system, the phase change carries the data, not the absolute phase, so the decoder [50] [64] is slightly different from the Viterbi-algorithm decoder used for CE8PSK signals.

When the $\{r_i\}$ are fed to the decoder, the decoder forms and stores a set of $m = 2^L$ vectors (sequences) $\{X_L\}$, where

$$X_L = [x_1 \;\; x_2 \;\; x_3 \;\; \ldots\ldots x_L] \qquad 5.4.1$$

and $x_h = 0$ or 1, for $h = 1, 2, \ldots, L$. x_h here represents a possible value of s_h. For each stored vector X_L the decoder forms eight different vectors

$$Y_i(j) = [y_1(j)\ \ y_2(j)\ \ y_3(j)\ \ \ldots.. y_i(j)] \qquad 5.4.2$$

where $y_i(j)$ is a possible value of r_i and $i = L/2$ (because a coded-symbol is transmitted for each pair of data symbols). The $\{y_h(j)\}$, for $h = 1, 2, \ldots, i$, have complex values and are the possible values of the transmitted signal values. Since the transmitted signal phases are differentially encoded, the first component (i.e., the initial phase), $y_1(j)$, for $j = 1, 2, \ldots..,8$, takes on 8 different possible values in the eight vectors. This takes into account the 8 possible initial reference phases $Y_i(j)$, for $j = 1, 2, \ldots..,8$, would have been transmitted in place of the sequence of the $\{q_i\}$ had the vector X_L been fed to the encoder at the transmitter in place of the vector

$$S_L = [s_1\ \ s_2\ \ s_3\ \ \ldots..s_L] \qquad 5.4.3$$

that was actually sent, subject to the constraint that $y_1(j)$ was the initial phase. Clearly, since the transmitted signal phases are differentially encoded, the possible values of $y_2(j), y_3(j), \ldots.., y_i(j)$ in each of the 8 vectors, $\{Y_i(j)\}$, depend on the first component (initial phase) of that vector. The ISI introduced by the channel is neglected in the decoding process in order to reduce the equipment complexity of the decoder. (This assumption is valid because the IF filters only introduce a low level of ISI). The decoder forms and stores together with each X_L, the corresponding 8 possible costs

$$C_i(j) = c_1(j) + c_2(j) + c_3(j) + \ldots. + c_i(j) \qquad 5.4.4$$

where for $h = 1, 2, \ldots, i$, $c_h(j) = |r_h - y_h(j)|^2$, $|r_h - y_h(j)|$ is the absolute value of the complex value $(r_h - y_h(j))$. Since for $j = 1, 2, \ldots.., 8$, there are 8 different vectors, $Y_i(j)$, which form 8 different values of $C_i(j)$, there are 8 possible costs associated with each X_L. This takes into account the 8 possible phase references (i.e., the eight-fold phase ambiguity) caused by the carrier recovery circuit.

Idealy, no firm decision is reached as to the value of any s_h until the whole sequence $\{r_i\}$ has been received, when all $\{s_h\}$ are decoded simultaneously from the received $\{r_i\}$. the decoded values $\{\hat{s}_h\}$ being the values of the $\{x_h\}$ in the stored vector X_L having the smallest cost $C_i(j)$. To reduce the equipment complexity, as for the Viterbi decoder, in determination of $(\hat{s}_{L-2n+1}\ \ \hat{s}_{L-2n+2})$ the decoder does not

consider the values of x_{L-2n}, x_{L-2n-1}, ... Thus, instead of storing m L-component vectors $\{X_L\}$, the decoder stores the corresponding $2n$-component vector $\{Z_L\}$, where

$$Z_L = [x_{L-2n+1} \;\; x_{L-2n+2} \;\; x_{L-2n+3} \;\; .....x_L] \qquad 5.4.5$$

so that Z_L is formed by the last $2n$ components of the corresponding vector X_L. The costs $\{C_i(j)\}$ for $j = 1, 2, ..., 8$, of this vector X_L are now said to be the cost of Z_L.

In practice, in the decoder the receiver holds in store the $m = 4^{K-1}$(K is the constraint length of the code) vectors $\{Z_L\}$, with the minimum costs of $C_i(j)$, for $j = 1, 2, ..., 8$, corresponding to the 4^{K-1} different possible combinations of values of x_{L-2n+3}, x_{L-2n+4}, $.....x_L$. Thus each stored vector Z_L forms the last $2n$ component of the vector X_L that minimizes $C_i(j)$, for $j = 1, 2, ..., 8$, subject to the constraint that x_{L-2n+3}, x_{L-2n+4}, $.....x_L$, have the given values. It is assumed for convenience here that $L>2K$. Associated with each stored vector Z_L is stored the corresponding $C_i(j)$, for $j = 1, 2, ..., 8$. Therefore, there are altogether $8m$ different values of $C_i(j)$. The decoded binary data-symbol $(\hat{s}_{L-2n+1} \;\; \hat{s}_{L-2n+2})$ are taken to be the values of $(x_{L-2n+1} \;\; x_{L-2n+2})$, respectively, in the vector Z_L associated with the smallest $C_i(j)$.

Following the receipt of the sample r_{i+1}, each of the stored vectors $\{Z_L\}$ forms a common part of 4 vectors $\{X_{L+2}\}$, having the 4 possible values of $(x_{L+1} \;\; x_{L+2})$. Each of these 4 possible vectors is associated with 8 corresponding costs

$$C_{i+1}(j) = C_i(j) + c_{i+1}(j) \qquad 5.4.6$$

for $j = 1, 2, ..., 8$

where
$$c_{i+1}(j) = \left| r_{i+1} - y_{i+1}(j) \right|^2 \qquad 5.4.7$$

and for $j = 1, 2, ..., 8$, the $C_i(j)$ are the costs of the original vector Z_L, and the $\{y_{i+1}(j)\}$ are complex values and have 8 possible received values. For each of the 4^{K-1} possible combinations of values x_{L-2n+5}, x_{L-2n+6}, $.....x_{L+1}, x_{L+2}$, the decoder now selects the vector Z_{L+2}, having the smallest $C_{i+1}(j)$ and then it stores the vector Z_{L+2} and the 8 smallest values $\{C_{i+1}(j)\}$, for $j = 1, 2, ..., 8$. $(\hat{s}_{L-2n+3} \;\; \hat{s}_{L-2n+4})$ are taken to be the values of $(x_{L-2n+3} \;\; x_{L-2n+4})$, respectively, in the stored vector Z_{L+2} associated with the smallest $C_{i+1}(j)$, and the process continues in this way.

r_{i+1} and $y_{i+1}(j)$ in Eqn. 5.4.7 are complex-valued:

$$c_{i+1}(j) = (\mathrm{Re}(r_{i+1} - y_{i+1}(j)))^2 + (\mathrm{Im}(r_{i+1} - y_{i+1}(j)))^2 \qquad 5.4.8$$

and so it requires two operations of squaring or multiplication to determine each value of 4 possible values of $c_{i+1}(j)$ (i.e., the unitary distance of two complex numbers). Hence for j = 1, 2, ..., 8, it requires 64 operations of squaring or multiplication to compute the 32 values of $c_{i+1}(j)$ for each vector X_{L+2}. There are m vectors Z_L. So that it requires altogether $64m$ operations of squaring or multiplication. However, $y_{i+1}(j)$, in Eqn. 5.4.8, has only 8 different values because it is one of the possible received complex-valued samples. Thus, of these $32m$ values of $c_{i+1}(j)$, many have the same values. There are only 8 possible values of $c_{i+1}(j)$, and each of them requires 2 operations of squaring or multiplication to be determine. Therefore, following the receipt of the sample r_{i+1}, the decoder has to carry out 16 operations of squaring or multiplication to compute the 8 different values of $c_{i+1}(j)$ which are used to form the $32m$ values $\{C_{i+1}(j)\}$. The starting up procedure can be exactly the same as that for decoding CE8PSK signals (Section 4.5).

In general, the processing of 4^K vectors and $8\text{x}4^K$ values of costs, followed by the storage of 4^{K-1} $2n$-component vectors $\{Z_L\}$ and $8\text{x}4^{K-1}$ values $\{C_{i+1}(j)\}$, are involved in the decoding of each received pair of data $(s_{L+1}\ \ s_{L+2})$. In the present case, K=3, it requires 16 vectors which expand into 64 vectors (i.e., each vector expands 4 ways, for 4 possible values of $(x_{L+1}\ \ x_{L+2})$) to form the decoder at the receiver, and each vector is now associated with eight different costs, i.e., a total of 128 costs. These 128 costs expand into 512 costs on the expansion of the vectors.(Each cost expands 4 ways, since there are 4 possible values of $(x_{L+1}\ \ x_{L+2})$). The decoder must store 4^{K-1} $2n$-component vectors and so requires the same amount of storage as for CE8PSK signals, but it requires 512 costs, instead of 64 in each decoding process.

Although the decoder resolves the 8-fold ambiguity in carrier recovery of CDE8PSK signals, because the differential encoder at the transmitter is a feedback loop, it is only a suboptimum decoder and not a true Viterbi decoder for the signal.

5.5 Performance of CDE8PSK signal

For DEQPSK signals, the differential decoding process is performed after signal detection. If one symbol is in error, the decoder output will tend to have double symbol errors because 2 symbols are compared for each output symbol. Thus the bit error rate of the Gray encoded DEQPSK signal is twice as much as the Gray encoded QPSK signal.

For CDE8PSK signals, the convolutional and differential encoding processes are carried out simultaneously in the decoder. If one symbol is in error, the decoder output will tend to have two, three or four symbol errors, because each symbol is correlated with three other symbols. The performance of the CDE8PSK signal, using

Code 1 (Table 4.3), over an AWGN channel, and with the suboptimum decoder used with a delay of 32 symbols in decoding, has been evaluated by computer simulation. The result, as shown in Fig. 5.3, indicates that the difference between the performances of CE8PSK and CDE8PSK signals increases as P_e increases. This cannot be caused by the correlation property of the transmitted symbols. If it were, the difference would have decreased as P_e increased. However, this is expected because the decoder is no longer the true Viterbi decoder.

5.6 Power spectra of CE8PSK and CDE8PSK signals

As with QPSK or DEQPSK signals, CE8PSK or CDE8PSK signals carry two information bits per symbol. If the same filtering is used, CE8PSK and CDE8PSK signals have the same signal spectra as those of QPSK or DEQPSK signals (Section 3.5).

5.6.1 Spectral estimation of CE8PSK and CDE8PSK signals by computer simulation

The basic principle of spectral estimation is described briefly in Section 3.5. The baseband equivalent model, used for spectral estimation of the transmitted CE8PSK or CDE8PSK signals, is shown in Fig. 5.2, which is very similar to that for QPSK spectral estimation shown in Fig. 3.9. The only difference is the encoder which convolutionally (for CE8PSK) and convolutionally and differentially (for CED8PSK) and Gray encodes the input data $\{s_i\}$. As with QPSK signals, the spectra of sampled signals are estimated at the output of the HPA.

The spectrum at the output of the HPA can be estimated as follows, a sequence of L quaternary dat-symbols $\{s_i\}$ is generated, where $\{s_i\}$ are taken to be statistically independent and equally likely to have value of 0 or 1. The encode symbols $\{q_i\}$ are obtained from $\{s_i\}$, by the encoder, after being S/P (serial-to-parallel) converted, convolutionally encoded (for CE8PSK), convolutionally and differentially encoded (for CDE8PSK) and then Gray encoded (Section 4.3). The ith symbol has the value

$$q_i = (\pm 0.924 \pm j0.383) \text{ or } (\pm 0.383 \pm j0.924) \qquad 5.6.1$$

where $j = \sqrt{-1}$, the $\{q_i\}$ being statistically independent and equally likely to have any of the eight possible values. The sequence $\{q_i\}$ is used to form the sequence of impulses $\{\sum_i q_i \delta(t - iT)\}$ which are fed into the modulation filter. The signal at the filter output is the complex-valued waveform

$$u(t) = \sum_{i}^{L} q_i h_t (t - iT) \qquad 5.6.2$$

with $h_t(t)$ the impulse response of the modulation filter. The waveform $u(t)$ is sampled, at time instants $\{mT_s\}$ (8 times per symbol), where $T_s = T/8$ and T is the symbol duration, to give the signal sequence $\{u_m\}$, with $u_m = u(mT_s)$.

The sample values $\{u_m\}$ are further filtered by the baseband equivalent model of the transmitter IF filter. The sampled impulse response of the baseband equivalent model of the transmitter IF filter, sampled at the rate of $1/T_s$ samples per second, is given by the $(g+1)$-component vector

$$F = [f_0 \; f_1 \; f_2 \; ..... f_g] \qquad 5.6.3$$

where the $\{f_m\}$, for $0 \le m \le g$, have real-valued components (Table 2.2), so that at time $t = mT_s$, the signal sample at the IF filter output is

$$e_m = \sum_{h=0}^{g} u_{m-h} f_h \qquad 5.6.4$$

The sample values $\{e_m\}$ are nonlinearly distorted by the HPA, so that at time $t = mT_s$, the signal sample at the output of the HPA is (Eqn. 2.5.30)

$$z_m = e_m M_c G(\hat{A}_m) \qquad 5.6.5$$

where $G(\hat{A}_m)$ is the conversion function of the baseband equivalent model of the HPA, M_c is the HPA backoff factor, and $\hat{A}_m$ is the one of the values $\{\lambda_n\}$ (Table 2.3) closest to the input signal envelope $|e_m M_c|$.

The FFT (Fast Fourier Transform) routine in the computer is used to evaluate the Fourier transform. Since the routine runs faster if the number of samples is a power of 2 (NAGF computer manual), the number of elements, in the resultant sequence $\{z_m\}$, is arranged to be $2^{10} = 1024$. Since the $\{u_m\}$, $\{e_m\}$ and $\{z_m\}$ have complex values, the amplitude spectra of the real and imaginary components of these signals, representing the spectra of the inphase and quadrature signals, respectively, are computed spearately by means of FFT and then added to form the amplitude spectrum of the CE8PSK signals. The 1024 samples are reduced to 128 samples by averaging every 8 samples. In order to obtain a good estimate of the amplitude spectrum of the sampled signal, the same procedure is repeated for 100 different sequence of data-symbols $\{q_i\}$ and then averaged. The signal power spectral density

of the sampled signal in dB is then obtained by taking the function $20\log_{10}(*)$ on each of these 128 sample values.

Since if the same filtering are used, CE8PSK and CDE8PSK signals have the same spectra as those of QPSK signals and do not modify the power spectral density.

5.7 Simulation results and discussion

To assess the error-rate performances for different systems, using CDE8PSK signals, computer simulation tests have been carried out , under different conditions, with the equipment filters and HPA described in Section 2.4 and 2.5. The simulation models and methods used to obtain the results in this section are described in Sections 5.3, and 5.4. In all simulation tests, it is assumed that the receiver provides the required ideal carrier and timing signals, and the data-transmission systems are optimized by sharing the overall filtering equally between the transmitter and receiver filters, and the sub-optimum decoder at the receiver uses 16 stored vectors with a delay of 32 symbols in decoding, for CDE8PSK signals.

For DEQPSK signals, it is shown in Section 3.6.1 that, the minimum truncation lengths of the sampled impulse responses of the modulation and demodulation filters, with $\alpha = 100\%,\ 40\%$ and 25% required to approximate to the theoretical ideal error-rate performance at $P_e \geq 10^{-4}$, are 5T, 5T and 8T, respectively, and they are denoted as signals 1A, 2A and 3A, respectively. Now for CDE8PSK signals, the same wave shapes of the modulating signals are used in the simulation tests, but they are known here as signals 1C, 2C and 3C, instead of signals 1A, 2A and 3A, respectively. Thus signals 1C, 2C and 3C apply to CDE8PSK signals, with $\alpha = 100\%$, 40% and 25%, and with truncation lengths of the sampled impulse responses of 5T, 5T and 8T respectively.

5.7.1 Performances of signals 1C, 2C and 3C over a nonlinear and bandlimited channel

To evaluate the error-rate performances of CDE8PSK signals, over a nonlinear and bandlimited channel, the same model as shown in Fig.4.9 is used. Here the encoder at the transmitter carries out convolutional, differential and Gray encoding of the input data, as described in Section 5.2, while the decoder at the receiver is that described in Section 5.4. As mentioned before, to avoid confusion, the CDE8PSK signals here called signals 1C, 2C and 3C, instead of signals 1B, 2B and 3B, respectively. Thus signals 1C, 2C and 3C are referred to CDE8PSK signals with $\alpha = 100\%,\ 40\%$ and 25%, respectivelly, and with truncation lengths of the sampled impulse responses of 5T, 5T and 8T respectively. The results for signals 1C, 2C and 3C, with the HPA operating at 0, 0.315 and 0.7 dB OBO, are shown in Figs. 5.4-5.6.

At 0 dB OBO (Fig. 5.4), signals 1C and 2C has a degradations in tolerance to noise about 1.6 dB at $P_e = 10^{-4}$, while signal 3C, being a relatively narrowband signal, has a degradation of about 2.2 dB at $P_e = 10^{-4}$, in comparison with that of an ideal CDE8PSK system.

At 0.315 dB HPA OBO, (i.e., slightly backed-off below saturation), Fig. 5.5 shows that signals 1C and 2C have improved in performance, and reduced the degradation to about 1.2 dB, that 0.4 dB improvement in comparison with that with 0 dB HPA OBO. Although signal 3C has reduced the degradation from 2.2 dB to about 1.8 dB, at $P_e = 10^{-4}$, in comparison with that with 0 dB HPA OBO.

With the HPA OBO value increased from 0.315 dB to 0.7 dB (Fig. 5.6), the error-rate performance of signals 1C, 2C and 3C have improved by about 0.2 dB, in comparison with the same signals when the HPA is at 0.315 dB OBO.

Figures 5.7, 5.8 and 5.9 shows the error-rate performances for signals 1C, 2C and 3C respectively, with the HPA OBO operating at 0, 0.315 or 0.7 dB for each of the signals, the results show that the degradations in tolerance to noise of the signals decreases when the HPA operating point is further below saturation (i.e., 0.7 dB OBO).

Table 5.2, shows the degradation in tolerance to noise of the CDE8PSK signals, at $P_e = 10^{-4}$, with the HPA operating at 0, 0.315 and 0.7 dB OBO, measured in comparison with that of an ideal CDE8PSK system. It can be seen that, with the HPA operating in the nonlinear mode at the earth station, the degradations in tolerance to noise of CDE8PSK signals due to nonlinear distortion are insignificant. The worst case is when signal 3C is used with the HPA operating at 0 dB OBO, and the degradation is about 2.2 dB at $P_e = 10^{-4}$, in comparison with that of an ideal CDE8PSKsystem.

3-bit binary sequence			Phase (degrees)	Magnitude of quadrature components	
$d_i(1)$	$d_i(2)$	$d_i(3)$		$q_{1,i}$	$q_{2,i}$
0	0	0	+ 22.5	+ 0.924	+ 0.383
0	0	1	+ 67.5	+ 0.383	+ 0.924
0	1	0	+ 112.5	- 0.383	+ 0.924
0	1	1	+ 157.5	- 0.924	+ 0.383
1	0	0	- 157.5	- 0.924	- 0.383
1	0	1	-112.5	- 0.383	- 0.924
1	1	0	- 67.5	+ 0.383	- 0.924
1	1	1	- 22.5	+ 0.924	- 0.383

Table 5.1 Gray encoding for CDE8PSK signals.

HPA OBO (in dB)	Signal		
	1C	2C	3C
0	1.6	1.7	2.2
0.315	1.15	1.25	1.8
0.7	0.95	1.1	1.55

Table 5.2 Degradations in tolerance to noise of signals 1C, 2C and 3C over a nonlinear and bandlimited channel, with the HPA operating at 0, 0.315 and 0.7 dB OBO, at $P_e = 10^{-4}$, expressed in dB, measured in comparison with that of the ideal CDE8PSK system (from Figs. 4.16, 4.17 and 4.18).

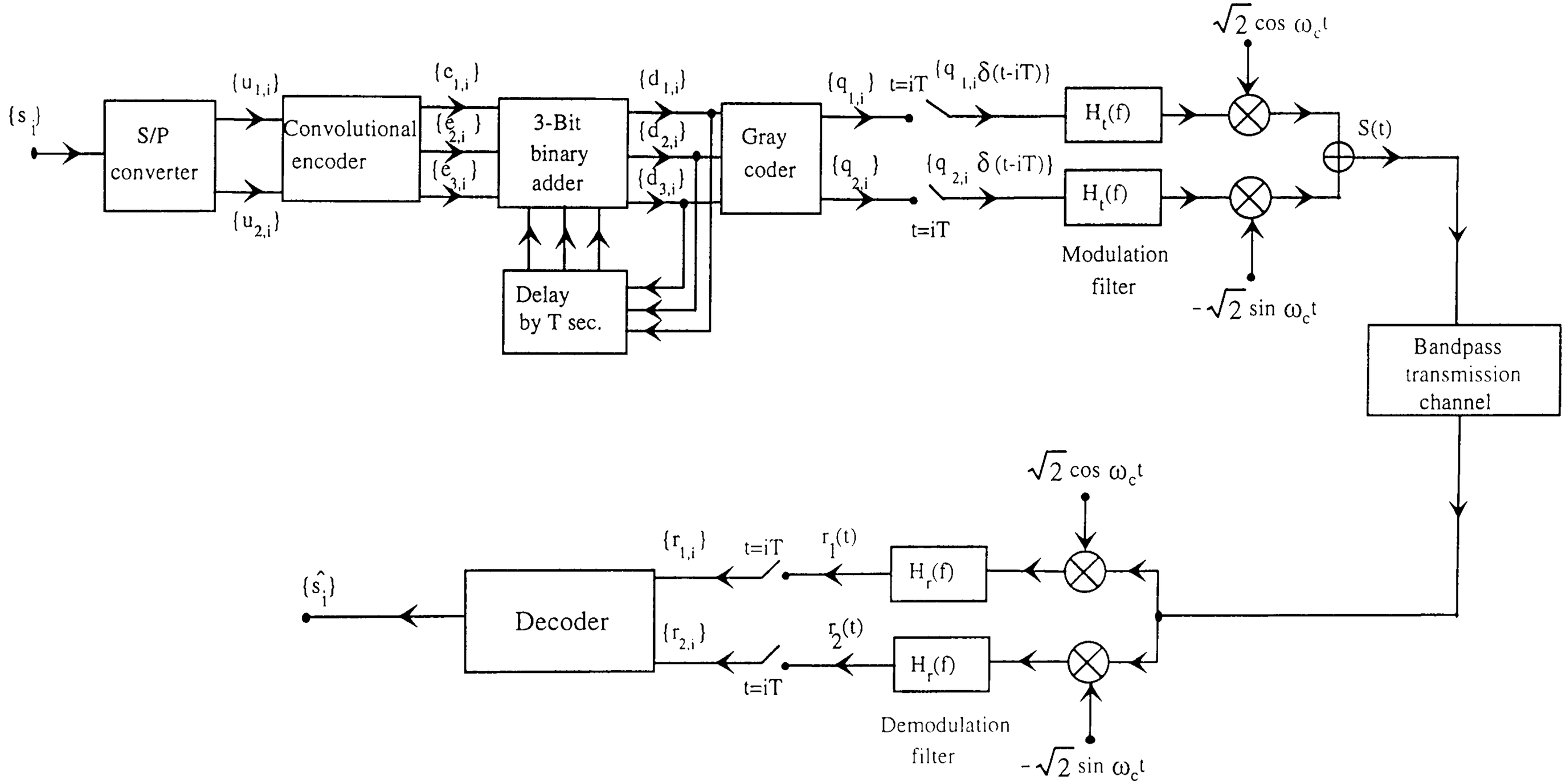

Figure 5.1 Block diagram of a convolutionally and differentially encoded 8PSK (CDE8PSK) system. S/P means serial-to-parallel.

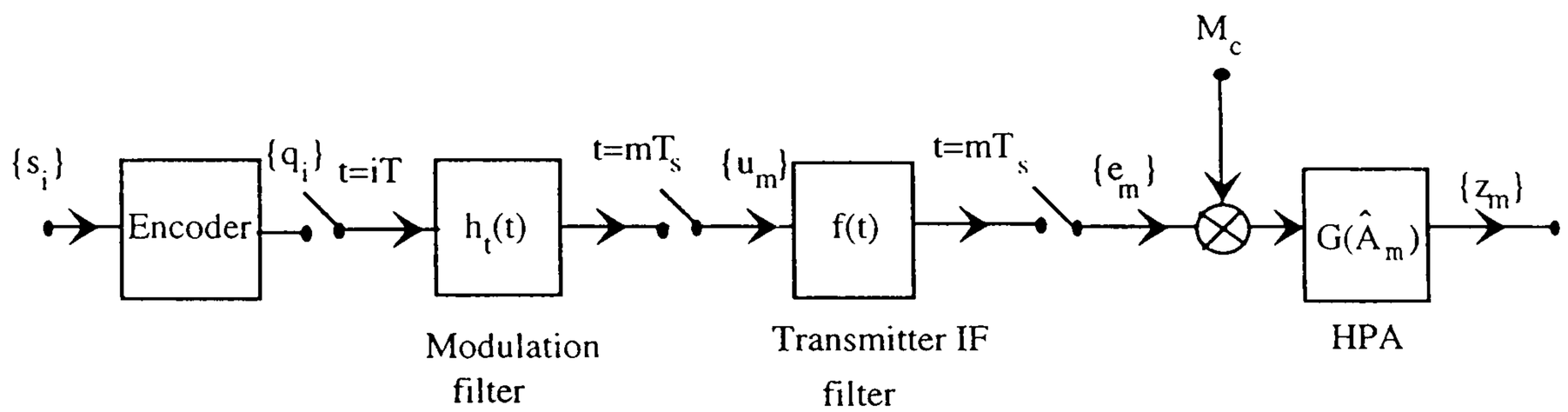

Figure 5.2 Baseband equivalent model for spectral estimation of CE8PSK or CDE8PSK signals at the output of the transmission path.

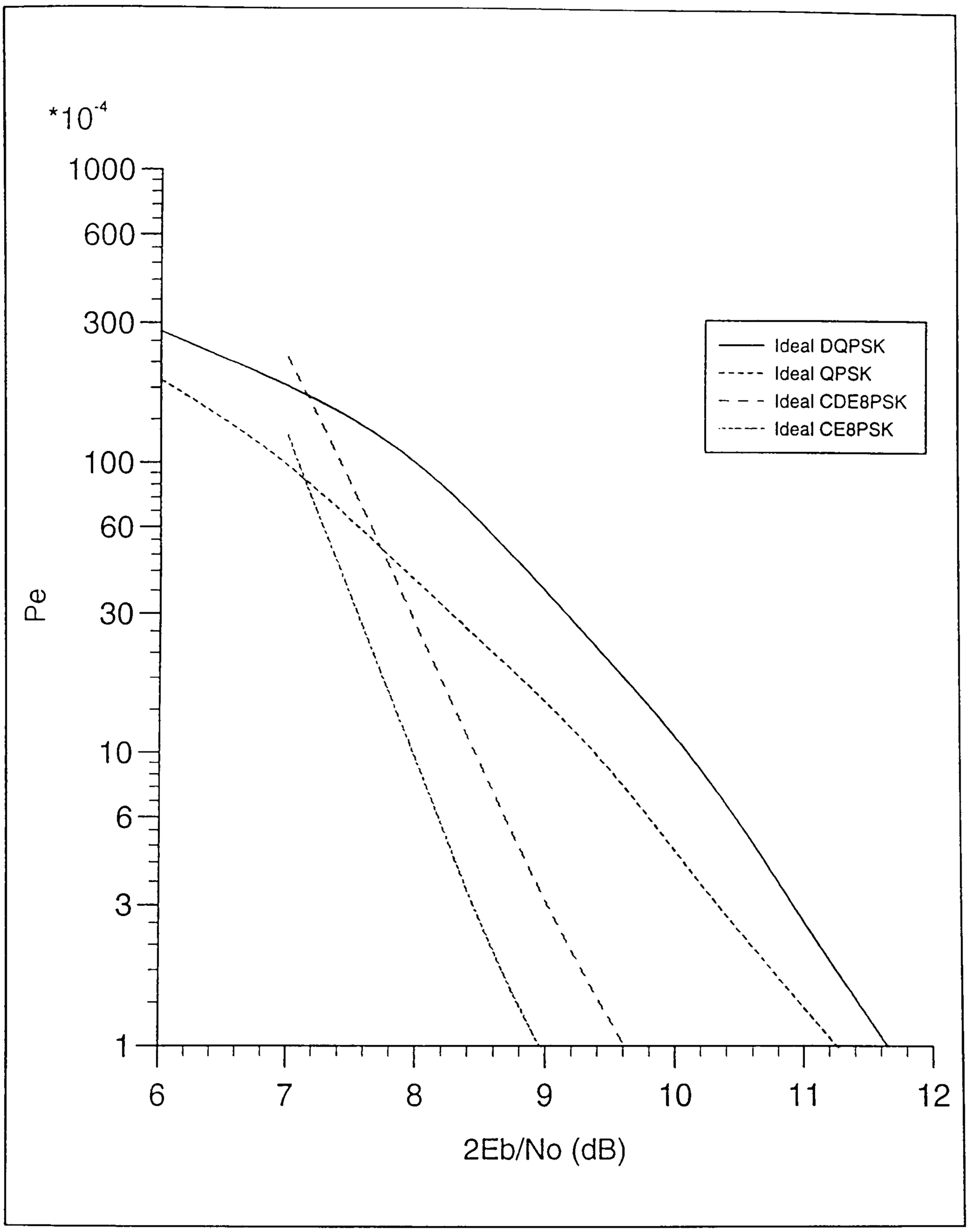

Figure 5.3 Error-rate performances of CE8PSK and CDE8PSK signals over an AWGN channel.

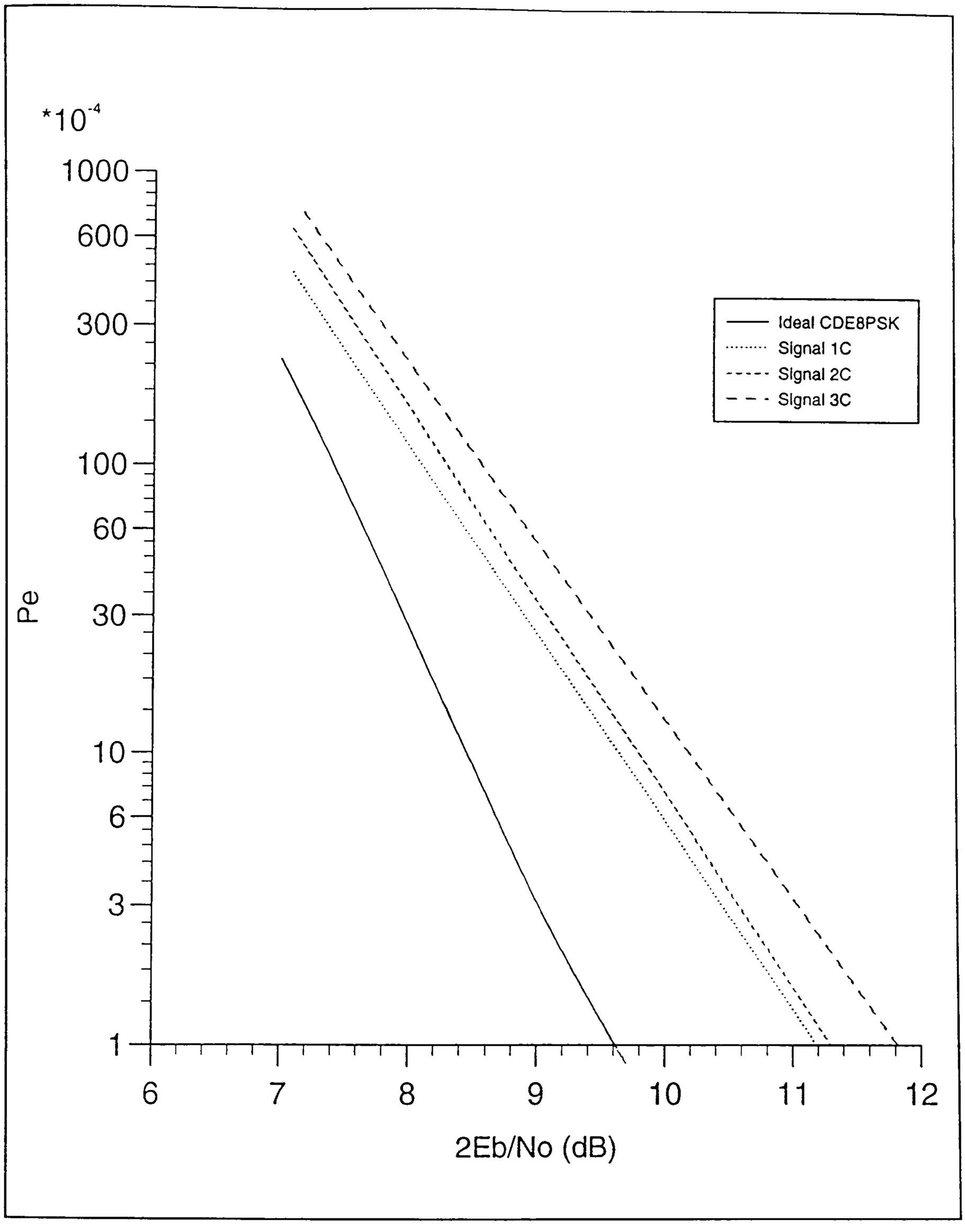

Figure 5.4 Error-rate performances of signals 1C, 2C and 3C, over a nonlinear and bandlimited channel, with the HPA operating at 0 dB OBO.

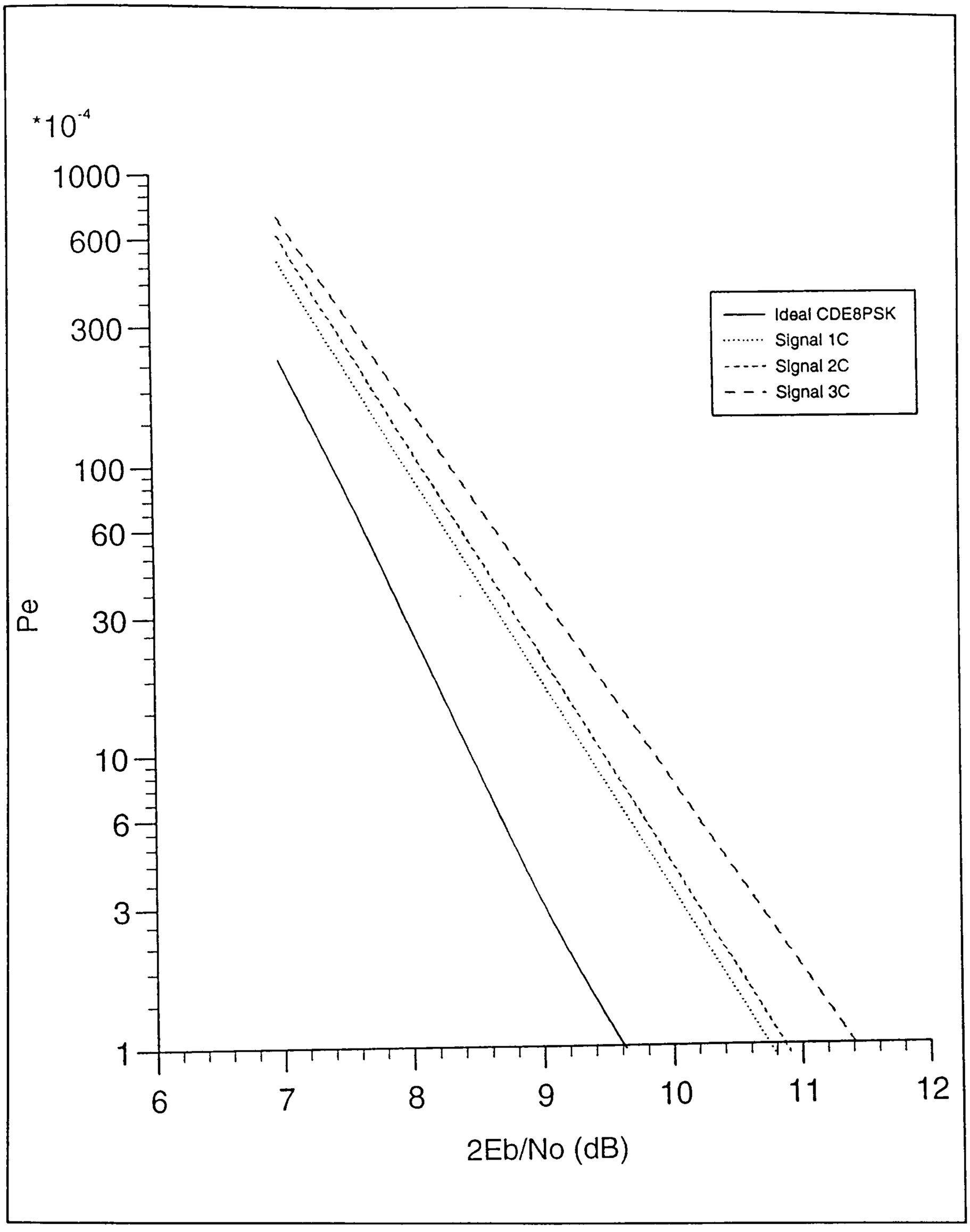

Figure 5.5 Error-rate performances of signals 1C, 2C and 3C, over a nonlinear and bandlimited channel, with the HPA operating at 0.315 dB OBO.

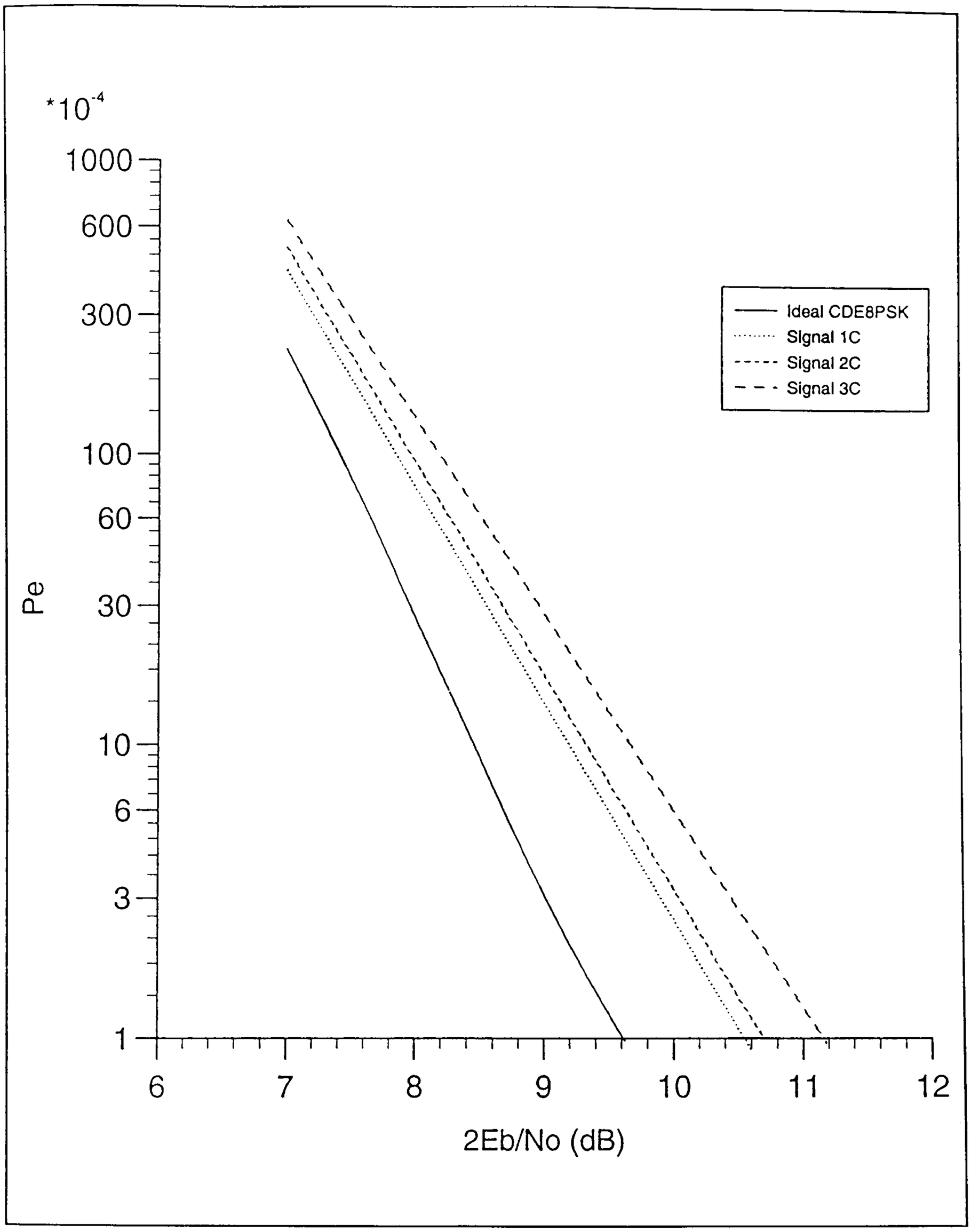

Figure 5.6 Error-rate performances of signals 1C, 2C and 3C, over a nonlinear and bandlimited channel, with the HPA operating at 0.7 dB OBO.

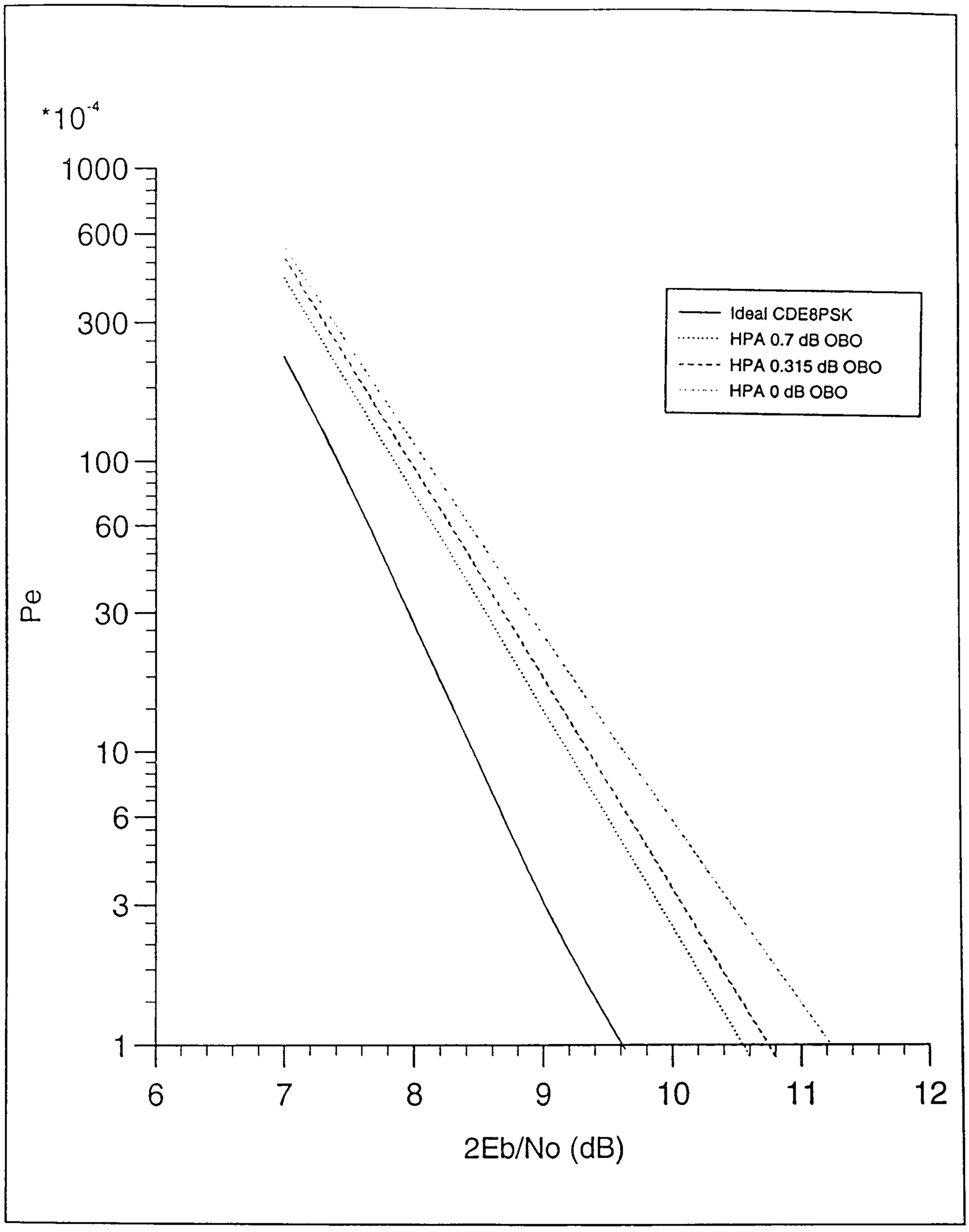

Figure 5.7 Error-rate performances of signal 1C over a nonlinear and bandlimited channel, with the HPA operating at 0, 0.315 or 0.7 dB OBO.

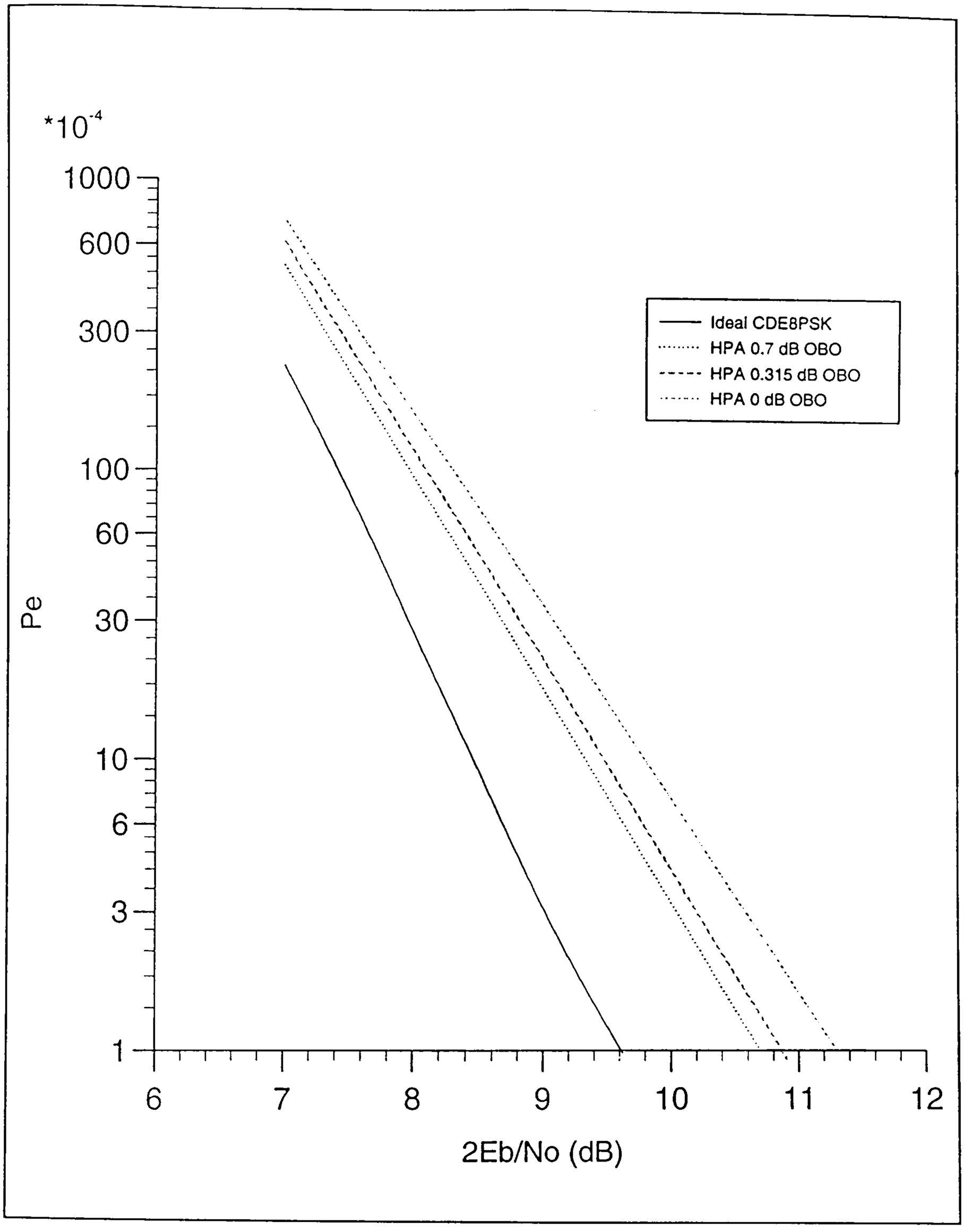

Figure 5.8 Error-rate performances of signal 2C over a nonlinear and bandlimited channel, with the HPA operating at 0, 0.315 or 0.7 dB OBO.

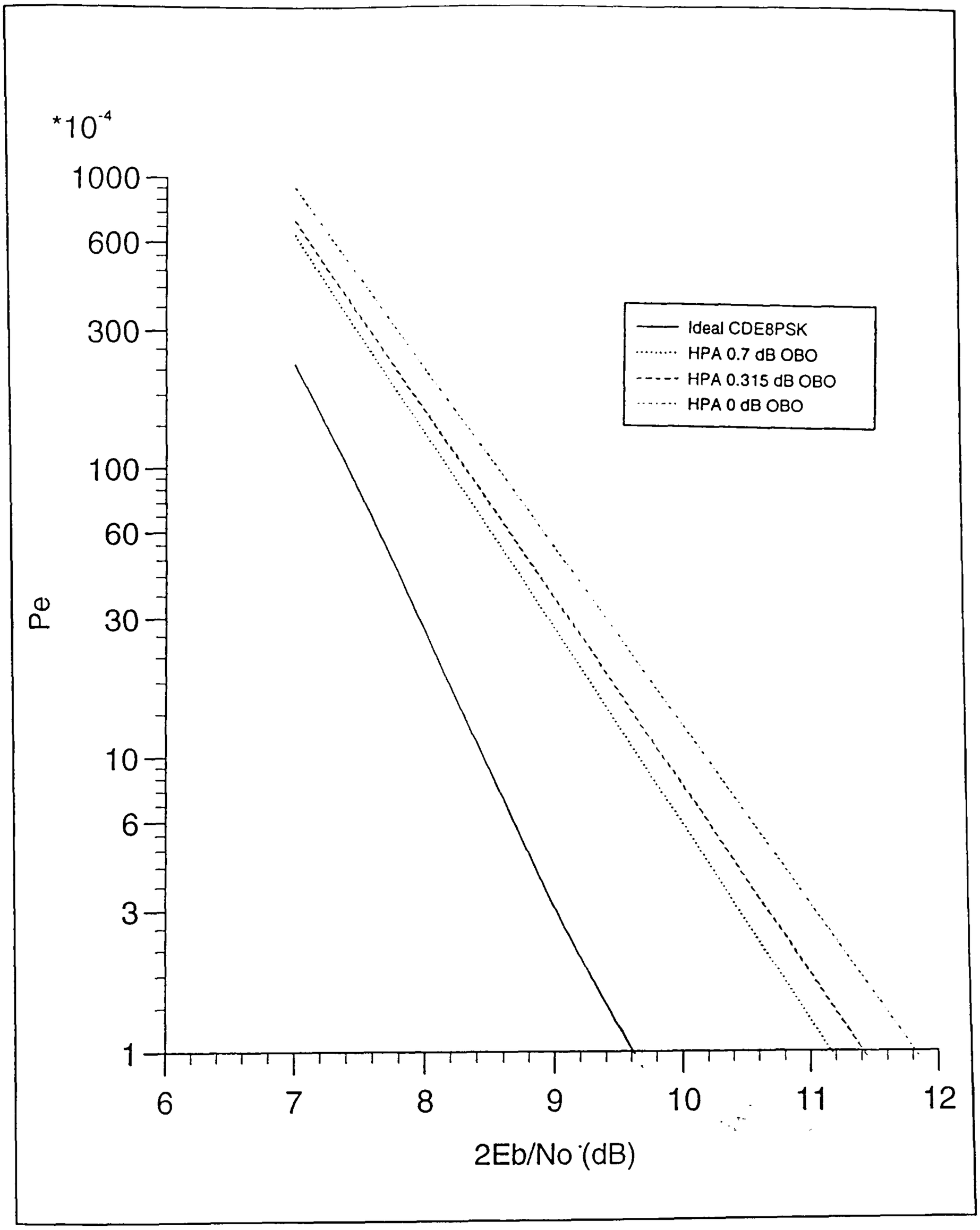

Figure 5.9 Error-rate performances of signal 3C over a nonlinear and bandlimited channel, with the HPA operating at 0, 0.315 or 0.7 dB OBO.

CHAPTER 6

BASEBAND LINEARIZER TECHNIQUE APPLIED TO PSK SIGNALS

6.1 Baseband linearizer technique

6.1.1 Introduction

For high power microwave amplification the HPA, TWT and FET (Field Effect Transistor) amplifiers are generally used. The linearity of the FET amplifier is somewhat superior to that of the HPA and TWT, as its nonlinear effects are considered negligible with reasonable output backoff. However, the maximum FET amplifier output is about 10's Watts in 2-8 GHz. The HPA and TWTA are used exclusively in high power amplifiers, for high capacity satellite transmission. For the present case, although the satellite TWTA is assumed to be operating in the linear mode, the HPA at the earth station distorts the pulse shape, which results in a reduction in tolerance to noise of the system, also it causes spectral spreading. Hence, without nonlinear compensation, efficient high capacity digital transmission can only be achieved by operating with a large backoff.

Baseband linearizing or simply predistortion is one of the best of the many methods of nonlinear compensation [67], [68], [69]. By using this technique, inverse distortion is added to the HPA input to cancel HPA nonlinear distortion. Because of the high microwave power, most predistortion circuit realizations have been achieved by predistortion of the microwave signal. In this thesis a presentation for a scheme [70] [71] which compensates the nonlinear effects of the HPA by predistorting the baseband signal prior to modulation, as opposed to correcting the distortion after modulation. It is assumed that the characteristics and the operating point of the HPA are known. The circuit realization advantages of the baseband predistorter are greatest in low data rate applications because the component costs are much smaller

than the equivalent microwave realization. The following sections describe a baseband linearizer and the improvements that can be obtained with it when applied to different PSK signals.

6.1.2 Description of the baseband linearizer

From Section 2.5.2, for a modulation signal (Eqn. 2.5.1)

$$S(t) = \sqrt{2}a(t)\cos\omega_c t - \sqrt{2}b(t)\sin\omega_c t \qquad 6.1.1$$

with the equivalent baseband signal represented (Appendix A6) as the complex-valued signal (Eqn. 2.5.12)

$$s(t) = a(t) + jb(t) \qquad 6.1.2$$

where $j = \sqrt{-1}$, input to the HPA, the equivalent baseband signal at the HPA output, with the use of the HPA backoff factor M_c, is given by (Eqn. 2.5.20, 2.5.21 and 2.5.18)

$$z(t) = s(t)M_c G(\hat{A}) \qquad 6.1.3$$

$$= [a(t) + jb(t)]M_c[G_p(\hat{A}) + jG_q(\hat{A})] \qquad 6.1.4$$

where $$G(\hat{A}) = [G_p(\hat{A}) + jG_q(\hat{A})] \qquad 6.1.5$$

is the conversion function of the HPA and is dependent on the envelope $\hat{A}$. $\hat{A}$ is a short-hand notation for

$$\hat{A}(t) = M_c[a^2(t) + b^2(t)]^{1/2} \qquad 6.1.6$$

from Eqn. 2.5.18.

The baseband linearizer, described here, adds inverse distortion to the inphase and quadrature components, $a(t)$ and $b(t)$, of the modulation signal, $S(t)$, in order to cancel HPA nonlinear distortion. Note that $a(t)$ and $b(t)$ are the inphase and quadrature modulated waveforms, respectively, so that baseband linearizer is carried out on the baseband signal. The baseband linearizer consists of two circuits, as shown in Fig. 6.1; the envelope predistortion circuit and the phase predistortion circuit. The former predistorts the (inphase and quadrature) components of the signal equally; however, this does not change the signal phase, while the latter in cascade with the

envelope predistortion circuit predistorts the phase of the signal, yet, does not affect the amplitude of the envelope.

Figure 6.1 shows a block diagram of the baseband predistorter. It has two major parts:

1) A circuit that predistorts the amplitude of the baseband signal $s(t)$. It is a hardware realization of the operation

$$[a(t)+jb(t)]|D(E)| \qquad 6.1.7$$

where $|D(E)|$ is the predistorter amplitude conversion function, whose value is dependent on the signal envelope E. E is a short-hand notation for

$$E(t)=[a^2(t)+b^2(t)]^{1/2} \qquad 6.1.8$$

2) A circuit that predistorts the phase angle of the complex-valued baseband signal $s(t)$ (Eqn. 6.1.2). It is a hardware realization of the operation

$$[a(t)+jb(t)]\{\cos[f(E)]+j\sin[f(E)]\} \qquad 6.1.9$$

where $f(E)$ is the predistorter phase conversion function, whose value is dependent on E.

In fact, these two operations can be combined by using a single ciruit with a hardware realization given by

$$x(t)=[a(t)+jb(t)]|D(E)|\{\cos[f(E)]+j\sin[f(E)]\} \qquad 6.1.10$$

$$=[a(t)+jb(t)]\{|D(E)|\cos[f(E)]+j|D(E)|\sin[f(E)]\} \qquad 6.1.11$$

$$=[a(t)+jb(t)][D_p(E)+jD_q(E)] \qquad 6.1.12$$

with $$D_p(E)=|D(E)|\cos[f(E)] \qquad 6.1.13a$$

and $$D_q(E)=|D(E)|\sin[f(E)] \qquad 6.1.13b$$

where $x(t)$ is the predistorted baseband (modulating) signal, and $D_p(E)$ and $D_q(E)$ are the inphase and quadrature conversion functions, respectively, of the baseband linearizer. A lookup table may be used to supply these multiplicative factors, $D_p(E)$ and $D_q(E)$, (which will be derived later in this Chapter), to apply to each of

the baseband signal components, for any given value of E, as shown in Fig. 6.2. These values are calculated such that they cancel as much as possible the nonlinear effects of the HPA.

6.2 Modelling of the baseband linearizer

Let $D(E) = D_p(E) + jD_q(E)$, where $j = \sqrt{-1}$. Then Eqn. 6.1.12 becomes

$$x(t) = [a(t) + jb(t)]D(E) \qquad 6.2.1$$

where $D(E)$ represents the conversion function of the baseband linearizer. The equivalent model of the baseband linearizer is shown in Fig. 6.3a, where the baseband linearizer is represented by the conversion function $D(E)$. Since the value of $D(E)$ is dependent on the input signal envelope $E(t)$, it can be varied by multiplying $E(t)$ by a constant factor L_c (as in the case of the HPA) to give the signal envelope (Eqn. 6.1.8)

$$\hat{E}(t) = L_c[a^2(t) + b^2(t)]^{1/2} \qquad 6.2.2$$

This is equivalent to shifting the operating point along the baseband linearizer transfer characteristics by using the value of L_c, so that L_c can be used to locate the operating point at the required backoff value. L_c is called the baseband linearizer backoff factor. Hence, with the use of the baseband linearizer backoff factor, the signal from the baseband linearizer output, for an input signal of

$$u(t) = a(t) + jb(t) \qquad 6.2.3$$

is given by (Eqn. 6.1.12 and 6.2.1)

$$x(t) = [a(t) + jb(t)]L_c[D_p(E) + jD_q(E)] \qquad 6.2.4$$

$$= [a(t) + jb(t)]L_c D(\hat{E}) \qquad 6.2.5$$

$$= u(t)L_c D(\hat{E}) \qquad 6.2.6$$

In practice, the analogue baseband signal components, $a(t)$ and $b(t)$, are generated by using a pair of digital filters and then an D/A conversion process (Section 2.4.1). Thus predistortion can be carried out digitally on the baseband signal, before the D/A conversion process. Samples of $D(\hat{E})$ which provide sufficient

resolution can be stored in a lookup table (Fig. 6.2), and used to determine the required output signal samples. The samples are obtained as follows

1) The baseband linearizer AM-AM characteristic is obtained by graphically inverting the HPA AM-AM characteristic, so that the input of the HPA AM-AM characteristic becomes the output of the baseband linearizer AM-AM characteristic. This is illustrated in Fig. 6.4b. Since the baseband linearizer can not cancel the nonlinear effect of the HPA over the region above saturation, no attempt is made to invert this region. To represent the baseband linearizer AM-AM characteristic by, say h discrete values of $|D(E)|$, the baseband linearizer voltage transfer characteristic is quantized into regular intervals of δ volts, along the input axis. The values of $|D(\delta_m)|$, where $\delta_m = m\delta$, for m= 1, 2, ..., h, are obtained using the baseband linearizer AM-AM characteristic and the equation

$$|D(\delta_m)| = \frac{\text{Output voltage for an input value of } m\delta \text{ volts}}{m\delta \text{ volts}} \qquad 6.2.7$$

This is the AM-AM conversion function of the baseband linearizer.

2) The baseband linearizer AM-PM characteristic is the negative of the phase rotation introduced by the HPA. Hence by drawing horizontal lines from the baseband linearizer AM-AM characteristic to the HPA AM-AM characteristic, the baseband linearizer AM-PM characteristic can be obtained by taking the negative sign of the corresponding HPA AM-PM values. For example, the negative phase rotation marked as point 'X' on the baseband linearizer AM-PM characteristic is shown by the path 'X' on Fig. 6.4. The complete baseband linearizer AM-PM characteristic is shown in Fig. 6.4b. The quadrature components, $D_p(\delta_m)$ and $D_q(\delta_m)$, of the baseband linearizer characteristic function, for m= 1, 2, ..., h, are then obtained using the baseband linearizer phase characteristic and $|D(\delta_m)|$ with the following two equations

$$D_p(\delta_m) = |D(\delta_m)|\cos[f(\delta_m)] \qquad 6.2.8$$

and

$$D_q(\delta_m) = |D(\delta_m)|\sin[f(\delta_m)] \qquad 6.2.9$$

where $f(\delta_m)$ is the AM-PM conversion function of the baseband linearizer and $|D(\delta_m)|$, for m= 1, 2, ..., h, have been obtained in (1).

3) The values of $D_p(\delta_m)$ and $D_q(\delta_m)$, for m= 1, 2, ..., h, are then taken as real and imaginary values, respectively, such that

$$D(\delta_m) = D_p(\delta_m) + jD_q(\delta_m) \qquad 6.2.10$$

Hence, the conversion function of the baseband linearizer, $\{D(\delta_h)\}$, are obtained.

Since the modulation filter is digital, consider time $t = iT_s$, where $1/T_s$ is the sampling rate. The digital baseband signal, at the filter output, at time $t = iT_s$, is given by (Eqn. 6.2.3)

$$u_i = a_i + jb_i \qquad 6.2.11$$

where $a_i = (iT_s)$ and $b_i = b(iT_s)$. So from Eqns. 6.2.6, 6.2.5 and 6.2.4, the signal sample from the baseband linearizer output, at time $t = iT_s$, is

$$x_i = u_i L_c D(\hat{E}_i) \qquad 6.2.12$$

$$= (a_i + jb_i) L_c D(\hat{E}_i) \qquad 6.2.13$$

$$= (a_i + jb_i) L_c [D_p(\hat{E}_i) + jD_q(\hat{E}_i)] \qquad 6.2.14$$

$$= [L_c a_i D_p(\hat{E}_i) - L_c b_i D_q(\hat{E}_i)] + j[L_c a_i D_q(\hat{E}_i) + L_c b_i D_p(\hat{E}_i)] \qquad 6.2.15$$

where now $\hat{E}_i$ is a quantized value which may not be equal to, but is at least close to, the signal envelope $|u_i L_c|$ at the baseband linearizer input. Equation 6.2.15 shows that, it is possible to achieve a considerable reduction in equipment complexity by combining the operation of modulation filtering and predistortion in a single lookup table.

The model shown in Fig. 6.3b is used to assess the performance of the baseband linearizer, in computer simulation tests. The value of $\{D(\delta_h)\}$, for h = 1, 2, 3, ..., 32, obtained by quantizing the baseband linearizer characteristics (Fig. 6.4b) into regular intervals along the input axis and using Eqns. 6.2.7, 6.2.8 and 6.2.9, are shown in Table 6.1.

From Fig. 6.4b, it can be seen that the baseband linearizer introduces nonlinear AM-AM and AM-PM conversion effects. This results in spectral spreading of a signal with a nonconstant envelope, as is seen from the results shown in Section 6.6.1. However, the predistorted signal, at the output of the baseband linearizer, must not be bandlimited if it is used to cancel the HPA nonlinear distortion. This is because the high frequency components in the signal, generated in the predistortion process, are needed to cancel the nonlinear distortion of the HPA. Results of computer simulation tests suggest that, if the predistorted signal is bandlimited by the transmitter IF filter F_{IF}, then it ceases to cancel the nonlinear distortion introduced by

the HPA. Thus the predistorted signal must not be bandlimted before feeding it into the HPA.

Predistortion is carried out on the sampled baseband signal, whereas the HPA is operating on continuous bandpass signal. However, as mentioned before, a D/A conversion process is used at the output of the baseband linearizer to obtain the required shape of the analoge modulating baseband waveforms, and so a pair of post D/A lowpass filters have to be used to reject spurious signals (Section 2.4.3). It is assumed here that, in all the transmission system models which use the baseband linearizer, the post D/A filters have a rectangular frequency response and a linear phase characteristic over the predistorted signal bandwidth. Clearly, the predistorted signal has a bandwidth of half of the digital sampling rate, i.e., $1/2T_s$. These filters do not distort the signal and so are not included in the simulation models.

6.3 Model of the baseband linearizer in cascade with the HPA, used for computer simulation

The baseband equivalent model of the HPA is shown in Fig. 2.11c and discussed in Section 2.5. Here the model of the baseband linearizer in cascade with the HPA, used for the computer simulation tests, is shown in Fig. 6.5. The signal sample value, at the input to the baseband linearizer, at time $t = iT_s$, is (Eqn. 6.2.11)

$$u_i = a_i + jb_i$$

From Eqn. 6.2.12, the output signal sample from the baseband linearizer, at time $t = iT_s$, is

$$x_i = u_i L_c D(\hat{E}_i) \qquad 6.3.1$$

where x_i and $D(\hat{E}_i)$ have complex values. $D(\hat{E}_i)$ is the conversion function of the baseband linearizer, and $\hat{E}_i$ is the quantized value which may not be equal, but is at least close to the input signal envelope $|u_i L_c|$ (the absolute value of $u_i L_c$). L_c is the baseband linearizer backoff factor used to locate the required operating point on the baseband linearizer characteristics. The predistorted signal sample x_i is then backed off by the HPA backoff factor M_c and fed into the HPA, which gives at its output the signal sample, at time $t = iT_s$,

$$y_i = x_i M_c G(\hat{A}_i) \qquad 6.3.2$$

Hence, from Eqns. 6.3.1 and 6.3.2,

$$v_i = u_i L_c D(\hat{E}_i) M_c G(\hat{A}_i) \qquad 6.3.3$$

where v_i and $G(\hat{A}_i)$ have complex values. $G(\hat{A}_i)$ is the conversion function of the HPA, $\hat{A}_i$ is a quantized value which may not be equal, but is at least close to the input signal envelope $\left|u_i L_c D(\hat{E}_i) M_c\right|$, and M_c is the HPA backoff factor used to locate the required operating point on the HPA characteristics.

6.4 Backoff factor of the baseband linearizer

The baseband linearizer adds inverse distortion to the baseband signal to cancel HPA nonlinear distortion. The distortion varies as the operating point (output power) of the HPA is varied, and so the baseband linearizer must be backed off at a suitable operating point in order to obtain the optimum performance (i.e., optimum cancellation of nonlinear distortion).

Figure 6.6 shows how the HPA AM-AM conversion effect on a signal is cancelled by using the baseband linearizer. It can be seen that, when an input signal with a sinusoidal envelope is fed into the baseband linearizer, the envelope of the signal at its output is amplitude distorted, but if the predistorted signal is fed into the HPA backed off at the right operating point, the original envelope could be recovered. Figure 6.6 shows that, when the signal with an average voltage of QA volts is fed into the baseband linearizer, the average output voltage is not QB volts, but QC volts. This is caused by the nonlinear AM-AM conversion effects of the baseband linearizer. So when the predistorted signal is fed into the HPA, it should be backed off at QC volts, instead of QB volts, in order to obtain the optimum cancellation of the nonlinear distortion, because the average voltage into the HPA is now QC volts.

Since the AM-AM conversion effect of the baseband linearizer is nonlinear, the optimum operating point for compensating the nonlinear effects of the HPA operating at a given backoff value can not be found directly or simply from the baseband linearizer characteristics. Computer simulation tests were, in fact, used to find this. Extensive computer simulation tests, have carried out and the results suggest that 0.7 and 1 dB IBO (Input Backoff) of the baseband linearizer are the optimum values (i.e., give the best error-rate performances) for the HPA operating at 0.315 and 0.7 dB OBO, respectively. Since the baseband linearizer can only cancel the HPA nonlinear effects ocuring below saturation, when predistortion is used, the HPA should be operating below saturation. Thus in all the transmission systems which use the baseband linearizer described here, the HPA is operating either at

0.315 or 0.7 dB OBO with the baseband linearizer operating at 0.7 or 1 dB IBO, respectively.

6.5 Baseband equivalent model of the DEQPSK or CE8PSK system (or CDE8PSK system) with the use of the baseband linearizer

Since the predistorted signal at the baseband linearizer output must not be bandlimited in order to cancel the HPA nonlinear distortion (Section 6.2), the transmitter IF filter F_{IF} cannot be used. In order to maintain the equal sharing of the overall filtering between the transmitter and receiver filters (as assumed in all the transmission systems discussed so far), the modulation filter should now have the characteristics of the baseband equivalent model of the receiver IF filter in cascade with the demodulation filter. In practice, since this filter is digital, it is not difficult to realize. So in all the transmission system models with the use of the baseband linearizer technique described in this thesis, the above filter arrangement is assumed. Hence the equal sharing of the overall filtering between the transmitter and receiver filters is maintained.

The baseband equivalent model of a DEQPSK or CE8PSK system (or CDE8PSK system), with the use of the baseband linearizer, is shown in Fig. 6.7. (The model is modified from the model shown in Fig. 3.8 or 4.9). For DEQPSK systems, the transmitter has a differential and Gray encoder, and the receiver has a threshold detector, a Gray and differential decoder. Whereas for CE8PSK systems, the transmitter has a convolutional and Gray encoder, and the receiver has a Viterbi decoder while for CDE8PSK systems, the transmitter has a differential, a convolutional and Gray encoder, and the receiver has a suboptimum decoder that is described in Section 5.4. The simulation methods are exactly as described in Section 3.3 (and 4.4 for CE8PSK signal), except that with e_m in Eqn. 3.3.8 replaced by x_m (Eqn. 6.3.1)

$$x_m = u_m L_c D(\hat{E}_m) \qquad 6.5.1$$

Thus Eqn. 3.3.8 becomes

$$z_m = u_m L_c D(\hat{E}_m) M_c G(\hat{A}_m) + n_m \qquad 6.5.2$$

where z_m, u_m, $D(\hat{E}_m)$, $G(\hat{A}_m)$ and n_m all have complex values. $\hat{E}_m$ and $\hat{A}_m$ are the quantized values which are closest to the corresponding input signal envelope $|u_m L_c|$ and $|u_m L_c D(\hat{E}_m) M_c|$, respectively.

6.6 Simulation results and discussion

In this section the improvements achieved by the use of the baseband linearizer will be shown. Computer simulation tests of the different systems have been carried out to assess the error-rate performances, with the use of the baseband linearizer, used for DEQPSK, CE8PSK and CDE8PSK signals, with the preferred equipment filters and HPA. In all simulation tests, it is assumed that the receiver provides the ideal required carrier and timing signals, and the data-transmission systems are optimized by sharing the overall filtering equally between the transmitter and receiver. In the cases of CE8PSK and CDE8PSK signals, the decoder uses 16 stored vectors with a delay of 32 symbols in decoding.

6.6.1 Reduction in spectral spreading

Computer simulation tests have been carried out to estimate the signal spectra at the output of the HPA for different types of signals. The results show that, if the same transmitting filtering is used, DEQPSK, CE8PSK and CDE8PSK signals all have similar shapes of signal spectra. With the use of the baseband linearizer prior to the HPA, the power spectra of DEQPSK, CE8PSK and CDE8PSK signals at the output of the HPA, with and without the baseband linearizer, over the nonlinear channel, were estimated. The results suggest that, with the same modulation filter, the baseband linearizer has the same effect on all the signals, i.e., DEQPSK, CE8PSK and CDE8PSK signals all have the similar spectra. With the HPA operating at 0.315 and 0.7 dB OBO, the estimated signal power spectra of signals 1A, 2A and 3A at the output of the HPA, with and without the use of the baseband linearizer, are shown in Figs. 6.8-6.13. The results show that, since the baseband linearizer is a nonlinear device, it causes spectral spreading to the signals, but the consequent spectral spreading at the output of the HPA is siginificantly reduced. Comparing the power spectra at the output of the HPA, without the use of the baseband linearizer, against the power spectra with the use of the baseband linearizer, it can be seen that a siginificant reduction in spectral spreading at the HPA output has been achieved by the use of the baseband linearizer.

6.6.2 Performance of signals 1A, 2A and 3A with the use of the baseband linearizer.

The simulation model, used to evaluate the error-rate performances of the DEQPSK signals, is shown in Fig. 6.7. The perfromances of signals 1A, 2A and 3A, with the HPA operating at 0.315 and 0.7 dB OBO, are shown in Figs. 6.14, and 6.15 respectively.

At 0.315 dB OBO (Fig. 6.14), signal 1A has the best performance. Table 6.2 shows the degradations in tolerance to noise of the signals at $P_e = 10^{-4}$, with the HPA operating at 0.315 and 0.7 dB OBO, measured in comparison with that of an ideal DEQPSK system. Comparing with the degradations in tolerance to noise of the signals under the same conditions, but without the use of the baseband linearizer, as shown in Table 3.5, it can be seen that the baseband linearizer has improved the performances of all signals.

The largest improvement of about 1.1 dB at $P_e = 10^{-4}$, are made by signal 3A. These improvements are expected since the spectral spreading have been reduced significantly by the baseband linearizer, as can be seen in Figs, 6.12 and 6.13. Figure 6.15 shows that very little improvement can be obtained by increasing the HPA OBO from 0.315 dB to 0.7.

From the above results, it can be concluded that, under the assumed conditions, for the preferred filters, baseband linearizer and HPA, the most cost effective arrangement is to use signal 2A, and to operate the HPA slightly below saturation (say 0.315 dB OBO). The degradation in tolerance to noise is about 0.5 dB at $P_e = 10^{-4}$, in comparison with that of an ideal DEQPSK system. Even signal 3A can provide a better power-bandwidth efficiency, but it still has about 1.2 dB degradation at $P_e = 10^{-4}$, in comparison with that of an ideal DEQPSK system.

6.6.3 Performances of signals 1B, 2B and 3B with the use of the baseband linearizer.

The results in Section 4.10.1 have shown that the nonlinear effects of the HPA on the error-rate performances of signals 1B, 2B and 3B are quite insignificant. Obviously, with the use of the baseband linearizer, these effects will be further reduced.

At 0.315 dB OBO (Fig. 6.16), signal 1B and 2B provide the best performances. Table 6.3 shows the degradations in tolerance to noise of the signals at $P_e = 10^{-4}$, measured in comparison with that of an ideal CE8PSK system. comparing the result without the use of the baseband linearizer, as shown in Table 4.3a, it can be seen that the baseband linearizer has further reduced the degradations, due to the HPA, of all the signals. These improvements in P_e degradations are expected since the spectral spreading has been reduced significantly (Figs. 6.8-6.13).

Now, if the degradations in Table 6.3 are compared with those in Table 6.2 obtained in the previous section, it can be seen that, under the same assumed conditions, the CE8PSK signals show very little degradation compared to the DEQPSK signals. This is because CE8PSK signals suffer less degradation in tolerance to noise, than DEQPSK signals.

From the above results, it can be concluded that, under the assumed conditions, for the prefered filters, baseband linearizer and HPA, the most cost effective arrangement is to use signal 2B, with the HPA is slightly below saturation (say 0.315 dB OBO), the degradation in tolerance to noise is less than 0.2 dB, at $P_e = 10^{-4}$, in comparison with that of an ideal CE8PSK system.

6.6.4 Performances of signals 1C, 2C and 3C with the use of the baseband linearizer.

To evaluate the error-rate performances of CDE8PSK signals with the use of the baseband linearizer, the same model as shown in Fig. 6.7 is used. The encoder at the transmitter now carries out convolutional, differential and Gray encoding of the input data, as described in Section 5.2, while the decoder at the receiver is that described in Section 5.4.

The error-rate performances of signals 1C, 2C and 3C with the HPA operating at 0.315 dB and 0.7 dB OBO, are shown in Figs. 6.18 and 6.19, respectively.

At 0.315 dB OBO (Fig. 6.18), signals 1C and 2C provide the best performances. Table 6.4 shows the degradations in tolerance to noise of the signals at $P_e = 10^{-4}$, measured in comparison with that of an ideal CDE8PSK system. Fig. 6.19 shows that very little improvement can be obtained by increasing the HPA OBO value from 0.315 to 0.7 dB.

Comparing the results in Table 6.4 with those in Table 5.2, it can be seen that the degradation is about 1.3 dB, at $P_e = 10^{-4}$, for signal 3C, when the HPA 0.315 dB OBO, and the baseband linearizer has reduced the degradation by 0.5 compared with that without the use of baseband linearizer (Table 5.2). The most cost effective signal to use with this system is signal 1C or 2C.

m	$D(\delta_m) = D_p(\delta_m) + jD_q(\delta_m)$		m	$D(\delta_m) = D_p(\delta_m) + jD_q(\delta_m)$	
1	0.280	-0.005	17	0.492	-0.251
2	0.280	-0.012	18	0.504	-0.315
3	0.280	-0.015	19	0.574	-0.425
4	0.285	-0.020	20	0.594	-0.544
5	0.309	-0.033	21	0.594	-0.544
6	0.309	-0.038	22	0.594	-0.544
7	0.319	-0.051	23	0.594	-0.544
8	0.341	-0.063	24	0.594	-0.544
9	0.357	-0.076	25	0.594	-0.544
10	0.358	-0.086	26	0.594	-0.544
11	0.386	-0.104	27	0.594	-0.544
12	0.399	-0.122	28	0.594	-0.544
13	0.418	-0.136	29	0.594	-0.544
14	0.432	-0.157	30	0.594	-0.544
15	0.453	-0.188	31	0.594	-0.544
16	0.468	-0.218	32	0.594	-0.544

Table 6.1 Sampled representation of baseband linearizer conversion function or (characteristics) shown in Fig. 6.4b.

HPA OBO (in dB)	Signal		
	1A	2A	3A
0.315	0.2	0.5	1.2
0.7	0.2	0.3	1

Table 6.2 Degradations in tolerance to noise of signals 1A, 2A and 3A, with the use of baseband linearizer, over a nonlinear and bandlimited channel, with the HPA operating at 0.315 and 0.7 dB OBO, at $P_e = 10^{-4}$, expressed in dB, measured in comparison with that of the ideal DEQPSK system (from Figs. 6.14 and 6.15).

HPA OBO (in dB)	Signal		
	1B	2B	3B
0.315	0.1	0.15	0.3
0.7	0.1	0.1	0.3

Table 6.3 Degradations in tolerance to noise of signals 1B, 2B and 3B, with the use of baseband linearizer, over a nonlinear and bandlimited channel, with the HPA operating at 0.315 and 0.7 dB OBO, at $P_e = 10^{-4}$, expressed in dB, measured in comparison with that of the ideal CE8PSK system (from Figs. 6.16 and 6.17).

HPA OBO (in dB)	Signal		
	1C	2C	3C
0.315	0.8	0.95	1.3
0.7	0.55	0.7	0.95

Table 6.4 Degradations in tolerance to noise of signals 1C, 2C and 3C, with the use of baseband linearizer, over a nonlinear and bandlimited channel, with the HPA operating at 0.315 and 0.7 dB OBO, at $P_e = 10^{-4}$, expressed in dB, measured in comparison with that of the ideal CDE8PSK system (from Figs. 6.18 and 6.19).

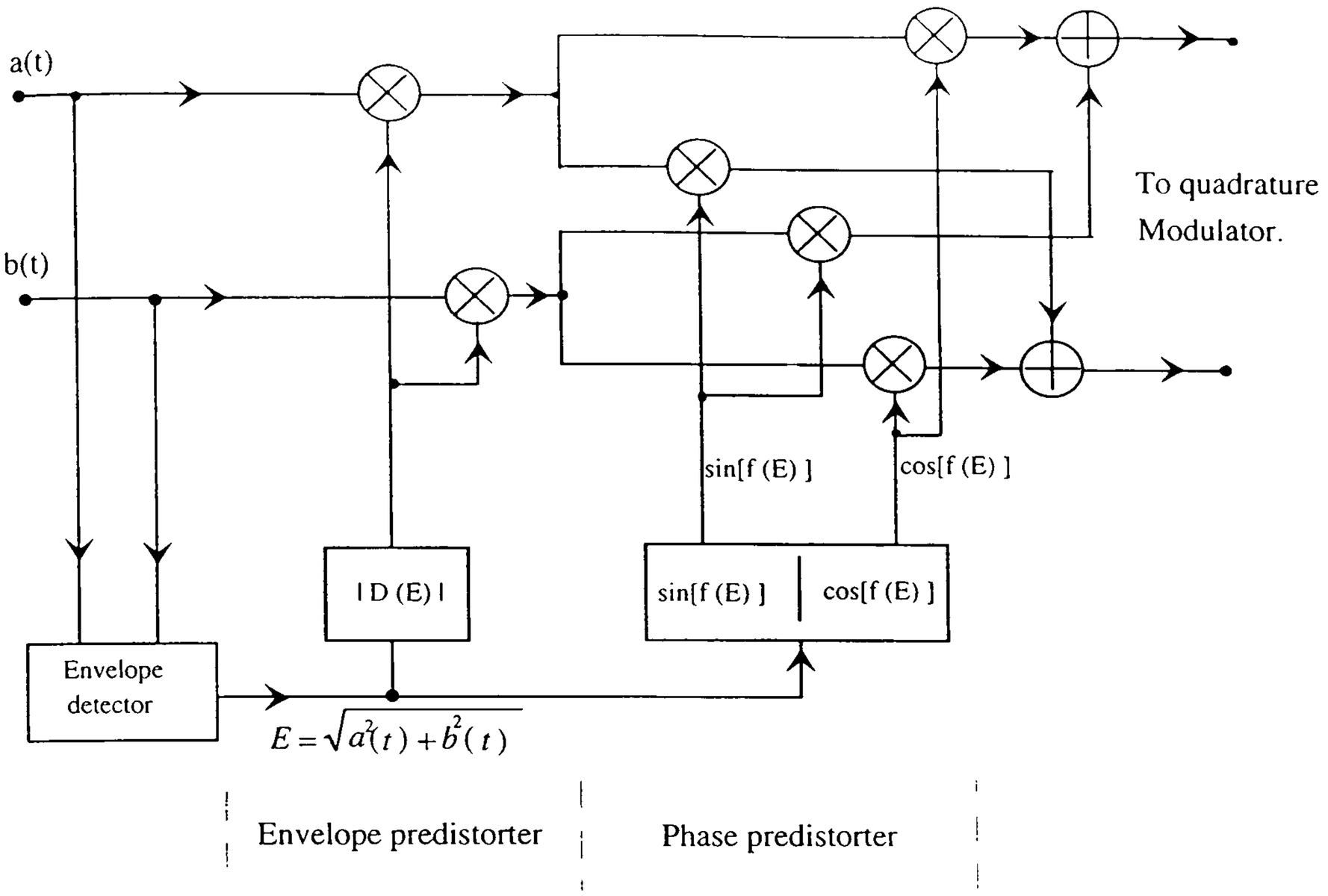

Figure 6.1 Baseband linearizer block diagram.

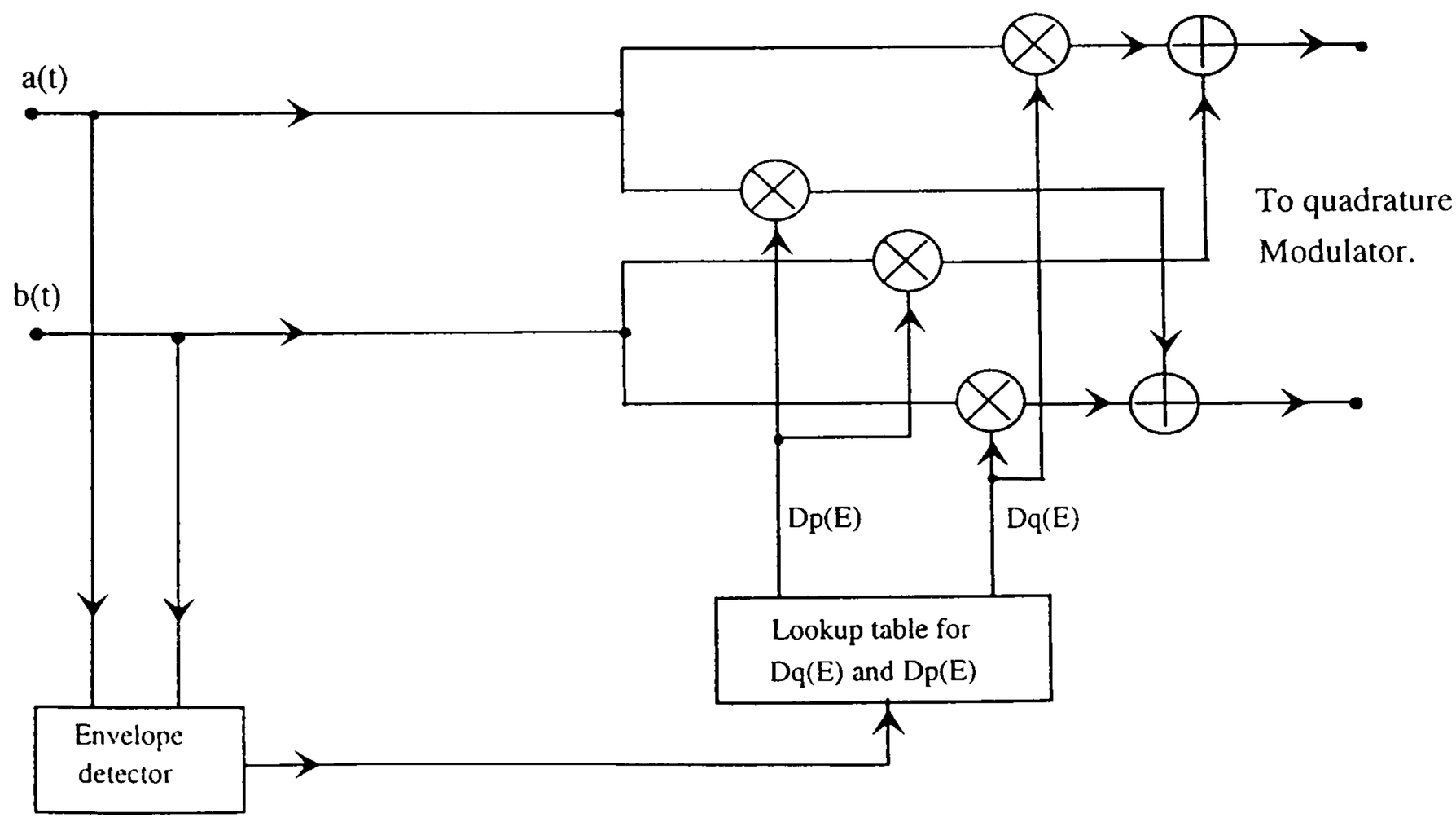

Figure 6.2 A simplified model of the one shown on Fig. 6.1.

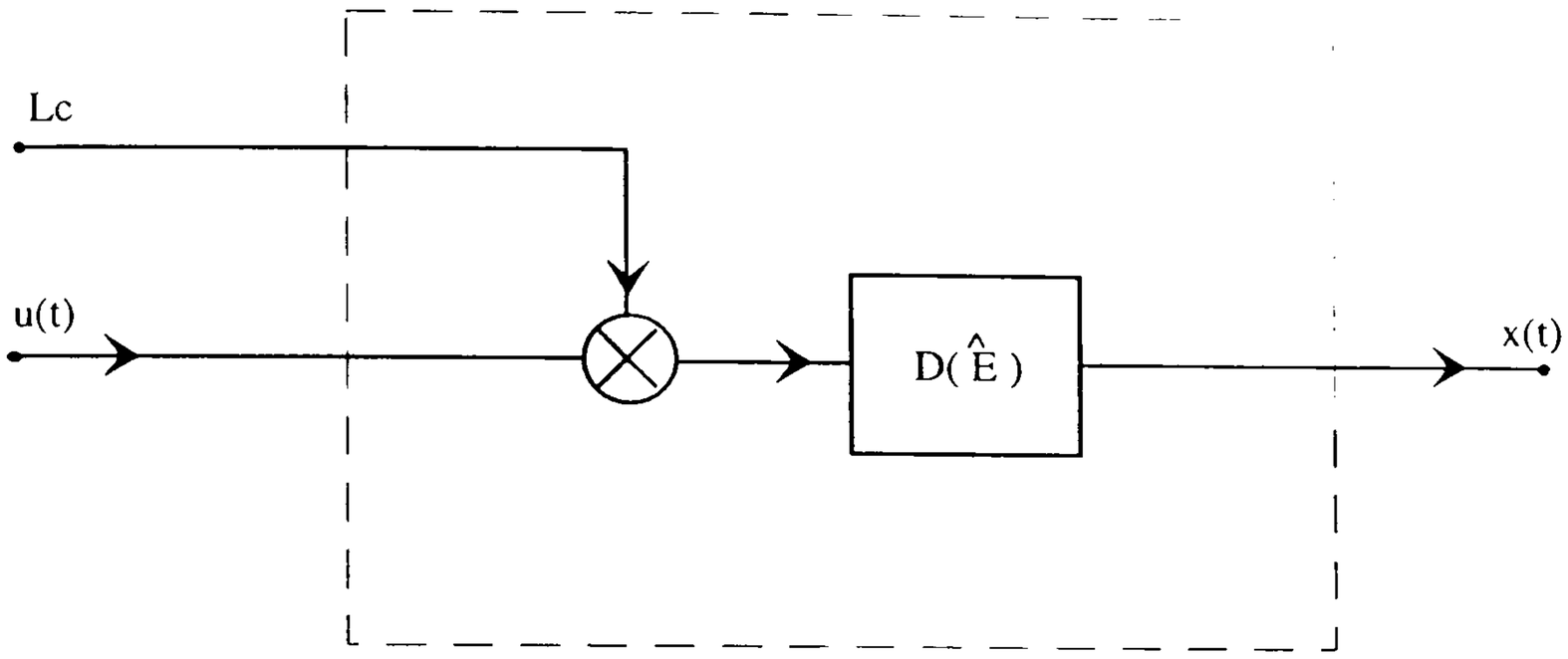

(a)

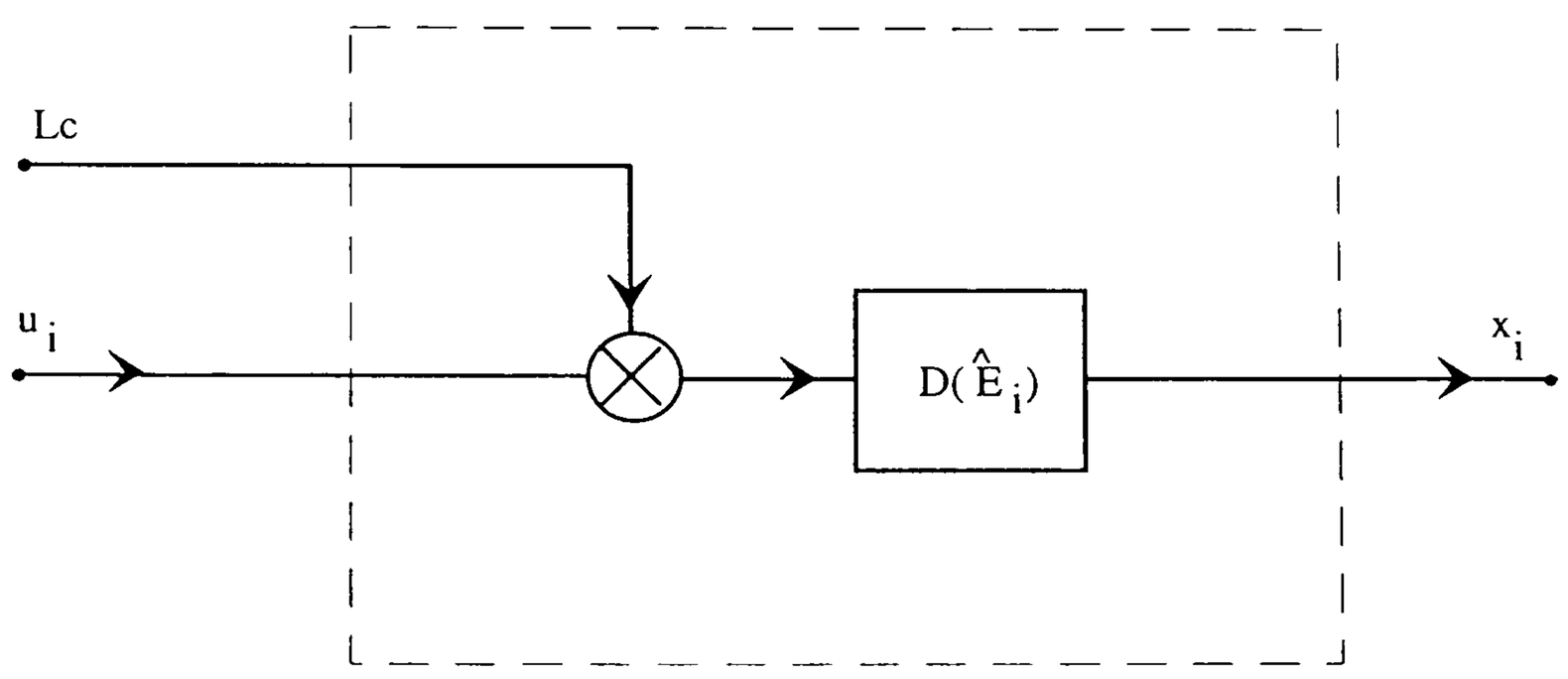

(b)

Figure 6.3 a) Equivalent model of the baseband linearizer. b) Equivalent model of the baseband linearizer for computer simulation.

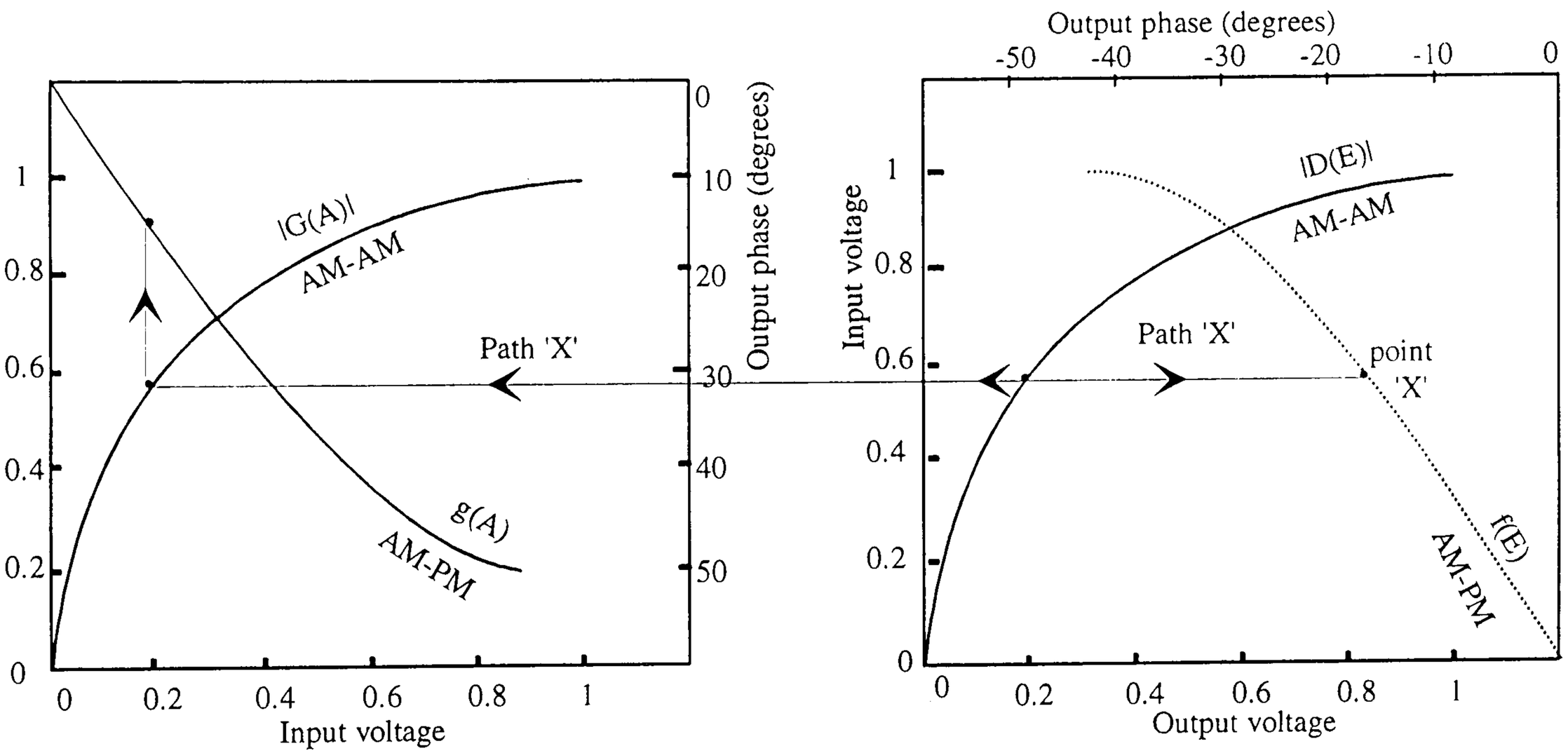

(a) (b)

Figure 6.4 (a) HPA characteristics. (b) Baseband linearizer characteristics.

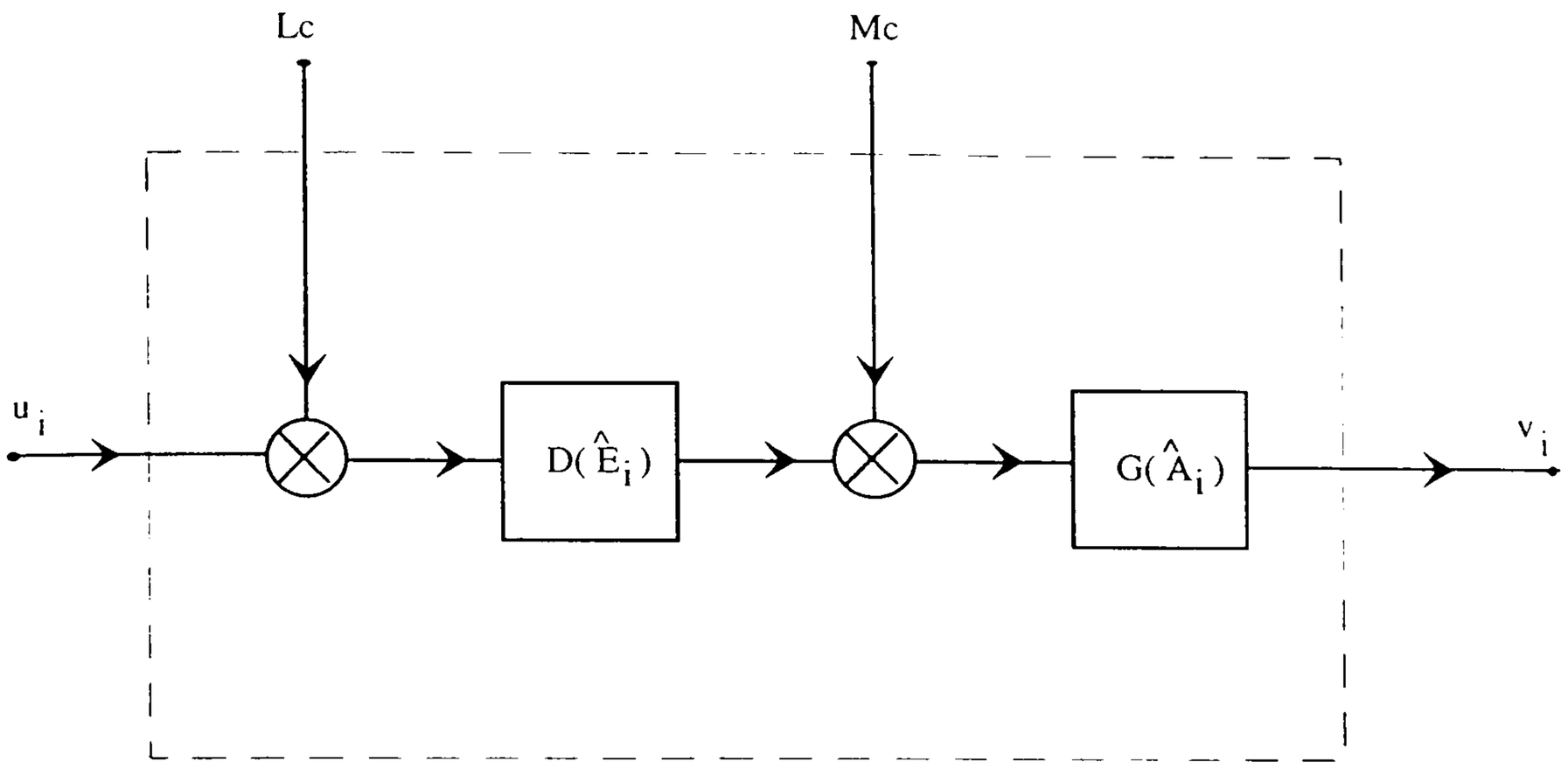

Figure 6.5 Baseband equivalent model of the baseband linearizer in cascade with the HPA.

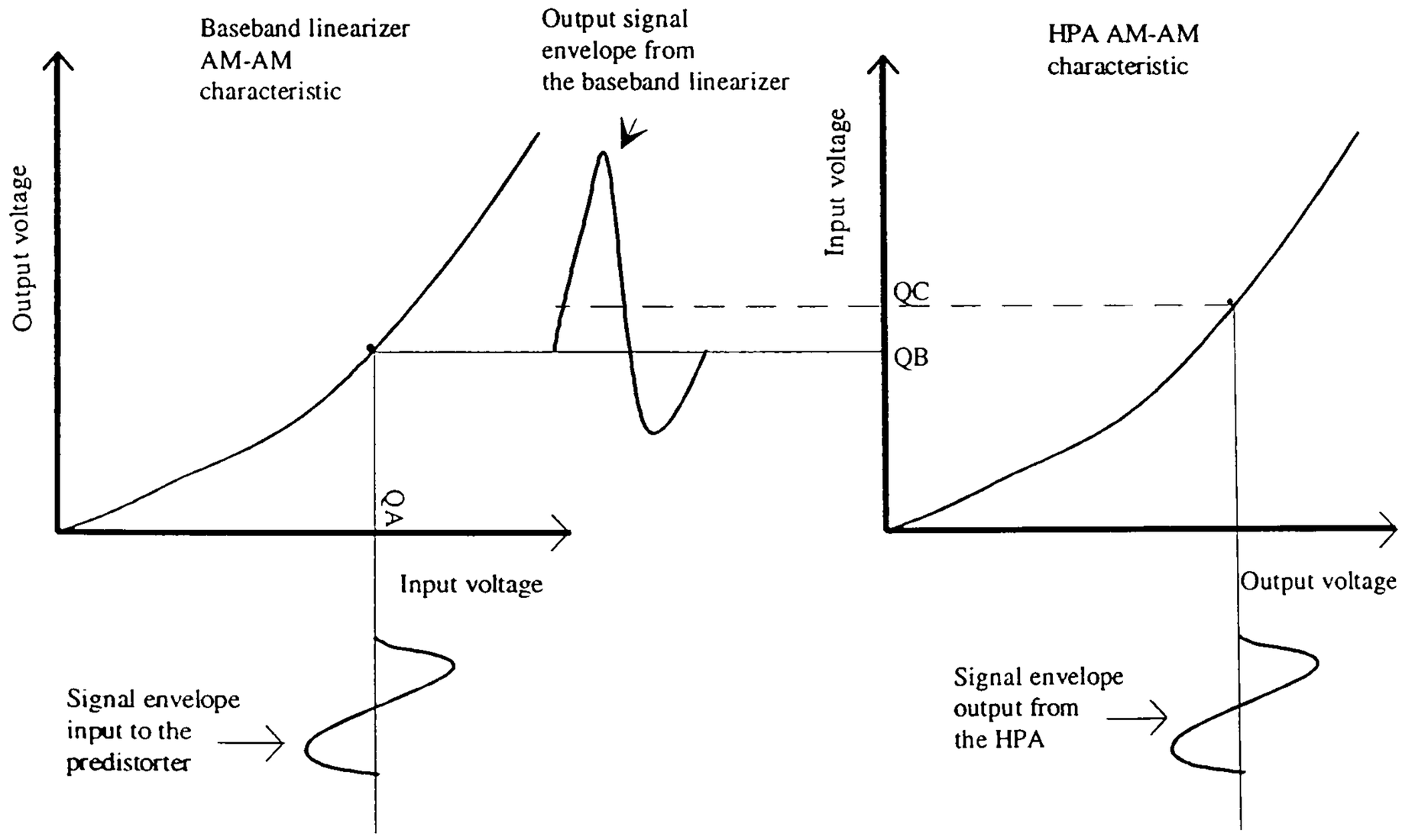

Figure 6.6 How the baseband linearizer removes HPA amplitude distortion.

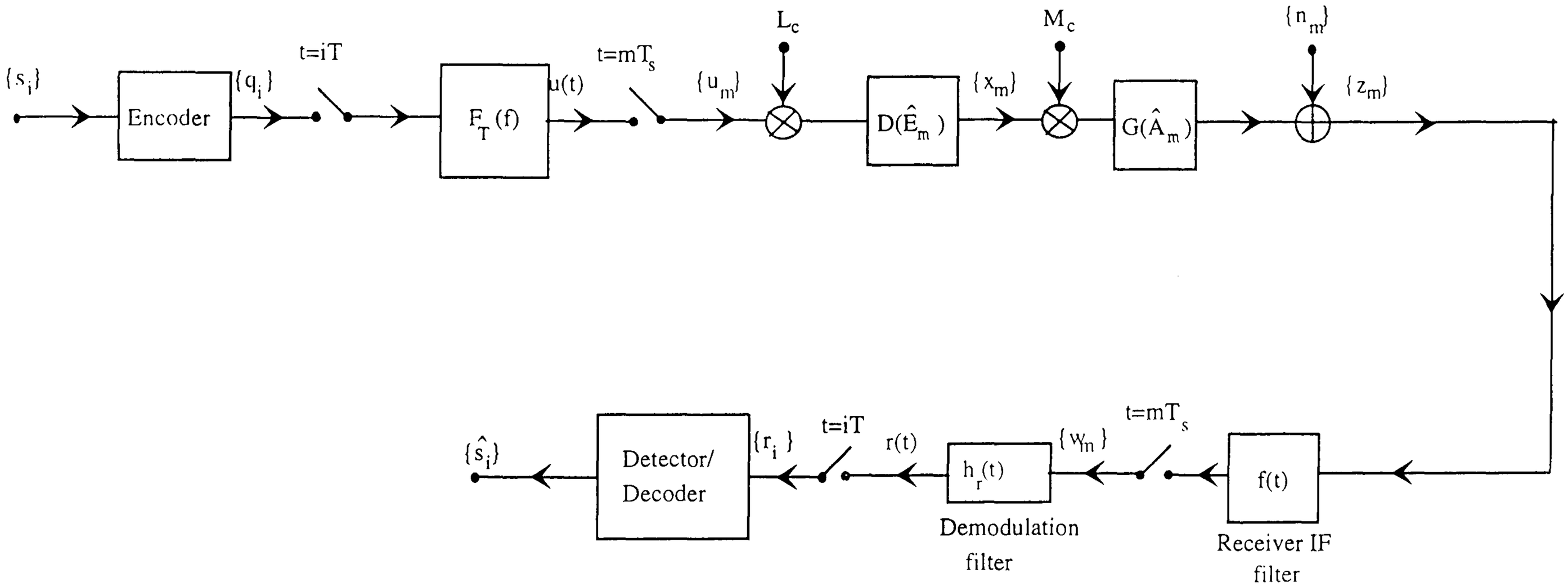

Figure 6.7 Baseband equivalent model of the DEQPSK or CE8PSK (or CDE8PSK) system, with the use of baseband linearizer and with a nonlinear satellite channel, for computer simulation. $F_T(f)$ is the resultant transfer function of the baseband equivalent model of the IF filter in cascade with the modulation filter.

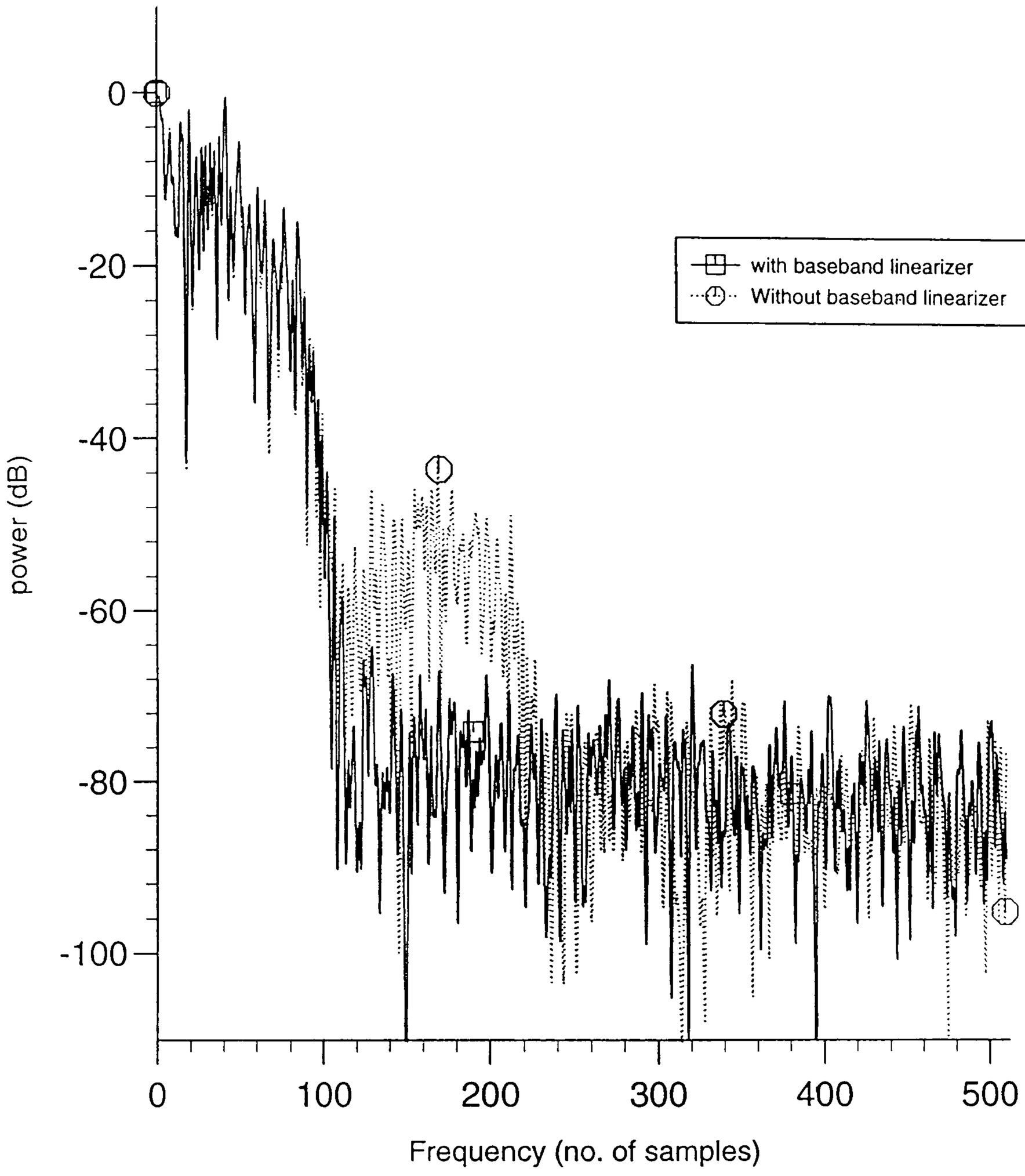

Figure 6.8 Power spectral densities of signal 1A, at the output of the HPA, with and without the use of baseband linearizer, with the HPA and baseband linearizer operating at 0.7 dB OBO and 1 dB IBO, respectively.

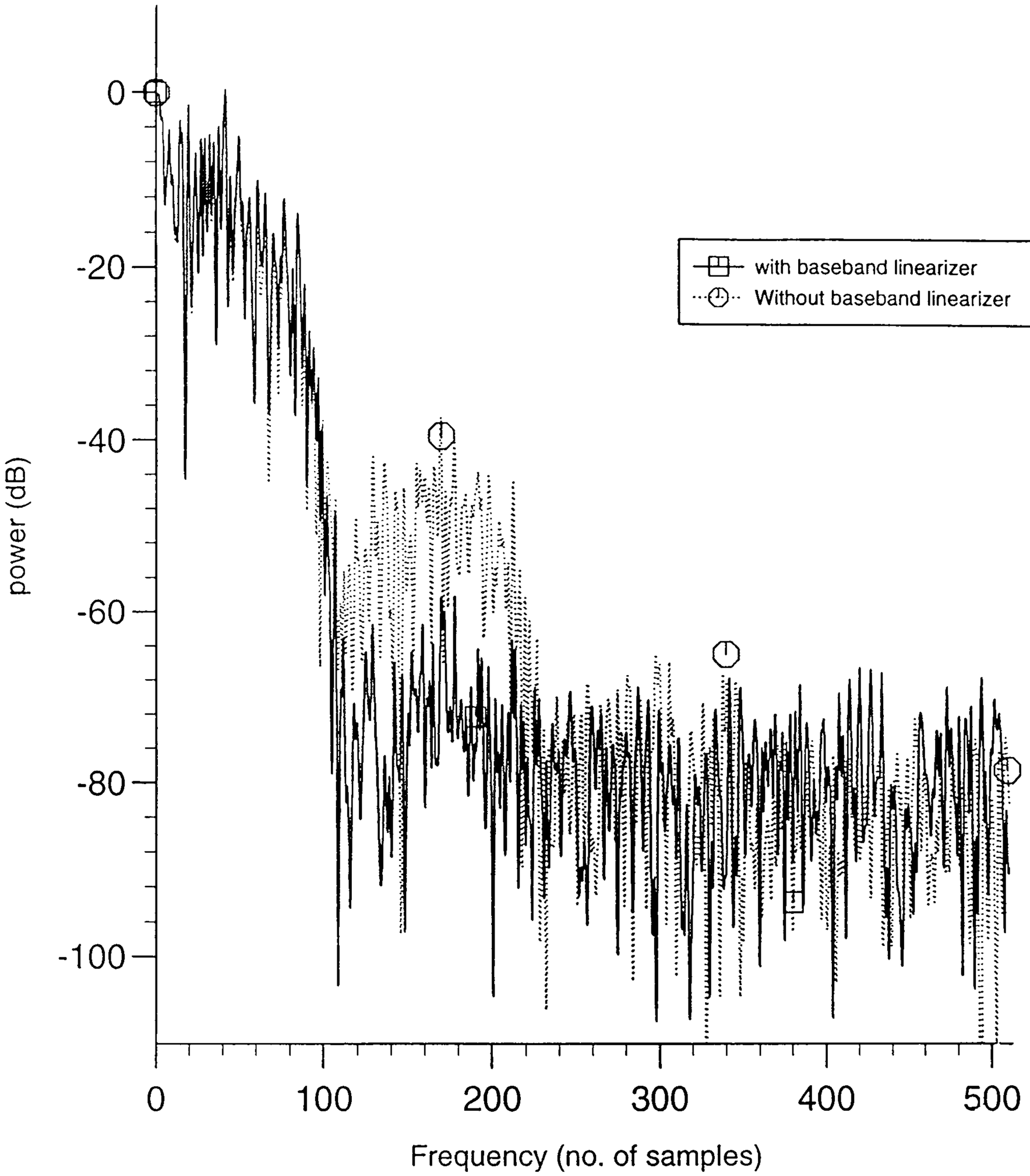

Figure 6.9 Power spectral densities of signal 1A, at the output of the HPA, with and without the use of baseband linearizer, with the HPA and baseband linearizer operating at 0.315 dB OBO and 0.7 dB IBO, respectively.

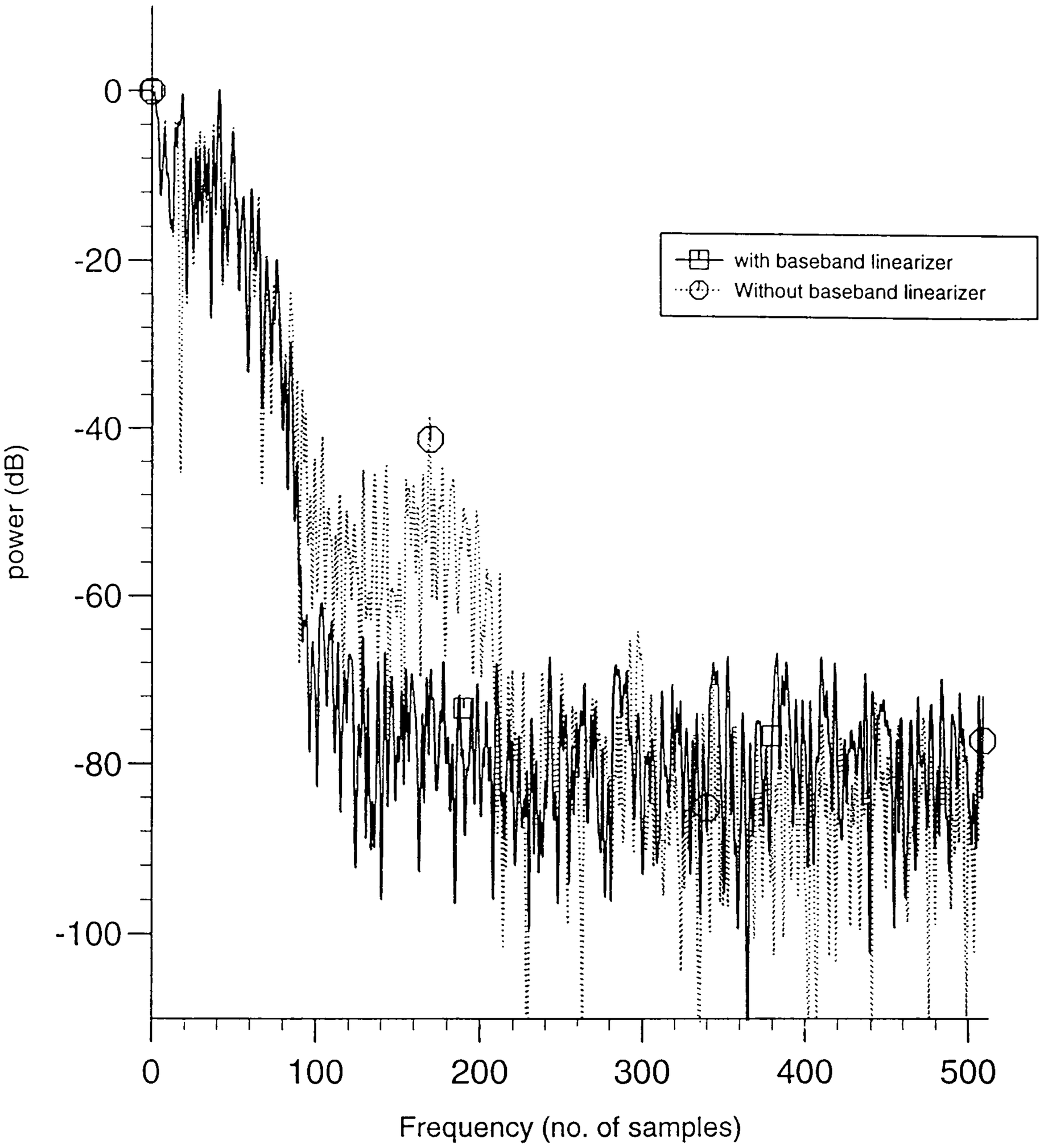

Figure 6.10 Power spectral densities of signal 2A, at the output of the HPA, with and without the use of baseband linearizer, with the HPA and baseband linearizer operating at 0.7 dB OBO and 1 dB IBO, respectively.

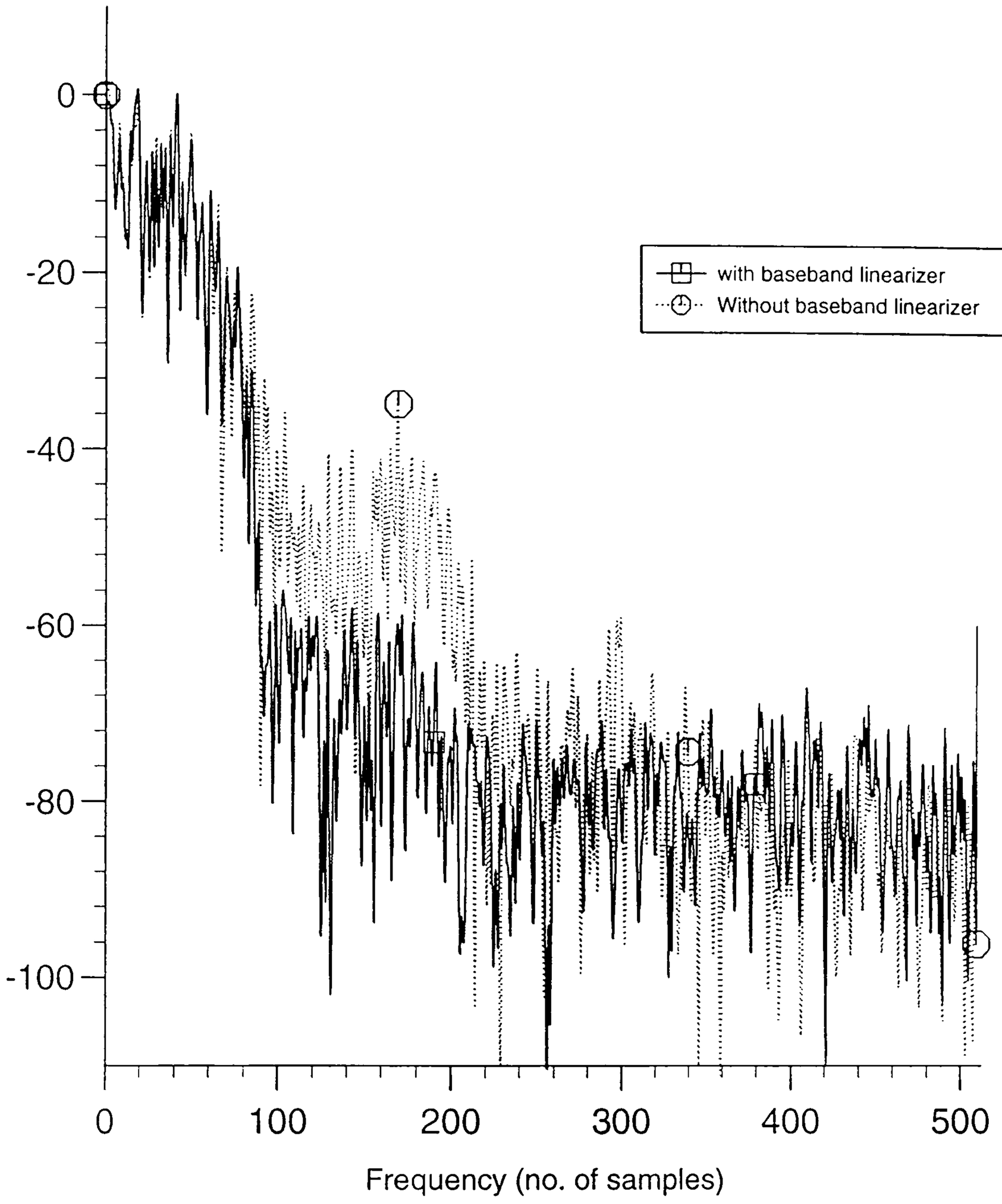

Figure 6.11 Power spectral densities of signal 2A, at the output of the HPA, with and without the use of baseband linearizer, with the HPA and baseband linearizer operating at 0.315 dB OBO and 0.7 dB IBO, respectively.

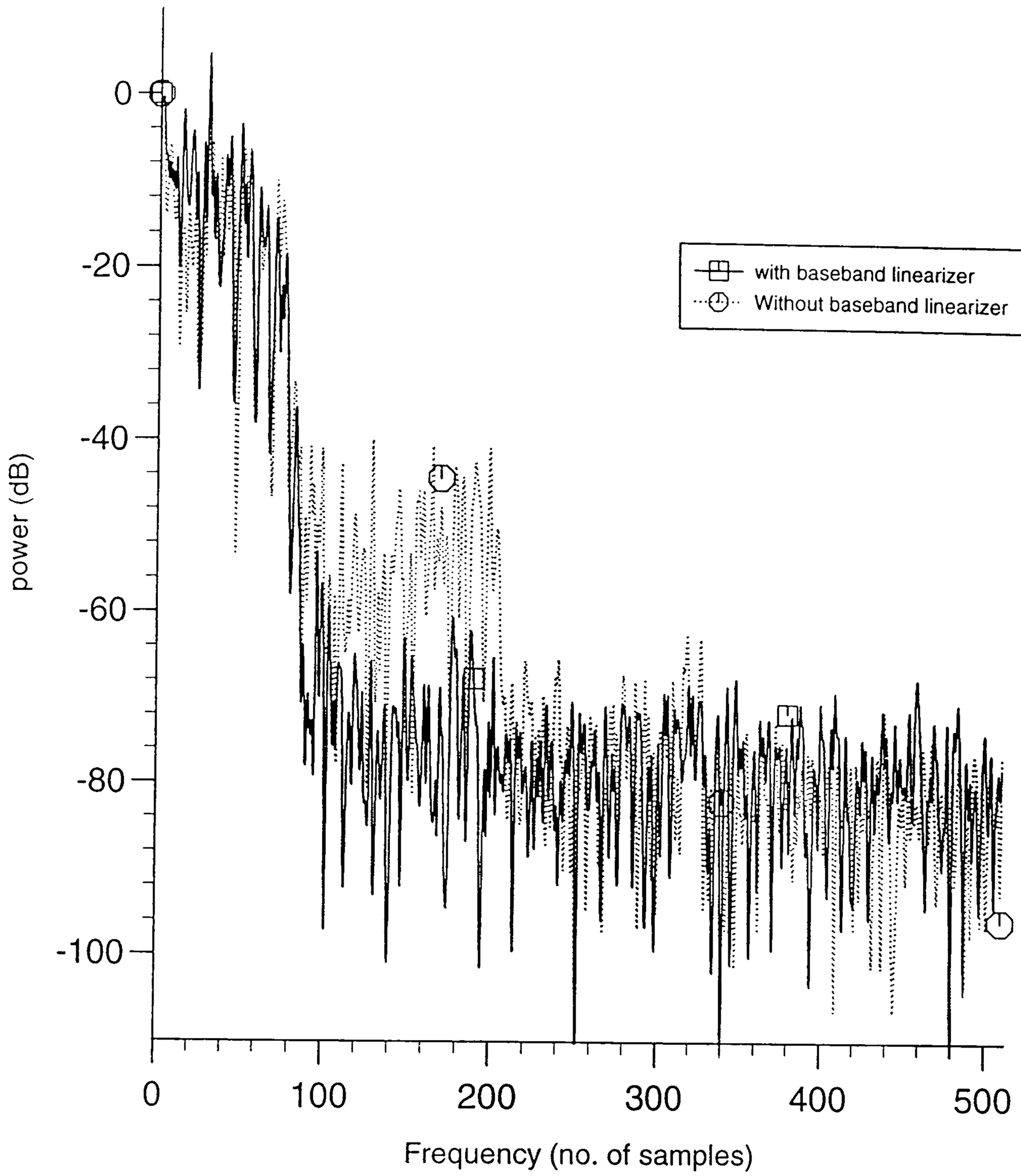

Figure 6.12 Power spectral densities of signal 3A, at the output of the HPA, with and without the use of baseband linearizer, with the HPA and baseband linearizer operating at 0.7 dB OBO and 1 dB IBO, respectively.

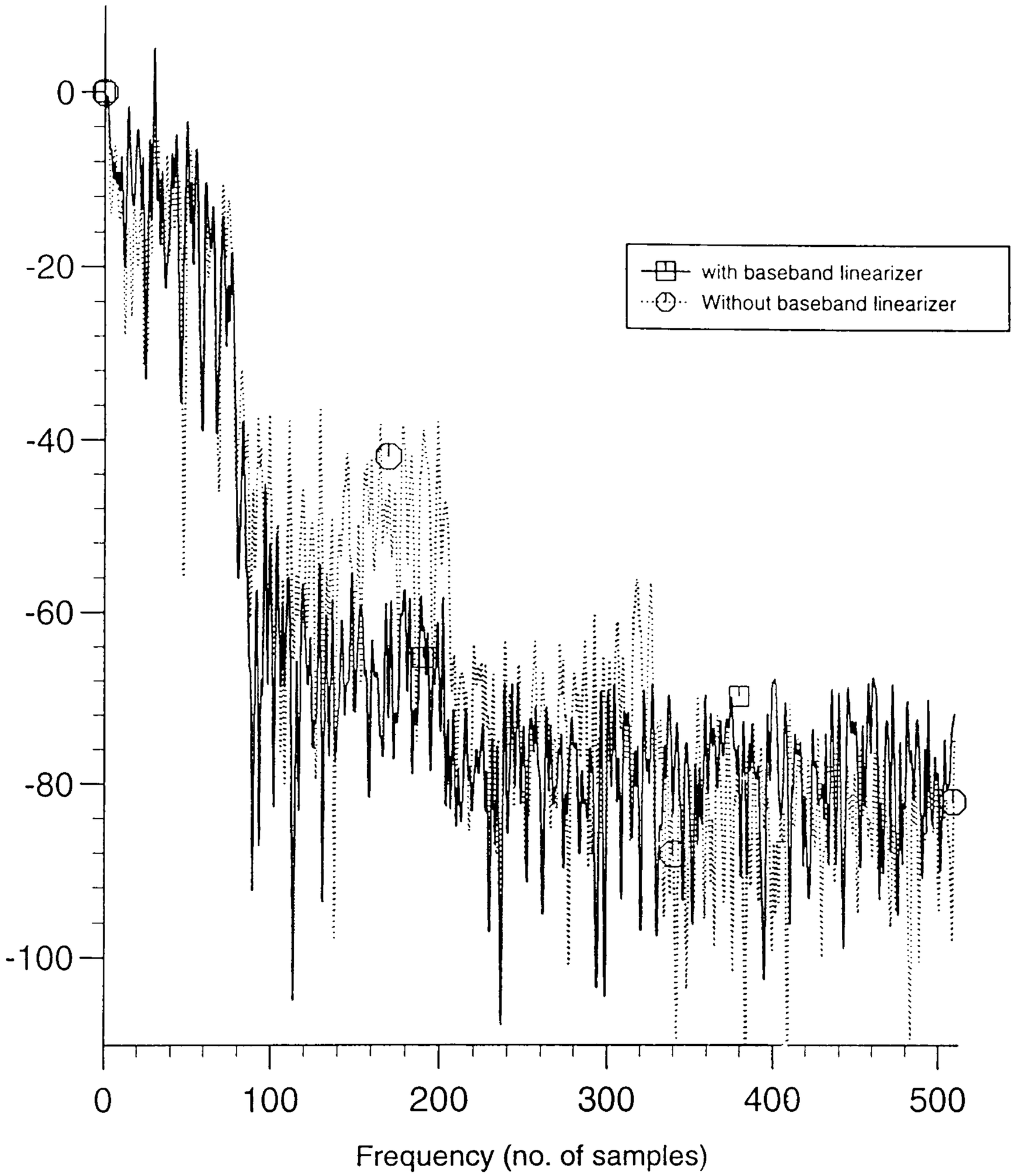

Figure 6.13 Power spectral densities of signal 3A, at the output of the HPA, with and without the use of baseband linearizer, with the HPA and baseband linearizer operating at 0.315 dB OBO and 0.7 dB IBO, respectively.

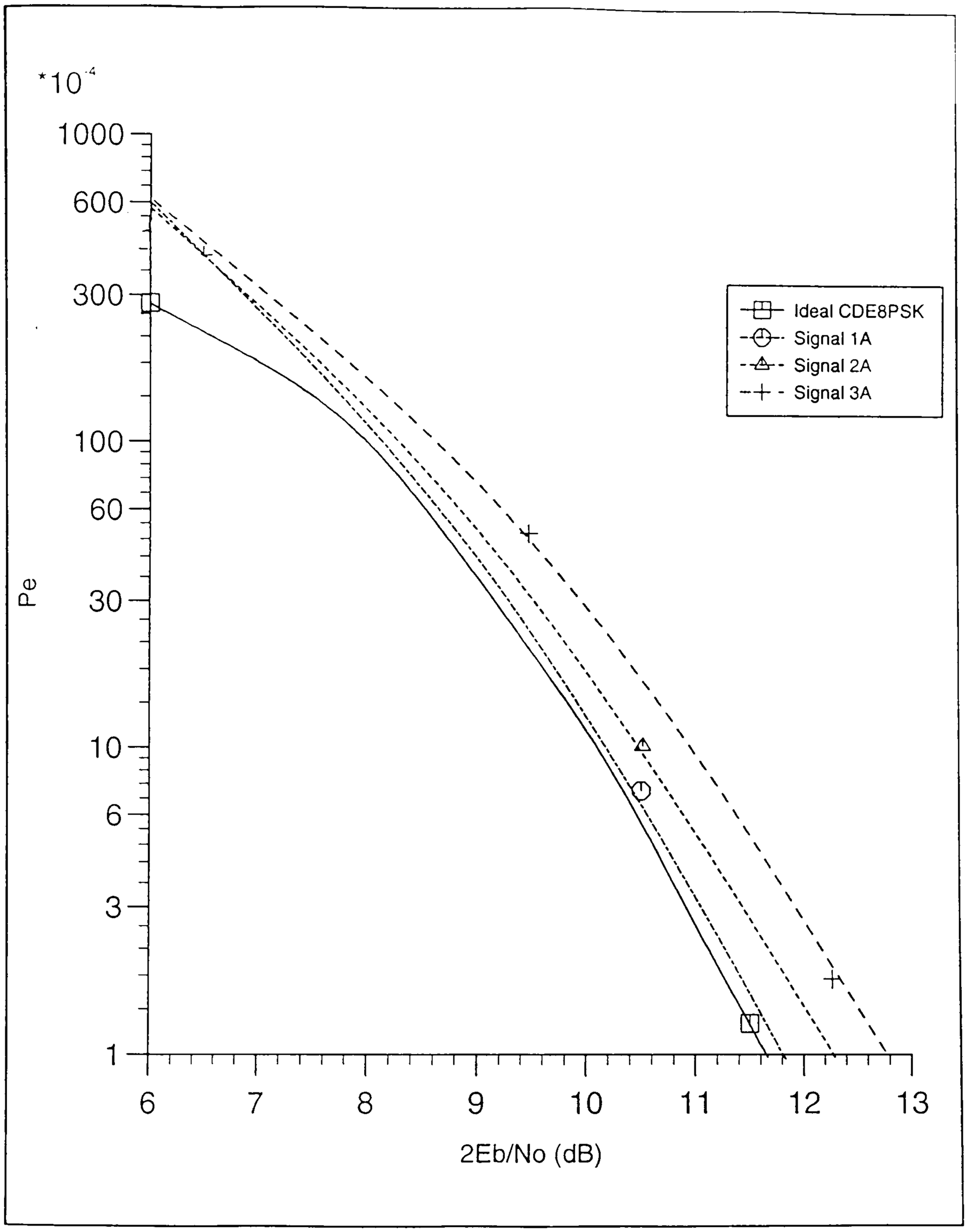

Figure 6.14 Error-rate performances of signals 1A, 2A and 3A, with the use of baseband linearizer, over a nonlinear and bandlimited channel, with the HPA operating at 0.315 dB OBO.

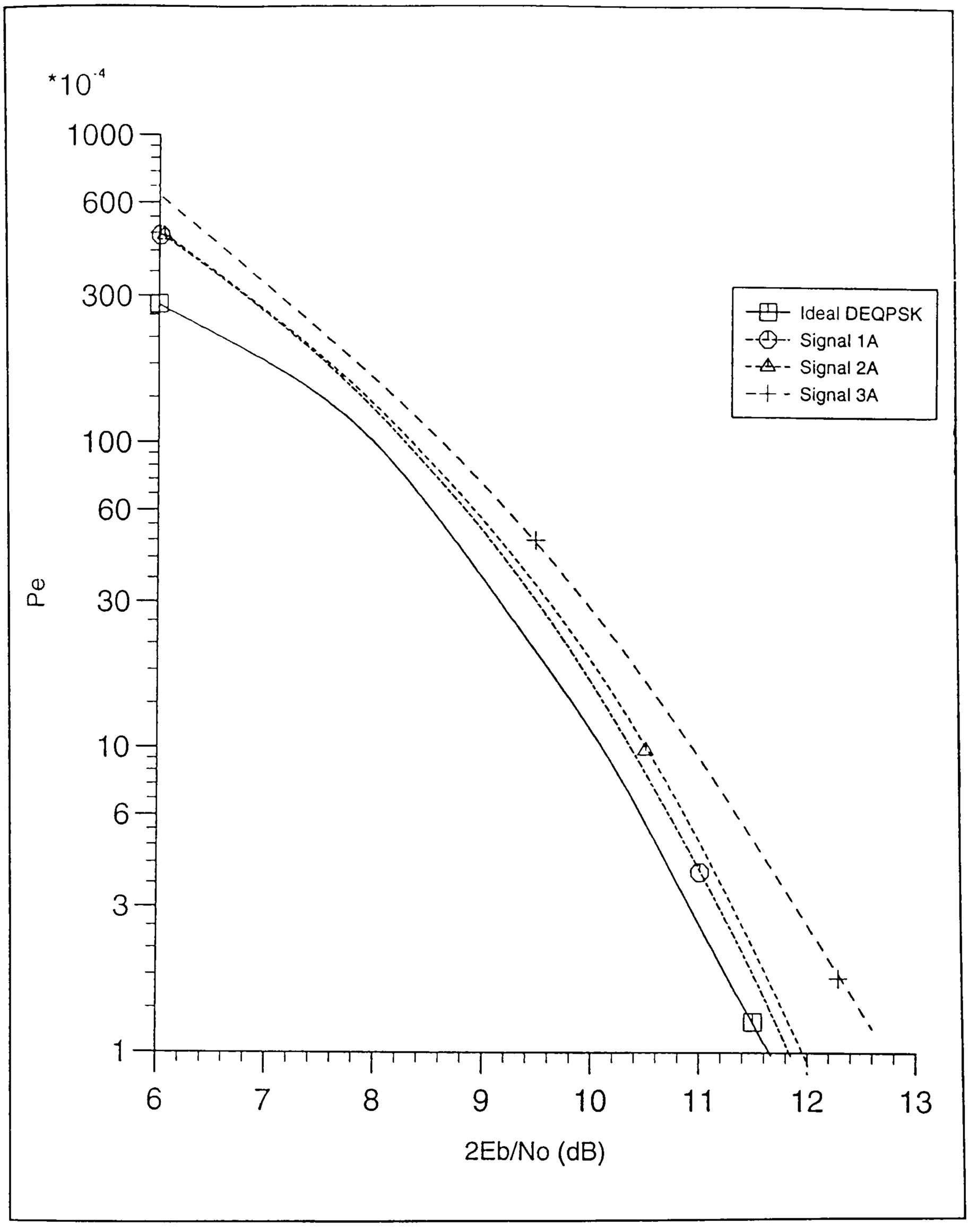

Figure 6.15 Error-rate performances of signals 1A, 2A and 3A, with the use of baseband linearizer, over a nonlinear and bandlimited channel, with the HPA operating at 0.7 dB OBO.

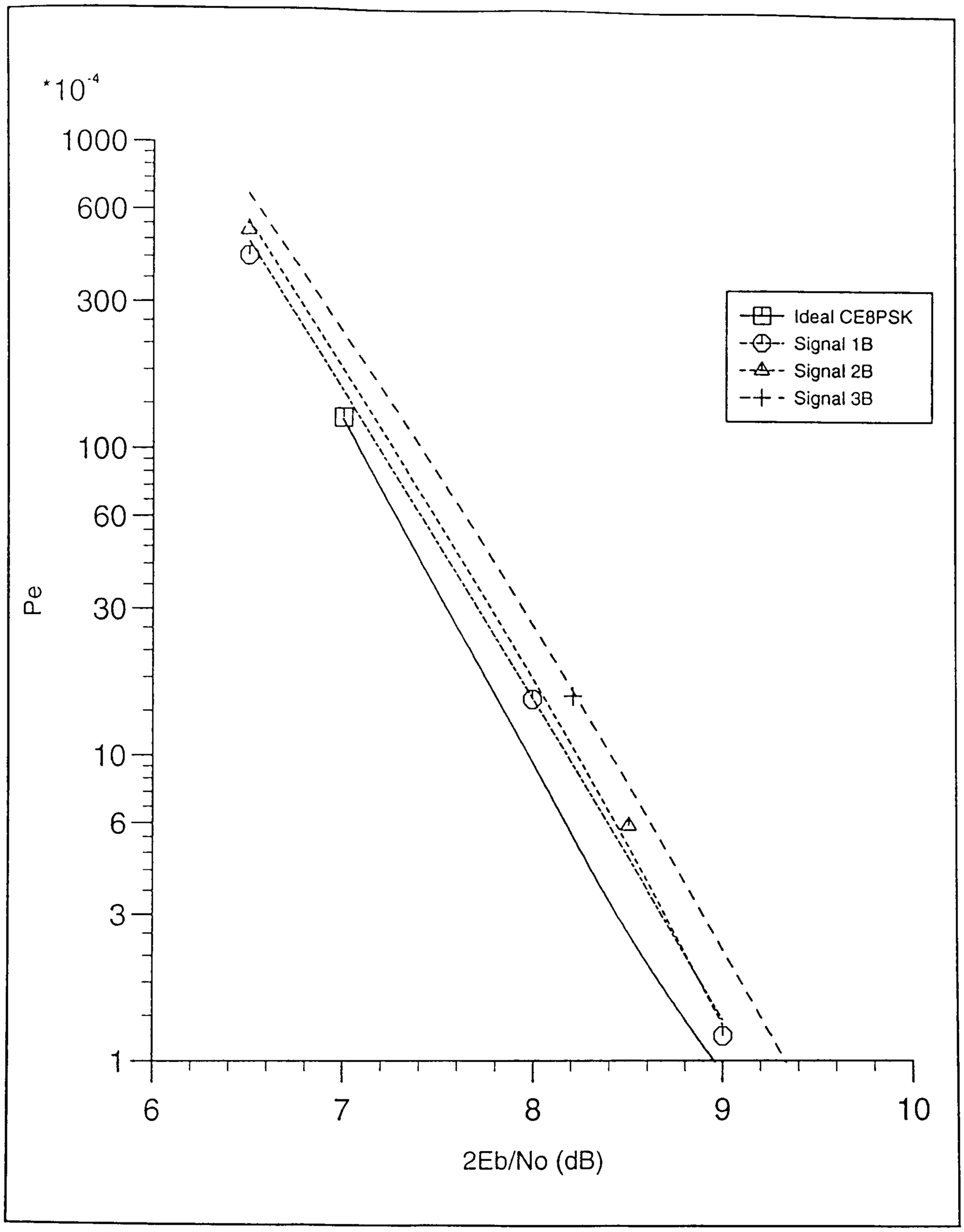

Figure 6.16 Error-rate performances of signals 1B, 2B and 3B, with the use of baseband linearizer, over a nonlinear and bandlimited channel, with the HPA operating at 0.315 dB OBO.

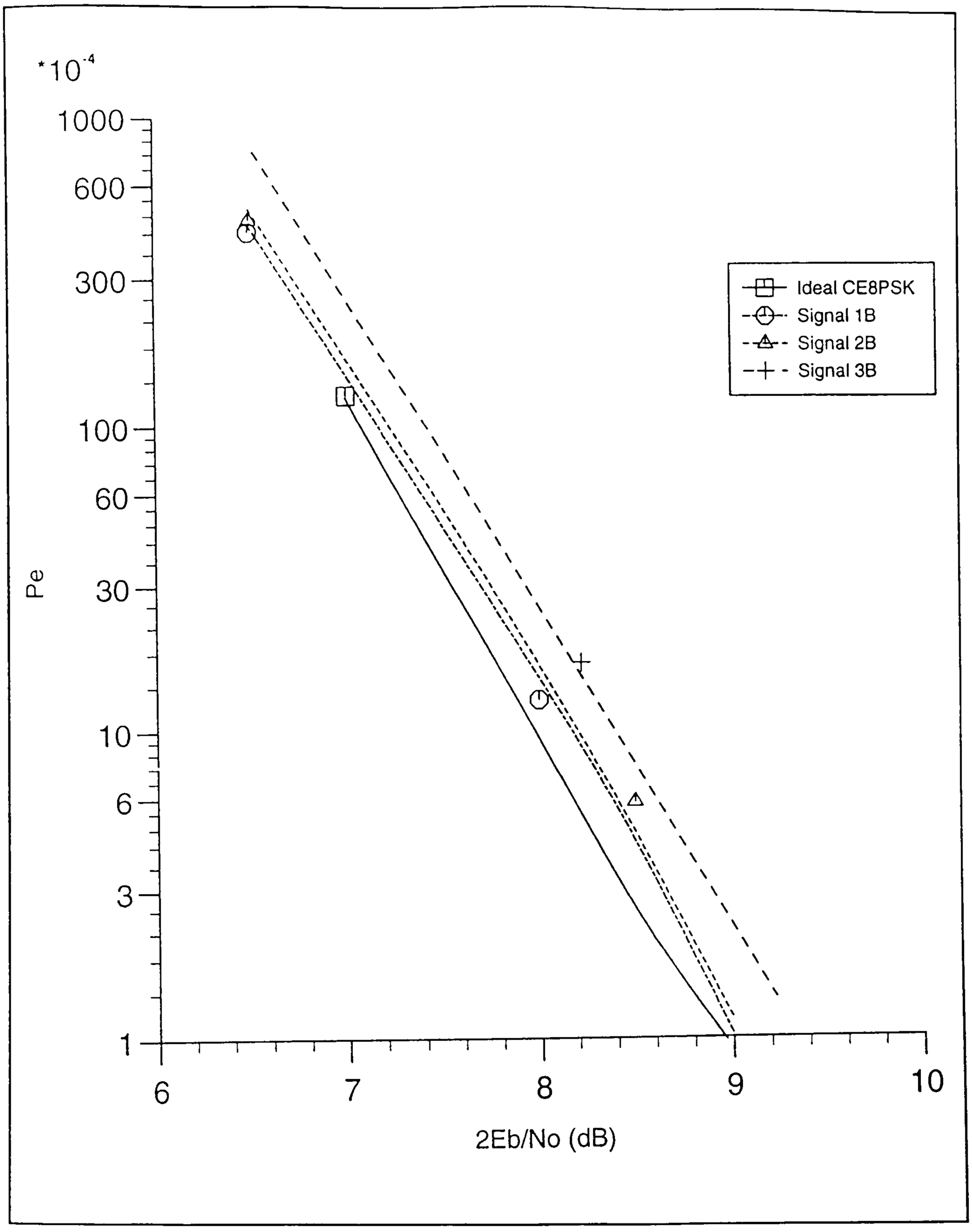

Figure 6.17 Error-rate performances of signals 1B, 2B and 3B, with the use of baseband linearizer, over a nonlinear and bandlimited channel, with the HPA operating at 0.7 dB OBO.

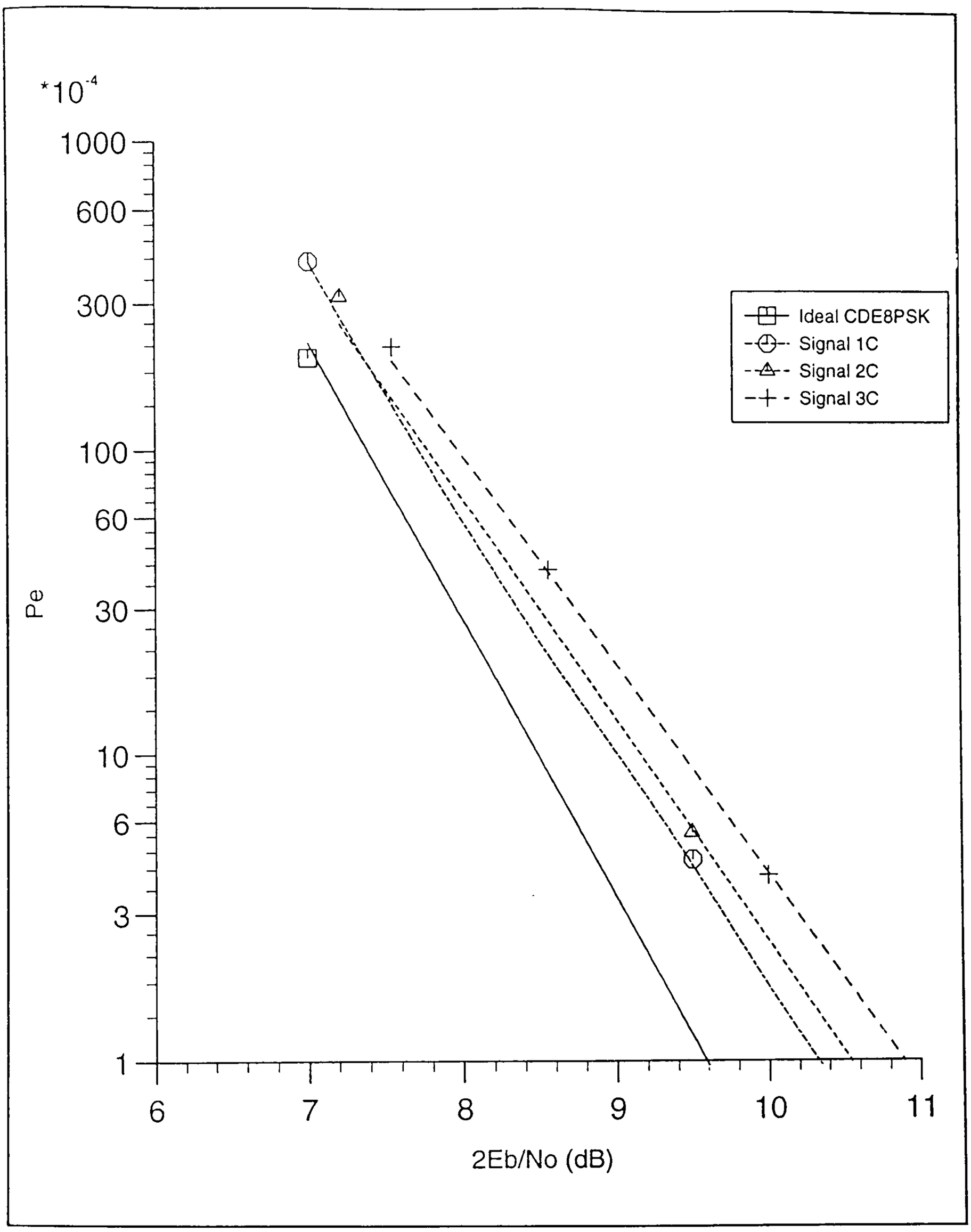

Figure 6.18 Error-rate performances of signals 1C, 2C and 3C, with the use of baseband linearizer, over a nonlinear and bandlimited channel, with the HPA operating at 0.315 dB OBO.

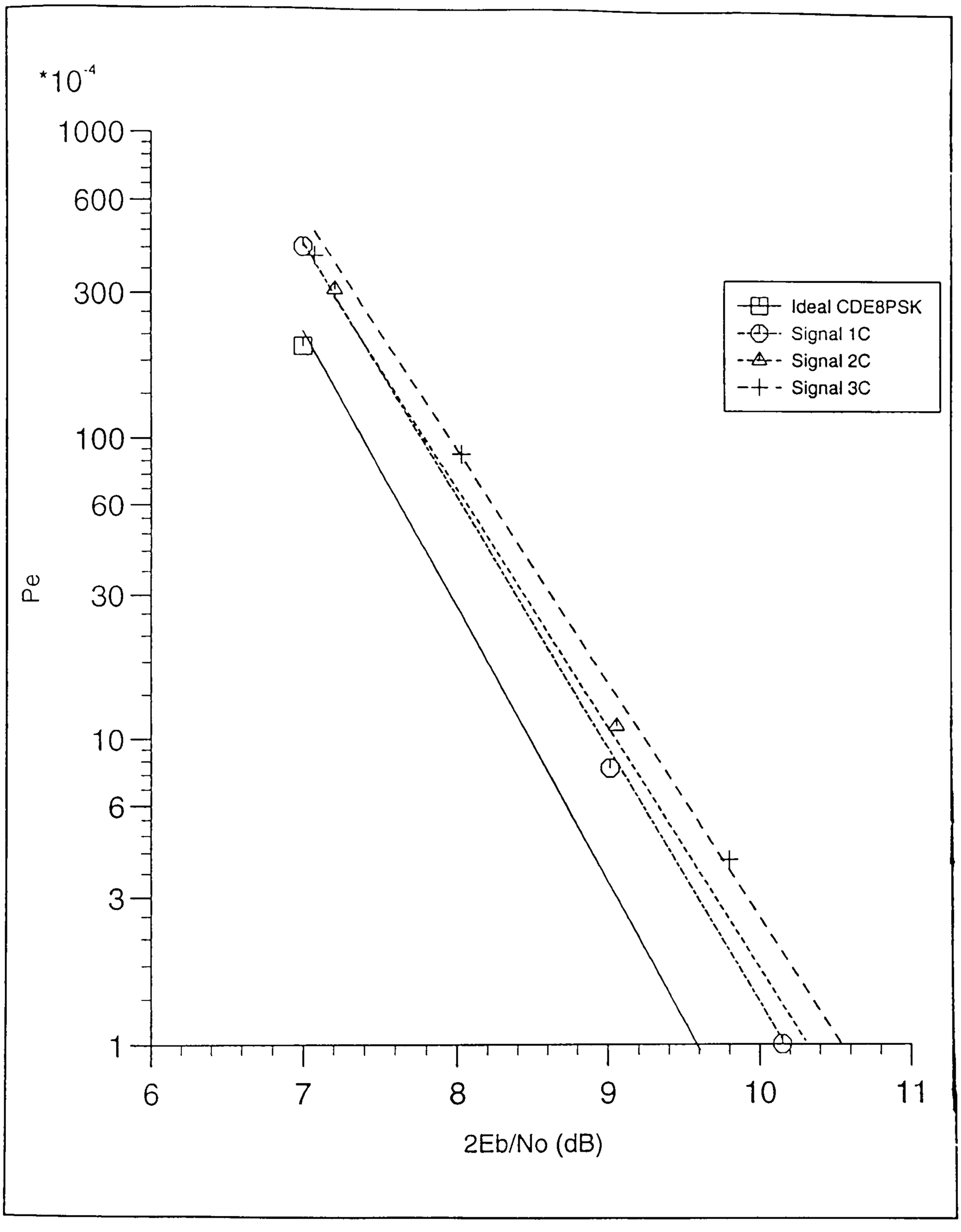

Figure 6.19 Error-rate performances of signals 1C, 2C and 3C, with the use of baseband linearizer, over a nonlinear and bandlimited channel, with the HPA operating at 0.7 dB OBO.

CHAPTER 7

IMPLEMENTATION OF A DEMODULATION AND FILTERING OF THE T-SAT MODEM USING A DIGITAL SIGNAL PROCESSOR (DSP)

7.1 Introduction

This chapter outlines the development of the demodulator and the baseband filter of the T-SAT modem using the new technology of digital signal processing, built using discrete hardware. With the high processing speed achieved in modern digital signal processors, it is now possible to implement the digital demodulation and digital filter of a modulated PSK signals using software algorithms in real time, rather than using conventional discrete hardware. This technique is cost and size effective, also allows an easy way for any modifications, as it is done in software.

The digital signal processor (DSP) devices have a highly specialized instruction set, which forms the basis of the operational flexibility and speed of these devices. Texas Instruments DSP device TMS320C50 has been chosen for this development of the T-SAT modem. This device is designed to execute more than 28 MIPS (million instructions per second) [72].

With the use of an advanced DSP device, large parts of the design can be implemented using a single chip. The processing system to be described in this thesis forms part of a TDMA modem for an experimental satellite project known as T-SAT.

The following sections describe the T-SAT modulation and demodulation parts in general, and the other sections outline the development of the demodulation and digital filters in the T-SAT modem using a DSP.

7.2 The T-SAT modem

The TDMA modem [74], [75] was built for the T-SAT satellite project, the specifications of which are as follows:

- Bit rate 256, 128, 64 Kbit/sec.
- Baseband carrier 256 KHz.
- Modulation methods Phase Shift Keying (BPSK, QPSK and DQPSK).

In the following sections a general description of the T-SAT is given, to assess the development of the demodulation and filtering section.

7.2.1 Modulation and filtering

The modulator part of the modem is standard [73], [74]. Fig. 7.1a shows the modulation, filtering and up converter parts of the modem. The incoming data stream is split into two channels by taking alternate bits. The two channels are each baseband filtered using a root-raised-cosine characteristic with 40% roll-off factor, this is achieved using an EPROM as a look-up table [73], [74].

One channel is mixed with the carrier signal which becomes the In-phase or I-channel while the other is mixed with the same carrier shifted $\pi/2$ in phase, producing the Quadrature or Q-channel. The two are then added to form a QPSK signal. A sampled-carrier approach has been used so that at a sampling clock of 1024 KHz the 256 KHz In-phase carrier reduces to a 0 +1 0 -1 sequence, and the quadrature carrier reduces to +1 0 -1 0, as shown in Fig. 7.2. The 4 samples/carrier cycle means that each carrier reduces to:

$$\begin{aligned} \cos\omega t &\Rightarrow +1 \quad 0 \quad -1 \quad 0 \\ \sin\omega t &\Rightarrow \quad 0 \quad +1 \quad 0 \quad -1 \end{aligned} \qquad 7.2.1$$

When mixed with each data channel alternate output samples are zero. When the two channels are added the resulting modulated carrier signal is composed of alternating samples of I and Q multiplied by +1 or -1. Hence modulation consists of multiplying the added I and Q filtered signals by ±1, so separation back into individual channels is easy at the demodulator.

An 8-bit DAC (digital to analogue converter) converts the digital samples to an analogue waveform. After the digital to analogue conversion the signal fed to low pass filter to compensate for sinx/x distortion, and then upconverted to the IF frequency. Unwanted frequency components are then removed by a SAW (surface acoustic wave) filter having the centre frequency of the IF signal.

7.2.2 The demodulator

The receiver circuitry is a lot more complicated, because of the need for synchronization with the incoming signal. The conversion of the IF signal down to a 256 KHz modulated signal is performed by a circuit almost the same as the one in the modulator for up conversion, the circuit here consists of down conversion and low pass filtering to remove high frequency components resulting from the conversion. At the output of the low pass filter a baseband modulated signal with a carrier frequency of 256 KHz is obtained, Fig. 7.1b shows a block diagram of the demodulator part of the modem.

The demodulation process is the same as the modulation process. The incoming data is split into I and Q channels. Each is then digitally filtered and demodulated by multiplying by $\cos \omega t$ and $\sin \omega t$ respectively.

Unfortunately, a look-up table cannot be used to perform demodulation. The input signals to the modulator digital filter only has two levels. Each sample from the demodulator ADC (analogue to digital converter) has 256 possible levels, so the necessary EPROM capacity would be huge. This means that the I and Q data outputs must be individually calculated in real-time.

The output from the down converter filter with its 256 KHz carrier is sampled at 1024 Ksamples/sec by an 8-bit flash ADC, with the results clocked into an 8 byte deep First-In-First-Out (FIFO) buffer at the same rate. The FIFO buffers up 8 samples during the 8 μsec symbol period (1/128 KHz) while the rest of the system processes the last 8 and produces a single output symbol.

Data is clocked out of the FIFO and into a high-speed RAM known as the circular buffer. This transfer takes place as a rapid burst of 8 samples every symbol period (8 μsec). Data is clocked out and processed to produce the symbol using a digital sequencer running at a very high speed.

The following operations must be performed for each symbol period (8 μsec)

-Extract the data from the circular buffer and demodulate it back into I and Q channels.

-Perform 40 multiply/accumulate operations per channel, using supplied Tap-gains (digital filter).

-Produce carrier phase correction angle θ and, perform the following to produce the final values of I' and Q'

$$I' = I\cos\theta - Q\sin\theta$$
$$Q' = Q\cos\theta + I\sin\theta \qquad 7.2.2$$

-Transfer 8 samples from FIFO to circular buffer.

All the above operations are a combination process of the circular buffer, the MAC (multiply/accumulate) circuit and the sequencer [74].

The synchronization technique used in the T-SAT modem is one in which the demodulated output data samples are 'corrected' for errors caused by carrier phase timing and bit timing. This method is known as 'feed forward' [56], [74], [75], [77], as opposed to the normal 'feed back' approach. So, a fixed frequency type quartz oscillator is used, and a high speed digital signal processors (DSPs) used to calculate the resulting phase and bit timing errors. The output data is then corrected for these errors (Eqn. 7.2.2). Two DSP chips were used to process the two tasks. A TMS320C25 was chosen in the original T-SAT design for the synchronization tasks [75].

7.3 Development of the demodulation and digital filtering in the T-SAT using digital signal processor(DSP)

With the advanced technology of digital signal processors (DSPs), large parts of the design relating to the demodulation section, consists of removing the carrier signal from the data, the digital filter with 40 Taps and the operation of the sequencer in the T-SAT modem can be implemented using a single DSP chip, rather than using many conventional digital chips. The processing system to be described in this thesis uses the Texas Instruments processor TMS320C50 DSP.

The demodulation digital section programmed in the DSP must perform the following operations in less than 8 μsec the symbol period

- Demodulation (extraction of data from 256 KHz carrier).
- 40-Tap digital filtering on each In-phase and Quadrature (I and Q) baseband channel.
- Carrier phase correction using the correction angle θ supplied by the carrier-phase processor, producing the final values of I' and Q' using equations 7.2.2.
- Detection of I and Q data.

With a DSP TMS320C50 running at 57 MHz (28 MIPS), an algorithm was written to carry out the above jobs, replacing all the discrete hardware of the sequencer, circular buffer, and MAC circuits. This was considered to be too heavy a load for the DSP chip in such a limited time. Hence, the algorithm was written to do these jobs, but the processing time needed was calculated to be 14 μsec, therefore it was not possible to carry out the jobs in less than 8 μsec (symbol period).

The proposal of replacing all of the discrete hardware now involved modifying the modem specifications as follows:

- Bit rate 128, 64, 32 Kbit/sec.
- Baseband carrier 128 KHz.
- Modulation methods Phase Shift Keying (BPSK, QPSK and DQPSK).

In this case the symbol period becomes 16 μsec, and the DSP algorithm would fit within the symbol period, and large parts of discrete hardware could be replaced using a single DSP chip.

Demodulation of a modulated PSK signal involves carrier removal from the signal. The sampling rate 512 KHz on the ADC was chosen to be exactly 4 times the carrier frequency 128 KHz. That means alternate input samples contain I or Q channel information only (Fig. 7.2).

Once separate, alternate samples in each channel are negated to remove the carrier. Hence, the digital filter procedures involve 20 operations of multiplication by zero, reducing the total number of digital filter operations to 20 for each of the I and Q channels per symbol period instead of 40.

The 40-Tap square-root-raised cosine shaping filter has been implemented with impulse response $p(t)$ and frequency response of the raised cosine shaping filter is given by [51]

$$H(f)=\begin{cases} T & 0\le|f|\le\frac{1}{2T}(1-\alpha) \\ \frac{T}{2}\left[1-\sin\frac{\pi T}{\alpha}\left(|f|-\frac{1}{2T}\right)\right] & \frac{1}{2T}(1-\alpha)\le|f|\le\frac{1}{2T}(1+\alpha) \\ 0 & \text{elsewhere} \end{cases} \qquad 7.3.2$$

The parameter T is the nominal duration of a signal element, being the time interval between adjacent impulses, and α is the roll-off factor of the frequency response, the filter is shared between the transmitter and receiver with α = 40% the roll-off factor. Filter coefficient calculations were obtained using Fast-Fourier Transform (FFT) techniques. Table 7.1 shows the 40% square-root-raised cosine filter coefficients in decimal and the Hex decimal scaled value needed for the TMS320C50 algorithm, and Fig. 7.3 shows the impulse response of the filter. Figure 7.4 shows the 40-Tap

gains of the digital filter of 40% square-root-raised cosine shape, which is implemented in the DSP algorithm.

7.3.1 Hardware and interface circuit

The TMS320C50 was chosen for the development of the T-SAT modem, because of its 57 MHz clock rate (28 MIPS), 35 nsec single-cycle instruction execution time. In addition, the CMOS technology together with the software-operated low power IDLE mode makes the device suitable for limited-power environments. It has a large set of instructions, including MAC, MACD for digital filtering applications, and an on-board parallel multiplier providing a 16*16 bit with 32-bit product capability. Many algorithms such as convolution, correlation, and FIR filters can make use of circular buffers in memory. In these algorithms, a circular buffer is used to implement a sliding window, which contains the most recent data to be processed and other powerful features [72]. All of these make the device suitable for this development.

The incoming signal with its 128 KHz carrier is sampled at 512 KHz (4 times the carrier frequency) by an 8-bit flash ADC (Fig. 7.5), with the result clocked at the same rate into an 8 byte deep First-In-First-Out (FIFO) buffer. Figure 7.5 shows the interface circuit with the TMS320C50 development board and Table 7.2 gives the truth table of the control signals of the interface circuit. The FIFO buffers up 8 samples during the 16 μsec symbol period while the rest of the system processes the last 8 samples and produces a single output symbol. Data is clocked out of the FIFO into a software circular buffer in the TMS320C50. Every symbol period (16 μsec) 8 samples are transferred as a rapid burst to be processed to produce the symbol.

After processing the samples, which involves carrier removal and digital filtering with a root-raised-cosine shape in the TMS320C50's software, one I data sample and one Q data sample is produced and output to DACs, and subsequent display as a 'constellation ' on a scope.

The processor is interrupted every symbol period (16 μsec). This has been derived from the sampling clock (512 KHz Timer output), via a counter. Figure 7.6 shows the timing diagram of the symbol interrupt and other control signals of the FIFO and output DACs, controlled by software.

7.3.2 Digital signal processor software algorithm

Each channel at the modulator is processed by a 40-Tap digital filter. The demodulator does the same, normally requiring a total of 80 multiply-accumulate operations per symbol period. The sampled carrier system used (4 samples/carrier cycle), resulting in alternate samples of each channel being zero, this means that the

multiply-accumulate operations per symbol period required for the digital filter is reduced to 40. In addition the carrier is removed by negating alternate values of each channel (I and Q).

The RAM (circular buffer) in the T-SAT modem demodulater part has been replaced by a software circular buffer in the TMS320C50, which makes the operation easy. Since the circular buffer in the TMS320C50 can be organized in the data memory, start and end addresses should first be loaded into the corresponding buffer registers; next an auxiliary register can be specified to point at the data memory address between the start and end registers for the circular buffer, so when the read pointer reaches the end of circular buffer address it jumps automatically back to the start address. The write and read pointers are organized to be 128 samples apart. This is essential for the bit timing procedure used by the synchronization processor in the T-SAT modem.

Flowchart of the algorithm (software program) is shown in Fig. 7.9. The algorithm starts by initialization of the processor as follows:

- Timer set-up to give 512 KHz sampling frequency.
- Enable INT3 for symbol interrupt (16 μsec).
- Circular buffer set-up, for 256 locations in data memory. Set-up start and end addresses, and assign auxiliary register as pointer for the circular buffer.
- Filter coefficients at block B0.

After initialization has been done the processor waits in the IDLE state until symbol interrupt occurs, and the following algorithm is executed:

1-Input 8 samples from FIFO into circular buffer.
2-Take 20 samples from alternate locations in circular buffer, and negate alternate values (this is carrier removal for I samples).
3-Perform 20-Tap root-raised-cosine digital filter, by taking 20-Tap gains from coefficient memory and multiply/accumulate with the 20 demodulated data samples from circular buffer, and store the result. This is the demodulated filtered I symbol sample.
4-Take 20 interleaving samples from alternate locations in circular buffer, and negate alternate values (this is carrier removal for Q samples).
5-Perform 20-Tap root-raised-cosine digital filter, by taking 20-Tap gains from coefficient memory and multiply/accumulate with the 20 demodulated data samples from circular buffer, and store the result. This is the demodulated filtered Q symbol sample.

6-Perform carrier phase correction.

7-Output I and Q data to DACs (this is the detected I and Q data).

8-Return and enable symbol interrupt, to process next symbol.

All the above is performed in less than 16 μsec (symbol period).

7.4 Discussion and results

The technique described here has been operated and tested for the T-SAT modem running at 128, 64, 32 Kbit/sec, with PSK modulated signal, and is valid for use in other applications. The error-rate performances for the T-SAT modem using a single DSP TMS320C50 chip are shown in Fig. 7.8, which gives a good performance in comparison with the systems discussed in Chapter 3 by computer simulations. Figure 7.7 shows the resultant TMS320C50 real time processed signal constellation of the detected data (I and Q) .

By using the DSP techniques described in this chapter, large parts of the design of discrete hardware in the T-SAT modem can be replaced using a single TMS320C50 DSP chip, rather than using conventional digital chips. Also this scheme provides an easy way for any modifications, which could be done on software only. That makes the design of the modem, cost and size effective. All the techniques used here are valid for use in other applications where cost, size and limited-power environment of the hardware are important.

Filter coefficient			Filter coefficient		
Sample No.	Decimal	Hex	Sample No.	Decimal	Hex
1	-0.019	FFFE	21	1.000	0080
2	-0.003	FFFF	22	0.858	006E
3	0.026	0003	23	0.511	0041
4	0.050	0006	24	0.139	0012
5	0.060	0008	25	-0.054	FFF9
6	0.025	0003	26	-0.140	FFEE
7	-0.028	FFFC	27	-0.025	FFFD
8	-0.053	FFF9	28	0.035	0004
9	-0.049	FFFA	29	0.071	0009
10	-0.020	FFFD	30	0.046	0006
11	0.008	0001	31	0.008	0001
12	0.046	0006	32	-0.020	FFFD
13	0.071	0009	33	-0.049	FFFA
14	0.035	0004	34	-0.053	FFF9
15	-0.025	FFFD	35	-0.028	FFFC
16	-0.140	FFEE	36	0.025	0003
17	-0.054	FFF9	37	0.060	0008
18	0.139	0012	38	0.050	0006
19	0.511	0041	39	0.026	0003
20	0.858	006E	40	-0.003	FFFF

Table 7.1 40% Square-root raised cosine filter coefficients.

Software control signals from the TMS320C50				Control signal at the output of the decoder			Control signals
IOE	A6	A5	R/$\overline{w}$	$\overline{WR1}$	$\overline{SO}$	$\overline{WR2}$	
L	H	L	H	H	L	H	Input 8 samples from FIFO
L	H	H	L	L	H	H	Output I data to DAC1
L	H	L	L	H	H	L	Output Q data to DAC2

L = 0, H = +5 V.

Table 7.2 Truth table for interface circuit in Fig. 7.5.

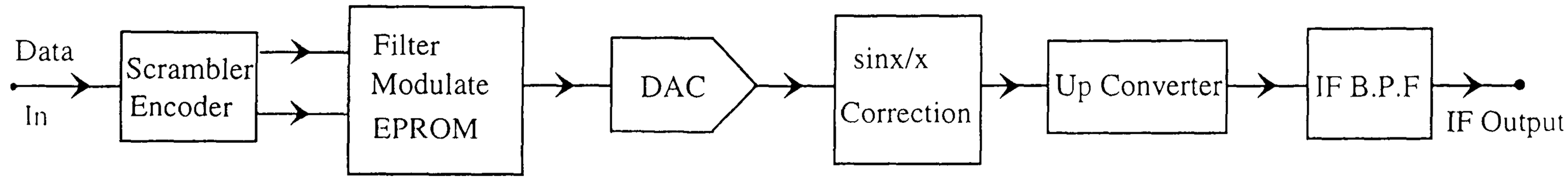

(a)

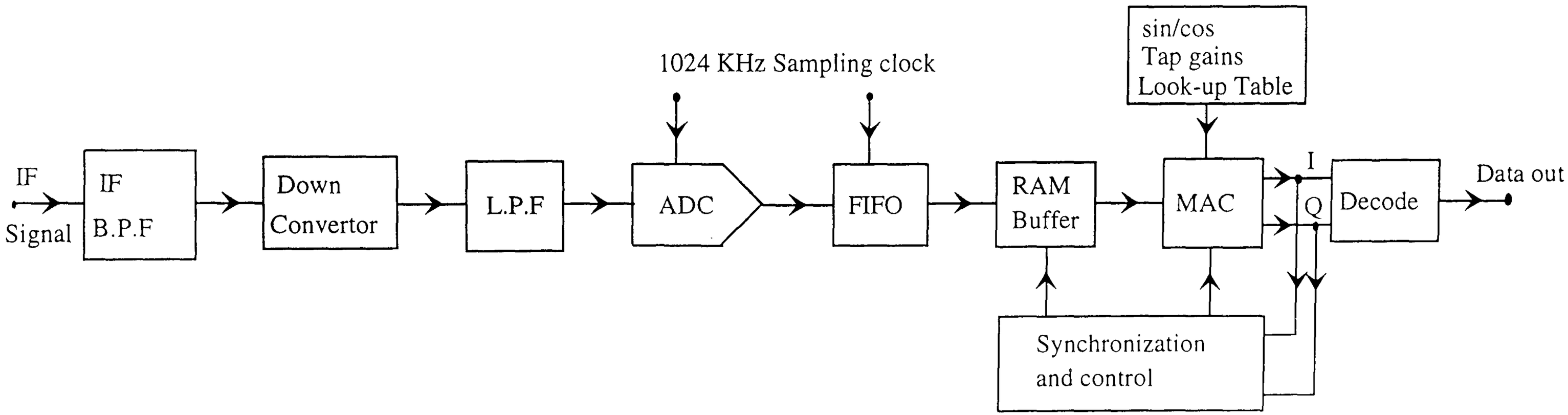

(b)

Figure 7.1 Block diagram of the T-SAT modem, a) Modulator, b) Demodulator and synchronization.

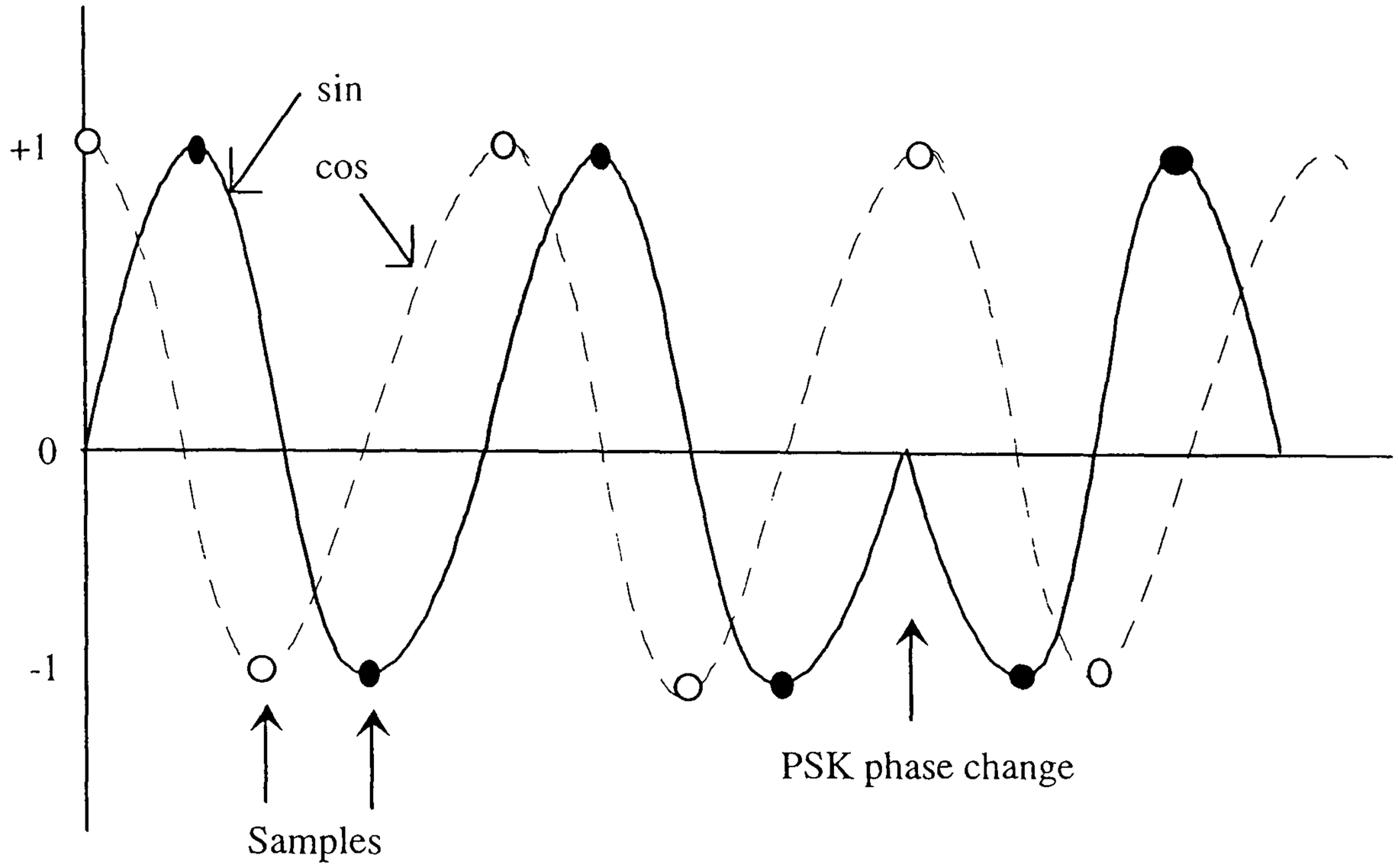

$\cos \omega t \longrightarrow +1 \quad 0 \quad -1 \quad 0$

$\sin \omega t \longrightarrow 0 \quad +1 \quad 0 \quad -1$

Figure 7.2 Sampling the carrier frequency 4 samples/carrier.

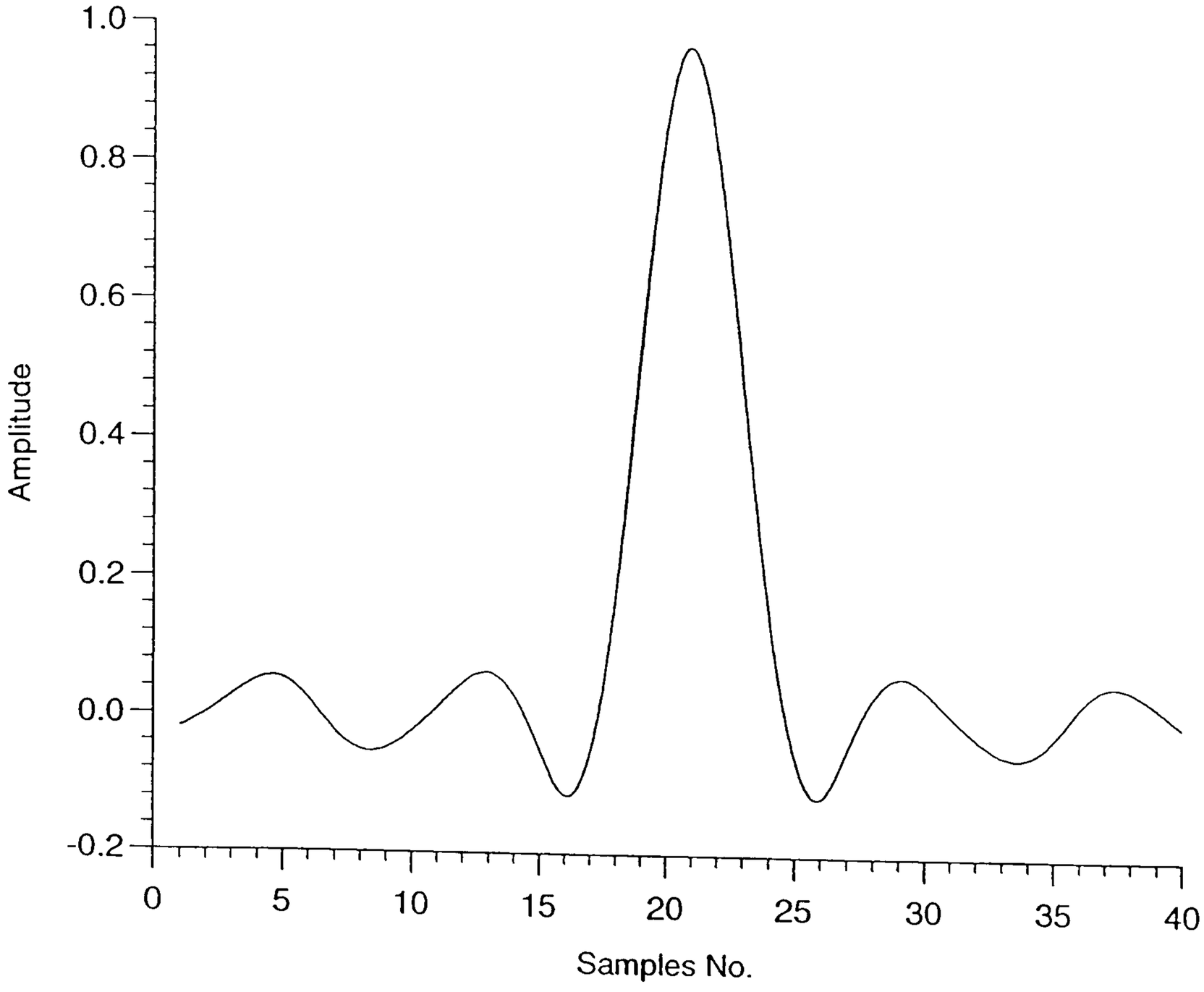

Figure 7.3 Sample impulse response of the 40% square-root raised cosine filter.

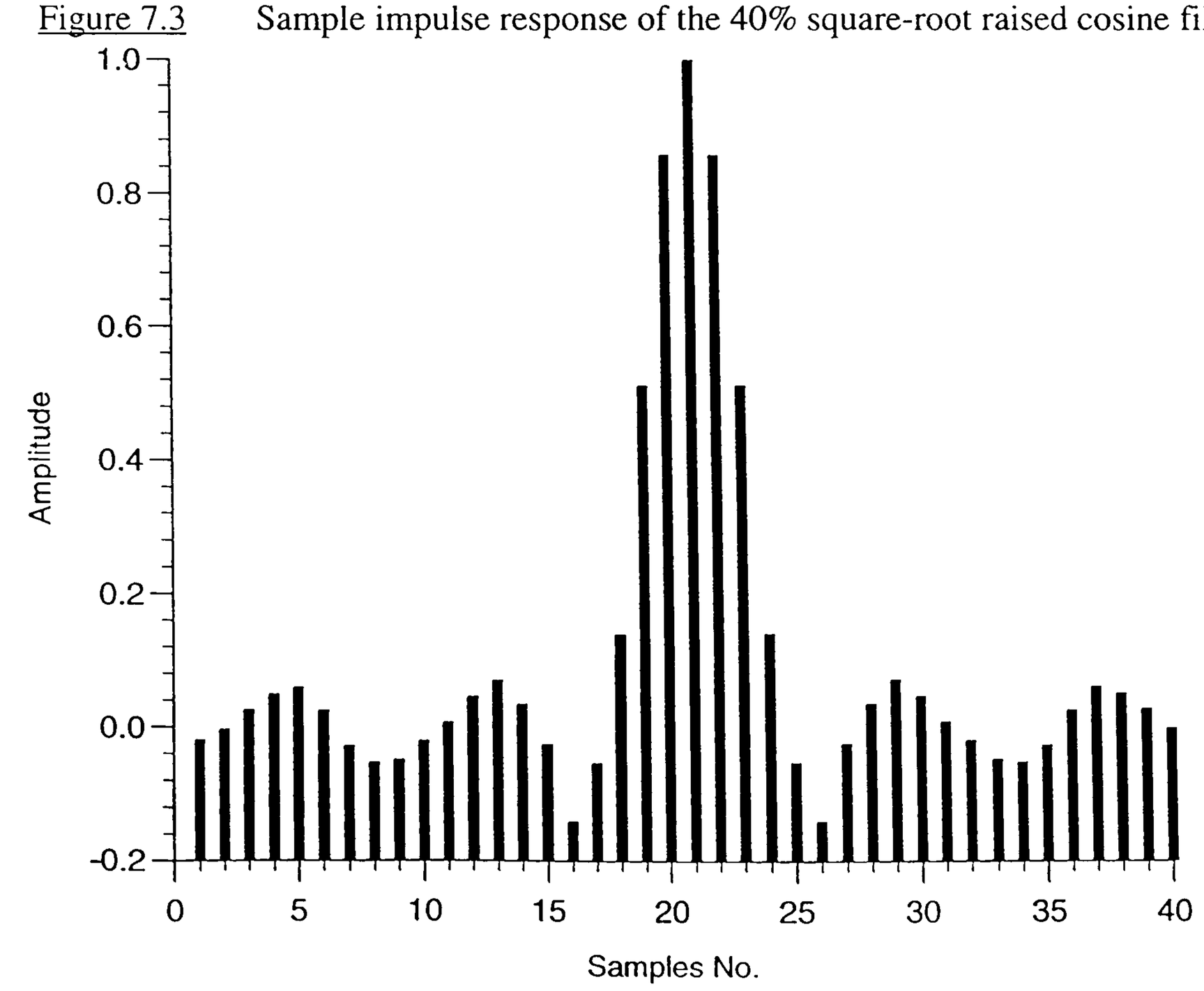

Figure 7.4 40-Tap gain of the digital filter with 40% square-root raised cosine shape.

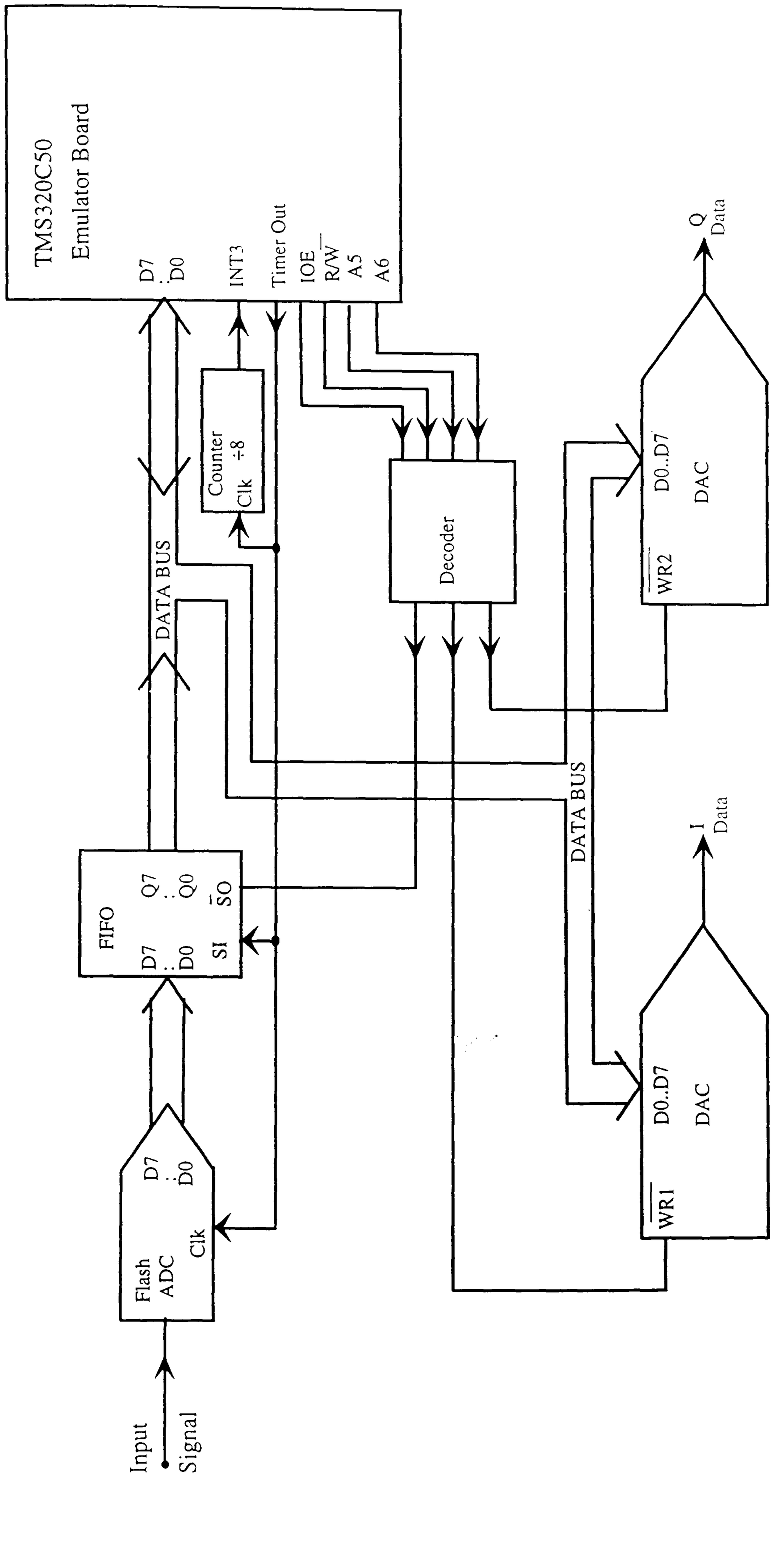

Figure 7.5 Interface circuit diagram of the TMS320C50.

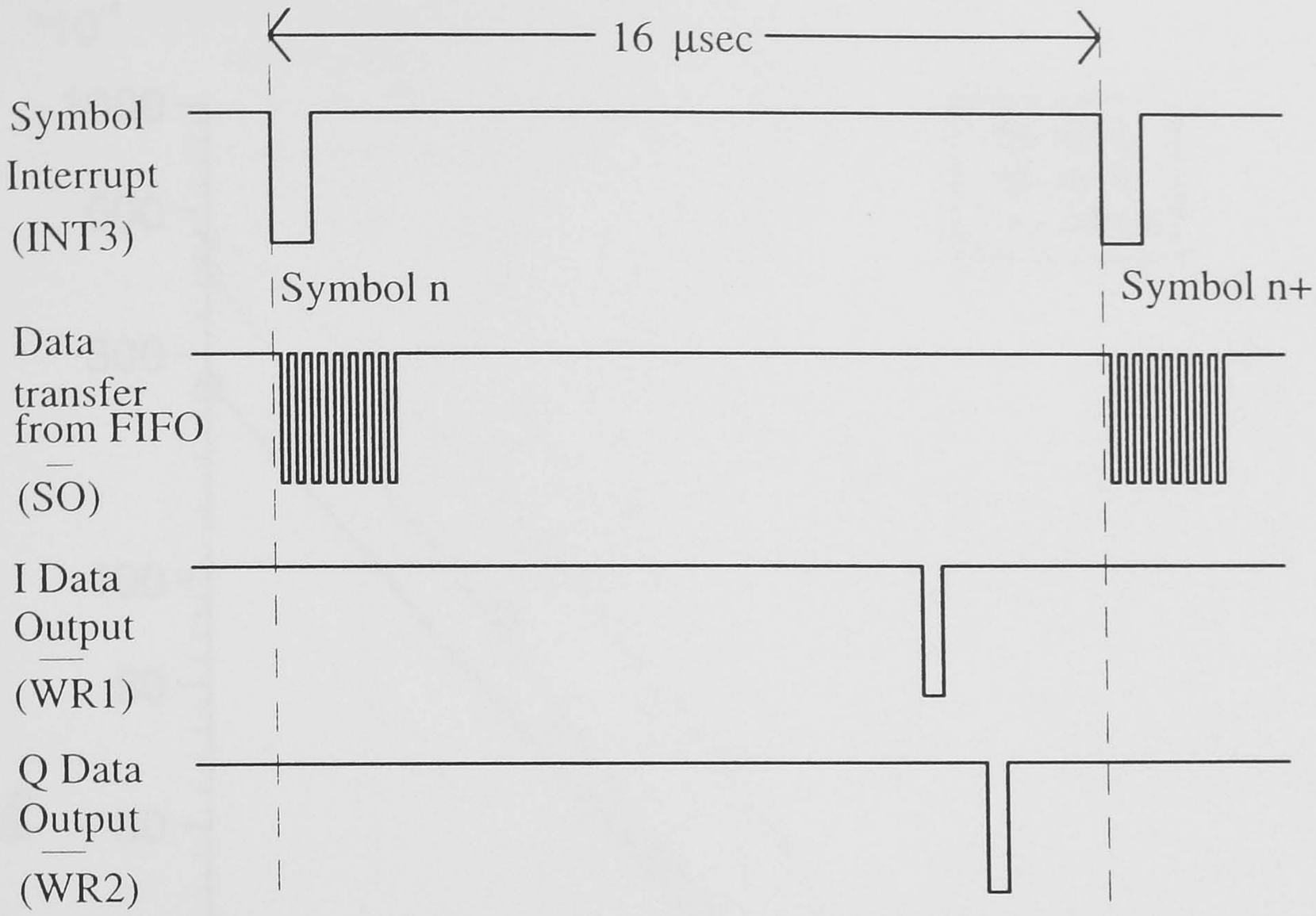

Figure 7.6 Symbol interrupt and control signals activity.

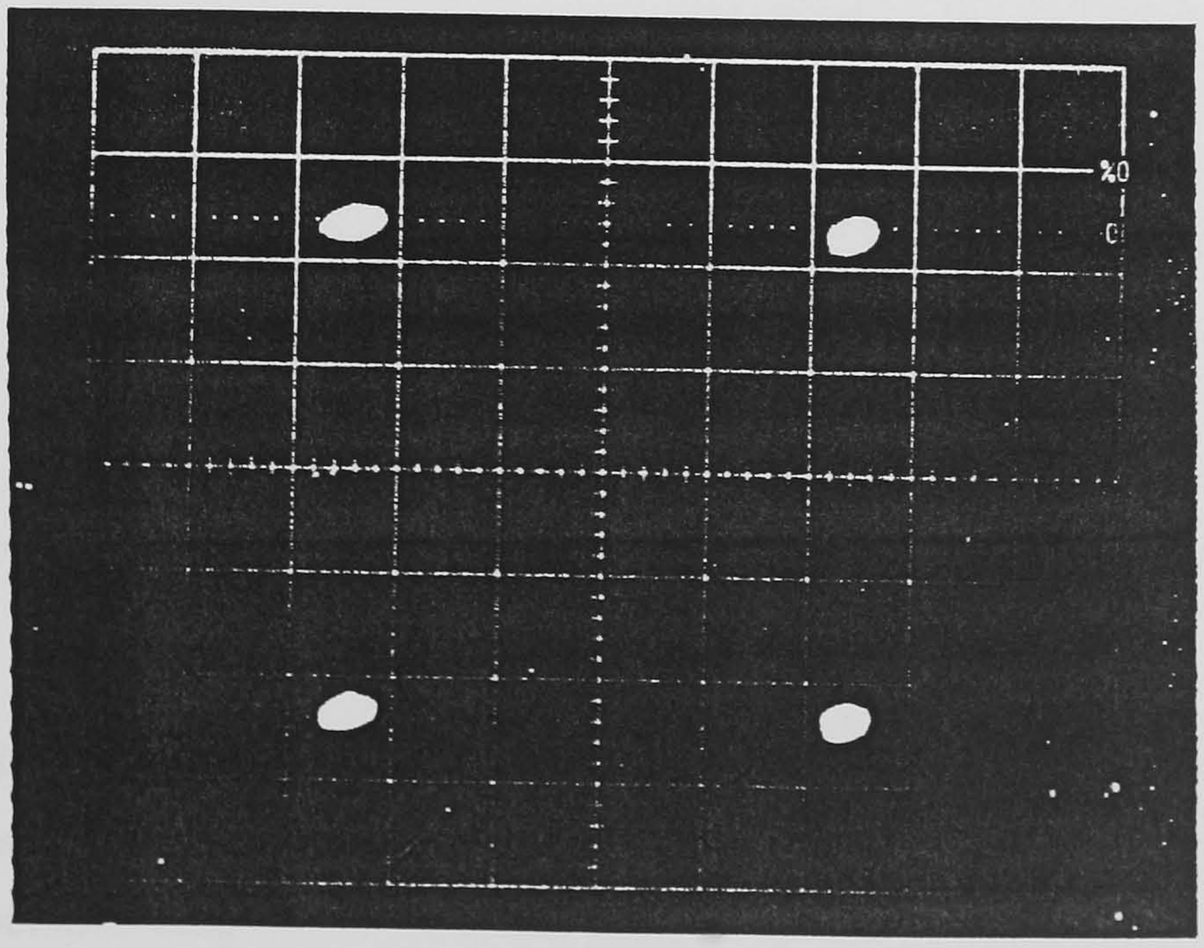

Figure 7.7 Signal constellation of the detected data.

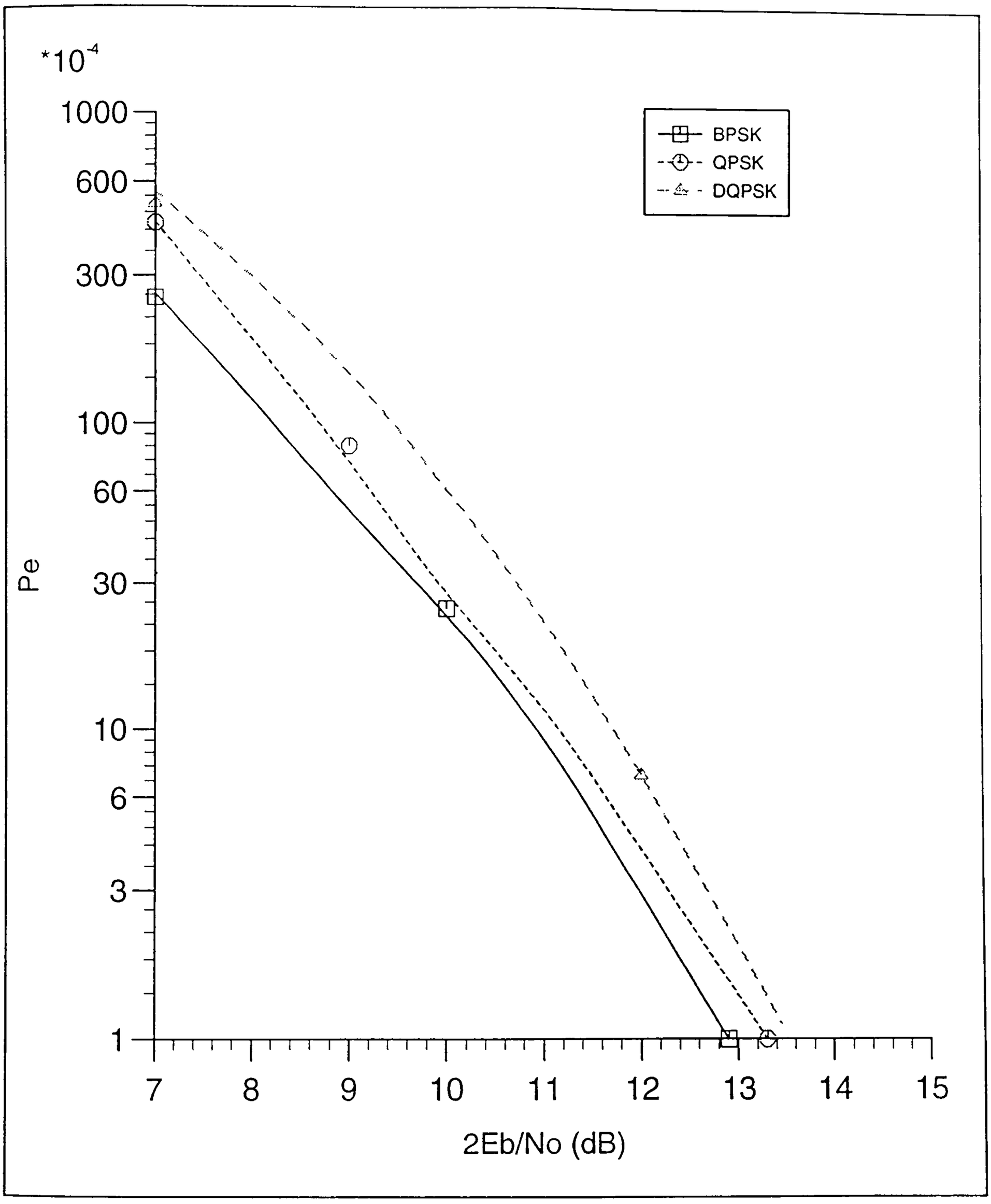

Figure 7.8 Error-rate performances of PSK signals for the T-SAT modem, where the demodulation and digital filtering parts of the modem implemented in digital signal processor chip.

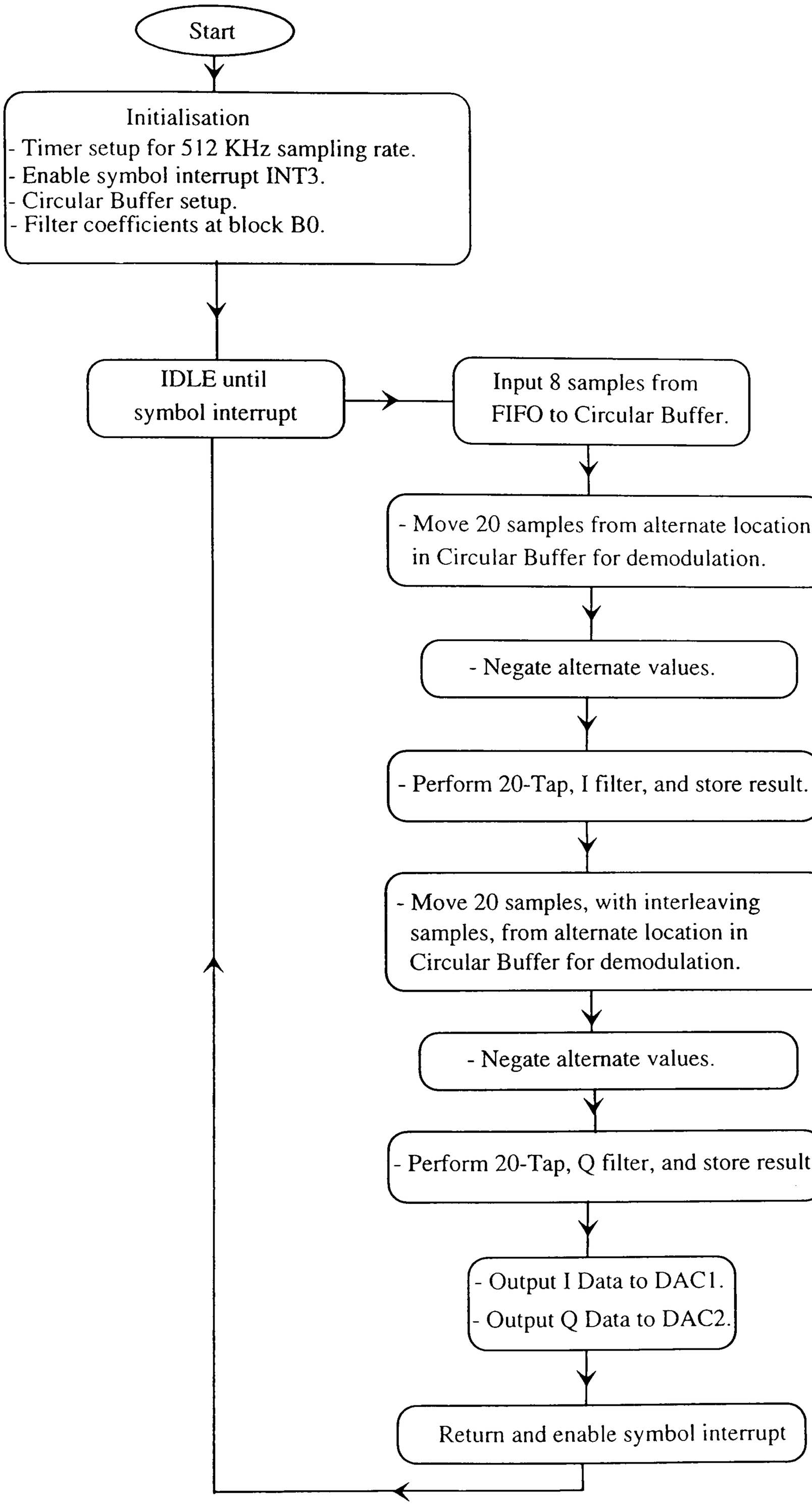

Figure 7.9 Flowchart of the demodulation and filtering algorithm.

CHAPTER 8

DIGITAL SIGNAL PROCESSOR IMPLEMENTATION OF A VITERBI-ALGORITHM DECODER FOR A CONVOLUTIONALLY ENCODED 8PSK SIGNAL

8.1 Introduction

In satellite communication systems, or in any digital data transmission system, it is well known that convolutional coding can be used to provide an improved tolerance to noise over the corresponding uncoded system, in cases where the tolerance to noise of the uncoded system is insufficient for the intended application [78]. Convolutionally encoded eight-phase-shift keyed (CE8PSK) signals have been proposed for use over satellite links [31], [32], [40].

In QPSK signals, two information bits are mapped into one of four possible phases; but in CE8PSK signals, two information bits (together with the previous four information bits) are convolutionally encoded into three bits, which are mapped into one of eight possible phases. The additional phases provide the redundancy needed for FEC (forward error correction) coding. The signals still have two information bits/symbol, but each symbol now has eight possible values. Thus the signal element rate remains the same as that of the QPSK signals, and the bandwidth does not change.

When an uncoded data transmission system is used, the detection process which is required to detect the received data sequence is usually relatively simple, if the channel introduces only limited intersymbol interference [50]. Conversely, coded systems usually require considerably more complex detectors [78]. The detector which minimizes the probability of error in the detection of the whole received coded sequence is a maximum likelihood detector [43]. This is usually implemented by means of the Viterbi-algorithm [43] [41] which is however, often too complex for the intended application.

With the advanced technology of digital signal processors (DSPs), it is possible to implement the Viterbi-algorithm decoder in a single DSP chip, for high bit-rate data.

Many researchers have investigated the implementation of the Viterbi-algorithm decoder using discrete logical chips [79], and others developed the Viterbi-algorithm decoder using Microprocessors [80]. Also, many have discussed the development and implementation of the decoder using VLSI technology [81,82], [84,85], and others have developed different approaches of the Viterbi-algorithm decoder [26,83]. Memory management of the memory contents in a Viterbi decoder is a major design problem for both hardware and software realization [86].

In this chapter the investigation of a digital signal processor Viterbi-algorithm decoder is described and the implementation of that algorithm is performed using a single chip digital signal processor.

8.2 Convolutionally encoded 8PSK signals

To assess the description of the Viterbi-algorithm decoder, a convolutional encoder which is used in this thesis for the rate-2/3 is described as follows. The model of the transmitter is shown in Fig. 8.1, which consists of a convolutional encoder and Gray encoder to map the signal into the corresponding complex-valued symbol.

The model of the rate-2/3 convolutional encoder is shown in Fig. 8.2. It consists of a shift register and modulo-2 adders. The information to be transmitted is carried by the binary digits $\{s_i\}$, where s_i= 0 or 1, when the encoder has received $IS1$ and $IQ1$, it convolutionally encodes these into the corresponding octal coded signal

$$e_i = [e_i(1) \quad e_i(2) \quad e_i(3)] \qquad 8.2.1$$

where $e_i(h) = 0$ or 1 for $h = 1,\ 2,\ 3$, which encoded according to the equations as follows

$$\begin{aligned} e_i(1) &= IS3 \oplus IS1 \oplus IQ2 \\ e_i(2) &= IS1 \oplus IQ3 \oplus IQ2 \oplus IQ1 \qquad 8.2.2 \\ e_i(3) &= IS2 \end{aligned}$$

where $\oplus$ denotes modulo-2 addition.

For every two bits fed into the encoder, it generates three binary digits (binary code symbols) whose values are determined, not only by the two bits, but also by the K

preceding bits, therefore by the 1/2 K preceding 4-level data-symbols, the value of K being the memory (in bits) of the code used [31], [33].

The Gray encoder converts the three bits at its input into the corresponding complex number of constant

$$q_i = q_{1,i} + jq_{2,i} \qquad 8.2.3$$

according to Table 8.1, where $j = \sqrt{-1}$ and where $q_{1,i}$ and $q_{2,i}$ are the real and imaginary parts of q_i. In every case $|q_i| = 1$, where $|q_i|$ is the absolute value of q_i.

Signal $\{q_i\}$ represents the convolutional encoded 8PSK signal, with the corresponding real and imaginary parts of $q_{1,i}$ and $q_{2,i}$. The value of q_i is uniquely related to the value of e_i in Fig. 8.3, which in turn is uniquely related to $e_i(1)$, $e_i(2)$ and $e_i(3)$ by the equation

$$\text{Mapping position} = e_i = 4e_i(1) + 2e_i(2) + e_i(3) + 1 \qquad 8.2.4$$

8.3 Viterbi-algorithm decoder

The i^{th} symbol at the output of the convolutional encoder and the Gray encoder has the value

$$q_i = (\pm 0.924 \pm j0.383) \text{ or } (\pm 0.383 \pm j0.924) \qquad 8.3.1$$

according to Table 8.1, where $j = \sqrt{-1}$, the $\{q_i\}$, of course, being statistically independent and equally likely to have any of the eight possible values.

Assume that the receiver provides the required ideal timing signal, so the signal is sampled once per symbol, at the time instants $\{iT\}$, to give the sequence $\{r_i\}$, where r_i has a complex value.

The received sample at time $t = iT$ is

$$r_i = r_{1,i} + jr_{2,i} \qquad 8.3.2$$

where

$$r_{1,i} = q_{1,i} + v_{1,i} \qquad 8.3.3$$

and

$$r_{2,i} = q_{2,i} + v_{2,i} \qquad 8.3.4$$

the signals $r_{1,i}$ and $r_{2,i}$ being the real and imaginary parts of r_i. The noise components $\{v_{1,i}\}$ and $\{v_{2,i}\}$ are statistically independent real-valued Gaussian random variables

with zero mean and fixed variance, being independent also of the symbol $\{s_i\}$ at the input to the encoder at the transmitter.

The $\{r_i\}$ are fed to the decoder which produces at its output the sequence of symbols $\{\hat{s}_i\}$ which form the sequence of decoded binary-data symbols. The decoded symbols $\{\hat{s}_i\}$, having the minimum probability of being incorrect, form the possible sequence data symbols at the input to the transmitter for which there is minimum mean-square difference (minimum unitary distance squared) [50], [51] between the corresponding received sequence of $\{q_i\}$ in the absence of noise and the samples $\{r_i\}$ actually received [41]. Thus, under these conditions, minimum-distance decoding, minimizes the probability of error in decoding the received signal. In the absence of noise, the $\{\hat{s}_i\}$ are the same as the $\{s_i\}$ at the input to the encoder at the transmitter.

The $\{r_i\}$ are fed to the decoder. In the Viterbi-algorithm decoder the receiver holds in store the $m = 4^{K-1} = 16$ vectors $\{Z_L\}$, where K=3 for the convolutional encoder used here, where

$$Z_L = [x_{L-2n+1} \quad x_{L-2n+2} \quad x_{L-2n+3} \ldots . \ x_L] \qquad 8.3.5$$

where $x_i = 0$ or 1 for $i = L\text{-}2n\text{+}1, L\text{-}2n\text{+}2, \ldots . , L$ and x_i represents a possible value of s_i. With each of the 16 stored vectors the receiver holds in store 16 minimum costs corresponding to the 4^{K-1} different possible combinations of values of $x_{L-2n+3}, x_{L-2n+4}, \ldots . x_L$. Thus each stored vector Z_L forms the last $2n$ component of the L component sequence $x_1, x_2, \ldots . x_L$, which is a possible sequence of values of the data-symbols $s_1, s_2, \ldots . s_L$. Associated with each vector Z_L is stored also the corresponding n component vector

$$Y_i = [y_1 \quad y_2 \quad y_3 \ldots . \ y_i] \qquad 8.3.6$$

where $i = L / 2$ (because a coded-symbol is transmitted for each pair of data symbols), where each y_i, for $k = 1, 2, \ldots . i$, takes on the value of q_i (Table 8.1) that have been obtained had the sequence of data-symbol $s_1, s_2, \ldots . s_i$ been given by the sequence $x_1, x_2, \ldots . x_L$, of which Z_L forms the last $2n$ components.

On the receipt of the sample r_{i+1} each of the 16 stored vectors $\{Z_L\}$ is used to form 4 vectors $\{X_{L+2}\}$, having the 4 possible values of $(x_{L+1} \quad x_{L+2})$. The cost of each vector X_{L+2} is given by the corresponding cost of

$$C_{i+1} = C_i + c_{i+1} \qquad 8.3.7$$

where

$$c_{i+1} = |r_{i+1} - y_{i+1}| \qquad 8.3.8$$

and C_i is the cost of the original vector Z_L. For each of the 4^{K-1} possible combinations of values x_{L-2n+5}, x_{L-2n+6}, ... x_{L+1}, x_{L+2}, the decoder now selects the vector Z_{L+2} and C_{i+1}. The resulting 16 vectors $\{Z_{L+2}\}$are then stored together with their costs $\{C_{i+1}\}$. The detected data-symbols $(\hat{s}_{L-2n+3}\ \hat{s}_{L-2n+4})$ are now given by the values of $(x_{L-2n+3}\ x_{L-2n+4})$ in the vector Z_{L+2} with the smallest cost C_{i+1}, and the process continues in this way.

r_{i+1} and y_{i+1} in Eqn. 8.3.8 are complex-valued, and so it requires two operations of squaring or multiplication to determine each value of C_{i+1}. In Eqn. 8.3.8, y_{i+1} has only 8 different values because it is one of the 8 possible received complex-valued samples (Fig. 8.3). Thus, of these $4m$ values of c_{i+1}, many have the same values. Therefore there are only 8 possible values of c_{i+1}, and each of them requires 2 operations of squaring or multiplication to be determined.

In practice, each time a new set of $\{C_i\}$ are determined, the value of the smallest cost C_i is subtracted from each C_i, thus setting the smallest C_i to zero. This prevents overflow in the values of the $\{C_i\}$, which would otherwise inevitably occur during the receipt of a long message [88].

Towards the end of the synchronizing or training signal, which normally precedes the transmission of data, one of the 16 vectors $\{Z_i\}$ is set to the correct sequence (which is known), and its cost C_i is set to zero. The remaining $\{Z_i\}$ may be set to any value and their costs are set to some very high values. After only a few received samples $\{r_i\}$, all vectors $\{Z_i\}$ will have been derived from the original correct vector, and correct operation of the Viterbi-algorithm decoder is now achieved [88].

In general, for each received sample r_i, the Viterbi-algorithm decoder must process 4^K vectors and 4^K values of costs, followed by the storage of 4^{K-1} $2n$-component vector $\{Z_L\}$ and 4^{K-1} values $\{C_i\}$ are involved in the decoding of each received pair of data $\{s_{L+1}\ s_{L+2}\}$. In the present case, studied in this thesis, K=3, it requires 16 vectors expanded into 64 vectors (i.e., each vector expands 4 ways, for 4 possible values of $(x_{L+1}\ x_{L+2})$) to form the Viterbi-algorithm decoder at the receiver. In receiving each sample r_{i+1} the decoder carries out two operations of squaring or multiplication to determine each of the 8 values of c_{i+1} (Eqn. 8.3.8), which are used to form the 64 values $\{C_{i+1}\}$.

8.4 Digital signal processor implementation of the Viterbi-algorithm decoder

The advanced technology of the digital signal processors (DSPs), makes the implementation of the Viterbi-algorithm decoder possible for the high data bit-rate used in satellite communications. The TMS320C50 generation of the Texas

Instruments TMS320 digital signal processors has been chosen for this implementation.

The TMS320C50 is fabricated with static CMOS integrated circuit technology. The combination of advanced Harvard architecture, on-chip peripherals, on-chip memory, and highly specialized instruction set is the basis of the operational flexibility and speed of the TMS320C50 device. It is designed to execute up to 28 MIPS (million instructions per second) [89].

The TMS320C50 architecture maximizes the processing power by maintaining two separate memory bus structures, program and data, for full-speed execution. Increased throughput on the 'C50 for many DSP applications is accomplished using single-cycle multiply/accumulate instructions with a data-move option, up to eight auxiliary registers with a dedicated arithmetic unit, a parallel logic unit, and faster I/O necessary for data-intensive signal processing. The 'C50 also implements a block-repeat feature that provides zero-overhead looping for implementation of FOR and DO loops. The equivalent of a WHILE loop can be implemented as well. In addition, it has a large instruction set, which makes this device suitable for such an application.

In the following section a system of the convolutionally encoded 8PSK and the Gaussian noise generator applied in the DSP is described, in order to assess the Viterbi-algorithm decoder which is implemented using the TMS320C50 DSP described later.

8.4.1 Model of the system using digital signal processor (DSP)

The model of the system is shown in Fig. 8.4, which implemented using digital signal processor chip TMS320C50. The encoder in Fig. 8.4 applies a process of rate-2/3 convolutional encoding to the input signal, which is a sequence of binary digits 0 and 1 that are fed to the encoder. A program is written in assembly language for the convolutional encoder and Gray coding to map the three bits convolutionally encoded into the mapping signal as shown in Fig. 8.3 and Table 8.1. When the encoder has received the data to be transmitted, it convolutionally encodes these into the corresponding octal signal, and then the Gray coder maps it into the corresponding complex number (Fig. 8.3 and Table 8.1).

The convolutionally encoded 8PSK signal is fed to another part of the program, where it is corrupted with noise. A program has been written in DSP assembly language to generate white Gaussian noise, in order to test the performance of the Viterbi-algorithm decoder.

The use of a DSP chip to produce white Gaussian noise is outlined in [90] [91]. A program was written for the DSP TMS320C50 to implement a random numbers algorithm and use the Central Limit Theorem to generate a Gaussian noise signal in

real time. The program uses the algorithm to generate batches of sixteen random numbers, which it then averages to generate a single value with Gaussian distribution which is added to the CE8PSK signal.

It has been shown in [90] [91] that algorithms carefully chosen to rely heavily on multiplication mathematics (the DSP forte) can be used to generate a suitably random output signal in real time, and from there the Central Limit Theorem can be used to approximate a Gaussian distribution. An example algorithm that relies heavily on the processor's multiplying capabilities is

$$r(n+1) = \mathrm{FRC}[9821.r(n) + 0.211327] \qquad 8.4.1$$

where FRC denotes the fractional part of an expression. It satisfies the Knuth [92] spectral test for randomness and with an arbitrary seed value $r(0)$ generates in excess of a million random numbers before repeating. Having generated a series of random numbers it is necessary to apply the Central Limit Theorem over batches of sample values to synthesise the Gaussian probability density function. The Central Limit Theorem is given by

$$y(n) = \frac{1}{n}\sum_{i=0}^{n-1} x(i) \qquad 8.4.2$$

where $x(i)$ represents a set of equally weighted random numbers. The set of numbers $y(n)$ will have a distribution that is close to Gaussian provided that $n>10$.

Having generated white Gaussian noise, it is then added to the received CE8PSK signal at the input of the decoder. Fig. 8.5 shows the received signal constellation of CE8PSK signal without noise added, and Fig. 8.6 shows the same signal with added white Gaussian noise generated by the DSP program.

The signal in Fig. 8.6 is fed to the Viterbi-algorithm decoder software program to decode the signal. Detected data is obtained at the output of the decoder, which is fed back to the BER test equipment to assess the BER performance of the Viterbi-algorithm decoder.

8.4.2 Viterbi-algorithm decoder software

A large number of calculations, comparisons and decisions are involved in the implementation of the Viterbi-algorithm decoder, and time available is very limited in this implementation.

An algorithm has been written in the DSP assembly language for the TMS320C50 to implement the Viterbi-algorithm decoder. As it is described in

Section 8.3, the Viterbi-algorithm decoder in the receiver holds in store 16 vectors with their minimum costs corresponding to the 16 different possible combinations of values x_{L-2n+3}, x_{L-2n+4}, ... x_L of the vector Z_L.

Upon the receipt of the sample r_{i+1}, each of the 16 vectors $\{Z_L\}$ forms a common part of 4 vectors $\{Z_{L+2}\}$, having the 4 possible values of $(x_{L+1} \quad x_{L+2})$. Each of these 4 possible vectors is associated with the corresponding cost (Eqn. 8.3.7)

$$C_{i+1} = C_i + c_{i+1} \qquad 8.4.3$$

where
$$c_{i+1} = |r_{i+1} - y_{i+1}| \qquad 8.4.4$$

and C_i is the cost of the original vector Z_L.
Since there are 8 possible values of y_{i+1} which is in the algorithm has real part $ci(i)$ and an imaginary part $cq(i)$ for i=1, 2, ... 64, for 64 expanded vectors, the decoder has to carry out 16 operations of squaring or multiplication to compute the 8 different values of c_{i+1}($ce(i)$ for i=1, 2, ... 8) which are used to form the 64 values $\{C_{i+1}\}$ ($cc(i)$ for $i = 1, 2, ... 64$) (Fig. 8.7), r_{i+1} has complex value, re is the real part and im is the imaginary part

$$\begin{aligned}
ce(1) &= (re - ci(1))^2 + (im - cq(1))^2 \\
ce(2) &= (re - ci(9))^2 + (im - cq(9))^2 \\
ce(3) &= (re - ci(2))^2 + (im - cq(2))^2 \\
ce(4) &= (re - ci(10))^2 + (im - cq(10))^2 \\
ce(5) &= (re - ci(4))^2 + (im - cq(4))^2 \\
ce(6) &= (re - ci(12))^2 + (im - cq(12))^2 \\
ce(7) &= (re - ci(5))^2 + (im - cq(5))^2 \\
ce(8) &= (re - ci(11))^2 + (im - cq(11))^2
\end{aligned} \qquad 8.4.5$$

After computing the 8 different values of $c_{i+1}(ce(i))$, the decoder uses these values to compute the 64 costs values $\{C_{i+1}\}$, according to Table 8.2 and Fig. 8.7, the 64 costs of the 64 expanded vectors are computed according to the following equations:

- $ce(1)$ is used to compute the costs of the vectors which have the same mapping position

$$c(1) = ce(1) + cc(1)$$

$$c(18) = ce(1) + cc(2)$$

$$c(36) = ce(1) + cc(4)$$

$$c(51) = ce(1) + cc(3)$$

8.4.6

$$c(7) = ce(1) + cc(7)$$

$$c(24) = ce(1) + cc(8)$$

$$c(38) = ce(1) + cc(6)$$

$$c(53) = ce(1) + cc(5)$$

- $ce(2)$ is used to compute the costs of the vectors which have the same mapping position

$$c(9) = ce(2) + cc(9)$$

$$c(26) = ce(2) + cc(10)$$

$$c(44) = ce(2) + cc(12)$$

$$c(59) = ce(2) + cc(11)$$

8.4.7

$$c(15) = ce(2) + cc(15)$$

$$c(32) = ce(2) + cc(16)$$

$$c(46) = ce(2) + cc(14)$$

$$c(61) = ce(2) + cc(13)$$

- $ce(3)$ is used to compute the costs of the vectors which have the same mapping position

$$c(2) = ce(3) + cc(2)$$

$$c(17) = ce(3) + cc(1)$$

$$c(35) = ce(3) + cc(3)$$

$$c(52) = ce(3) + cc(4)$$

$$c(8) = ce(3) + cc(8) \qquad 8.4.8$$

$$c(23) = ce(3) + cc(7)$$

$$c(37) = ce(3) + cc(5)$$

$$c(54) = ce(3) + cc(6)$$

- $ce(4)$ is used to compute the costs of the vectors which have the same mapping position

$$c(10) = ce(4) + cc(10)$$

$$c(25) = ce(4) + cc(9)$$

$$c(43) = ce(4) + cc(11)$$

$$c(60) = ce(4) + cc(12)$$

$$c(16) = ce(4) + cc(16) \qquad 8.4.9$$

$$c(31) = ce(4) + cc(15)$$

$$c(45) = ce(4) + cc(13)$$

$$c(62) = ce(4) + cc(14)$$

- $ce(5)$ is used to compute the costs of the vectors which have the same mapping position

$$c(4) = ce(5) + cc(4)$$

$$c(19) = ce(5) + cc(3)$$

$$c(33) = ce(5) + cc(1)$$

$$c(50) = ce(5) + cc(2)$$

8.4.10

$$c(6) = ce(5) + cc(6)$$

$$c(21) = ce(5) + cc(5)$$

$$c(39) = ce(5) + cc(7)$$

$$c(56) = ce(5) + cc(8)$$

- $ce(6)$ is used to compute the costs of the vectors which have the same mapping position

$$c(12) = ce(6) + cc(12)$$

$$c(27) = ce(6) + cc(11)$$

$$c(41) = ce(6) + cc(9)$$

$$c(58) = ce(6) + cc(10)$$

8.4.11

$$c(14) = ce(6) + cc(14)$$

$$c(29) = ce(6) + cc(13)$$

$$c(47) = ce(6) + cc(15)$$

$$c(64) = ce(6) + cc(16)$$

- $ce(7)$ is used to compute the costs of the vectors which have the same mapping position

$$c(5) = ce(7) + cc(5)$$

$$c(22) = ce(7) + cc(6)$$

$$c(40) = ce(7) + cc(8)$$

$$c(55) = ce(7) + cc(7)$$

$$c(3) = ce(7) + cc(3) \qquad 8.4.12$$

$$c(20) = ce(7) + cc(4)$$

$$c(34) = ce(7) + cc(2)$$

$$c(49) = ce(7) + cc(1)$$

- $ce(8)$ is used to compute the costs of the vectors which have the same mapping position

$$c(11) = ce(8) + cc(11)$$

$$c(28) = ce(8) + cc(12)$$

$$c(42) = ce(8) + cc(10)$$

$$c(57) = ce(8) + cc(9) \qquad 8.4.13$$

$$c(13) = ce(8) + cc(13)$$

$$c(30) = ce(8) + cc(14)$$

$$c(48) = ce(8) + cc(16)$$

$$c(63) = ce(8) + cc(15)$$

where $cc(i)$ for i=1, 2, ... 16 is the cost of the original vector, for all vectors set (Eqns. 8.4.6-8.4.13).

Having computed the 64 costs of the expanded 64 vectors, the decoder now selects the 16 of the 64 vectors with the smallest cost. The algorithm choosing the minimum costs starts by comparing each set of 4 costs with arbitrary value of a cost (*ccc*). Of these costs, the algorithm selects 16 of the 64 vectors with a minimum cost.

Now the decoder has 16 selected vectors with 16 minimum costs, the algorithm now selects one vector with a smallest cost of the 16 vectors. After choosing the

vector with a smallest cost, the lowest cost $cc(i)$ for i=1, 2, ... 16 is subtracted from all costs, setting the smallest cost to zero, thus preventing overflow.

The detected vector is the one with cost equal to zero. The algorithm then stores the 16 selected vectors with their 16 costs, for next detection of sample r_{i+2}, and the process continues in this way.

The flowchart of the algorithm is shown in Fig. 8.8, and it's program was written in the digital signal processor assembly language.

The program starts by initialising the timer period for the specified data bit-rate of the system, and then enabling one of the DSP's interrupts to be used as symbol interrupt. Thus when a symbol has been detected the symbol interrupt enables the processor to execute the algorithm to decode the data for next symbol received. In the decoder initialisation, a map has been set-up for the 8 possible received samples, and setting one of the 16 vectors to the correct value and it's cost to zero, the rest of the 16 vectors are set to any value and their costs are set to a very high values.

Upon receiving sample r_{i+1}, the algorithm compute the 8 possible costs $ce(i)$, for i=1, 2, ... 8 (Eqn. 8.4.5) for 8 possible received samples r_{i+1}. These 8 costs $ce(i)$ are used to compute the 64 costs (Eqns. 8.4.6-8.4.13) of the expanded vectors. After computing the 64 costs, the algorithm selects 16 vectors associated with 16 minimum costs of the 64 expanded vectors. The algorithm sets the 64 vectors into a group of 4 vectors and selects one vector with its minimum cost of the 4 expanded vectors, which have the 4 possible transmitted symbols (s_{L+1} s_{L+2}) (Table 8.2). After examining the 64 vectors and their associated costs, the algorithm selects 16 vectors with their 16 minimum costs.

Having selected the 16 vectors with their 16 minimum costs, the algorithm starts examining the 16 costs and selects the lowest one of the 16 costs. The lowest cost is then subtracted from all 16 selected costs, setting the lowest cost to zero, thus preventing overflow in the values.

The vector with cost equal to zero is the detected vector. The processor then outputs this vector as the detected symbol, the program enables the symbol interrupt for next received sample, and the process continues in this way.

8.4.3 Performance of the Viterbi-algorithm decoder

The Viterbi-algorithm decoder has been presented as a practical method of decoding a convolutionally encoded 8PSK signal operating in a noisy environment using a single chip digital signal processor.

To evaluate the performance of the Viterbi-algorithm decoder, Fig. 8.4 shows a block diagram of the evaluation system used. In Fig. 8.4 a convolutionally encoded

8PSK signal is generated using a program written in assembly language, and white Guassian noise, generated by the DSP's software is added to the signal before being decoded by the Viterbi-algorithm decoder.

A bit error-rate test set is used to generate the transmitted data input to the convolutional encoder, and a received data from the test set, which is the output of the Viterbi-algorithm decoder is taken as the detected data symbols. The test set then calculates the bit error-rate for a given value of noise added to the received signal at the input of the decoder.

Preliminary investigation of the implementation of the Viterbi-algorithm decoder using a DSP, shows that the algorithm needs 60 μsec to detect one symbol of the received data when it is executed.

The error-rate performances of the Viterbi-algorithm decoder is plotted in Fig. 8.9, which gives a gain in bit-energy-to-noise density ratio ($2E_b/N_0$) of 2.5 dB at BER $\leq 10^{-4}$ probability of error in comparison with those of uncoded QPSK signals. The results here are the same as the CE8PSK signal discussed in Chapter 4 with a computer simulation system, in AWGN environment, for a non-linear satellite channel.

8.5 Discussion and results

The implementation of the Viterbi-algorithm decoder for a convolutionally encoded 8PSK signal has been discussed. The implementation using a single digital signal processor chip TMS320C50 was constructed and successfully demonstrated in running order and showed good agreement with simulated performance figures. The resultant implementation shows that with a single DSP chip, the Viterbi-algorithm decoder could be constructed, which results in a decoder of moderate software complexity, small size, and low cost.

The rate 2/3 convolutional encoder, with a Viterbi decoder implemented in a single digital signal processor chip, has achieved a gain of 2.5 dB at a BER of $\leq 10^{-4}$ illustrated in Fig. 8.9 when compared with those of uncoded QPSK signals.

An all digital signal processors satellite modem could be implemented, using the development implementation parts of the modem discussed in Section 7.3 and Section 8.4.

Mapping position e_i	$e_i(1)$	$e_i(2)$	$e_i(3)$	$q_{1,i}$	$q_{2,i}$
1	0	0	0	+0.924	+0.383
2	0	0	1	+0.383	+0.924
3	0	1	0	-0.383	+0.924
4	0	1	1	-0.924	+0.383
5	1	0	0	-0.924	-0.383
6	1	0	1	-0.383	-0.924
7	1	1	0	+0.383	-0.924
8	1	1	1	+0.924	-0.383

Table 8.1 Relationship between $[e_i(1)\ \ e_i(2)\ \ e_i(3)]$ and q_i.

Table 8.2

Vector No.	Mapping position	*ci*	*cq*	IS1	IS2	IS3	IQ1	IQ2	IQ3
1	1	+0.924	+0.383	0	0	0	0	0	0
2	3	-0.383	+0.924	0	0	0	1	0	0
3	7	+0.383	-0.924	1	0	0	0	0	0
4	5	-0.924	-0.383	1	0	0	1	0	0
5	7	+0.383	-0.924	0	0	0	0	1	0
6	5	-0.924	-0.383	0	0	0	1	1	0
7	1	+0.924	+0.383	1	0	0	0	1	0
8	3	-0.383	+0.924	1	0	0	1	1	0
9	2	+0.383	+0.924	0	1	0	0	0	0
10	4	-0.924	+0.383	0	1	0	1	0	0
11	8	+0.924	-0.383	1	1	0	0	0	0
12	6	-0.383	-0.924	1	1	0	1	0	0
13	8	+0.924	-0.383	0	1	0	0	1	0
14	6	-0.383	-0.924	0	1	0	1	1	0
15	2	+0.383	+0.924	1	1	0	0	1	0
16	4	-0.924	+0.383	1	1	0	1	1	0
17	3	-0.383	+0.924	0	0	0	0	0	1
18	1	+0.924	+0.383	0	0	0	1	0	1
19	5	-0.924	-0.383	1	0	0	0	0	1
20	7	+0.383	-0.924	1	0	0	1	0	1
21	5	-0.924	-0.383	0	0	0	0	1	1
22	7	+0.383	-0.924	0	0	0	1	1	1
23	3	-0.383	+0.924	1	0	0	0	1	1
24	1	+0.924	+0.383	1	0	0	1	1	1
25	4	-0.924	+0.383	0	1	0	0	0	1
26	2	+0.383	+0.924	0	1	0	1	0	1
27	6	-0.383	-0.924	1	1	0	0	0	1
28	8	+0.924	-0.383	1	1	0	1	0	1
29	6	-0.383	-0.924	0	1	0	0	1	1
30	8	+0.924	-0.383	0	1	0	1	1	1
31	4	-0.924	+0.383	1	1	0	0	1	1
32	2	+0.383	+0.924	1	1	0	1	1	1

Continue Table 8.2

Vector No.	Mapping position	*ci*	*cq*	IS1	IS2	IS3	IQ1	IQ2	IQ3
33	5	-0.924	-0.383	0	0	1	0	0	0
34	7	+0.383	-0.924	0	0	1	1	0	0
35	3	-0.383	+0.924	1	0	1	0	0	0
36	1	+0.924	+0.383	1	0	1	1	0	0
37	3	-0.383	+0.924	0	0	1	0	1	0
38	1	+0.924	+0.383	0	0	1	1	1	0
39	5	-0.924	-0.383	1	0	1	0	1	0
40	7	+383	-0.924	1	0	1	1	1	0
41	6	-0.383	-0.924	0	1	1	0	0	0
42	8	+0.924	-0.383	0	1	1	1	0	0
43	4	-0.924	+0.383	1	1	1	0	0	0
44	2	+0.383	+0.924	1	1	1	1	0	0
45	4	-0.924	+0.383	0	1	1	0	1	0
46	2	+0.383	+0.924	0	1	1	1	1	0
47	6	-0.383	-0.924	1	1	1	0	1	0
48	8	+0.924	-0.383	1	1	1	1	1	0
49	7	+0.383	-0.924	0	0	1	0	0	1
50	5	-0.924	-0.383	0	0	1	1	0	1
51	1	+0.924	+0.383	1	0	1	0	0	1
52	3	-0.383	+0.924	1	0	1	1	0	1
53	1	+0.924	+0.383	0	0	1	0	1	1
54	3	-0.383	+0.924	0	0	1	1	1	1
55	7	+0.383	-0.924	1	0	1	0	1	1
56	5	-0.924	-0.383	1	0	1	1	1	1
57	8	+0.924	-0.383	0	1	1	0	0	1
58	6	-0.383	-0.924	0	1	1	1	0	1
59	2	+0.383	+0.924	1	1	1	0	0	1
60	4	-0.924	+0.383	1	1	1	1	0	1
61	2	+0.383	+0.924	0	1	1	0	1	1
62	4	-0.924	+0.383	0	1	1	1	1	1
63	8	+0.924	-0.383	1	1	1	0	1	1
64	6	-0.383	-0.924	1	1	1	1	1	1

Table 8.2 Possible combinations of convolutional encoding bits, and their mapping position with the associated vectors.

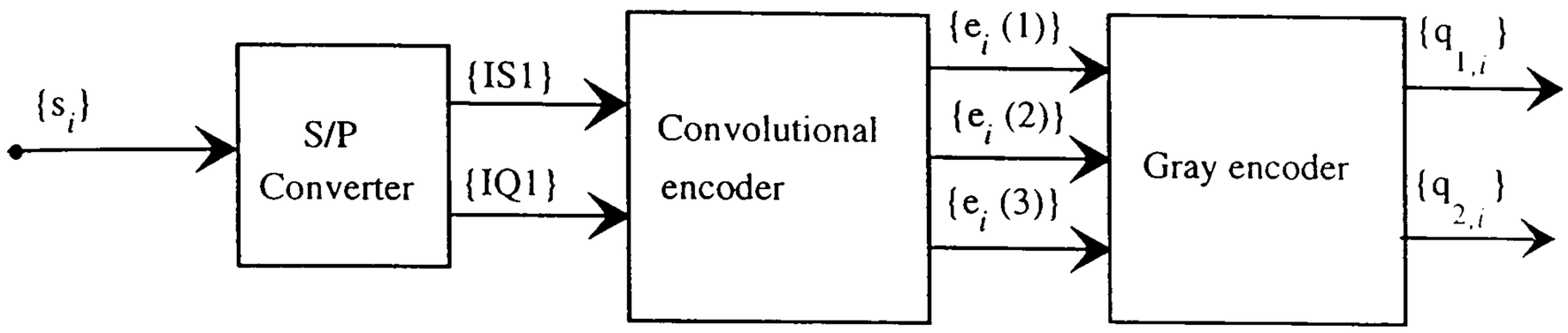

Figure 8.1 Model of CE8PSK signal encoder.

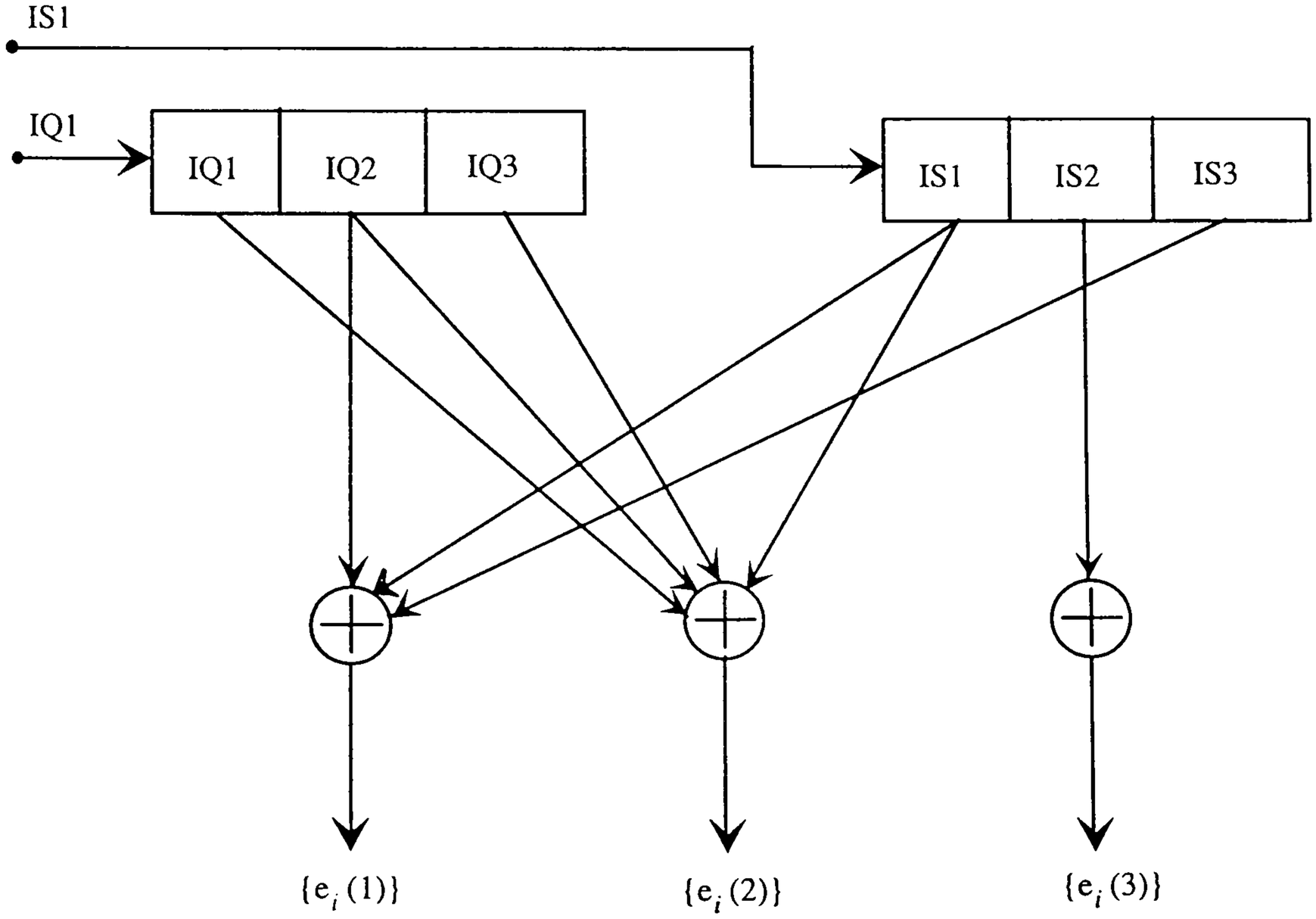

Figure 8.2 Rate-2/3 convolutional encoder.

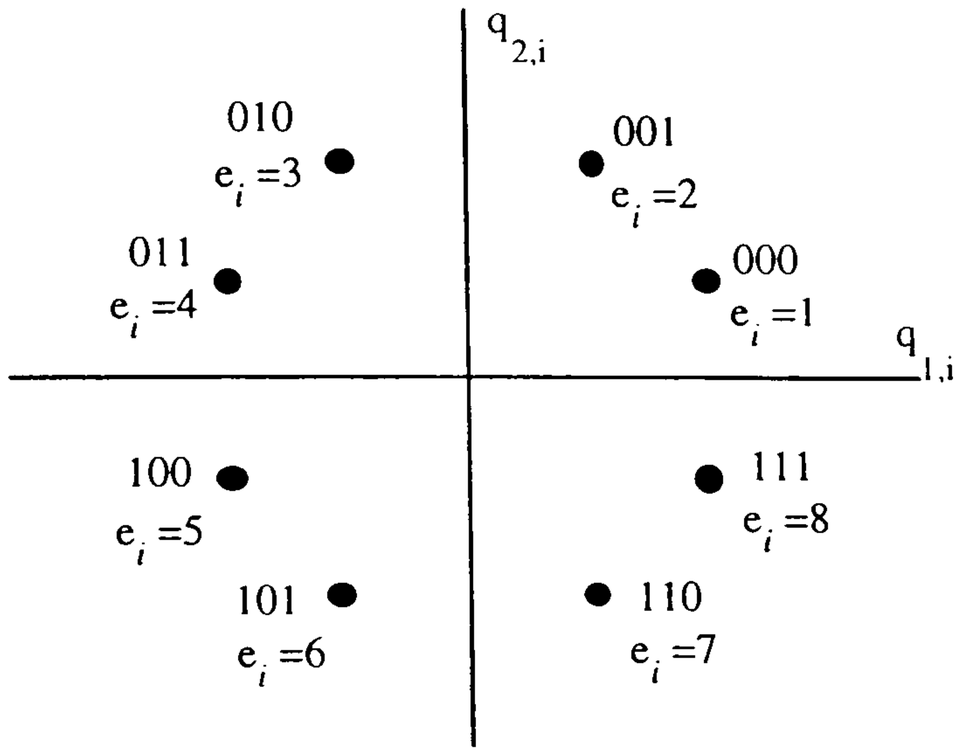

Figure 8.3 Mapping of three bits into a complex-valued symbol.

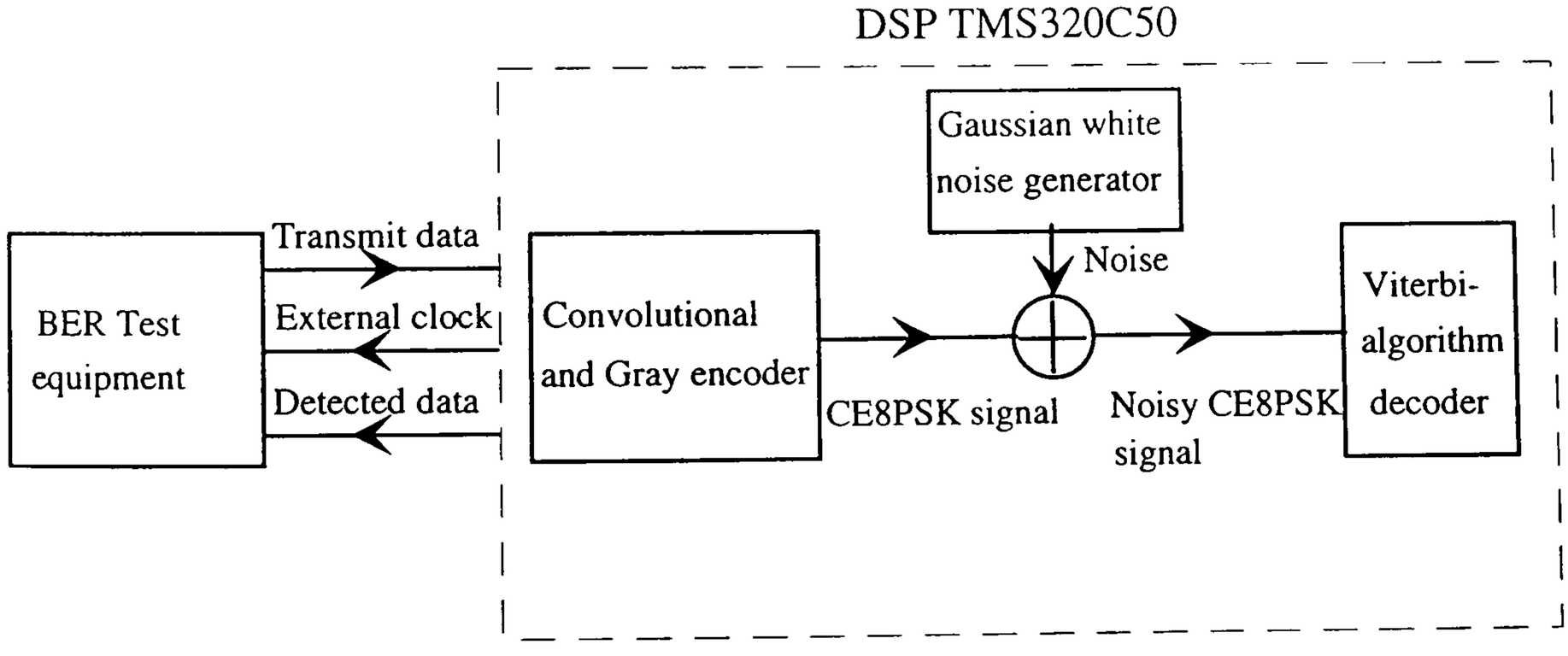

Figure 8.4 Model of the system using digital signal processor, used to evaluate error-rate performances of the Viterbi-algorithm decoder.

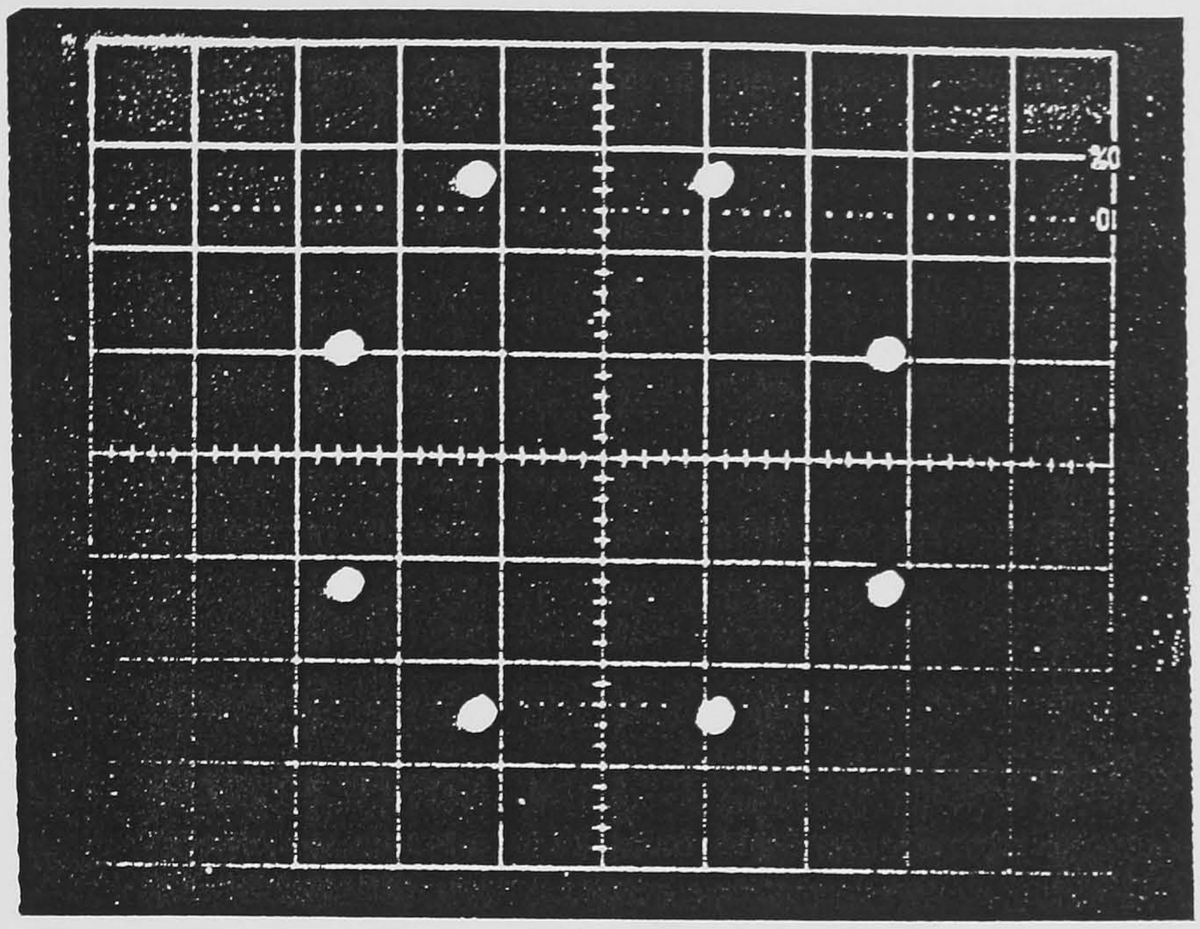

Figure 8.5 Received signal constellation for CE8PSK signal (without noise added).

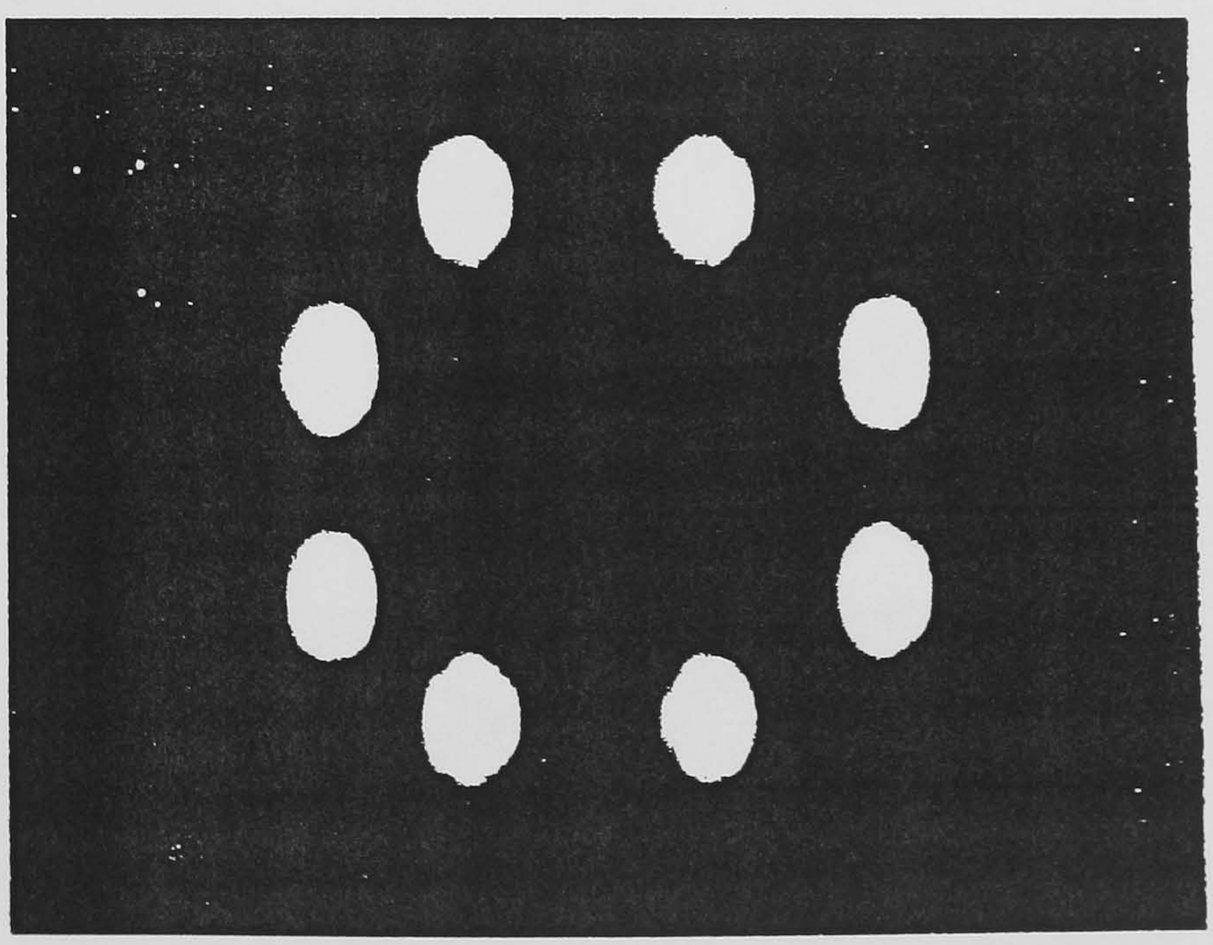

Figure 8.6 Received noisy signal constellation for CE8PSK signal.

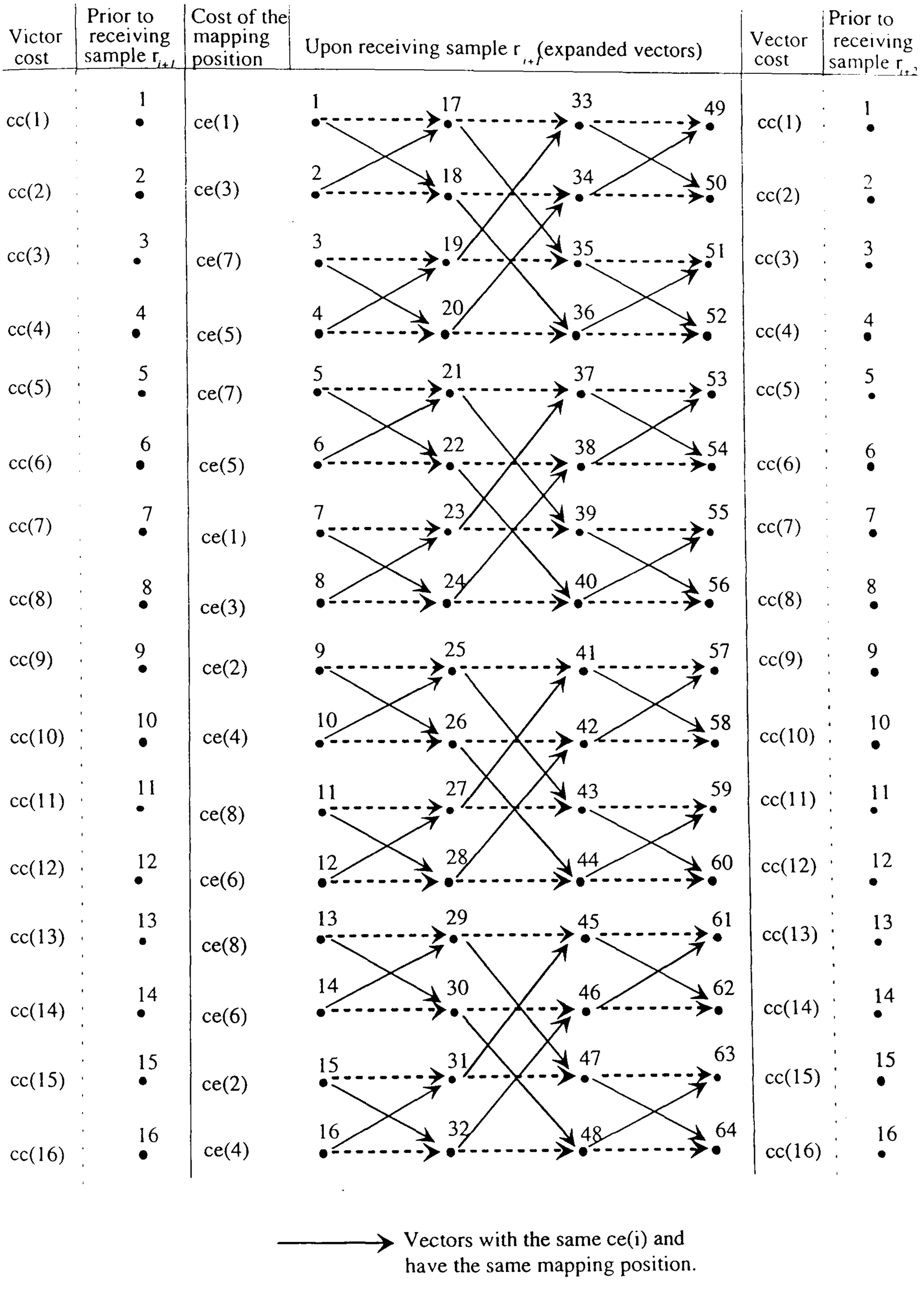

Figure 8.7 Viterbi-algorithm decoder vectors representation, expanded vectors and their costs.

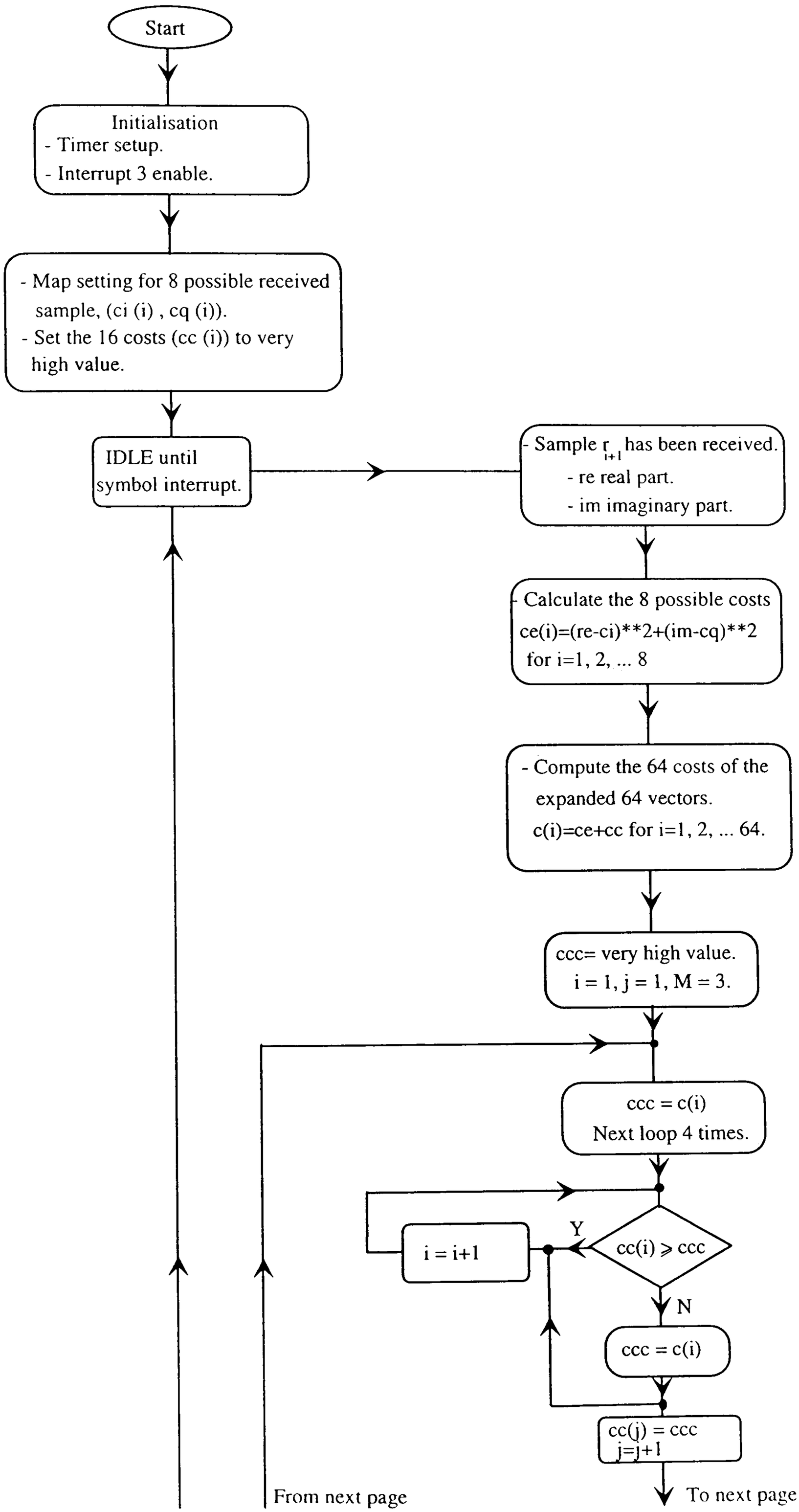
Start
Initialisation
- Timer setup.
- Interrupt 3 enable.
- Map setting for 8 possible received sample, (ci (i) , cq (i)).
- Set the 16 costs (cc (i)) to very high value.
IDLE until symbol interrupt.
- Sample r i+1 has been received.
- re real part.
- im imaginary part.
- Calculate the 8 possible costs
ce(i)=(re-ci)**2+(im-cq)**2
for i=1, 2, ... 8
- Compute the 64 costs of the expanded 64 vectors.
c(i)=ce+cc for i=1, 2, ... 64.
ccc= very high value.
i = 1, j = 1, M = 3.
ccc = c(i)
Next loop 4 times.
cc(i) ⩾ ccc
Y
i = i+1
N
ccc = c(i)
cc(j) = ccc
j=j+1
From next page
To next page

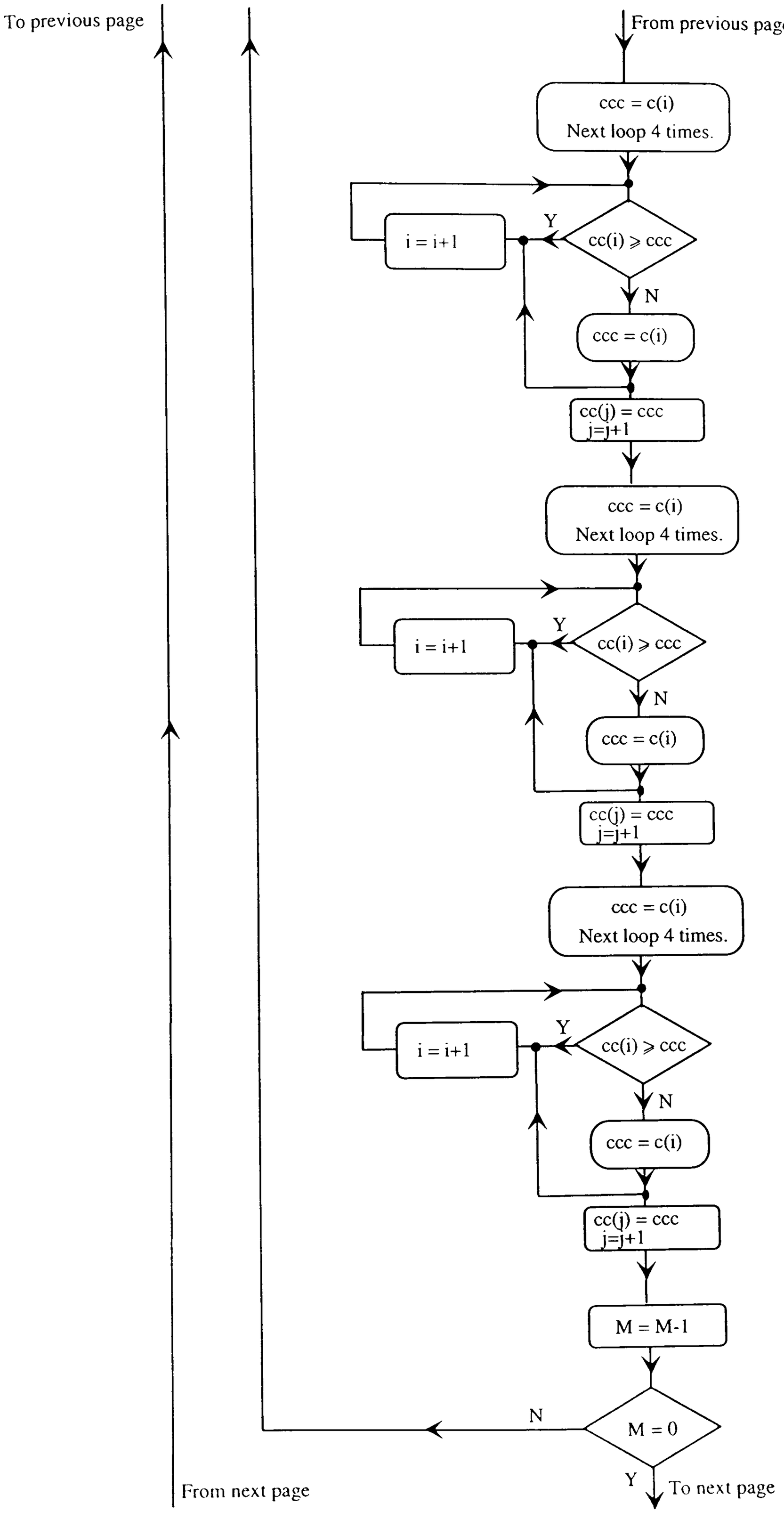
To previous page
From previous page
ccc = c(i)
Next loop 4 times.
i = i+1
Y
cc(i) ⩾ ccc
N
ccc = c(i)
cc(j) = ccc
j=j+1
ccc = c(i)
Next loop 4 times.
i = i+1
Y
cc(i) ⩾ ccc
N
ccc = c(i)
cc(j) = ccc
j=j+1
ccc = c(i)
Next loop 4 times.
i = i+1
Y
cc(i) ⩾ ccc
N
ccc = c(i)
cc(j) = ccc
j=j+1
M = M-1
M = 0
N
Y
From next page
To next page

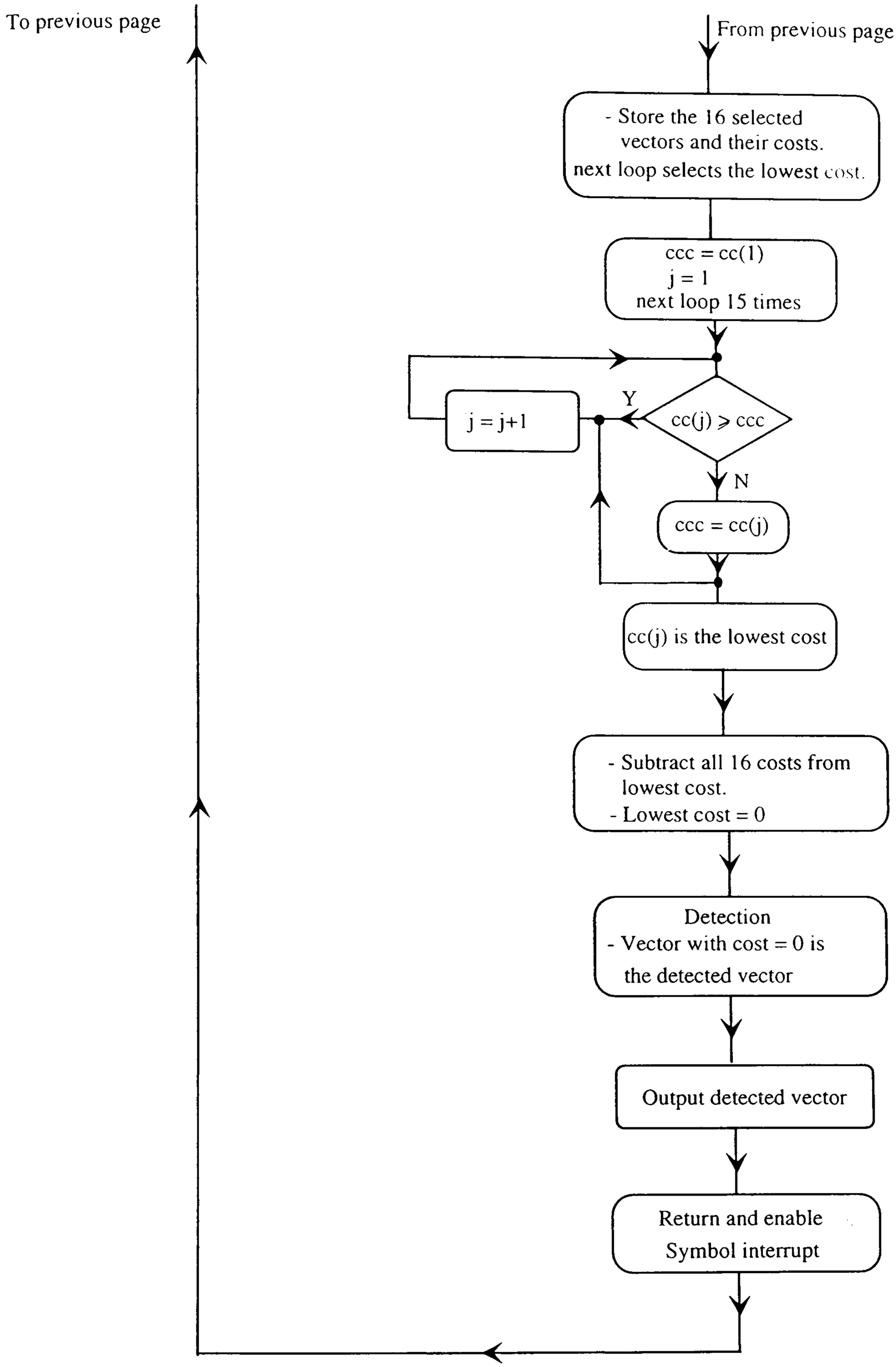

Figure 8.8 Flowchart of the DSP TMS320C50 algorithm for the Viterbi-algorithm decoder.

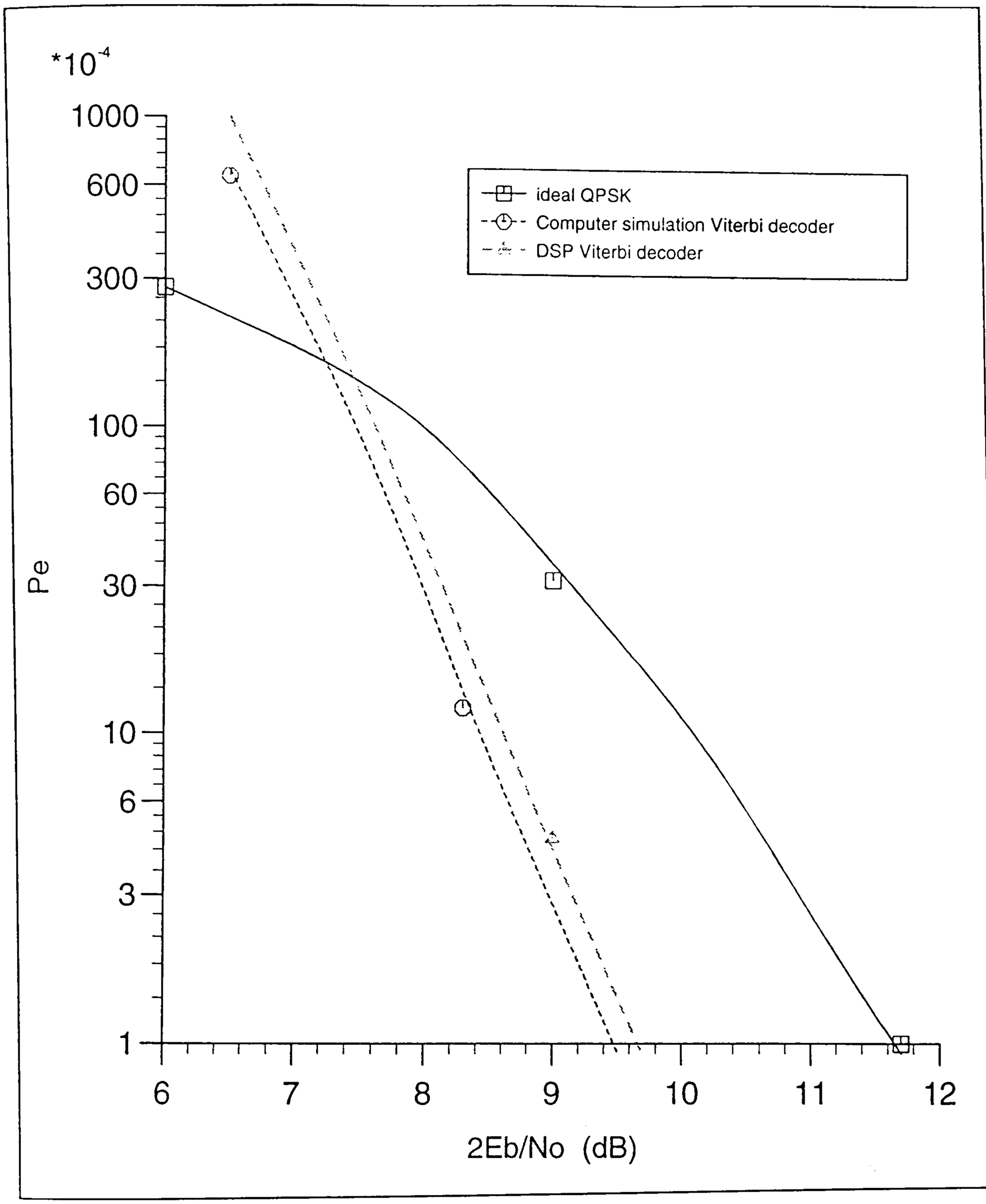

Figure 8.9 Error-rate performances of CE8PSK signal using Viterbi-algorithm decoder implemented in digital signal processor.

CHAPTER 9

COMMENTS ON THE PROJECT

9.1 Recommendations for further study

The aim of this section is to outline further areas of work which are required to prove the worth of the modem design, and to investigate the possible implementation of the other sections of the modem using digital signal processor. The thesis contains various results of data-transmission systems using DEQPSK, OQPSK, CE8PSK and CDE8PSK signals under different assumed conditions as well as hardware implementation for some parts of the modem using digital signal processor (DSP). The following is a list of the possible objectives worthy of further study.

(1) The baseband linearizer is found to be very promising for using with phase-shift keying signals which have a low-spectral efficient modulation techniques e.g., 16-ary quadrature amplitude modulation technique, requires investigation.

(2) In the channel modelling described in the thesis, it is assumed that the TWTA on the satellite is operating in the linear mode. Further study is required to investigate the performance of the system if the TWTA is also operating in a nonlinear mode. This is essential for TDMA systems.

(3) The predistortion technique described in the thesis is used for a single nonlinearity. Predistortion of two nonlinearities in cascade is worth studying, as for the case when the HPA and TWTA both are operating in a nonlinear mode.

(4) One method of carrier synchronisation is discussed, other methods of the feasibility of carrier synchronisation require investigation.

(5) A more detailed study of possible practical implementations is required for various applications. This would include the feasibility of high bit-rate schemes using more parallel processing, and lower bit-rate schemes where digital signal

processors (DSPs) are an attractive solution in terms of cost and flexibility, (including the option of reprogramming), require investigation.

Depending on the development of the demodulation and filtering parts of the T-SAT modem discussed in Section 7.3, the synchronisation described in [74] [75] and Section 4.7, and the implementation of the Viterbi-algorithm decoder for convolutionally encoded 8PSK signal as discussed in Section 8.4, it is possible to construct a satellite modem using digital signal processors, as shown in Fig. 9.1.

The modulator part of the modem could be built using a single DSP chip, where that DSP would process the coding of the signal, which is convolutional and Gray encoded. A square-root raised cosine with a roll-off factor of 40% digital filter will be implemented for signal shaping. After filtering, the convolutionally encoded 8PSK signal, modulated by a carrier, forms the input to a digital to analogue converter (DAC). The resultant modulated convolutionally encoded 8PSK signal is obtained at the output of the DAC.

Both the modulator and demodulator IF sections and channel filters could be implemented using analogue circuitry, to convert the baseband signal to IF frequency and back from IF to baseband signal, respectively.

The demodulator part of the modem could be implemented using three DSPs as shown in Fig. 9.1. DSP2 is used for demodulation, which consist of carrier removal and carrier phase correction (Section 4.7 and 7.3). The demodulated signal is then filtered by a 40% square-root raised cosine digital filter. The resultant data symbol is then passed to DSP4 for carrier and bit-timing synchronisation [74] [75] and Section 4.7. Data symbols are passed to DSP3 from the demodulation and filtering DSP which decodes the signal using the Viterbi-algorithm decoder described in Section 8.4. A good speed up procedure is to use DSP2 to process symbol r_{i+1} while the rest of the system (DSP3 and DSP4) are processing symbol r_i.

At the end of every symbol period, DSP3 (Viterbi-algorithm decoder) outputs a detected symbol-sample to the output device. The whole demodulation part (DSP2, DSP3 and DSP4) must process and detect a symbol-sample within a symbol period, which could be used as a symbol interrupt for all DSPs in the demodulator part of the modem.

The possibility of implementing the required functions using a very small number of Very Large Scale Integration, (VLSI), integrated circuits requires further studies.

9.2 Conclusions

Several shapes of modulating waveforms have been tested for data-transmission systems, using DEQPSK, OQPSK, CE8PSK and CDE8PSK signals, over a nonlinear and bandlimited satellite channel. The results indicate that the most cost effective arrangement is to use signals 2A or 2B (with α = 40%, a signal with a truncation length of $5T$ (40 taps), and depending upon whether a DEQPSK or OQPSK (signal 2A) or a CE8PSK (signal 2B) is used), with the HPA operating slightly below saturation, which is a very promising system to be used in TDMA environment and gives 2.4 dB improvement in comparison with uncoded QPSK signal. Bandwidth and power efficiency cannot be improved by increasing the HPA OBO value. Using a Viterbi-algorithm decoder for convolutionally encoded 8PSK signals is a very promising technique in that it yields relatively small degradation in tolerance to noise in comparison with uncoded PSK signals. The method of feed forward carrier synchronisation for CE8PSK is a promising technique with the use of phase estimator, which gives excellent performance and small degradation in tolerance to noise in comparison with that of an uncoded QPSK signal.

A method of predistorting the baseband signal which compensates the nonlinear effects of the HPA has been presented in the thesis, and the results of the tests show that a significant reduction in spectral spreading at the HPA output and better bandwidth and power efficiency can be achieved by using the baseband linearizer. The results of the investigation indicate that, with the use of baseband linearizer, the most cost effective arrangement are signals 2A or 2B (with α = 40%, a signal with a truncation length of $5T$ (40 taps), and depending upon whether a DEQPSK or OQPSK (signal 2A) or a CE8PSK (signal 2B) is used), with the HPA operating slightly below saturation.

The catastrophic failure of CE8PSK signals, caused by a wrong reference carrier phase recovered at the receiver, has been prevented by using a convolutionally and differentially encoding (CDE8PSK) technique. The penalty for this is about 0.8 dB at $P_e = 10^{-4}$.

Large parts of the hardware in the T-SAT modem have been replaced using a single digital signal processor chip rather than conventional digital circuits. The technique described in the thesis has been operated and tested for the T-SAT modem and gives excellent performance. The technique described is valid for use in other applications for a digital modem using PSK signals.

Hardware implementation of the Viterbi-algorithm decoder for convolutionally encoded 8PSK (CE8PSK) signals using a single digital signal processor chip has

been designed. The system has been constructed and successfully demonstrated in running order and showed good agreement with simulated performance figures. The Viterbi-algorithm decoder for convolutionally encoded 8PSK (CE8PSK) signals, implemented in the thesis is valid for use in other applications for a digital modem.

9.3 Originality of the study

This investigation was originated to study various types of PSK signals design for a satellite modem and a TDMA access scheme is used at the satellite. It was hoped that such an investigation may lead to the development of more promising and/or more cost-effective signal design schemes for digital satellite communication systems.

Different shapes of modulating waveforms have been considered for data-transmission systems, using different modulation signal schemes over a bandlimited and nonlinear satellite channel. Different simulation models are used to evaluate the effects of nonlinear distortion on the error-rate performances for DEQPSK and OQPSK signals when the HPA operating point at saturation and slightly backed off, this was the author's own work.

The design of rate-2/3 convolutionally encoded 8PSK (CE8PSK) signals to be used over a nonlinear and bandlimited satellite channel, in a TDMA scheme is the author's own work. The feed-forward synchronisation using phase estimator scheme for CE8PSK signals is the author's own work, although the original idea was proposed in [56] for PSK modulated carrier phase, the idea was further developed and tested by the author for CE8PSK signals. The catastrophic failure of CE8PSK signals, caused by a wrong reference carrier phase recovered at the receiver, has been prevented by using a differential encoding scheme (CDE8PSK), the decoder was originally presented in [50] [64] for different environment, but the sub-optimum decoder was proposed for use in a TDMA scheme was the author's own work.

Baseband linearizer scheme, which compensates the nonlinear effects of the HPA was designed for DEQPSK, OQPSK, CE8PSK and CDE8PSK signals, was the author's own work, although it was proposed in [70] for QPSK signals. The proposal was further developed and tested by the author for DEQPSK, OQPSK, CE8PSK, and CDE8PSK signals for use in a TDMA environment.

The development of the hardware in the T-SAT modem using single chip digital signal processor, which leads to cost and small size effective modem design, was the author's own work. The implementation of the Viterbi-algorithm decoder for convolutionally encoded 8PSK (CE8PSK) signals using a single digital signal processor chip, was the author's own work.

Finally, all computer simulation tests on the various systems were carried out by the author, and all the performance results presented in this thesis are attributed to the author. All computer programs used in the tests and digital signal processor's assembly language programs were also written by the author.

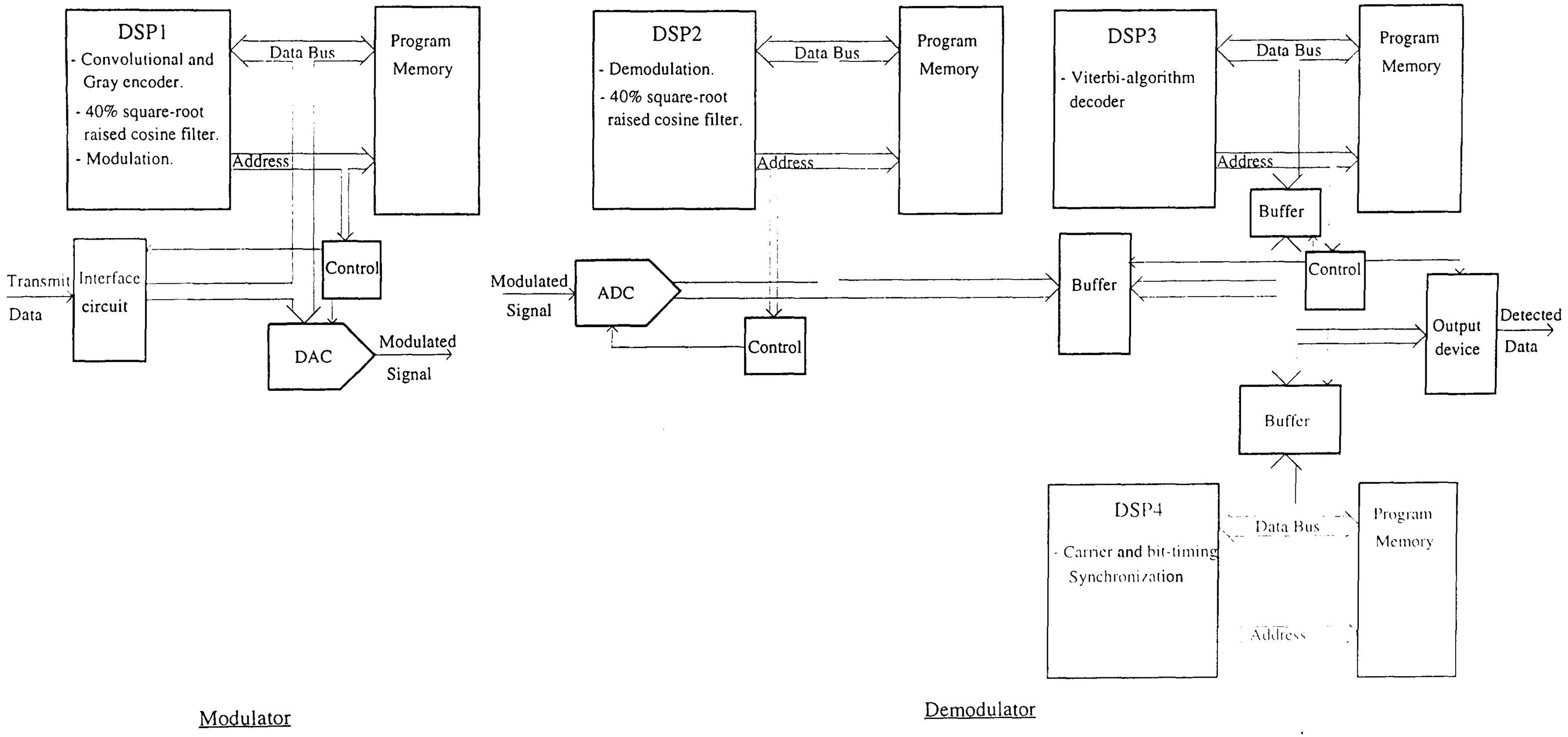

Modulator

Demodulator

Figure 9.1 An all digital signal processors satellite modem.

APPENDICES

APPENDIX A1

MATCHED-FILTER DETECTION [1]

Consider an arbitrary signal waveform $s(t)$, with a duration of T seconds, such that $s(t)$ is zero for $t < 0$ and $t > T$. This signal waveform is received in the presence of AWGN (additive white Gaussian noise) $w(t)$ having zero means and a two-sided power spectral density $\frac{1}{2}N_0$ over all positive and negative frequencies. Thus the received signal is

$$r(t) = s(t) + w(t) \qquad \text{A1.1}$$

The received signal $r(t)$ is fed to a linear filter whose transfer function is $H(f)$ and impulse response $h(t)$. The signal and noise waveforms at the filter output are $s_o(t)$ and $w_o(t)$, respectively, as shown in Fig. A1.1.

The problem is to determine the filter charateristics which maximize the signal/noise power ratio at the output of the linear filter at time $t = T$.

The output signal/noise power at time $t = T$ is

$$SNR_0 = \frac{s_0^2(T)}{\mathrm{E}[w_0^2(T)]} \qquad \text{A1.2}$$

where, this is, of course, the ratio of the instantaneous signal power to the expected noise power.

If the spectrum (Fourier transform) of $s(t)$ is $G(f)$, then

$$G(f) = \int_{-\infty}^{\infty} s(t)\exp(-j2\pi ft)dt \qquad \text{A1.3}$$

and

$$s(t) = \int_{-\infty}^{\infty} G(f)\exp(j2\pi ft)df \qquad \text{A1.4}$$

where f is the frequency in Hz and $j = \sqrt{-1}$.

The spectrum of $s_o(t)$ is $G(f)H(f)$, and

$$s_o(t) = \int_{-\infty}^{\infty} G(f)H(f)\exp(j2\pi ft)df \qquad \text{A1.5}$$

so that the magnitude of the output signal $s_o(t)$ at time $t = T$ is

$$|s_o(T)| = \left| \int_{-\infty}^{\infty} G(f)H(f)\exp(j2\pi ft)df \right|$$

and the power of the output signal at this time instant is

$$|s_o(T)|^2 = \left| \int_{-\infty}^{\infty} G(f)H(f)\exp(j2\pi fT)df \right|^2 \qquad \text{A1.6}$$

The power spectral density of $w_o(t)$ is

$$\tfrac{1}{2} N_0 |H(f)|^2$$

and the expected power level of $w_o(t)$ is

$$N = \tfrac{1}{2} N_0 \int_{-\infty}^{\infty} |H(f)|^2 df \qquad \text{A1.7}$$

Thus the ratio of instantaneous signal power to the expected noise power, at the output of the linear filter at time $t = T$ seconds, is

$$SNR_o = \frac{\left| \int_{-\infty}^{\infty} G(f)H(f)\exp(j2\pi fT)df \right|^2}{\tfrac{1}{2} N_0 \int_{-\infty}^{\infty} |H(f)|^2 df} \qquad \text{A1.8}$$

By the Schwartz inequality [3]

$$\left| \int_{-\infty}^{\infty} U(f)V(f)df \right|^2 \le \int_{-\infty}^{\infty} |U(f)|^2 df \int_{-\infty}^{\infty} |V(f)|^2 df \qquad \text{A1.9}$$

where $U(f)$ and $V(f)$ may be any finite complex functions of f.

Equality holds in Eqn. A1.9 when

$$U(f) = cV^*(f) \qquad \text{A1.10}$$

for any real constant c. $V^*(f)$ is the complex conjugate of $V(f)$.

In Eqn. A1.9 substitute $H(f)$ for $U(f)$ and $G(f)\exp(j2\pi fT)$ for $V(f)$, so that

$$\left|\int_{-\infty}^{\infty} H(f)G(f)\exp(j2\pi fT)df\right|^2 \le \int_{-\infty}^{\infty}|H(f)|^2 df \int_{-\infty}^{\infty}|G(f)\exp(j2\pi fT)|^2 df$$

$$= \int_{-\infty}^{\infty}|H(f)|^2 df \int_{-\infty}^{\infty}|G(f)|^2 df \qquad \text{A1.11}$$

From Eqn. A1.8 and A1.11, the maximum of signal/noise power is given by

$$SNR_{o(\max)} = \frac{\int_{-\infty}^{\infty}|H(f)|^2 df \int_{-\infty}^{\infty}|G(f)|^2 df}{\tfrac{1}{2}N_0\int_{-\infty}^{\infty}|H(f)|^2 df} \qquad \text{A1.12}$$

$$= \frac{1}{\tfrac{1}{2}N_0}\int_{-\infty}^{\infty}|G(f)|^2 df \qquad \text{A1.13}$$

From Parseval's theorem [3],

$$\int_{-\infty}^{\infty}|G(f)|^2 df = \int_{-\infty}^{\infty}s^2(t)dt = E \qquad \text{A1.14}$$

where E is the total signal energy of the signal waveform $s(t)$.

Thus
$$SNR_{o(\max)} = \frac{E}{\tfrac{1}{2}N_0} \qquad \text{A1.15}$$

From Eqn. A1.10, the signal/noise power ratio has its maximum value when

$$\begin{aligned} H(f) &= c[G(f)\exp(j2\pi fT)]^* \\ &= cG^*(f)\exp(-j2\pi fT) \\ &= cG(-f)\exp(-j2\pi fT) \end{aligned} \qquad \text{A1.16}$$

and
$$h(t) = \int_{-\infty}^{\infty}H(f)\exp(j2\pi ft)df$$

$$= c\int_{-\infty}^{\infty} G(-f)\exp[-j2\pi f(T-t)]df$$

$$= cs(T-t) \qquad \text{A1.17}$$

so that $$H(f) = cG^{*}(f)\exp(-j2\pi fT) \qquad \text{A1.18}$$

$$h(t) = cs(T-t) \qquad \text{A1.19}$$

From Eqns. A1.13 and A1.18, the signal power at the output of the linear filter at $t = T$, under the assumed conditions of $SNR_{o(\max)}$, is

$$\int_{-\infty}^{\infty}|H(f)|^2 df \int_{-\infty}^{\infty}|G(f)|^2 df = c^2\int_{-\infty}^{\infty}|G(f)|^2 df \int_{-\infty}^{\infty}|G(f)|^2 df$$

$$= c^2E^2 \qquad \text{A1.20}$$

Also the average noise power at the output of the linear filter is

$$N = \tfrac{1}{2}N_0\int_{-\infty}^{\infty}|H(f)|^2 df = \tfrac{1}{2}N_0c^2\int_{-\infty}^{\infty}|G(f)|^2 df = \tfrac{1}{2}N_0c^2E \qquad \text{A1.21}$$

The filter satisfying Eqns. A1.18 and A1.19 is said to be matched to the receiver signal $s(t)$ and is known as a matched filter [20], [66].

Since $s(t) = 0$ for $t < 0$ and $t > T$, it follows from Eqn. A1.19 that, $h(t) = 0$, for $t < 0$ and $t > T$, so that $h(t)$ is physically realisable.

Suppose now that the received signal is $ks(t)$ where $s(t)$ is known at the receiver but k is an unknown real number, whose value it is required to estimate as accurately as possible at the receiver. If the signal $ks(t)$ is fed to the matched filter given by Eqn. A1.19, then in the absence of noise, the output signal at time $t = T$ is the convolution of $ks(t)$ and $h(t)$, and is

$$\int_{-\infty}^{\infty} ks(t)h(T-t)dt = \int_{0}^{T} ks(t)cs(t)dt$$

$$= kc\int_{0}^{T} s^2(t)dt$$

$$= kcE \qquad \text{A1.22}$$

from Eqns. A1.14 and A1.19, E is the energy of $s(t)$, but not of $ks(t)$.

When $ks(t)$ is received in the presence of AWGN $w(t)$, the input signal to the matched filter becomes

$$r(t) = ks(t) + w(t) \qquad \text{A1.23}$$

and the output signal from the matched filter at time $t = T$ is now

$$r_o(t) = \int_0^T r(t)h(T-t)dt = \int_0^T [ks(t) + w(t)]cs(t)dt$$

$$= kc\int_0^T s^2(t)dt + c\int_0^T w(t)s(t)dt$$

$$= kcE + w_o \qquad \text{A1.24}$$

where $$w_o = c\int_0^T w(t)s(t)dt \qquad \text{A1.25}$$

w_o is a sample value of a Gaussian random variable with zero mean.

Equation A1.24 shows that

$$r_o = c\int_0^T r(t)s(t)dt \qquad \text{A1.26}$$

so that r_o could alternatively be obtained by multiplying $r(t)$ by $cs(t)$ and integrating the product over the time interval 0 to T. This operation is performed by the appropriate correlation receiver, which is therefore equivalent to the matched filter.

In order to estimate k, assuming a prior knowledge of c and E at the receiver, r_o is multiplied by $1/cE$ to give

$$\frac{r_o}{cE} = k + \frac{w_o}{cE} \qquad \text{A1.27}$$

r_o/cE is the estimate of k given by the matched filter. w_o/cE is the error in this estimate and is introduced by the Gaussian noise. The matched filter maximizes the ratio of instantaneous signal power to average noise power in the estimate of k.

Suppose now that k is equally likely to have one of two values k_1 and k_2, where $k_2 > k_1$, and where k_1 and k_2 are both known at the receiver. $ks(t)$ is here a binary signal element.

It can be seen from Eqn. A1.27 that in the absence of noise

$$\frac{r_o}{cE} = k \qquad \text{where } k = k_1 \text{ or } k_2 \qquad \text{A1.28}$$

so that k is now given exactly by the value of r_o/cE. However, when $ks(t)$ is received together with the noise waveform $w(t)$, r_o/cE will not normally have the correct value k_1 or k_2.

To detect the value of k with the minimum probability of error, r_o/cE is now compared with a threshold level of $\frac{1}{2}(k_1 + k_2)$, which lies half way between k_1 and k_2.

When

$$r_o < \tfrac{1}{2}cE(k_1 + k_2), \qquad k \text{ is detected as } k_1,$$

and when

$$r_o > \tfrac{1}{2}cE(k_1 + k_2), \qquad k \text{ is detected as } k_2.$$

It can be shown that this arrangment minimizes the probability of error under the assumed conditions [50].

The probability of error in a detection process may be determined as follows. From Eqn. A1.24

$$r_o = kcE + w_o$$

where

$$w_o = c\int_0^T w(t)s(t)dt \qquad \text{A1.29}$$

From Eqn. A1.21, w_o is sample value of a Gaussian random variable with zero mean and variance

$$\eta^2 = \tfrac{1}{2}N_0c^2E \qquad \text{A1.30}$$

Thus

$$r_o/cE = k + w_o/cE \qquad \text{A1.31}$$

where w_o/cE is a sample value of a Gaussian random variable with zero mean and variance

$$\sigma^2 = \eta^2 / c^2 E^2 = \tfrac{1}{2} N_0 / E \qquad \text{A1.32}$$

when k_1 is received, k is wrongly detected if

$$r_o / cE > \tfrac{1}{2}(k_1 + k_2)$$

or
$$w_o / cE > d$$

where
$$d = \tfrac{1}{2}(k_1 + k_2) \qquad \text{A1.33}$$

so that the probability of error is

$$P_{e1} = \int_d^\infty \frac{1}{\sqrt{2\pi\sigma^2}} \exp(\frac{-w^2}{2\sigma^2}) dw = \int_{d/\sigma}^\infty \frac{1}{\sqrt{2\pi}} \exp(\frac{-w^2}{2}) dw$$

$$= Q(\frac{d}{\sigma}) \qquad \text{A1.34}$$

where
$$Q(y) = \int_y^\infty \frac{1}{\sqrt{2\pi}} \exp(\frac{-w^2}{2}) dw \qquad \text{A1.35}$$

is called the Q-function.

When k_2 is received, k is wrongly detected if

$$r_o / cE < \tfrac{1}{2}(k_1 + k_2)$$

or
$$w_o / cE < -d$$

so that the probability of error is

$$P_{e2} = \int_{-\infty}^{-d} \frac{1}{\sqrt{2\pi\sigma^2}} \exp(\frac{-w^2}{2\sigma^2}) dw = \int_d^\infty \frac{1}{\sqrt{2\pi\sigma^2}} \exp(\frac{-w^2}{2\sigma^2}) dw$$

$$= Q(\frac{d}{\sigma}) \qquad \text{A1.36}$$

Clearly, the probability of error is the same, whether k_1 or k_2 is received, and is

$$P_e = P_{e1} = P_{e2} = Q(\frac{d}{\sigma}) = Q(\frac{d}{\sqrt{\tfrac{1}{2} N_0 / E}}) = Q(\sqrt{\frac{d^2 E}{\tfrac{1}{2} N_0}}) \qquad \text{A1.37}$$

It can be seen from Eqn. A1.37 that the error probability is independent of the shape of the signal waveform, and is dependent only on d, E and N_0.

It has been shown that the matched filter maximizes the signal/noise power at its output, so that for given values of k_1 and k_2 and therefore for a given value of d, it minimizes the average noise power at its output.

In a situation such as that considered here, where the wanted signal k is equally likely to have one of the two values k_1 and k_2, and is received in the presence of a zero-mean Gaussian random variable, the detection process that minimizes the probability of error compares the received signal (in this case $r_o/cE = k + w_o/cE$) with a threshold level half way between the two possible values k_1 and k_2 of the wanted signal. The wanted signal k is now detected as k_1 or k_2 depending upon whether the received signal lies below or above the threshold, that is depending upon whether the received signal is nearer to k_1 or k_2, respectively.

The combination of the matched filter and the following detection process in which the output from the matched filter is compared with the appropriate threshold level, is an arrangement of matched filter detection. This is the optimum detection process for the wanted signal, under the assumed conditions, and it minimizes the probability of error in a detection process.

The average energy of the two waveforms $k_1 s(t)$ and $k_2 s(t)$ is

$$\tfrac{1}{2}(k_1^2 + k_2^2)E = \tfrac{1}{4}(k_1 - k_2)^2 E + \tfrac{1}{4}(k_1 + k_2)^2 E \qquad \text{A1.38}$$

where E is the energy of $s(t)$. For any given values of $k_1 - k_2$ and E, the average of the two signal waveforms has a minimum value of d^2E when $k_1 = k_2 = -d$. But from Eqn. A1.37, the probability of error is dependent only on d, E and N_0, so that for a given probability of error and given values of d, and E, the average signal/noise power ratio at the input to the matched-filter has its minimum value when $k_1 = -k_2 = -d$. In other words, the tolerance to AWGN is maximized under these conditions.

When $k_1 = -d$ and $k_2 = d$ the optimum decision threshold is zero, so that k is detected as k_1, when $r_o < 0$, and k is detected as k_2 when $r_o > 0$.

The probability of error in the detection of k is now

$$Q(\frac{d}{\sigma}) = Q(\sqrt{\frac{d^2E}{\tfrac{1}{2}N_0}}) = Q(\sqrt{\frac{E_d}{\tfrac{1}{2}N_0}}) \qquad \text{A1.39}$$

where E_d is the energy of each signal waveform $k_1 s(t)$ and $k_2 s(t)$. The error probability is a function only of the signal/noise power ratio at the input to the matched filter, and has its minimum value for any given signal/noise ratio.

This is clearly the optimum combination of signal design and detection process for a binary-coded signal, where the two binary values are equally likely and the signal is received in the presence of AWGN. Any waveform of duration T seconds may be used for the transmitted signal-element, so long as it has the required energy and so long as the waveform corresponding to one of the two binary values is the negative of that corresponding to the other binary value. Such a signal is known as a binary antipodal signal-element.

Since a decision threshold of zero is used for the detection of the binary value, the receiver requires no prior knowledge of the values of k_1 and k_2 other than that k_1 is negative and k_2 is positive. In other words, the receiver requires no prior knowledge of the received signal level in order to achieve optimum detection of the element binary value.

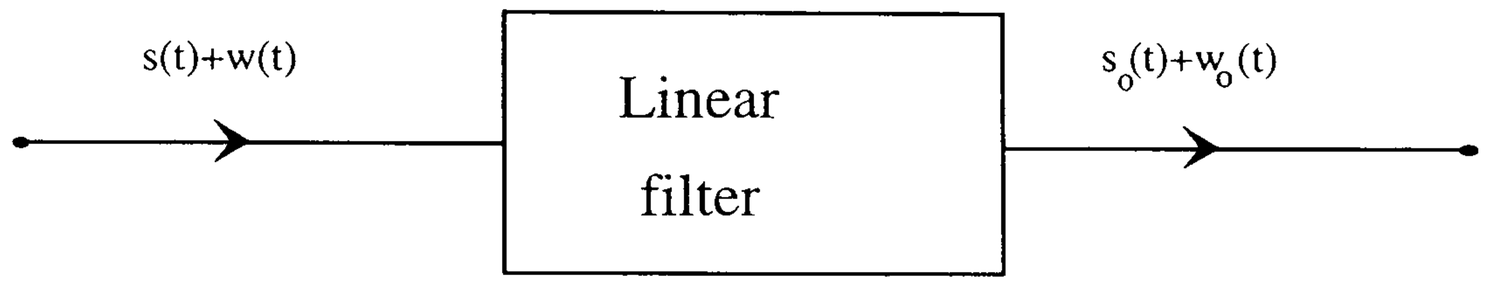

Figure A1.1 Linear filtering of $r(t)$.

APPENDIX A2

IMPULSE RESPONSES OF THE TRANSFER FUNCTIONS GIVING A RECTANGULAR SPECTRUM AND A SINUSOIDAL ROLL-OFF SPECTRUM

A2.1 Rectangular spectrum

The transfer function giving a rectangular spectrum is

$$H(f)=\begin{cases}T, & -\dfrac{1}{2T}<f<\dfrac{1}{2T}\\ 0, & \text{elsewhere}\end{cases} \qquad \text{A2.1}$$

as shown in Fig. 2.3a in Section 2.2.1.

The impulse response of the transfer function is

$$h(t)=\int_{-\infty}^{\infty}H(f)\exp(j2\pi ft)\,df=\int_{-1/2T}^{1/2T}T\exp(j2\pi ft)\,df$$

$$=T\left[\frac{\exp(j2\pi ft)}{j2\pi f}\right]_{-1/2T}^{1/2T}=\frac{\exp(j\pi t/T)-\exp(-j\pi t/T)}{j2\pi t/T}$$

$$=\frac{\sin(\pi t/T)}{\pi t/T} \qquad \text{A2.2}$$

as shown in Fig. 2.3b in Section 2.2.1.

A2.2 Sinusoidal roll-off spectrum

The transfer function of a sinusoidal roll-off spectrum is

$$H(f)=\begin{cases}T & 0\le|f|<\dfrac{(1-\alpha)}{2T}\\ \dfrac{T}{2}\left[1-\sin\dfrac{\pi T}{\alpha}\left(|f|-\dfrac{1}{2T}\right)\right] & \dfrac{(1-\alpha)}{2T}\le|f|\le\dfrac{(1+\alpha)}{2T}\\ 0 & \text{elsewhere}\end{cases} \qquad \text{A2.3}$$

as shown in Fig. A2.1a, where the ratio $\alpha = f_x/f_c$ is called the roll-off factor. Equation A2.3 can be written as

$$H(f) = \begin{cases} T + H_1(f) & f_c - f_x < |f| < f_c \\ H_1(f) & f_c < |f| < f_c + f_x \\ 0 & \text{elsewhere} \end{cases} \qquad \text{A2.4}$$

where $f_c = 1/2T$ and

$$H_1(f) = \begin{cases} \frac{T}{2}\{\cos\frac{\pi[|f| - (f_c - f_x)]}{2f_x} - 1\} & f_c - f_x < |f| < f_c \\ \frac{T}{2}\{\cos\frac{\pi[|f| - (f_c - f_x)]}{2f_x} + 1\} & f_c < |f| < f_c + f_x \\ 0 & \text{elsewhere} \end{cases} \qquad \text{A2.5}$$

Assume that the overall filter has zero phase shift. (A linear phase term of course results in a corresponding time delay.) Assume further that $H_1(f)$ has odd symmetry about f_c. Then

$$H_1(f_c + |f|) = -H_1(f_c - |f|) \qquad \text{for } f_x < |f| \qquad \text{A2.6}$$

The sinusoidal roll-off spectrum has this property, as shown in Fig. A2.1b, with the overall characteristic shown in Fig. A2.1a.

Taking the Fourier transform of Eqn. A2.4, by superposition, the impulse is given by

$$h(t) = \frac{\sin(\pi t/T)}{\pi t/T} + h_1(t) \qquad \text{A2.7}$$

as can be seen from Eqn. A2.2, and

$$h_1(t) = \int_{-\infty}^{\infty} H_1(f)\exp(j2\pi ft)df \qquad \text{A2.8}$$

But $H_1(f)$, having zero (or linear) phase shift, must be even in f (Fig. A2.1b) [15,p.182]. Then

$$h_1(t) = \int_{-\infty}^{\infty} H_1(f)\exp(j2\pi ft)df$$

$$= 2\int_{f_c - f_x}^{f_c + f_x} H_1(f)\cos(2\pi ft)df$$

$$= 2\int_{f_c - f_x}^{f_c} H_1(f)\cos(2\pi ft)df + 2\int_{f_c}^{f_c + f_x} H_1(f)\cos(2\pi ft)df \qquad \text{A2.9}$$

using the fact that $H_1(f) = 0$, for $|f| > f_c + f_x$.

Using the property of odd symmetry about f_c by letting $f = f_c - x$ in the first integral of Eqn. A2.9 and $f = f_c + x$ in the second integral. The new dummy variable x ranges between 0 and f_c in both integrals, and the two may be combined into the following one integral, after using the odd-symmetry property:

$$h_1(t) = -2\int_{f_x}^{0} H_1(f_c - x)\cos 2\pi(f_c - x)t\, dx + 2\int_{0}^{f_x} H_1(f_c + x)\cos 2\pi(f_c + x)t\, dx$$

$$= 2\int_{0}^{f_x} [H_1(f_c + x)\cos 2\pi(f_c + x)t + H_1(f_c - x)\cos 2\pi(f_c - x)t]\ dx \qquad \text{A2.10}$$

After using the odd-symmetry property (Eqn. A2.6), it becomes

$$h_1(t) = 2\int_{0}^{f_x} [H_1(f_c + x)\cos 2\pi(f_c + x)t - H_1(f_c + x)\cos 2\pi(f_c - x)t]\ dx$$

$$= 2\int_{0}^{f_x} H_1(f_c + x)[\cos 2\pi(f_c + x)t - \cos 2\pi(f_c - x)t]\ dx$$

$$= -4\sin 2\pi f_c t \int_{0}^{f_x} H_1(f_c + x)\sin 2\pi xt\ dx$$

$$= -4\sin(\pi t/T)\int_{0}^{f_x} H_2(f)\sin 2\pi xt\ dx \qquad \text{A2.11}$$

where $$H_2(f) = \begin{cases} \dfrac{T}{2}\left(1 - \sin\dfrac{\pi x}{2f_x}\right) & , x < f_x \\ 0 & , x > f_x \end{cases} \qquad \text{A2.12}$$

as shown in Fig. A2.1c.

Using Eqn. A2.11, A2.7 can be written as

$$h(t)=\frac{\sin(\pi t/T)}{\pi/T}\{\frac{1}{t}-2\pi\int_0^{f_x}(1-\sin\frac{\pi x}{2f_x})\sin 2\pi xt\ \ dx\}$$

$$=\frac{\sin(\pi t/T)}{\pi/T}\{\frac{1}{t}-2\pi\int_0^{f_x}[\sin 2\pi xt+\frac{1}{2}\cos(\frac{\pi}{2f_x}+2\pi t)x-\frac{1}{2}\cos(\frac{\pi}{2f_x}-2\pi t)x]\ \ dx\}$$

$$=\frac{\sin(\pi t/T)}{\pi/T}\{\frac{1}{t}-2\pi\left[\frac{-\cos 2\pi xt}{2\pi t}+\frac{\frac{1}{2}\sin(\pi x/(2f_x)+2\pi xt)}{\pi/(2f_x)+2\pi t}-\frac{\frac{1}{2}\sin(\pi x/(2f_x)-2\pi xt)}{\pi/(2f_x)-2\pi t}\right]_0^{f_x}\}$$

$$=\frac{\sin(\pi t/T)}{\pi/T}\{\frac{1}{t}-2\pi\left[\frac{1-\cos 2\pi f_x t}{2\pi t}+\frac{\frac{1}{2}\cos(2\pi f_x t)}{\pi/(2f_x)+2\pi t}-\frac{\frac{1}{2}\cos(2\pi f_x t)}{\pi/(2f_x)-2\pi t}\right]\}$$

$$=\frac{\sin(\pi t/T)}{\pi/T}\{\frac{1}{t}-\left[\frac{1-\cos 2\pi f_x t}{t}+\frac{\cos(2\pi f_x t)}{1/(2f_x)+2t}-\frac{\cos(2\pi f_x t)}{1/(2f_x)-2t}\right]\}$$

$$=\frac{\sin(\pi t/T)}{\pi/T}\{\frac{\cos 2\pi f_x t}{t}+\frac{2f_x\cos(2\pi f_x t)}{1+4f_x t}-\frac{2f_x\cos(2\pi f_x t)}{1-4f_x t}\}$$

$$=\frac{\sin(\pi t/T)}{\pi/T}\cos 2\pi f_x t[2f_x\{\frac{1}{2f_x t}+\frac{1}{1+4f_x t}-\frac{1}{1-4f_x t}\}]$$

$$=\frac{\sin(\pi t/T)}{\pi/T}\frac{\cos 2\pi f_x t}{t[1-(4f_x t)^2]}\qquad\text{A2.13}$$

But $\alpha=f_x/f_c$ and so $f_x=\alpha f_c=\alpha/2T$, thus Eqn. A2.13 can be written as

$$h(t)=\frac{\sin(\pi t/T)}{\pi t/T}\frac{\cos(\alpha\pi t/T)}{1-4\alpha^2t^2/T^2}\qquad\text{A2.14}$$

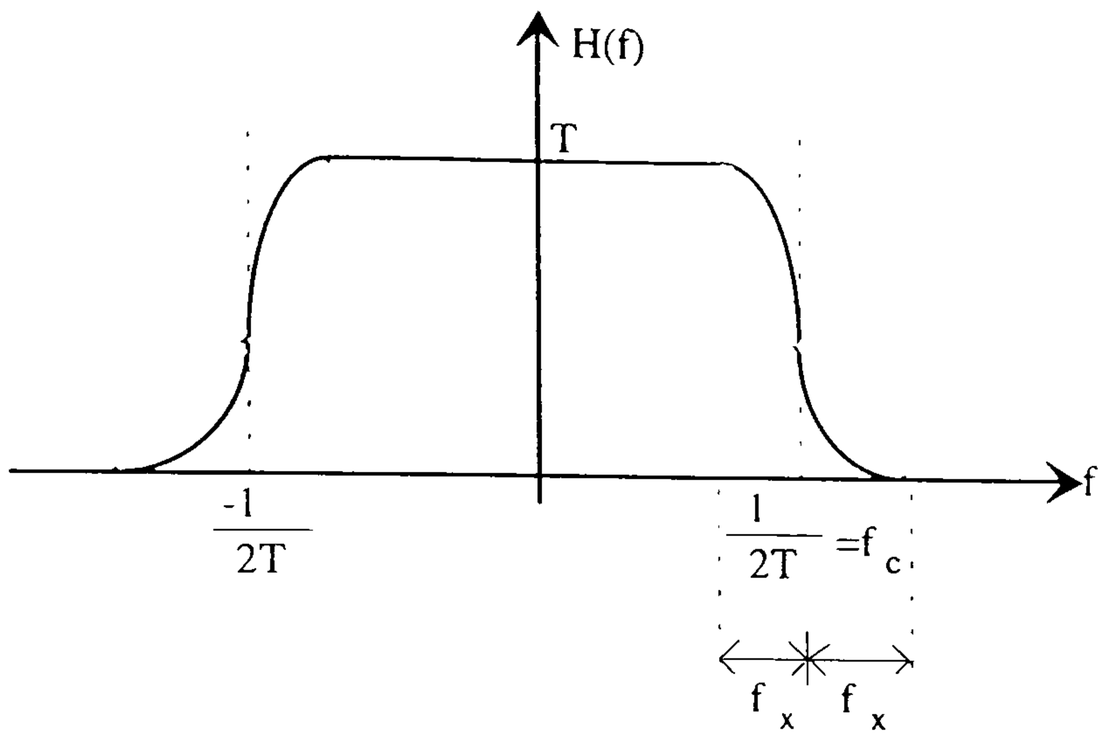

(a)

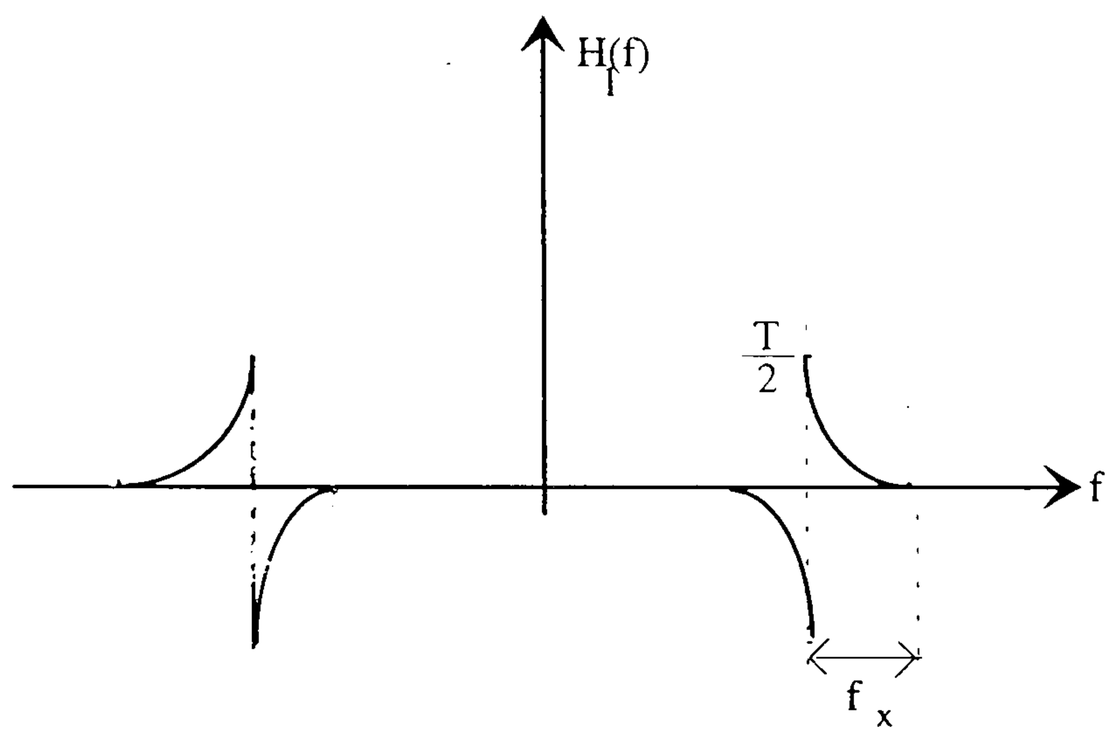

(b)

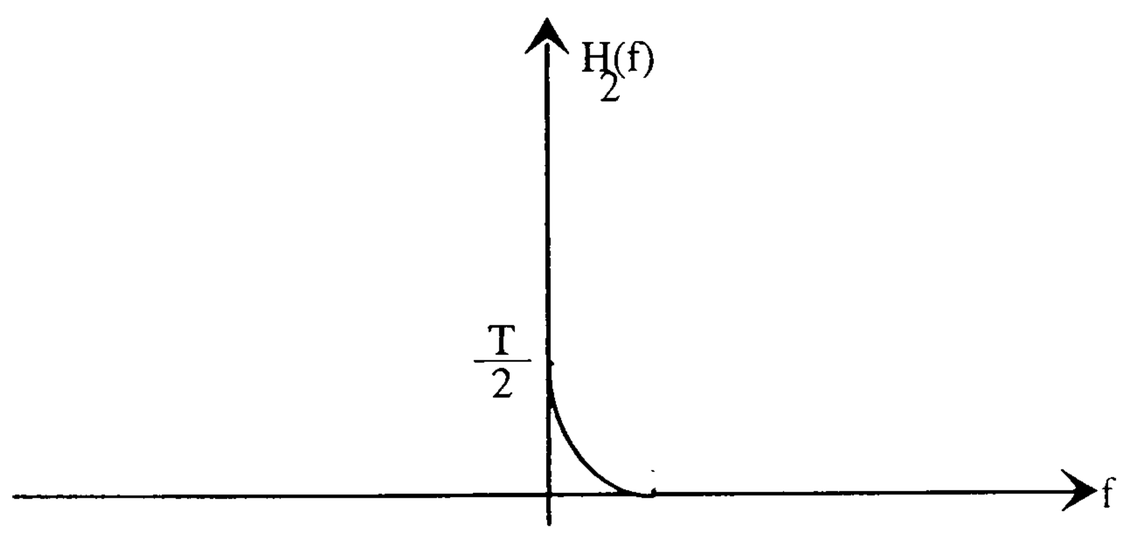

(c)

Figure A2.1 (a) Sinusoidal rolloff spectrum. (b) and (c) spectra of $H_1(f)$ and $H_2(f)$, respectively.

APPENDIX A3

THE RELATIONSHIP OF $2E_b/N_0$ BETWEEN THE UPLINK AND DOWNLINK OF A SATELLITE CHANNEL

In conventional amplifier satellite transponders, the noise contributions of the uplink and downlink are added according to the following expression [6, p42]:

$$(2E_b/N_0)_{\mathrm{T}}^{-1} = (2E_b/N_0)_{\mathrm{U}}^{-1} + (2E_b/N_0)_{\mathrm{D}}^{-1} \qquad \text{A3.1}$$

where E_b is the energy per bit, $\frac{1}{2}N_0$ is the two-sided noise power spectral density, and the subscripts U, D, and T denote the uplink, downlink and total, respectively. In Eqn. A3.1, the quantities are in ratios and not dBs.

Normally the value of $2E_b/N_0$ in the uplink is made high enough to compensate for the restricted performance caused by the fact that less power is available in the downlink.This is because the noise and interference contributions in the uplink are passed together with the wanted signal to the downlink where further noise and interference are added. If the same value of E_b/N_0 is used for both up and downlink, so that

$$(2E_b/N_0)_{\mathrm{T}} = (2E_b/N_0)_{\mathrm{U}} = (2E_b/N_0)_{\mathrm{D}} \qquad \text{A3.2}$$

then $2E_b/N_0$ must be at least 3dB greater than before in order to achieve the required value of $(2E_b/N_0)_{\mathrm{T}}$.

Appendix A4

BASEBAND EQUIVALENT MODELS OF SYMMETRICAL BANDPASS FILTERS

Figure A4.1 shows the baseband equivalent model of bandpass modulated signals. The bandpass filter, with a limited bandwidth, represents the cascade of the transmitter BPF (bandpass filter), the channel filter, and receiver BPF. It is assumed that perfect carrier and symbol timing synchronization signals are available, the noise is negligible on the channel, and the channel is linear. Note that due to the linearity of the system, the conclusions are not restricted to the noiseless case.

A4.1 Baseband equivalent model of the BPF at the transmitter [6, p131]

In Fig. A4.1b, the modulator contains only a premodulation lowpass filter, LPF_T. The modulated signal is

$$s_1(t) = [a(t) * h_L(t)]c(t) \qquad \text{A4.1}$$

where $a(t)$ is the input signal, $h_L(t)$ is the impulse response of the lowpass filter, $c(t)$ is the sinusoidal carrier signal, and * denotes the convolution, defined by

$$a(t) * h_L(t) = \int_{-\infty}^{\infty} a(\tau) h_L(t-\tau) d\tau \qquad \text{A4.2}$$

Taking the Fourier transform of Eqn. A4.1 and noting that convolution in the time domain corresponds to multiplication in frequency domain, and that convolution in the frequency domain corresponds to multiplication in the time domain, the spectrum of $s_1(t)$ can be written as

$$S_1(f) = [A(f) H_L(f)] * C(f) \qquad \text{A4.3}$$

where $A(f)$, $H_L(f)$ and $C(f)$ are the Fourier transforms of $a(t)$, $h_L(t)$ and $c(t)$, respectively. Since convolution of a baseband spectrum with a sinusoidal carrier results in a double-side band (DSB) spectrum centered around the carrier frequency f_c, Equation A4.3 can be written as

$$S_1(f) = \tfrac{1}{2}\{A(f-f_c)H_L(f-f_c) + A(f+f_c)H_L(f+f_c)\} \qquad \text{A4.4}$$

In Fig. A4.1c, the linear modulator contains only a postmodulation bandpass filter, BPF_T. The modulating signal is

$$s_2(t) = [a(t)c(t)] * h_B(t) \qquad \text{A4.5}$$

where $h_B(t)$ is the impulse response of the BPF_T. The corresponding Fourier transform is

$$S_2(f) = [A(f) * C(f)]H_B(f)$$

$$= \tfrac{1}{2}[A(f - f_c) + A(f + f_c)]H_B(f) \qquad \text{A4.6}$$

where $H_B(f)$ is the Fourier transform of $h_B(t)$.

The amplitude spectra of the premodulated and postmodulated filter signals, represented by Eqns. A4.4 and A4.6, respectively, are the same if $S_1(f) = S_2(f)$, that is

$$H_L(f - f_c) = H_L(f + f_c) = H_B(f) \qquad \text{A4.7}$$

bearing in mind that the bandpass filter has a limited bandwidth. Hence, the equivalent condition is satisfied if the bandpass filter, $H_B(f)$, has the same transfer function as lowpass filter, $H_L(f)$, shifted so as to be centered around the carrier frequency f_c. Thus if a transmitter bandpass filter is symmetrical around the center frequency, the baseband equivalent model of it can be easily obtained by shifting the center frequency to zero frequency.

A4.2 Baseband equivalent model of the BPF at the receiver

In Fig. A4.1d, the demodulator contains a predemodulated bandpass filter, BPF_R. The signal to the demodulator is

$$s_{11}(t) = [a(t)c(t)] * h_B(t)c(t)$$

The corresponding spectrum is

$$S_{11}(f) = \tfrac{1}{2}[A(f - f_c) + A(f + f_c)]H_B(f) * C(f)$$

$$= \tfrac{1}{2}[A(f - f_c)H_B(f) + A(f + f_c)H_B(f)] * C(f)$$

$$= \tfrac{1}{4}[A(f - f_c - f_c)H_B(f - f_c) + A(f - f_c + f_c)H_B(f + f_c)$$

$$+ A(f + f_c - f_c)H_B(f - f_c) + A(f + f_c + f_c)H_B(f + f_c)] \qquad \text{A4.8}$$

The wide LPF will block the second-order spectral components, so that amplitude spectrum of the signal to the detector is

$$\hat{S}_{11}(f) = \tfrac{1}{4} A(f)[H_B(f - f_c) + H_B(f + f_c)] \qquad \text{A4.9}$$

In Fig. A4.1e, the linear demodulator contains only a postdemodulator lowpass filter, LPF_R. The demodulated signal is

$$s_{22}(t) = [a(t)c(t)c(t)] * h_L(t)$$

The corresponding Fourier transform is

$$S_{22}(f) = [A(f) * C(f)] * C(f)H_L(f)$$

$$= \tfrac{1}{2}[A(f - f_c) + A(f + f_c)] * C(f)H_L(f)$$

$$= \tfrac{1}{4}[A(f - f_c - f_c) + A(f - f_c + f_c) + A(f + f_c - f_c) + A(f + f_c + f_c)]H_L(f)$$

A4.10

The second-order spectral components are blocked by the LPF_R, so that the amplitude spectrum of the signal to the detector becomes

$$\hat{S}_{22}(f) = \tfrac{1}{4}[A(f)H_L(f) + A(f)H_L(f)] \qquad \text{A4.11}$$

The amplitude spectra to the detector, represented by Eqns. A4.9 and A4.11, are the same if $\hat{S}_{11}(f) = \hat{S}_{22}(f)$, that is

$$H_L(f) = H_B(f - f_c) = H_B(f + f_c) \qquad \text{A4.12}$$

bearing in mind that the bandpass filter has a limited bandwidth. Therefore the equivalent condition is satisfied if the bandpass filter, $H_B(f)$, has the same transfer function as the lowpass filter, $H_L(f)$, shifted so as to be centered around zero frequency. Thus if a receiver bandpass filter is symmetrical around the center frequency, the baseband equivalent model of it can be easily obtained by shifting the center frequency to zero frequency.

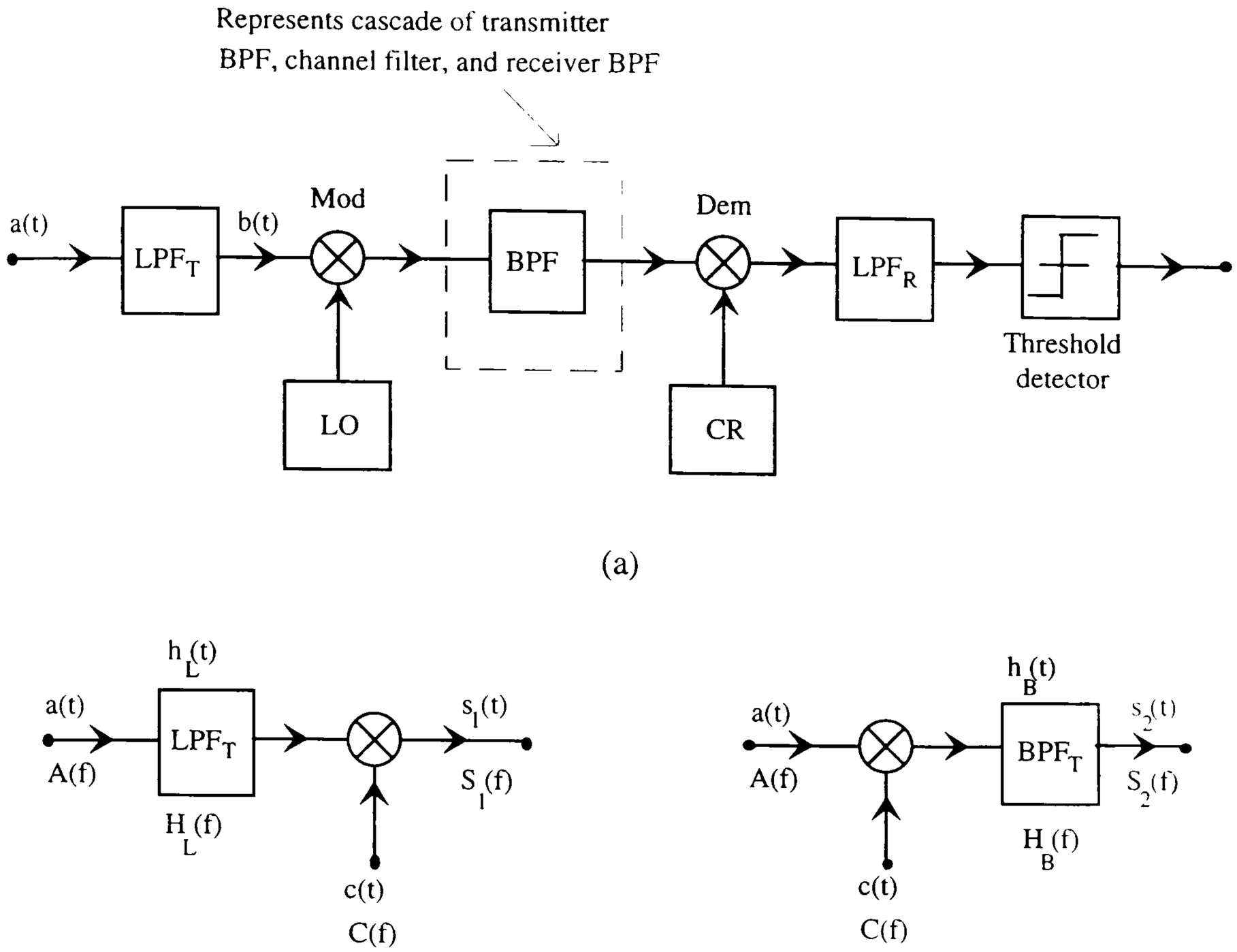

Figure A4.1 Baseband equivalent model of bandpass modulated signals, (a) Modulator, channel, demodulator. Mod is modulator, Dem is demodulator, LPF is lowpass filter, BPF is bandpass filter, LO is local oscillator, CR is carrier recovery, and Det is detector. (b) Linear modulator having a premodulation LPF only. (c) Modulator having a postmodulation BPF only. $h_L(t)$ and $h_B(t)$ are impulse responses of the LPF and BPF, respectively. (d) Demodulator having a predetection BPF. (e) Demodulator having a postdetection LPF only.

APPENDIX A5

ANALYSIS OF QUADRATURE CROSSTALK IN BANDPASS SIGNALS [93]

Consider a bandpass signal $s(t)$ is given by

$$s(t) = a(t)\cos 2\pi f_c t - b(t)\sin 2\pi f_c t$$

$$= \tfrac{1}{2}c(t)\exp(j2\pi f_c t) + \tfrac{1}{2}c^*(t)\exp(-j2\pi f_c t) \qquad \text{A5.1}$$

where

$$c(t) = a(t) + jb(t) \qquad \text{A5.2a}$$

$$c^*(t) = a(t) - jb(t) \qquad \text{A5.2b}$$

where $j = \sqrt{-1}$ and f_c is the carrier frequency.

The signal $c(t)$ is the complex lowpass envelope of $s(t)$ while $a(t)$ and $b(t)$ are the inphase and quadrature components of $s(t)$, respectively.

Hence, the Fourier transform of $s(t)$, giving by the frequency translation theorem, is

$$S(f) = \tfrac{1}{2}C(f - f_c) + \tfrac{1}{2}C^*(-f - f_c) \qquad \text{A5.3}$$

where $C(f)$ is the Fourier transform of $c(t)$.

The process of bandpass filtering $s(t)$ through a bandpass filter is

$$y(t) = h(t) * s(t) \qquad \text{A5.4}$$

where $h(t)$ is the impulse response of the bandpass filter and * denotes the convolution (see Eqn. A4.2 for the definition).

The corresponding Fourier transform is

$$Y(f) = H(f)S(f) \qquad \text{A5.5}$$

where $Y(f)$, $H(f)$ and $S(f)$ are the Fourier transform of $y(t)$, $h(t)$ and $s(t)$, respectively.

The impulse response of the bandpass filter can be expressed as

$$h(t) = r(t)\cos 2\pi f_c t - q(t)\sin 2\pi f_c t \qquad \text{A5.6}$$

$$= \tfrac{1}{2} d(t)\exp(j2\pi f_c t) + \tfrac{1}{2} d^*(t)\exp(-j2\pi f_c t) \qquad \text{A5.7}$$

where

$$d(t) = r(t) + jq(t) \qquad \text{A5.8a}$$

$$d^*(t) = r(t) - jq(t) \qquad \text{A5.8b}$$

and f_c is the centered frequency of the bandpass filter. (Assume it is the same as the carrier frequency of $s(t)$.

The signal $d(t)$ is the complex lowpass envelope of $h(t)$, while $r(t)$ and $q(t)$ are the inphase and quadrature components of $h(t)$, respectively.

The Fourier transform of $h(t)$ is given by

$$H(f) = D(f - f_c) + D^*(-f - f_c) \qquad \text{A5.9}$$

where $D(f)$ is the Fourier transform of $d(t)$.

The bandpass signals of $d(t)$ and $d^*(t)$ in Eqn. A5.7 can be written as

$$d(t)\exp(j2\pi f_c t) = r(t)\exp(j2\pi f_c t) + jq(t)\exp(j2\pi f_c t) \qquad \text{A5.10a}$$

and $$d^*(t)\exp(j2\pi f_c t) = r(t)\exp(j2\pi f_c t) - jq(t)\exp(j2\pi f_c t) \qquad \text{A5.10b}$$

The corresponding Fourier transforms are

$$D(f - f_c) = R(f - f_c) + jQ(f - f_c) \qquad \text{A5.11a}$$

$$D^*(-f - f_c) = R(f - f_c) - jQ(f - f_c) \qquad \text{A5.11b}$$

where $R(f)$ and $Q(f)$ are the Fourier transform of $r(t)$ and $q(t)$, bearing in mind that $r(t)$ and $q(t)$ are the inphase and quadrature components of the impulse response. Thus

$$R(f - f_c) = \tfrac{1}{2}[D(f - f_c) + D^*(-f - f_c)] \qquad \text{A5.12}$$

and $$jQ(f - f_c) = \tfrac{1}{2}[D(f - f_c) - D^*(-f - f_c)] \qquad \text{A5.13}$$

If the signal from the output of the baseband equivalent model of the filter is not real for a real input, or if the output from it is not purely imaginary for an imaginary input, there is crosstalk introduced by the bandpass filter. From Eqn. A5.13, the crosstalk interference (CI) is represented by

$$CI = jQ(f - f_c) \qquad \text{A5.14}$$

Case I <u>Symmetrical bandpass filter</u>

If the bandpass filter transfer function $H(f)$ is symmetrical in amplitude and asymmetrical in phase about f_c (i.e., $D(f - f_c) = D^*(-f - f_c)$), then $jQ(f - f_c) = 0$ and so CI=0. Since there is no interference between the inphase and quadrature components, there is no crosstalk.

Case II <u>Nonsymmetrical bandpass filter</u>

If the bandpass filter transfer function $H(f)$ is not symmetrical in amplitude or not asymmetrical in phase about f_c (i.e., $D(f - f_c) \neq D^*(-f - f_c)$), then $jQ(f - f_c) \neq 0$ and $CI = jQ(f - f_c)$. There is crosstalk between the inphase and quadrature components, introduced by the bandpass filter.

APPENDIX A6

PROOF OF THE COMPLEX SIGNAL REPRESENTATION OF SYSTEMS USING QUADRATURE MODULATED SIGNAL [94]

A6.1 Representation of the modulated signal

Let $R(.)$ represent the real part of (.). If $a(t)$ and $b(t)$ are the information bearing signals then:

$$S(t) = \sqrt{2}\{a(t)\cos\omega_c t - b(t)\sin\omega_c t\} \quad \text{A6.1}$$

$$= \sqrt{2}\{a(t)\cos\omega_c t - b(t)\cos(\omega_c t - \pi/2)\} \quad \text{A6.2}$$

$$= \sqrt{2}R\{a(t)\exp(j\omega_c t) - b(t)\exp j(\omega_c t - \pi/2)\} \quad \text{A6.3}$$

$$= \sqrt{2}R\{a(t)\exp(j\omega_c t) - b(t)\exp(j\omega_c t)\exp(-j\pi/2)\} \quad \text{A6.4}$$

now $\exp(-j\pi/2) = \cos(-\pi/2) + j\sin(-\pi/2)$ A6.5

$$= 0 - j \quad \text{A6.6}$$

where $j = \sqrt{-1}$

$$\therefore S(t) = \sqrt{2}\{a(t) + jb(t)\}R\{\exp(j\omega_c t)\} \quad \text{A6.7}$$

If

$$s(t) = a(t) + jb(t) \quad \text{A6.8}$$

then

$$S(t) = \sqrt{2}s(t)R\{\exp(j\omega_c t)\} \quad \text{A6.9}$$

The auto-correlation function of $S(t)$ is

$$\psi_s(\tau) = 2\int_{-\infty}^{\infty} s(t-\tau)\cos\omega_c(t-\tau)s(t)\cos\omega_c t dt \quad \text{A6.10}$$

The energy of the waveform $S(t)$ is

$$\psi_s(\sigma) = 2\int_{-\infty}^{\infty}[s(t)\cos\omega_c t]^2 dt \quad \text{A6.11}$$

$$= \int_{-\infty}^{\infty} \{[s(t)]^2 + \cos 2\omega_c t\} dt \qquad \text{A6.12}$$

$$= \int_{-\infty}^{\infty} s^2(t) dt \qquad \text{after lowpass filtering} \qquad \text{A6.13}$$

which is also the energy of the modulating waveform. Hence, the process of modulation does not alter the energy content of the waveform to be transmitted. Consequently, the modulation of the two waveform $a(t)$ and $b(t)$ can, from Eqn. A6.7, be represented as

$$s(t) = a(t) + jb(t) \qquad \text{A6.14}$$

in a baseband equivalent model, because the term $\sqrt{2}R\{\exp(j\omega_c t)\}$ in Eqn. A6.7 only represents a shift of the spectrum of $s^2(t)$ by ω_c rad/sec and has a modulus of unity.

A6.2 Representation of the demodulated signal

Let the demodulated signal be represented by $r'(t)$ and let the received information bearing signal before demodulation be represented by $m(t)$, then

$$r'(t) = \sqrt{2} m_a(t) \cos(\omega_c t + \phi) - \sqrt{2} m_b(t) \sin(\omega_c t + \phi)$$

where $m_a(t)$ and $m_b(t)$ are the inphase and quadrature components of $m(t)$, and ϕ is an arbitrary phase. Hence

$$r'(t) = \sqrt{2}\{m_a(t)\cos(\omega_c t + \phi) - m_b(t)\cos(\omega_c t + \phi - \pi/2)\} \qquad \text{A6.15}$$

$$= \sqrt{2} R\{m_a(t)\exp[j(\omega_c t + \phi)] - m_b(t)\exp[j(\omega_c t + \phi - \pi/2)]\} \qquad \text{A6.16}$$

$$= \sqrt{2} R\{m_a(t)\exp[j(\omega_c t + \phi)] - m_b(t)\exp[j(\omega_c t + \phi)]\exp[-j\pi/2]\} \qquad \text{A6.17}$$

$$= \sqrt{2} R\{m_a(t) + jm_b(t)\}\exp[j(\omega_c t + \phi)] \qquad \text{A6.18}$$

where $\exp(-j\pi/2) = 0 - j$, $(j = \sqrt{-1})$;

hence $r'(t) = \sqrt{2} R\{[m_a(t) + jm_b(t)]\exp(j\omega_c t)\exp(j\phi)\}$ A6.19

From Eqns. A6.7 and A6.9, the term $\sqrt{2}R\{\exp(j\omega_c t)\}$ in Eqn. A6.19 only represents a shift of the spectrum of $m(t)$ by ω_c rad/sec and has an average value of unity. Thus, the demodulation of $m(t)$ into two separate waveforms, representing the demodulation of two double sideband suppressed carrier amplitude modulated signals which are in phase quadrature, gives

$$r(t) = \{m_a(t) + jm_b(t)\}\exp(j\phi) \qquad \text{A6.20}$$

$$= \{m_a(t)\cos\phi - m_b(t)\sin\phi\} + j\{m_a(t)\sin\phi + m_b(t)\cos\phi\} \qquad \text{A6.21}$$

in a baseband equivalent model.

If the channel introduces no signal distortion or noise then the representation of the bandpass signal in the baseband equivalent model from Eqns. A6.14 and A6.20, is

$$r(t) = s(t)\exp(j\phi)\} \qquad \text{A6.22}$$

The result of Eqn. A6.22 can be verified by demodulating the signal in Eqn. A6.9 with $\sqrt{2}R\{\exp[j(\omega_c t + \phi)]\}$ and gives

$$r(t) = \sqrt{2}s(t)R\{\exp[j\omega_c t]\}\sqrt{2}\{\exp[j(\omega_c t + \phi)]\}$$

$$= 2s(t)\exp(j\phi)\cos^2\omega_c t$$

$$= s(t)\exp(j\phi)\{1 + \cos 2\omega_c t\}$$

$$= s(t)\exp(j\phi) \text{ after lowpass filtering} \qquad \text{A6.23}$$

Equations A6.22 and A6.23 are the same. Thus a system using quadrature amplitude modulated signals can use the complex signal representation given by Eqns. A6.21 and A6.22 to represent a baseband equivalent model.

APPENDIX A7

NARROWBAND NOISE REPRESENTATION PROPERTIES

Consider a white Gaussian noise of zero-mean and spectral density $\frac{1}{2}N_0$ which is passed through an ideal narrow bandpass filter (i.e., the center frequency f_c is large compared with the half-bandwidth of the filter) of unit gain, midband frequency f_c, and bandwidth $2B$ Hz. The spectral density characteristic of the filtered noise process $N(t)$ will therefore be as shown in Fig. A7.1a. It may be written [19] that

$$N(t) = N_c(t)\cos 2\pi f_c t - N_s(t)\sin 2\pi f_c t \qquad \text{A7.1}$$

where $N_c(t)$ and $N_s(t)$ are referred as the inphase and quadrature components of the narrowband noise $N(t)$. Some properties of this expansion are as follows [19], [95]:

(1) Gaussian. If $N(t)$ is a sample function of a Gaussian process, then $N_c(t)$ and $N_s(t)$ are also sample functions of Gaussian random processes.

(2) Independence. The functions $N_c(t)$ and $N_s(t)$ are statistically independent.

(3) Mean. If $N(t)$ has zero mean, then $N_c(t)$ and $N_s(t)$ also have zero mean.

(4) Spectra and variance. Both $N_c(t)$ and $N_s(t)$ have the same spectral density, which related to the spectral density $\psi_n(f)$ of the narrowband noise $N(t)$ as follows.

$$\psi_c(f) = \psi_s(f) = \begin{cases} \psi_n(f+f_c) + \psi_n(f-f_c) & ,-B \le f \le B \\ 0 & ,\text{elsewhere} \end{cases} \qquad \text{A7.2}$$

where $\psi_n(f)$, and $\psi_c(f)$ and $\psi_s(f)$ are the specral density of $N(t)$, $N_c(t)$ and $N_s(t)$, respectively, and $2B$ Hz is the bandwidth of $N(t)$. $N_c(t)$ and $N_s(t)$ each occupy the frequency band from zero frequency to $\pm B$ Hz. Since $N(t)$ has a two-sided power spectral density of $\frac{1}{2}N_0$ over the frequency bandwidth, Eqn. A7.2 reduces to

$$\psi_c(f) = \psi_s(f) = \begin{cases} 2\psi_n(f+f_c) & ,-B \le f \le B \\ 0 & ,\text{elsewhere} \end{cases} \qquad \text{A7.3}$$

$$= \begin{cases} N_0 & ,-B \le f \le B \\ 0 & ,\text{elsewhere} \end{cases} \qquad \text{A7.4}$$

The two-sided power spectral density of $N_c(t)$ and $N_s(t)$ are twice that of $N(t)$. The variance of $N_c(t)$ and $N_s(t)$, is

$$\overline{N_s^2(t)} = \overline{N_c^2(t)} = \int_{-B}^{B} \psi_c(f)df = 2N_0B \qquad \text{A7.5}$$

The variance of $N(t)$ is

$$\overline{N^2(t)} = \int_{-f_c-B}^{-f_c+B} \psi_n(f)df + \int_{f_c-B}^{f_c+B} \psi_n(f)df \qquad \text{A7.6}$$

$$= 2N_0B$$

Thus, the variance of $N_c(t)$, $N_s(t)$ and $N(t)$ are equal.

(5) Autocorrelation function of $N_c(t)$ and$N_s(t)$.

The autocorrelation function of $N(t)$ is the inverse Fourier transform of the spectral density characteristic, i.e., [95, p.208]

$$R_n(\tau) = \int_{-f_c-B}^{-f_c+B} \tfrac{1}{2}N_0 \exp(j2\pi f\tau)df + \int_{f_c-B}^{f_c+B} \tfrac{1}{2}N_0 \exp(j2\pi f\tau)df$$

$$= N_0B\frac{\sin 2\pi B\tau}{2\pi B\tau}[\exp(-j2\pi f_c\tau) + \exp(j2\pi f_c\tau)]$$

$$= 2N_0B\frac{\sin 2\pi B\tau}{2\pi B\tau}\cos 2\pi f_c\tau \qquad \text{A7.7}$$

which is shown in Fig. A7.1b.

Applying Eqn. A7.4 to the spectral density characteristic of Fig. A7.1, which is symmetrical about $\pm f_c$, the corresponding spectral density characteristic of the inphase and quadrature noise components, $N_c(t)$ or $N_s(t)$, as shown in Fig. A7.1c.

The autocorrelation function of $N_c(t)$ or $N_s(t)$ is therefore

$$R_s(\tau) = R_c(\tau) = \int_{-B}^{B} N_0 \exp(j2\pi f\tau)df$$

$$= 2N_0B\frac{\sin 2\pi B\tau}{2\pi B\tau} \qquad \text{A7.8}$$

It can be seen that $R_s(\tau)$ or $R_c(\tau)$ passes through zero at $\tau = \pm n/B$, where n=1, 2, 3, ..., if $N_c(t)$ or $N_s(t)$ is sampled at the rate of $2B$ samples per second, the resulting noise samples are uncorrelated, being Gaussian, they are statistically independent.

(6) Equivalent baseband signal of $N(t)$.

From Appendix A6, the narrowband noise $N(t)$ can be represented as the complex-valued signal

$$N(t) = [N_c(t) + jN_s(t)]R[\exp(j\omega_c t)] \qquad \text{A7.9}$$

in a baseband equivalent model, where $j = \sqrt{-1}$, $\omega_c = 2\pi f_c$ and $R(.)$ represents the real part of (.). The demodulation of $N(t)$ with $\sqrt{2}R[\exp(j\omega_c t)]$ gives

$$N(t)\sqrt{2}R[\exp(j\omega_c t)] = [N_c(t) + jN_s(t)]R[\exp(j\omega_c t)]\sqrt{2}R[\exp(j\omega_c t)]$$

$$= \sqrt{2}[N_c(t) + jN_s(t)]\cos^2 \omega_c t$$

$$= [\sqrt{½}N_c(t) + j\sqrt{½}N_s(t)][1 + \cos 2\omega_c t]$$

$$= n(t)[1 + \cos 2\omega_c t]$$

$$= n(t) \qquad \text{after lowpass filtering} \qquad \text{A7.10}$$

where
$$n(t) = \sqrt{½}N_c(t) + j\sqrt{½}N_s(t) \qquad \text{A7.11}$$

$$= n_c(t) + jn_s(t) \qquad \text{A7.12}$$

with $n_c(t) = \sqrt{½}N_c(t)$ and $n_s(t) = \sqrt{½}N_s(t)$.

Since the variance of $N_c(t)$ and $N_s(t)$ are $2N_0B$, the variance of $n_s(t)$ and $n_c(t)$ are

$$\overline{n_c^2(t)} = \frac{\overline{N_c^2(t)}}{2} = \frac{2N_0B}{2} = N_0B \qquad \text{A7.13a}$$

and
$$\overline{n_s^2(t)} = \frac{\overline{N_s^2(t)}}{2} = N_0B \qquad \text{A7.13b}$$

respectively.

The equivalent baseband signal of the narrow noise is therefore

$$n(t) = n_c(t) + jn_s(t)$$

where $n_c(t)$ and $n_s(t)$ each occupy a bandwidth of $\pm B$ Hz with a two-sided power spectral density of $\frac{1}{2} N_0$ over the frequency bandwidth (Fig. A7.1d).

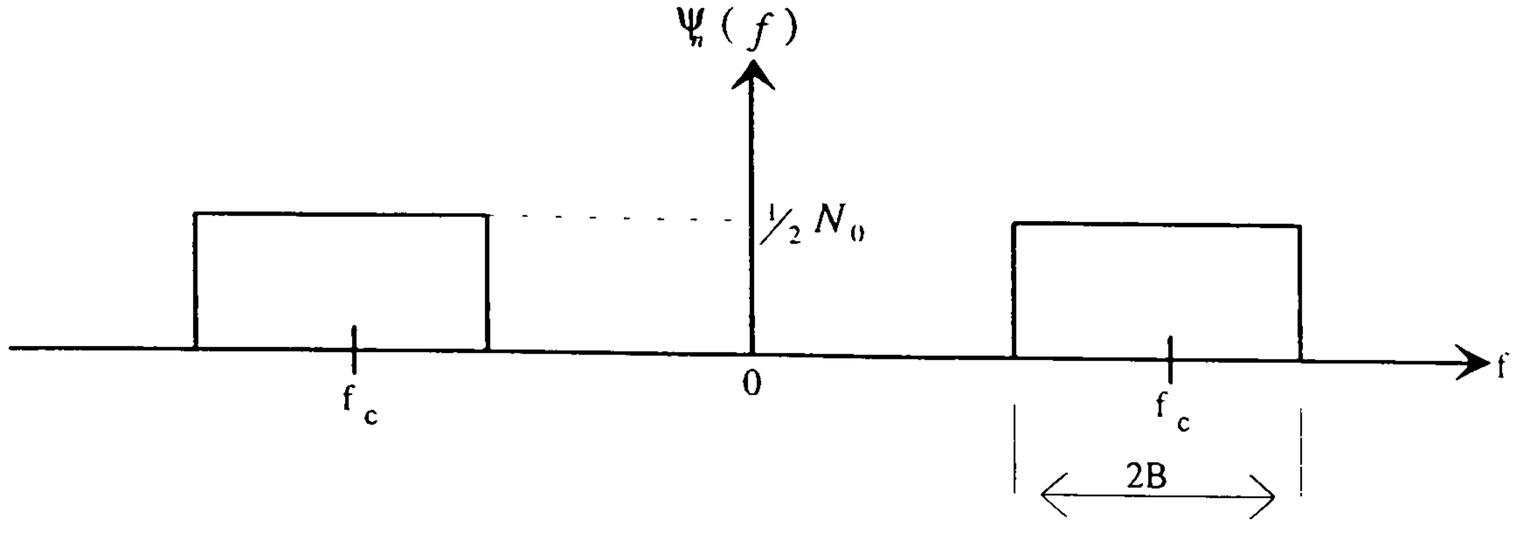

(a)

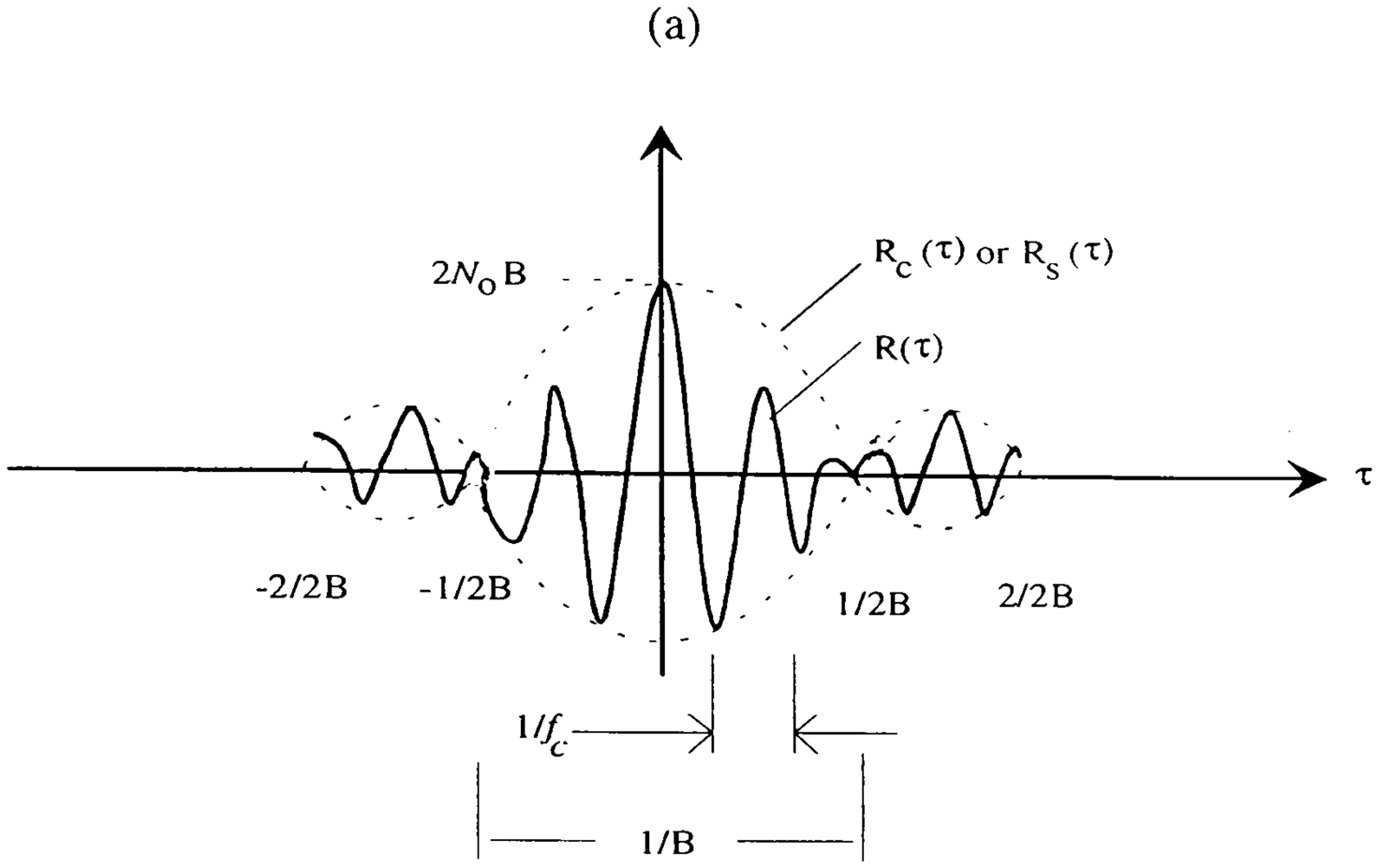

(b)

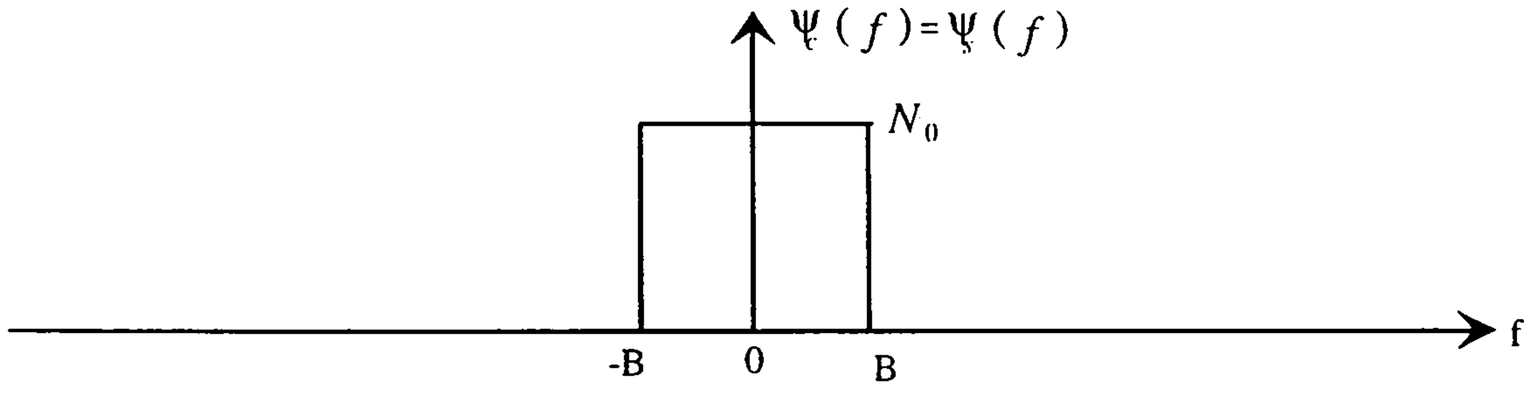

(c)

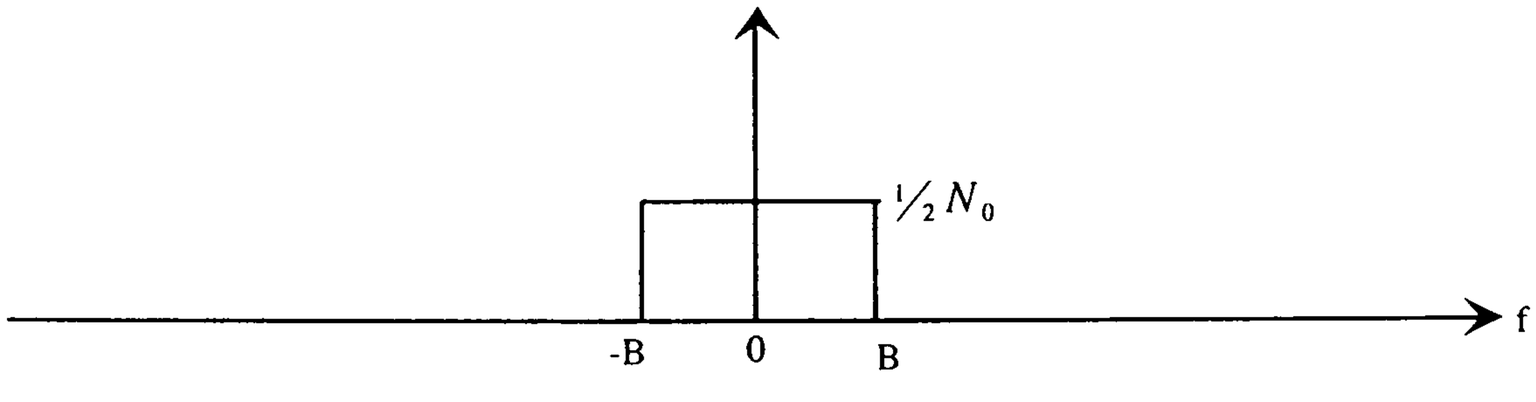

(d)

Figure A7.1 Characteristics of ideal bandpass filtered white noise. (a) Spectral density. (b) Autocorrelation function. (c) Spectral density of inphase and quadrature components. (d) Spectral density of the baseband inphase and quadrature components.

APPENDIX A8

BIT-ENERGY-TO-NOISE POWER DENSITY RATIO $(2E_b/N_0)$ CALCULATION FOR COMPUTER SIMULATION

A8.1 $\frac{1}{2}N_0$ determination for computer simulation

It is mentioned in Section 2.2.4 that the bit-energy-to-noise power spectral density ratio, $(2E_b/N_0)$ is frequently used in digital communication systems to enable a comparison of systems having variable transmission rates and of the performances of various modulation and coded systems in a complex interference environment. E_b is the energy per bit at the input to the receiver and $\frac{1}{2}N_0$ is the white Gaussian two-sided noise power spectral density measured at the same point. Here, it is to determine the white Gaussian two-sided noise power spectral density at the input to the receiver, for the different values of noise variance and sampling rate used in the simulation tests.

Consider a white Gaussian noise of zero mean and a two-sided power spectral density of $\frac{1}{2}N_0$ which is passed through an ideal narrow receiver bandpass filter of unit gain, mid-band frequency f_c, and bandwidth $2B$ Hz (Fig. A7.1). The baseband equivalent of the noise signal at the output of the filter can be written (Appendix A7) as the complex signal :

$$n(t) = n_c(t) + jn_s(t) \qquad \text{A8.1}$$

where $j = \sqrt{-1}$, and $n_c(t)$ and $n_s(t)$ are sample functions of Gaussian random processes with zero mean and two-sided power spectral density of $\frac{1}{2}N_0$ over the frequency band from -B Hz to B Hz (Fig. A7.1).

If $n(t)$ is sampled, at the time instants $\{iT\}$, where i takes all positive integer values, and

$$T = 1/2B \qquad \text{A8.2}$$

or

$$2B = 1/T \qquad \text{A8.3}$$

to give the noise sample value, at time $t = iT$,

$$n_i = n_{c,i} + jn_{s,i} \qquad \text{A8.4}$$

where $n_i = n(iT)$, $n_{c,i} = n_c(iT)$ and $n_{s,i} = n_s(iT)$, the resulting samples $\{n_i\}$ are uncorrelated and statistically independent (Appendix A7). The $\{n_{c,i}\}$ and $\{n_{s,i}\}$ each have the variance (Eqn. A7.13)

$$\sigma^2 = N_0 B \qquad \text{A8.5}$$

Thus, the two-sided noise power spectral density, $\frac{1}{2}N_0$, at the input to the ideal bandpass filter, in terms of variance σ^2 and bandwidth B Hz of the baseband equivalent model, can be written as

$$\frac{1}{2} N_0 = \sigma^2/(2B) \qquad \text{A8.6}$$

Hence, if the variance and bandwidth of the baseband equivalent model of the noise signal are known, the two-sided noise power spectral density at the input to the receiver filter can be found using Eqn. A8.6.

Now suppose a Gaussian random number generator generates the complex-valued samples, at the time instants $\{mT_s\}$, where m takes all positive integer values and

$$T_s = T/k \qquad \text{A8.7}$$

where k is an integer. The generating rate is k/T samples per second. So that at time $t = mT_s$, the generated complex-value sample is

$$n_m = n_{c,m} + jn_{s,m} \qquad \text{A8.8}$$

where $n_{c,m}$ and $n_{s,m}$ are sample values of uncorrelated and statistically independent Gaussian random variables with zero mean and fixed variance σ^2. This process is equivalent to obtaining the complex-valued Gaussian noise samples from the equivalent baseband model of an ideal narrow bandpass filter (Fig. A8.1). The ideal bandpass filter has a passband gain of one and a bandwidth of

$$2B = 1/T_s = k/T \qquad \text{A8.9}$$

as can be seen in an exactly analogous fashion expressed in Eqn. A8.3. So that by substituting $B = k/2T$ into Eqn. A8.6, the two-sided noise spectral power density at the input to the ideal bandpass filter can be found as

$$\frac{N_0}{2} = \frac{\sigma^2 T}{k} \qquad \text{A8.10}$$

Note that $\frac{1}{2}N_0$ is dependent on the generating rate k/T. This equation is very important in calculating the bit-energy-to-noise power density ratio in the computer simulation tests, because it relates the noise variance σ^2 and sampling rate used in the tests to the two-sided power density $\frac{1}{2}N_0$ at the input to the receiver.

Thus a Gaussian random number generator, generates uncorrelated complex-value samples $\{n_m\}$ with zero mean and fixed variance σ^2, at a rate of k/T samples per second, is equivalent to obtaining the complex-valued Gaussian noise samples from the baseband equivalent model of an ideal bandpass filter (Fig. A8.1). The ideal bandpass filter has a bandwidth k/T Hz and a gain of one. The two-sided noise power spectral density at the input to the baseband equivalent model of the ideal bandpass filter is

$$\frac{N_0}{2} = \frac{\sigma^2 T}{k} \qquad \text{A8.11}$$

This value can be used to compute the value $2E_b/N_0$ in the computer simulation tests.

A8.2 $2E_b/N_0$ value calculation for computer simulation

The equivalent baseband of a transmitted quadrature modulation signal (Section 2.6) can be represented as the complex signal (Appendix A6):

$$s(t) = a(t) + jb(t) \qquad \text{A8.12}$$

where $j = \sqrt{-1}$, and $a(t)$ and $b(t)$ are the equivalent baseband of the inphase and quadrature signal components, respectively.

The transmitted signal energy during the n^{th} T interval is

$$E_s = \int_{(n-1)T}^{nT} |s(t)|^2 \, dt \qquad \text{A8.13}$$

where T is the symbol duration.

Suppose the continuous waveform $s(t)$ of the transmitted signal is sampled at the time instants $\{mT_s\}$, for $m = 1, 2, 3, \ldots$, where

$$T = kT_s \qquad \text{A8.14}$$

and k takes a positive integer value (Eqn. A8.7), to give a sequence of samples $\{s_m\}$, where $s_m = s(mT_s)$ has a complex value. Assume that the sampling rate, $1/T_s = k/T$, is high enough to prevent alaising and L symbols are transmitted. There are altogether kL samples in the sequence $\{s_m\}$. The average energy per sample in $\{s_m\}$ is

$$P_a = \frac{1}{kL} = \sum_{m=1}^{kL} |s_m|^2 \qquad \text{A8.15}$$

Thus the average transmitted signal energy over a period of T seconds is

$$E_s = P_a T \qquad \text{A8.16}$$

This is also the average transmitted energy per signal element, and so the average transmitted bit energy (for DEQPSK, OQPSK, CE8PSK and CDE8PSK signals) can be written as

$$E_b = E_s/2 = P_a T/2 \qquad \text{A8.17}$$

Suppose the Gaussian noise sample value $\{n_m\}$ with zero mean and fixed variance σ^2, as described in Appendix A8.1, are used to add to the signal sample values at the time instants $\{mT_s\}$. So that at time $t = mT_s$, the added noise sample is

$$n_m = n_{c,m} + jn_{s,m} \qquad \text{A8.18}$$

with $n_{c,m}$ and $n_{s,m}$ the same definitions as in Eqn. A8.8.

From Appendix A8.1, it can be said that, under these assumed conditions, the two-sided power spectral density of $\frac{1}{2} N_0$ of the noise, measured at the same point as E_b, can be written as

$$\frac{N_0}{2} = \frac{\sigma^2 T}{k} \qquad \text{A8.19}$$

as can be seen in Eqn. A8.10. Of course, the signal is assumed to be all covered by the white Gaussian noise.

Using Eqns. A8.17 and A8.19, the bit-energy-to-noise power spectral density ratio can be written as

$$\frac{2E_b}{N_0} = \frac{P_a T k}{2\sigma^2 T} = \frac{P_a k}{2\sigma^2} \qquad \text{A8.20}$$

and the variance of the noise can be written as

$$\sigma^2 = \frac{N_0 P_a k}{4E_b} \qquad \text{A8.21}$$

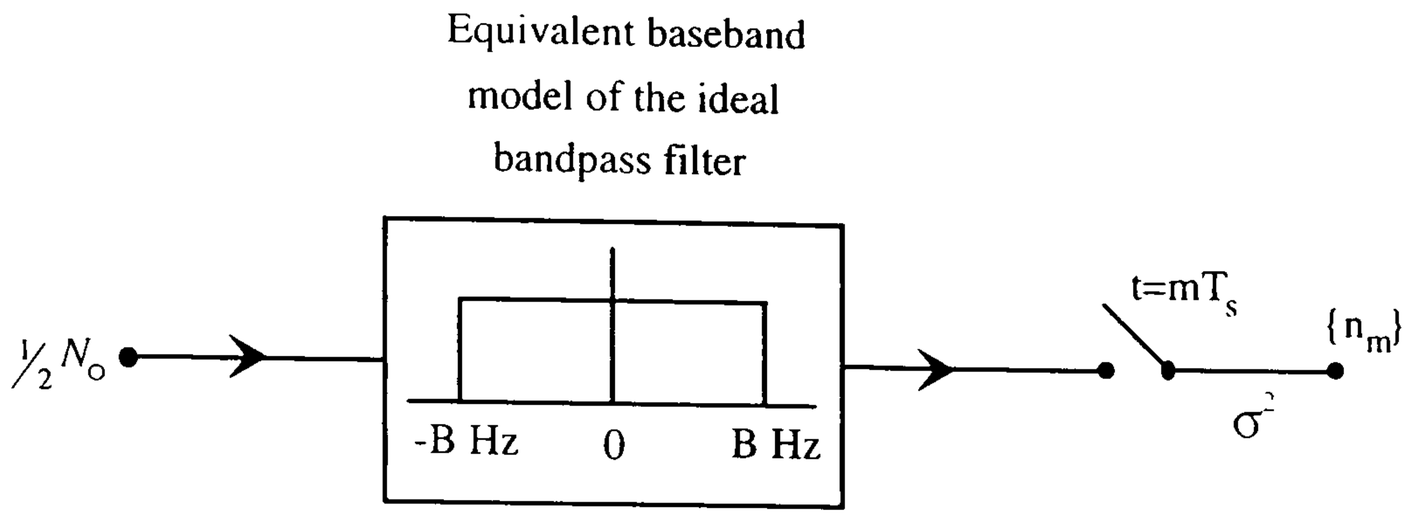

Figure A8.1 Equivalence of the noise model for computer simulation. (a) Model for obtaining the noise samples from the baseband equivalent model of the ideal bandpass filter. (b) Model for generating the noise samples for computer simulation. This is equivalent to the model shown in (a).

APPENDIX A9

THE SCALING RELATIONSHIP BETWEEN THE CONTINUOUS SIGNAL AND THE SAMPLED SIGNAL

Let $y(t)$ be a continuous waveform which is sampled at not less than the Nyquist rate to give the samples $\{y_m\}$, where

$$y_m = y(mT_s) \tag{A9.1}$$

and T_s is the sampling period. Now $y(t)$ may be expressed as [19]

$$y(t) = \sum_{m=-\infty}^{\infty} y_m \frac{\sin(t/T_s - m)}{\pi(t/T_s - m)} \tag{A9.2}$$

where the $\{\frac{\sin(t/T_s - m)}{\pi(t/T_s - m)}\}$, are a set of orthonormal functions. Thus

$$\int_{-\infty}^{\infty} |y(t)|^2 dt = \sum_{m=-\infty}^{\infty} |y_m|^2 \int_{-\infty}^{\infty} \frac{[\sin(t/T_s - m)]^2}{[\pi(t/T_s - m)]^2} dt \tag{A9.3}$$

The integral on the right-hand side is equal to T_s [96]. Therefore, Eqn. A9.3 becomes,

$$\int_{-\infty}^{\infty} |y(t)|^2 dt = T_s \sum_{m=-\infty}^{\infty} |y_m|^2 \tag{A9.4}$$

which means that the sampled signal must be scaled by sampling intervals T_s in order to give the same energy level as the continuous signal $y(t)$.

APPENDIX A10

PROBABILITY OF ERROR CALCULATION FOR BINARY SIGNALS [54, P499]

Consider two signal vectors S_i and S_j with a distance of d_{ij} units apart. With the two signals equally likely to be transmitted (as assumed here) it is to determine the probability of error for either one. By symmetry this is the same as for the other, and, averaging over both, is the system probability of error. This shows up in the decision regions of Fig. A10.1, since it is apparent that a signal vector V anywhere in the right-half plane should be associated with S_i, while any value in the left-half plane is associated with S_j. It is clear from Fig. A10.1 that the locus of all points ρ equally distant from S_i and S_j is the ϕ_2 axis. Thus an error occurs when S_j is transmitted if and only if the noise component N_j exceeds $d_{ij}/2$, where d_{ij} is the Euclidean distance between the two signals:

$$\mathrm{P}[\mathrm{E}|S_i] = \mathrm{P}[N_j > d_{ij}/2], \qquad \text{A10.1}$$

where

$$d_{ij}^2 = \left|S_i - S_j\right|^2 = \int_{-\infty}^{\infty} [s_i(t) - s_j(t)]^2 \, dt \qquad \text{A10.2}$$

is the square Euclidean distance, and $s_i(t)$ and $s_j(t)$ are the two corresponding timing signals in time domain. $\mathrm{P}[\mathrm{E}|S_i]$ is the conditional probability of error when S_i has been transmitted.

Let N_j be zero-mean Gaussian with variance $\frac{1}{2} N_0$, so that

$$\mathrm{P}[\mathrm{E}|S_i] = \int_{d_{ij}/2}^{\infty} \frac{1}{\sqrt{\pi N_0}} \exp\left(\frac{-\alpha^2}{N_0}\right) d\alpha \qquad \text{A10.3}$$

Setting $\gamma = \alpha/2/N_0$, Eqn. A10.3 becomes

$$\mathrm{P}[\mathrm{E}|S_i] = \int_{\frac{d_{ij}/2}{\sqrt{N_0/2}}}^{\infty} \frac{1}{\sqrt{2\pi}} \exp\left(\frac{-\gamma^2}{2}\right) d\gamma \qquad \text{A10.4}$$

$$= Q(\frac{d_{ij}}{\sqrt{2N_0}}) \qquad \text{A10.5}$$

where $$Q(y) = \int_y^{\infty} \frac{1}{\sqrt{2\pi}} \exp(\frac{-w^2}{2}) dw$$

Since, by symmetry, the conditional probability of error is the same for either signal, so the probability of error is

$$P_e = P(E) = P[S_i]P[E|S_i] + P[S_j]P[E|S_j] \qquad \text{A10.6}$$

$$= \tfrac{1}{2} P[E|S_i] + \tfrac{1}{2} P[E|S_j] \qquad \text{A10.7}$$

$$= Q(\frac{d_{ij}}{\sqrt{2N_0}}) \qquad \text{A10.8}$$

$$= Q(\sqrt{\frac{d_{ij}^{\ 2}}{2N_0}}) \qquad \text{A10.9}$$

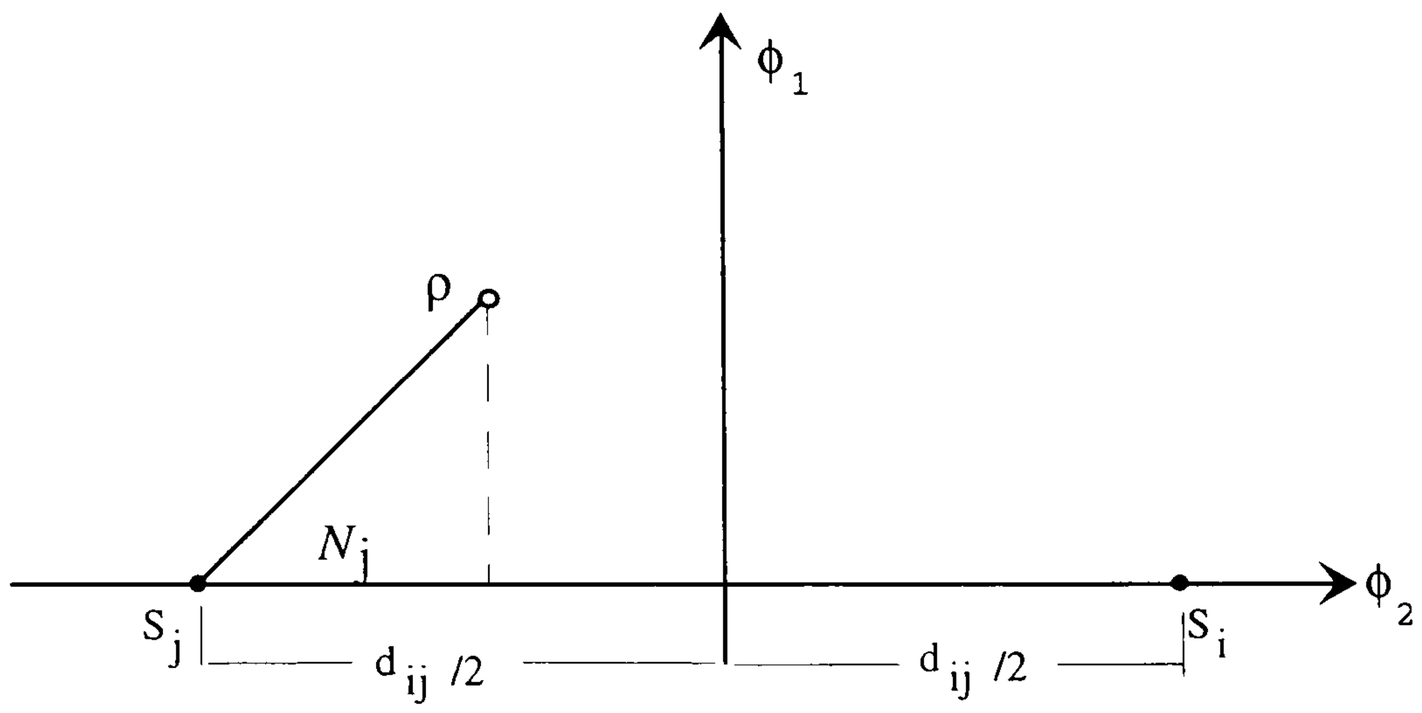

Figure A10.1 Two signal vectors and decision boundray in a subspace.

REFERENCES

1. Clark, A. P., *Principles of Digital Data Transmission*, Pentech Press, London (1976).

2. Davenport, W. B., *Probability and Random Processes*, McGraw-Hill, New York (1970).

3. Thomas, J. B., *An Introduction to Statistical Communication Theory*, pp.614-620,Wiley, New York (1969).

4. Bennet, W. R. and Davey, J. R., *Data Transmission*, McGraw-Hill, New York (1965).

5. Martin, J., *Communications Satellite Systems*, Prentice-Hall, Englewood Cliffs, NJ (1978).

6. Feher, K., *Digital Communications; Satellite/Earth Station Engineering*, Prentice-Hall, Englewood Cliffs, NJ (1978).

7. Miyauchi, K., Ito, M. and Okada, T., "A method to evaluate effective use of transmitting power in bandlimited psk channels", *Electronics and Commun. in Japan, Part 1 (Communications),* vol. 77, Iss.7, pp.81-92, July 1994.

8. Kato, S. et al, "A TDMA satellite communication system for ISDN services", *IEEE Journal on selected areas in communications.* vol.10, Iss.2, pp.456-464, Feb. 1992.

9. Dubey, V. K., Taylor, D. P., "Further results on receivers for the nonlinear channel including pre- and post- nonlinearity filtering", *IEE Proceeding-Communications.* vol. 141. Iss.5, pp.334-340, Oct. 1994.

10. Lunn, T. J., Burr, A. G., "Performance degradation of coded 8 PSK over a non-linear channel", *IEE Colloquium on 'Advanced Modulation and coding Techniques for satellite Communications'*, pp.8/1-6, IEE, 1992.

11. Lin, F., Song, T., and Jiang, S., "A modified IJF-OQPSK modulation technique", *IEEE MILCOM' 93. 'Communications on the Move', Conference Recoed,* pp. 944-947, vol.3, 1993.

12. DeJagar, F. de and Dekker, C. B., " Tamed frequency modulation, a novel method to achieve spectrum economy in digital transmission", *IEEE Trans. on Commun.*, vol. COM-20, pp.534-542, May 1978.

13. Lyons, R. G., " The effect of a bandpass nonlinearity on signal detectibility", *IEEE Trans. on Commun. Technol.*, vol. COM-2, pp.51-60, Jan. 1973.

14. Davisson, L. D., and Milstein, L. B., " On the performance of digital communication systems with bandpass limiters - Part I: One link system", *IEEE Trans. on Commun. Technol.*, vol. COM-20, pp. 972-975, Oct. 1972.

15. Jain, P. C. and Blachman, N. M., " Detection of a PSK signal transmitted through a hard-limited channel", *IEEE Trans. Inform. Theory*, vol. IT-19, No.5, pp.623-630, Sept. 1973.

16. Hetrakul, P. and Taylor, D. P., " The effects of transponder nonlinearity on binary CPSK signal transmission", *IEEE Trans. Commun.*, vol. COM-24, pp.546-553, May 1976.

17. Kaye, A. R., George, D. A. and Eric, M. J., " Analysis and compensation of bandpass nonlinearities for communications", *IEEE Trans. on Commun. Technol.*, vol. COM-20, pp. 965-972, Oct. 1972.

18. Bhargave, U. K., Hacocum, D., Matyas, R. and Nuspl, P. P., *Digital Communications by Satellite. Modulation, Multiple access and coding,* John Wiley & Sons (1982).

19. Taub, H. and Schilling, D. C., *Principles of communication systems*, pp. 235-281 McGraw-Hill (1971).

20. Schwartz, M., *Information transmission, modulation, and noise,* 2nd Edition, McGraw-Hill Kogakusha. Tokyo (1970).

21. Linsey, W. C. and Simon, M. K., *Telecommunication systems engineering,* Prentice-Hall, Englewood Cliffs, NJ (1978).

22. Wilson, S. G. and Gaus, R., "Power spectra of multi-h phase codes", *IEEE Trans. on Commun.*, vol. COM-29, pp. 250-256, March. 1981.

23. Schwartz, M. and shaw, L., *Signal processing: discrete spectra analysis, detection and estimation,* ch.3, McGraw-Hill (1975).

24. Oppenheim, A. V. and Schafer, R. W., *Digital signal processing,* ch.11, Prentice-Hall, Englewood Cliffs, NJ (1975).

25. Gauo, Y., Feher, K., "Frequency hopping F-QPSK for power and spectrally efficient cellular systems", *43rd IEEE Vehicular Technology Conferenve. Personal Commun.* pp.799-802, 1993.

26. Zhigang, C., Yongkun, L., "DSP-based implementation of Viterbi decoder for trellis-coded 8psk", *IEEE TENCON' 90, 1990 IEEE Region 10 Conference on Computer and Commun. Systems.* pp.697-700, vol.2, 1990.

27. Gunther, C. G., Habermann, J., "DOQPSK-differential demodulation of filtered offset QPSK", *VTC 1994. IEEE 44th Vehicular Technology Conference.* pp.1542-1546. vol.3. 1994.

28. Feher, K., Ed., *Advanced Digital communications: systems and signal processing Techniques*. Englewood Cliffs, NJ: Prentice-Hall, 1987.

29. Feher, K., *Wireless Digital communications: Modulation and spread spectrum,* Englewood Cliffs, NJ: Prentice-Hall, 1995.

30. Papoulis, A., *Signal analysis,* ch.12, McGraw-Hill (1971).

31. Lebowitz, S. H. and Rhodes, S. A., "Performance of 8PSK signaling for satellite communications", *IEEE Int. Conf. on Commun.*, Denver, Co, USA, vol. 3, pp. 47.4.1-47.4.8, June 1981.

32. Hui, J. and Fang, R. J. F., "Convolutional code and signal waveform design for band-limited satellite channels", *IEEE Int. Conf. on Commun.*, Denver, Co, USA, vol. 3, pp. 47.5.1-47.5.9, June 1981.

33. Rhodes, S. A, Fang, R. J., and Chang, P. Y.,"coded octal phase shift keying in TDMA satellite communications", *COMSAT Tech. Rev.* vol. 13, No. 2, pp. 221-257, Fall 1983.

34. Mulwijk, D., "Correlative phase shift keying- A class of constant envelope modulation techniques", *IEEE Trans. on Commun.*, vol. COM-29, pp. 226-236, March. 1981.

35. Benedetto, S., et al, "Receiver design for 8-PSK trellis coded modulation in a TDMA burst mode satellite link", *Proceeding of the 5th Tirrenia International workshop, 'Coded Modulation and Bandwidth-Efficient transmission'*. pp.103-116, Elsevier, Amsterdam, Netherlands, 1992.

36. Viterbi, A. J. and Omura, J. K, *Principle of digital communication and coding*, McGraw-Hill (1979).

37. Clark, A. P., "Minimum-distance decoding of binary convolutional codes", *Computer and Digital Techniques,* vol. 1, pp. 190-196, Oct. 1978.

38. Evans, B. G., Ed., *Satellite communication systems*, 2nd Edition, IEE Telecommunications, series 24, Peter Peregninus Ltd. London, 1991.

39. Ungerboeck, G., "Channel coding with multi-level/phase signals", *IEEE Int. Symp. on Inform. Theory*, Ronnedy, Sweden, June 1976.

40. Ungerboeck, G., "Channel coding with multi-level/phase signals", *IEEE Trans. Inform. Theory*, vol. IT-28, pp.55-67, Jan. 1982.

41. Viterbi, A. J., "Convolutional codes and their performance in communication systems", *IEEE Trans. on Commun.*, vol. COM-19, pp. 751-772, 1971.

42. Biglieri, E., "High-level modulation and coding for nonlinear satellite channels", *IEEE Trans. on Commun.*, vol. COM-32, pp. 616-626, May 1981.

43. Viterbi, A. J., "Error-bounds for convolutional codes and an asymptotically optimum decoding algorithm", *IEEE Trans. Inform. Theory*, vol. IT-13, pp.260-269, 1967.

44. Forny, JR. G. D., "The Viterbi algorithm", *Proceeding of the IEEE,* vol. 61, No. 3, pp.268-278, March 1973.

45. Nuspl, P. P., et al, "Synchronisation methods for TDMA", *Proceedings of the IEEE*, vol.65, No.3, pp.434-444, March 1977.

46. Christodoulides, L. M., et al, "Frame synchronisation using two frame alignment words", *Electronics Letters*, pp.104-106, vol.30, No.2, January 1994.

47. Wyk, J. V. and Linde, L. P., "Multidimensional frame synchronisation strategy for 4D-Q2PSK", *Electronics Letters*, pp.2077-2078, vol.31, No.24, November 1995.

48. Shark, L. K., Terrell, T. J. and Simpson, R. J., "Adaptive frame synchroniser for digital satellite communication systems", *IEE Proceedings*, vol.135, Pt. F, No.1, pp.51-59, feb. 1988.

49. Proakis, J., *Digital communications*, McGraw-Hill (1983).

50. Clark, A. P., *Advanced Data-Transmission systems*, Pentech Press, London (1977).

51. Aftelak, S. B. and Clark, A. P., "Adaptive reduced-state Viterbi algorithm detector", *J. IERE,* vol. 56, No. 5, pp.197-206, may 1986.

52. Pooiy, Y. K. and Sinha, P., "A Viterbi-type algorithm for efficient estimation of M-PSK sequences over the Gaussian channel with unknown carrier phase", *IEEE Trans. on Commun.*, vol. COM-43, Iss.9, pp.2429-2433, 1995.

53. Hemati, F. and Costello, D. J., "Truncation error probability in Viterbi decoding", Consie paper, *IEEE Trans. on Commun.*, vol. COM-25, pp.530-532, 1977.

54. Wozencraft, J. M. and Jacobs, I. M., *Principles of Communication Engineering*, John Wiley & sons, N. Y. (1967).

55. Gardner, F. M.,"Hang-up in phase-locked loops", *IEEE Trans. on Commun.*, vol. COM-25, No. 10, 1977.

56. Viterbi, A. J. and Viterbi, A. M., "Nonlinear estimation of PSK-modulated carrier phase with application to burst digital transmission", *IEEE Trans. on Info. Theory*, vol.IT-29, No.4, pp.543-551, July 1983.

57. Classen, F., Meyr, H. and Sehier, P., "An all feedforward synchronisation unit for digital radio", *43rd IEEE Vehicular Technology Conference*. Personal commun. pp.738-741, 1993.

58. Kobayashi, K. et al, "High speed QPSK/OQPSK burst modem VLSIC", *International Conf. on Commun. ICC' 93*, vol.3. pp.1735-1739, 1993.

59. Kato, S. et al, "Satellite TDMA system for DYNET II", *NTT Review* vol.4, part.6, pp.53-61, 1992.

60. Seki, K., et al, "A high speed QPSK/OQPSK digital burst modem for LSIC implementation", *Communication for Global users Conf. GLOBCOM' 92*, pp.422-426, Dec. 1992.

61. Aulin, I., "CPM- An efficient constant amplitude modulation scheme", *Int. J. of Sat. Commun.* April 1984.

62. Aulin, I., "CPM- The effect of filtering and bandlimiting", *Int. J. of Sat. Commun.* April 1984.

63. Gardner, F. M., *Phaselock Techniques*, 2nd Ed. John Wiley & sons (1979).

64. Clark, A. P. and Cheung, S. W., "Performance of a satellite modem transmiting convolutionally and differentially encoded 8psk signals", *International Journal of satellite commun.* vol.11, No.1, pp.19-32, 1993.

65. Clark, A. P., "Distance measures for Near-Maximum-Likelihood detection processes", *IEE Proc.*, vol. 128, Pt. E., No. 3, May 1981.

66. Lathi, B. P., *Random Signals and Communication Theory*, Intertext Books, London (1968).

67. Namiki, J., "An automatically controlled predistorter for multilevel quadrature amplitude modulation", *IEEE Trans. on Commun.*, vol. COM-31, No. 5, pp. 707-712, May 1983.

68. Hecken, P. and Heidt, R. C., "Prediction linearization of the AR-6A transmitter", in *Conf. Rec., ICC'80*, pp. 33.1.1-33.1.6.

69. Gray, L. F., Alstyne, J. V. and Sadrin, W. A., "Application of broadband linearizer to earth station", in *Conf. Rec., ICC'80*, pp. 33.4.1.

70. Girard, H. and Feher, K., "A new baseband linearizer for more efficient utilization of earth station amplifiers used for QPSK transmission", *IEEE Trans. on Selected Area in Commun.*, vol. SAC-1, No. 1, pp. 46-56, Jan. 1983.

71. Cheung, S. W. and Aghvami, A. H., "Performance of a 16-Ary DEQAM modem employing a baseband or RF predistorter over a regenerative satellite link", *IEE proceedings, vol.135, Pt. F, Commun., Rader and signal processing*, pp.547-557, No.6, Dec. 1988.

72. TMS320C5X Digital Signal Processor User's Guide. Texas Instruments, USA (1993).

73. Allan, R. D., Bramwell, J. R. and Saunders, D. A., "A high performance satellite modem using rael-time digital signal processing techniques", *J. IERE*. pp. 117-124, May 1988.

74. "High speed TDMA modem for the T-SAT satellite", Internal report, Loughborough University, Dept. of Elec. Engineering, March 1990.

75. Marshall, W. G., Hoare, D. W. and Clark, A. P., "Using DSPs to synchronize a digital satellite modem", *Microprocessors and Microsystems*. vol. 14, No. 2, pp. 97-100, March 1990.

76. Clark, A. P., *Priciples of digital data transmission*, Pentech press (1983).

77. Clark, A. P. and Tan, H. C., "Carrier phase synchronization for QPSK signals in satellite links", *IERE conf. Pubn.* No. 82. pp. 219-224, Sept. 1988.

78. Clark, G. C. and Cain, J. B., *Error-correction coding for digital communications*, Plenum press, New York, 1981.

79. Shenoy, A. and Johnson, P., "Serial implementation of Viterbi decoders", *COMSAT Technical review*, vol. 13, No. 2, pp. 315-330, Fall 1983.

80. Conan, J., "Implementation of Microprocessor based Viterbi decoders", *Conf. Microcomputers and their applications*, 6th International symposium, Mini'78, pp. 78-93, Zurich, switzerland, June 1978.

81. Fettweis, G. and Meyr, H. "High-speed parallel Viterbi decoding: algorithm and VLSI-Architecture", *IEEE Commun. Magazine*, pp. 46-55, May 1991.

82. Kubota, S. and Kato, S., "Novel Viterbi decoder VLSI implementation and its performance", *IEEE Trans. on Commun.*, vol. COM-41, No. 8, pp. 1170-1178, Aug. 1993.

83. Seshadri, N. and Sundberg, C. W., "List Viterbi decoding algorithms with applications", *IEEE Trans. on Commun.*, vol. COM-42, No. 2/3/4, pp. 313-323, Feb./March/April, 1994.

84. Stahl, J., Meyer, H. and Oerder, M., "Implementation of a high speed Viterbi decoder", *Signal processing III: Theory and applications* I. T. Young et al. (Editors), pp. 1117-1120, *EURASIP*, 1986.

85. Golda, J., Benzakein, A., Groenendaal, J. G. and Braun, R. M., "VLSI appropriate design of a Trace-back Viterbi decoder", *IEEE South African symposium on Commun. and signal processing*, COMSIG-94, pp. 76-80. October 1994.

86. Rader, C. M., "Memory mangement in a Viterbi decoder", *IEEE Trans. on Commun.*, vol. COM-29, No. 9, pp. 1399-1401, Sept., 1981.

87. Omura, J. K., "On the Viterbi decoding algorithm", *IEEE Trans. on Info. Theory*, pp. 177-179, January 1969.

88. Clark, A. P., *Equalizers for digital modems*, Pentech press, 1985.

89. TMS320C5X, TMS320LC5X, Digital signal processor, Texas Instrument, SPRS030- April 1995.

90. Brown, A., "Random noise generation for the TMS320", *Electronic production design*, pp. 21, Feb. 1988.

91. Brown, A., "Generate Gaussian noise with a DSP chip", *Electronic Design News*, June 23, 1988.

92. Knuth, D. E., *Seminumerical Algorithms*, Addison-wesley, pp. 26-27, 1969.

93. Brayer, k., "Analysis of Quadrature Crosstalk in Bandpass Siganls", *Proc. IEEE,* pp. 292-294, Feb. 1971.

94. Harvey, J. D., "*Adaptive Detection of Digital Suppressed-Carrier A.M. Signals*", pp.362-365, PhD Thesis, Loughborough University of Technology (1978).

95. Haykin, S., *Communication systems*, pp.206-207, John Wiley & Sons, Inc., New York (1979).

96. Maisel, L., *Probability, statistics and random processes,* Simon and Schuster Inc., NY, 1971.

97. Le-Ngoc, T., and Feher, K., "Performance of IJF-OQPSK modem in cascaded nonlinear and regenerative satellite systems", *IEEE Trans. on Commun.*, vol. COM-31, No. 2, pp. 296-301, 1983.

98. Gronemeyer, S. A. and McBride, A. L., "MSK and Offset QPSK modulation", *IEEE Trans. on Commun.*, vol. COM-24, pp. 809-820, Aug. 1976.

99. Buda, R. de, "Coherent demodulation of frequency shift keying with low deviation ratio", *IEEE Trans. on Commun.*, vol. COM-20, pp. 429-435, June 1972.

100. Murota, K. and Hirade K., "GMSK modulation for digital mobile radio telephony", *IEEE Trans. on Commun.*, vol. COM-29, No. 9, pp. 1044-1050, July 1981.

101. Murota, K., Kimoshita, K. and Hirade K., "Spectrum efficiency of GMSK land mobile radio", *IEEE Int. Conf. on Commun.*, pp. 23.8.1-23.8.5, June 1981.

102. Le-Ngoc, T., Feher, K. and Phan van, H., "New modulation techniques for low-cost power and bandwidth efficient satellite earth stations", *IEEE Trans. on Commun.*, vol. COM-30, Jan. 1982.

103. Kato, S. and Feher, K., "XPSK: A new cross-correlated phase-shift keying modulation technique", *IEEE Trans. on Commun.*, vol. COM-31, pp. 701-707, May 1983.